# HIGH RESOLUTION, U/TH DATED (32,000 TO 11,000 YEARS), OXYGEN AND CARBON ISOTOPE PROXY CLIMATE RECORDS FROM A STALAGMITE IN DESOTO CAVERNS, ALABAMA, USA

by

WILLIAM JOSEPH LAMBERT

A DISSERTATION

Submitted in partial fulfillment of the requirements
for the degree of Doctor of Philosophy
in the Department of Geological Sciences
in the Graduate School of
The University of Alabama

TUSCALOOSA, ALABAMA

2010

## ABSTRACT

This study addresses the question whether speleothems from DeSoto Caverns (Childersburg, AL) can serve as archives of paleoclimate conditions for the Southeast, USA. The focus of the study involves determining present-day controls of cave water $\delta^{18}O$ and $\delta^{13}C$ followed by interpretation of stalagmite $\delta^{18}O$ and $\delta^{13}C$ variability in comparison to climate events of the past.

The monitoring program involved a 3-year study of cave waters and local rainfall (Tuscaloosa, AL) during years characterized by a significant trend from wet to dry conditions. Decreasing recharge of the cave aquifer was expressed as an interannual trend of declining drip flow rates, which was punctuated by seasonal oscillations due to varying rates of evapotranspiration. Amount-weighted mean monthly rainwater $\delta^{18}O$ range from -1.5 to -8.3‰, show a mean seasonal amplitude of ~4‰, and exhibit an interannual trend toward $^{18}O$-enrichment that I interpret as being governed by global atmospheric circulation patterns. The cave's aquifer attenuates seasonal $\delta^{18}O$ variability, records 20% of rainfall's interannual $^{18}O$-enrichment, and is biased toward winter rainfall $\delta^{18}O$.

Cave waters display strong seasonal variability in dissolved inorganic carbon (DIC) and $\delta^{13}C$, which range from 0.2 to 6.0 mM and 2.7 to -12.9‰ (VPDB), respectively. The data suggest the strongest seasonal controls are cave air ventilation/stagnation and varying $CO_2$ fluxes through the soil horizon and epikarst. $\delta^{13}C$ of active speleothems imply the precipitating

aragonite captures the seasonality observed in source dripwaters and time-series $\delta^{13}C$ records of stalagmites carry the imprints of drip annual means entailing climate-driven $\delta^{13}C$ seasonal biases.

A fossil stalagmite provided a high-resolution proxy record of rainfall variability between 31.9 and 11.3 ka. I propose a more southerly polar jet stream (PJS) promoted increased winter rainfall amounts during cold phase events while warm phases result in a higher PJS position and decreased winter rainfall. The Younger Dryas was characterized by a dramatic change in the PJS path as warm air from the Gulf of Mexico infiltrated deep into the continent's interior and substantially decreased winter rainfall. Establishment of near modern climate conditions greatly enhanced deposition rates before changes in flow paths through the epikarst prevented stalagmite deposition since 11.3 ka.

# DEDICATION

I would like to dedicate this dissertation to my family, Bailee and Hayden, as well as my parents and grandparents. Thank you for your patience as I worked to complete this degree.

## LIST OF ABBREVIATIONS AND SYMBOLS

| | |
|---|---|
| A.D. | Anno Domini |
| Atm | Standard atmosphere |
| BH | Bermuda High |
| BP | Before present relative to 1950 A.D. |
| C | Carbon |
| Cal. | Calendar |
| CF-IRMS | Continuous flow isotope ratio mass spectrometer |
| cm | Centimeter: hundredth of a meter |
| $CO_2$ | Carbon dioxide |
| Corr. | Corrected |
| DBT | Depth below top |
| DCP | Dead carbon percent |
| *d-excess* | Deuterium excess |
| DIC | Dissolved Inorganic carbon |
| DO | Dansgaard-Oeschger Event |
| DSSG | DeSoto stalagmite |

| | |
|---|---|
| e.g. | For example (Latin: *exempli gratia)* |
| et al. | And others (Latin: *et alii*) |
| etc. | And the rest (Latin: *et cetera)* |
| ENSO | El Niño-Southern Oscillation |
| GCMWL | Gulf Coast Meteoric Water Line |
| GMWL | Global Meteoric Water Line |
| GOM | Gulf of Mexico |
| h | Hour |
| H | Hydrogen |
| HE | Heinrich Event |
| i.e. | That is to say (Latin: *id est*) |
| ka | kilo-annum |
| km | Kilometer |
| l | Liter |
| m | Meter |
| mm | Millimeter: thousandth of a meter |
| mM | Millimoles/liter |
| *n* | Number of observations |
| NBS | National Bureau of Standards |
| O | Oxygen |
| PJS | Polar jet stream |
| PMC | Percent modern carbon |
| $r^2$ | Coefficient of determination |

| | |
|---|---|
| s | Second |
| U/Th | Uranium to Thorium ratio |
| VPDB | Vienna Pee Dee Belemnite |
| VSMOW | Vienna standard mean ocean water |
| XRD | X-ray diffraction |
| YD | Younger Dryas |
| 10x | Magnified by 10 times |
| 20x | Magnified by 20 times |
| $^{18}O$ | Oxygen atom with atomic mass of 18 |
| $^{2}H$ | Hydrogen atom with atomic mass of 2 |
| $^{13}C$ | Carbon with atomic mass of 13 |
| $^{14}C$ | Radiocarbon |
| $\delta^{18}O$ | Oxygen isotopic composition |
| $\delta^{13}C$ | Carbon isotopic composition |
| $\delta^{13}C_{AR}$ | Carbon isotopic composition of aragonite |
| $\delta^{13}C_{DIC}$ | Carbon isotopic composition of dissolved organic carbon |
| μm | Micrometer: millionth of a meter |
| μl | Microliter: millionth of a liter |
| μg | Microgram: millionth of a kilogram |
| °C | Degrees Celsius |
| % | Percent |
| ‰ | Per mil |
| σ | Standard deviation |

# ACKNOWLEDGMENTS

First and foremost I would like to thank my family for their support in my pursuit of a Ph.D. Special thanks is due to committee chair Dr. Paul Aharon for his supervision during the planning, implementation, and completion of my dissertation research. His assistance guided me in further developing my scientific writing ability as well improving skills within the field and laboratory. Additionally, I would like to thank committee members Fred Andrus, Tim Masterlark, Geoff Tick, and David Kopaska-Merkel for their time investment from busy schedules and their support and encouragement along the way.

The list is long of both graduate and undergraduate students that have assisted me in the field and the laboratory. These students include but are not limited to: Michael Rasbury, Valeriu Murgulet, Sandip Bordoloi, Miguel Etayo, Montana Puscas, Rajesh Dhungana, Dave Aldridge, Hunter Phillips, and Maeve Yaden. I also thank George Ponta for his help with mapping the cave interior.

My research project would not have been possible without the generosity of cave owner Al Mathis and DeSoto Caverns' president Tim Lacy. They graciously allowed research within the cave and accommodated my schedule without hesitation.

Funding for this research was provided by: Gulf Coast Association of Geological Societies (GCAGS faculty and student grants), Geological Society of America, Evolving Earth Foundation, John G. Newton Scholarship of the Alabama Geological Society, and multiple University of Alabama student research and travel grants.

CONTENTS

LIST OF TABLES

LIST OF FIGURES

CHAPTER 1

# INTRODUCTION

Rainfall distribution across our planet defines a region's ecological diversity, economic infrastructure, and sustainable population, among many other important variables. The Southeast (USA) is heavily dependent upon all phases of the water cycle as moisture is transported from the Gulf of Mexico (GOM), falls as rainfall to support agriculture and natural ecosystems, and recharges surface reservoirs and aquifers. Reductions in normal moisture flux from the GOM, even for periods of less than one year, can drastically affect local economies and day-to-day activities (Dixon and Segerson, 1999). For instance, spring/summer rainfall deficiencies can result in near complete crop loss (Rosenzweig et al., 2001), while reduced winter rainfall fails to fully recharge already stressed reservoirs, often resulting in water conservation regulations (Rosen et al., 1999; Pirie et al., 2004). With human population continuing to grow, especially along the Gulf Coast (Hinrichsen, 1998), the need to better constrain the natural cycles of Southeast rainfall variability is of utmost importance (Alexandrov and Hoogenboom, 2000).

In the present climate state, atmospheric circulation patterns influence rainfall amounts throughout the year in the Southeast (Yin, 1994). During summer months, rainfall is typically delivered in the form of convection style thunderstorms where moisture is supplied by southerly winds from the warm GOM (Long, 1959). The Bermuda High (BH), which is a high-pressure

cell that migrates to the western Atlantic Ocean during the Northern Hemisphere summer, can strongly increase or limit this flow of moisture depending on the east-west position of the cell's western edge (Katz et al., 2003). Additionally, the BH position can act to steer tropical systems (i.e., depressions, storms, and hurricanes) from the Atlantic Coast to the Gulf Coast thereby altering the track of landfall and ensuing torrential rainfall (Knight and Davis, 2007). During winter months (as well as early spring/late fall) the north-south position of the polar jet stream plays a vital role in rainfall amounts (Cane, 2005). A southerly position of the jet stream carries storm systems across the Southeast increasing winter rainfall. Drier conditions in the Southeast occur when the jet stream is positioned farther to the north. Regardless of season, the dominant moisture source for rainfall associated with convection style storms and frontal systems is the GOM (Rasmusson, 1968; Bryson and Hare, 1974; Simpkins, 1995).

Unfortunately, historical rainfall records are too brief to accurately predict future trends in the variability of these rainfall controls. In order to circumvent this shortcoming, a number of proxies for past climate conditions have been explored with their reliability and temporal resolution increasing in concert with technological advances (Fairchild et al., 2006). In the Southeast, the majority of these studies have focused on pollen and tree-ring records. Stahle and Cleaveland (1992) and Stahle and Cleaveland (1994) used annual tree-ring data from scattered old-growth bald cypress stands to suggest the BH strongly affected Southeast rainfall at decadal time scales; however, their record only covered the past ~1000 years and is (by nature) ill-suited for detecting century-long variability. Changes in pollen assemblages have been used as proxy for climate-induced changes in vegetation type and density and is a viable tool for the Southeast given the number of depositional basins and plethora of vegetation. Studies by Delcourt (1980), Watts (1980), and Delcourt (1983) have provided >10 ka (kilo-annum) records of vegetation

characteristics for the Southeast. Although useful for understanding long-term changes in vegetation to new climate conditions, time lags between rainfall variation and vegetation response limit the insights to past atmospheric circulation patterns.

This dissertation utilizes speleothems (i.e., stalagmites) from DeSoto Caverns (Fig. 1.1; Childersburg, AL) to provide the highest resolution record produced to date for past rainfall variability for a Southeast study site. In part due to advances in radiometric dating techniques, speleothem-based studies have moved to the forefront of climate reconstructions from continental settings (Fairchild et al., 2006). These secondary cave deposits are often reliable climate archives because they: (i) preserve multiple proxies for climatic conditions outside the cave, (ii) have the potential to provide long and continuous high-resolution records, and (iii) can be accurately dated by more than one independent analytical method (McDermott, 2004; Fairchild et al., 2006: Baker et al., 2008; Lachniet, 2009). Despite the extensive karst systems in the Southeast, high-resolution paleoclimate reconstructions based on speleothem proxy data do not exist.

DeSoto Caverns was chosen for this research due to its central location within the Southeast, proximity to the Gulf Coast, historical significance, and numerous active and fossil speleothems. The cave intercepts moisture as it moves from the GOM inland across the Southeast and variations in moisture flux would be experienced by the karst aquifer above the cave. With regard to proxies archived in DeSoto speleothems, I investigate the variations in carbon ($\delta^{13}C$) and oxygen ($\delta^{18}O$) isotopes of modern and past cave deposition (as $CaCO_3$). Carbon isotopes, although complex, have been used as a proxy for changes in biological productivity (vegetation) directly above the cave. Oxygen isotopes, which have been used extensively from speleothems in the international paleoclimate community, tend to mimic changes in isotopic composition of

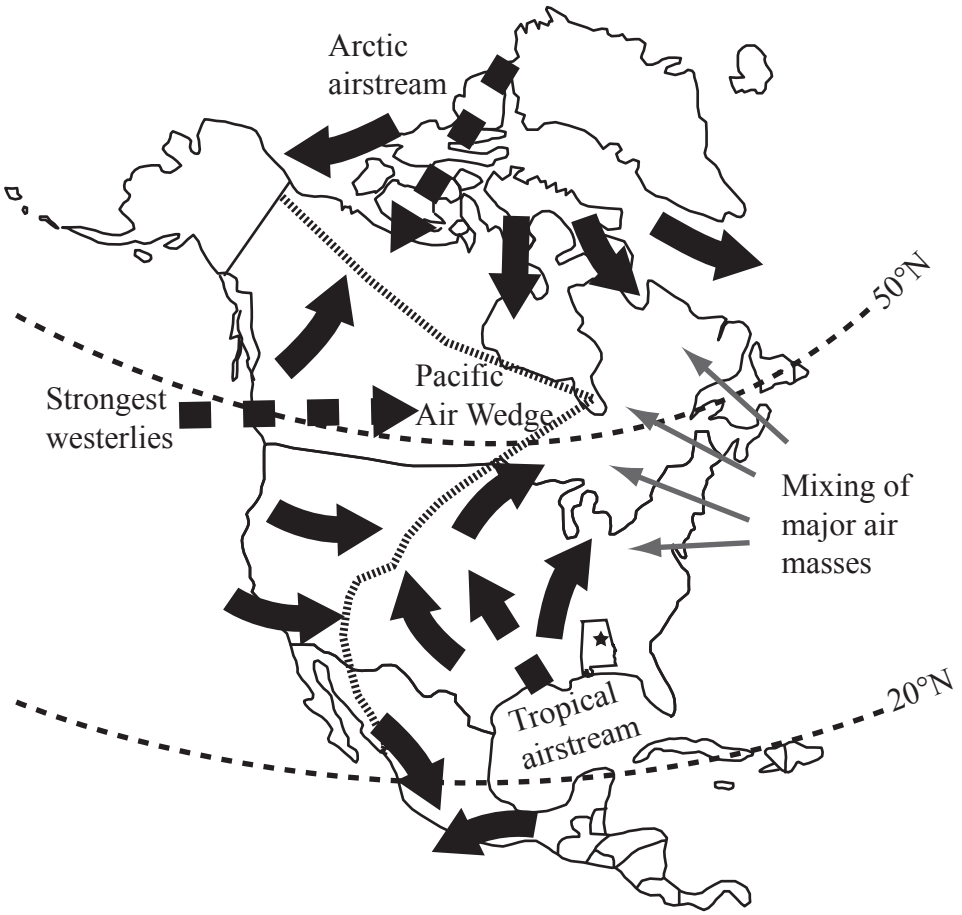


Fig. 1.1. Map of North America showing present-day geographic distribution of air masses and location of DeSoto Caverns (star). Map modified after Simpkins (1995) and Bryson and Hare (1974).

rainfall and can be used to infer changes in moisture source and/or rainfall amounts (Neff et al., 2001; Bar-Matthews et al., 2003; Cruz, et al., 2005; Baker et al., 2007).

The main objective of this dissertation research was to reconstruct past climate conditions (rainfall variability) for north central Alabama by means of proxy records and to compare these findings with past global climate events. A high-resolution record of how rainfall amounts varied under states of general global warming and cooling will allow better estimates of the region's response associated with future climate change. Although speleothems offer many advantages compared to other climate archives, each cave system is unique and the controls on the proxies of interest, as well as the degree of climate signal preservation within the speleothem, must be determined to ensure proper paleoclimate interpretation (Fig. 1.2). For example, depending on the extent of mixing in the aquifer above the cave and the atmospheric conditions within the cave, stalagmites may record: (i) both seasonal and interannual trends in external climate conditions (i.e., rainfall amount; Fig. 1.2a), (ii) only interannual (or greater) trends (Fig. 1.2b), or (iii) no meaningful signal whatsoever (Fig 1.2c). To determine the usefulness of isotope proxies of DeSoto stalagmites, additional objectives included monitoring $\delta^{18}O$ and $\delta^{13}C$ of the cave waters and addressing their present-day controls.

The body of the dissertation is divided into three additional chapters. The following chapter compares the isotopic composition and variability of cave waters relative to that of rainfall collected at the University of Alabama (Tuscaloosa, AL). The isotopic composition of local rainfall was determined because there are no monitoring stations near DeSoto Caverns that report current water isotope data. The nearest sites are in Waco, TX and Hatteras, NC, neither of which are currently in operation and do not characterize rainfall sourced from the GOM. The chapter describes the acquisition, results, and interpretation of water isotopes of the rainfall collected at

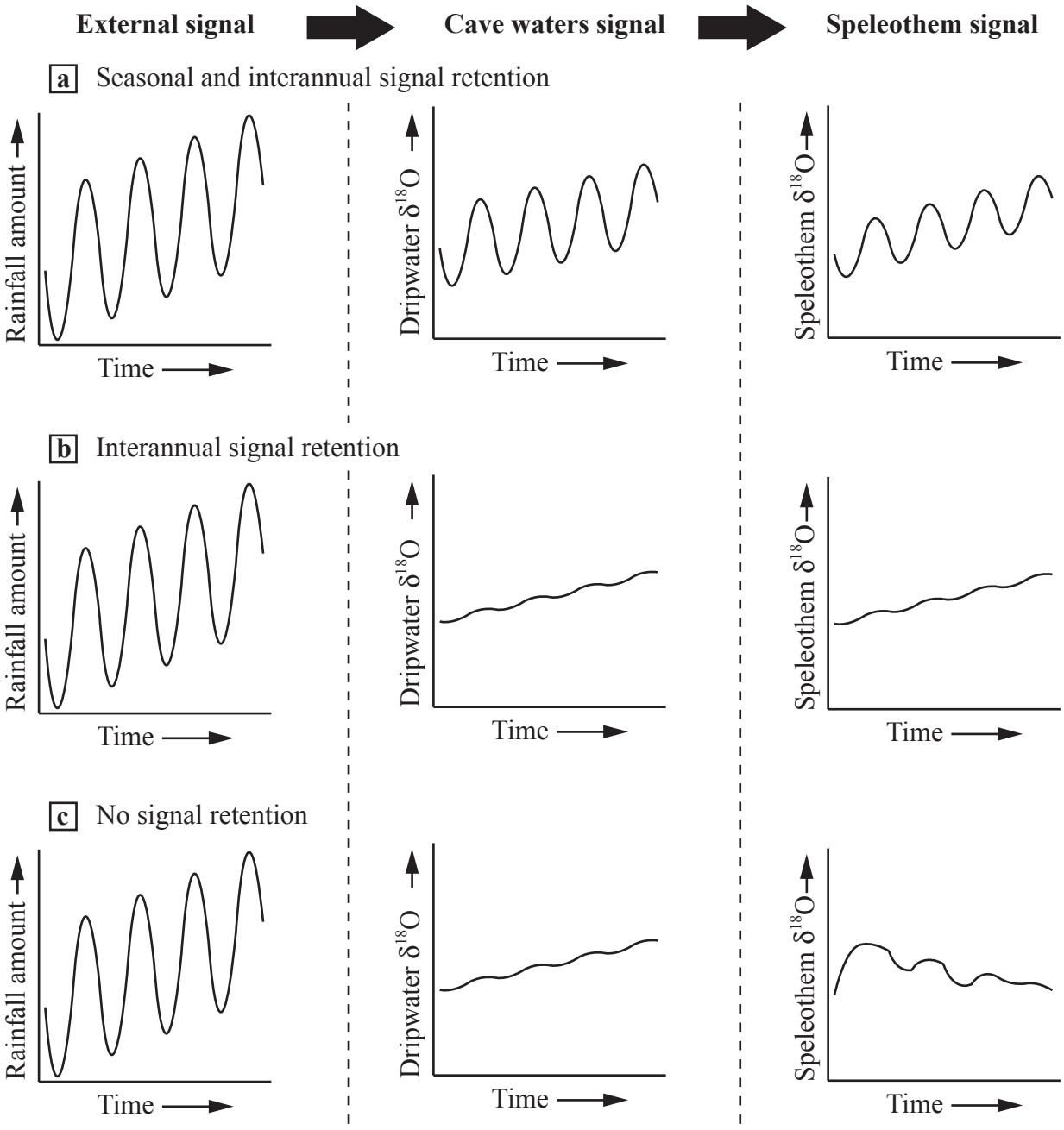


Fig. 1.2. Examples of possible relationships between external climate variables (rainfall amount shown here) and the signals experienced by the cave's aquifer as well as those preserved within speleothems. (a) Both seasonal variation and interannual trends recognized in cave waters and speleothem deposition. (b) The aquifer above the cave quickly homogenizes infiltrating water and results in only interannual signal retention. (c) Conditions (i.e., evaporation) within cave chamber prevent proxy records from properly preserving changes in dripwater.

weekly resolution over a 3-year period (2005-2008). Simultaneously, infiltrating waters were collected from the cave at 2-month intervals to determine the transmission of the rainfall isotope signal to the precipitating stalagmites. From this work the aim is to better understand the meaning of $\delta^{18}O$ variation through time preserved in DeSoto stalagmites.

The next chapter discusses the carbon isotope system. The $\delta^{13}C$ signals found in speleothems are much more difficult to interpret than $\delta^{18}O$ because of the multiple factors that can alter the final $^{13}C/^{12}C$ ratio of the stalagmite (McDermott, 2004). Within the chapter, carbon sources are identified and the expected isotopic composition of cave waters is modeled by applying published relationships between carbon species in aqueous solutions. To compare the observed chemistry of cave waters to the predicted values, the amount of carbon in solution (as bicarbonate) as well as its isotopic composition was measured from the same aliquots of cave waters collected in the $\delta^{18}O$ study. The variability and relationship between the two parameters are used to constrain their controls and to assess the meaning of observed speleothem $\delta^{13}C$ variability, both present and past.

Finally, the last chapter deals with the past record of climate conditions inferred from the $\delta^{13}C$ and $\delta^{18}O$ measured from a large stalagmite and the interpretations are primarily based on the findings of the previous two chapters. The stalagmite, which has partially inverted from primary aragonite to secondary calcite, is thoroughly examined in terms of mineralogy because of the important implications regarding possible diagenetic effects on the retained chemistry of the $CaCO_3$. Although monitoring the cave in its present state suggests whether or not the precipitating aragonite is in isotopic equilibrium with the cave waters, the chapter addresses carefully planned tests that were performed to determine if past aragonite was also precipitated under conditions promoting isotopic equilibrium. The chapter describes three methods (U-series,

radiocarbon, and band counting) used to construct an age model for the $\delta^{18}O$ and $\delta^{13}C$ profiles produced from this study. The data are compared to other North America paleoclimate records in order to better understand the atmospheric processes controlling rainfall variability for north central Alabama.

The results and interpretations of this dissertation help to fill a significant void in reconstructing the paleoclimate of the Southeast. This work lays the groundwork for future speleothem-based paleoclimate records that may cover time periods not addressed here. Furthermore, rainfall isotope data are now available for research projects whose focus is not limited to paleoclimate endeavors.

CHAPTER 2

# OXYGEN AND HYDROGEN ISOTOPES OF RAINFALL AND DRIPWATER AT DESOTO CAVERNS (ALABAMA, USA): KEY TO UNDERSTANDING PAST VARIABILITY OF MOISTURE TRANSPORT FROM THE GULF OF MEXICO

## ABSTRACT

The Southeast and the US Gulf Coast in particular are notably lacking isotope data in the water cycle despite the fact that moisture transport from the Gulf of Mexico (GOM) has a considerable influence on both regional and continental rainfall patterns. This study reports time-series of oxygen and hydrogen isotopes acquired over a 3-year period (2005-2008) from GOM-derived rainfall, cave dripwater and shallow groundwaters, and offers valuable insights on the links between factors controlling regional rainfall and the ubiquitous karst hydrology.

Amount-weighted mean monthly rainwater $\delta^{18}O$ and $\delta D$ values in Tuscaloosa, Alabama range from -1.5 to -8.3‰ and -1.2 to -49.5‰, respectively, and show mean seasonal amplitudes of ~4‰ ($\delta^{18}O$) and ~25‰ ($\delta D$). In comparison *d-excess* values display large seasonal amplitudes of 10‰ to 20‰ resulting from differences in the degree of evaporation from falling raindrops between summer and winter months, and correlate well with the coeval air temperature ($r^2$ = 0.59). Deviations of the Gulf Coast Meteoric Water Line (GCMWL) slope and *d-excess* from the Global Meteoric Water Line (GMWL) are attributed to different rates of evaporation after

condensation, and to humidity contrast between the cloud boundary layer and the surrounding atmosphere in the vapor source region, respectively. Rainfall amounts declined during the study interval from an excessive "wet" year, ascribed to six tropical storms incursions during an unusually active hurricane season in 2005, to an onset of a regional drought during 2007-2008 with monthly rainfall amounts substantially below normal values (30-year monthly means). An interannual trend of $^{18}O$ and $^{2}H$ enrichment is discerned from 2005 to 2008 (1.4‰ and 11.6‰, respectively) coeval with the decline in rainfall amounts.

Dripwater samples from nearby DeSoto Caverns show weak $\delta^{18}O$ and $\delta D$ seasonal variations and record only 20% and 51% of the $^{18}O$ and $^{2}H$ enrichments, respectively, discerned in the rainwater 3-year time-trends. The seasonal and interannual amplitude attenuations in the dripwaters are attributed to a relatively thick overlying bedrock (~30-40 m) and a relatively large, well-mixed, epikarst-storage reservoir. Residence time of water in the cave's epikarst is estimated to be 1-3 months based on high-resolution flow-rate data.

This investigation suggests that global atmospheric circulation patterns (ENSO and Bermuda High) likely govern the interannual $\delta^{18}O$ and $\delta D$ isotope trends discerned in the water cycle compartments but much longer time-series are required to confirm my conjectures. The results of this study form a solid basis for future acquisition and interpretation of climate proxy records from regional speleothems.

# 1. INTRODUCTION

Numerous investigations established that stable isotope composition of speleothems provide useful proxy records of continental climate change (e.g., recent reviews by McDermott, 2004; Fairchild et al., 2006; Lachniet, 2009). The most robust and commonly used climate proxy in carbonate speleothems is $\delta^{18}O$ that follows local rainwater $\delta^{18}O$ variability at the site assuming that: (i) cave dripwater $\delta^{18}O$ values covary with local rainwater $\delta^{18}O$ variability, (ii) cave air temperature is invariable through time, and (iii) isotope quasi-equilibrium is attained between the cave dripwater and the precipitated carbonate (Hendy, 1971). Stalagmite oxygen isotope records from tropical to subtropical sites largely reflect rainfall amounts (e.g., Neff et al., 2001; Bar-Matthews et al., 2003; Baker et al., 2007) whereas air temperature is the dominant controlling factor at high latitudes (Lachniet, 2009). Other controlling factors invoked to explain oxygen isotope shifts in stalagmites include changes in the moisture source (Cruz et al., 2005), variations in monsoon intensity (Wang et al., 2001), and hurricane landfalls (Frappier et al., 2007). A simple isotope-based rainwater-dripwater relationship, however, is rarely attained because of cave-specific complicating factors such as the degree of signal attenuation from surface to cave drips affected by the thickness of the overlying bedrock that control aquifer residence times (Bar-Matthews et al., 1996; Ayalon et al., 1998; McDermott, 2004; Fairchild et al., 2006; Lachniet, 2009). Modern-day monitoring studies investigating the link between high-resolution (measurements) of rainwater and contemporaneous cave dripwater isotope time-series over several seasons can offer an important guide to stalagmite paleoclimate proxy records from a

particular cave site (Bar-Matthews et al., 1996; Ayalon et al., 1998; Spötl et al., 2005; Mattey et al., 2008; Lachniet, 2009).

The Southeast USA in general, and the Gulf Coast in particular, are notably lacking in high-resolution continental climate records such as those from speleothems. This deficiency is striking considering that moisture transport from the Gulf of Mexico has a considerable influence on North American rainfall patterns (Rasmusson, 1968; Bryson and Hare, 1974; Simpkins, 1995), and this dominant role likely extended through the past glacial/interglacial cycles (Oglesby et al., 1989; Maasch and Oglesby, 1990).

This study investigates the relationship between stable oxygen and hydrogen isotopes in rainwater at Tuscaloosa, AL and cave dripwater in nearby DeSoto Caverns (Fig. 2.1). The rainwater study examines the: (i) seasonal and interannual variability in isotope time-series and the link to the dominant moisture source region (Gulf of Mexico) and (ii) relationship of the isotope compositions to rainfall amount, surface air temperature, and evaporation. Multi-year monitoring of oxygen and hydrogen isotopes of cave dripwater sites provides insight into: (i) spatial and temporal dripwater variability, (ii) relationship between drip rates, major rainfall events, monthly precipitation amounts, and estimated monthly water budget (rainfall minus evapotranspiration), and (iii) residence time of the water in the vadose zone above the cave. The data and interpretations reported here will likely lead to a better understanding of the proxy climate records preserved in regional speleothems.

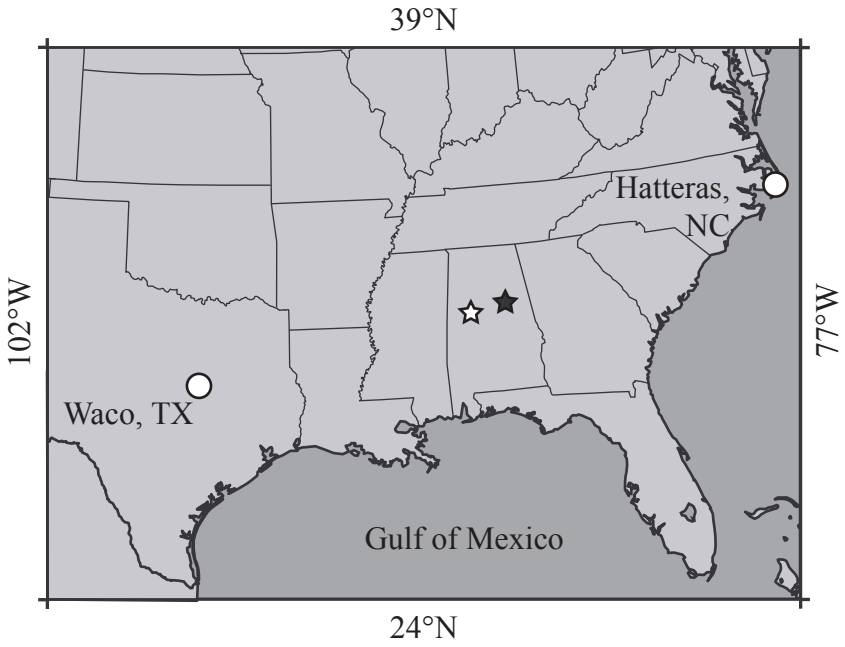


Fig. 2.1. Tuscaloosa (open star) and DeSoto Caverns (solid star) in relation to IAEA rainfall-isotopes monitoring stations (open circles).

# 2. **STUDY SITES**

## 2.1. DeSoto Caverns

DeSoto Caverns (Childersburg, AL; 33°18’26” N, 86°16’36” W) occur within an Upper Ordovician-age dolomite karst system. The cave is ornately decorated with massive stalagmites and stalactites, and has an unusually rich human history (Downs, 2005). Native Americans used the cave as a burial ground at least 2000 years ago; they were living in the area in 1540 A.D. when the Hernando de Soto Spanish expedition spent 5 weeks at the then Coosa Indian capital. In 1796 it became the first officially recorded cave when field scout Benjamin Hawkins reported his findings of the majestic cave to President George Washington. Additionally, “saltpeter” was extensively mined from DeSoto Caverns during the Civil War to supply the Confederate Army with a crucial gunpowder ingredient.

The cave is roughly 150 m in length and has two continuous sections: (i) a large chamber (70 m long, 50 m wide, 36 m high) with approximately 10 m of overlying bedrock, and (ii) smaller chambers in the back of the cave with substantially thicker (30 – 40 m) bedrock (Fig. 2.2). Deciduous hardwood forest grows above the cave in soil that is thin and poorly developed. Both active and fossil speleothems in DeSoto Caverns are composed predominantly of aragonite. The current study of cave dripwater was carried out in the distal portion of the cave, ~120 m from the cave entrance where the atmosphere is believed to be stable and is proximal to stalagmites currently under study (Fig. 2.2).

Because of logistic constraints, rainwater was collected on the University of Alabama campus (33°13’2” N, 86°32’35” W) in Tuscaloosa at 65 m above mean sea level. DeSoto

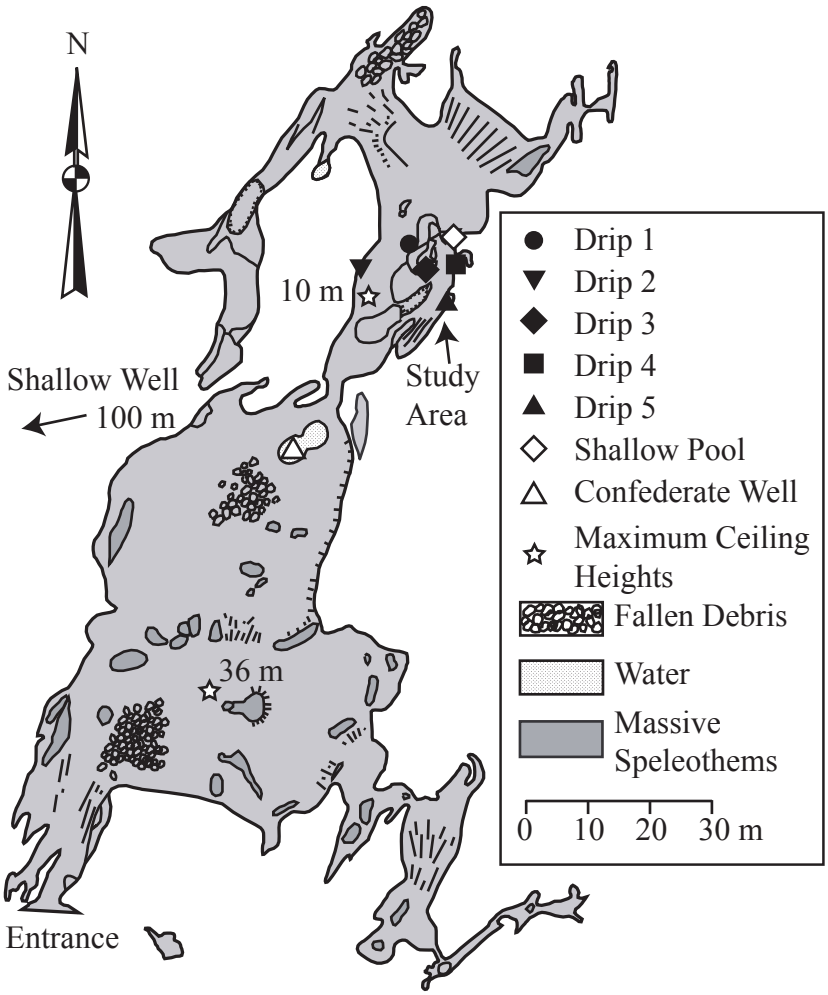


Fig. 2.2. Map (plan view) of DeSoto Caverns with water sampling locations (modified from an unpublished map by Michael T. Laing and Allen W. Mathis III, 1976).

Caverns is located about 120 km east of Tuscaloosa at 170 m in elevation at the cave entrance. Both sites are separated from the Gulf of Mexico by approximately 325 km of low elevation coastal plains.

## 2.2. Regional Climate

Long-term rainfall and air temperature records (1958-2004) indicate that Tuscaloosa and Childersburg are subject to the same climate variability regime (Fig. 2.3). The two sites experience moderate seasonality with average monthly air temperatures ranging from ~7 °C (January) to ~27 °C (July) while mean monthly rainfall ranges from ~80 mm (October) to ~150 mm (March). Mean annual air temperatures are 17.2 °C and 17.6 °C for Childersburg and Tuscaloosa, respectively, while average annual rainfall totals are 1417 mm and 1396 mm based on 1958 to 2004 data (www.ncdc.noaa.gov). The study sites intercept north-tracking moisture from tropical maritime air masses that originate over the Gulf of Mexico with no orographic interference.

In general, convection style thunderstorms deliver rainfall during the summer months while fall, winter, and spring rainfall often is associated with frontal systems that are driven west to east by the polar jet stream. Tropical systems (i.e., hurricanes, tropical storms, tropical depressions) add 40-60 mm of rainfall to north central Alabama each hurricane season (June-November; Knight and Davis, 2007). It must be noted, however, that delivery of rainfall by tropical systems is stochastic in nature with large interannual variability.

Extended periods of droughts and wet spells in the Southeast USA, including central Alabama, have been linked to changes in global atmospheric circulation patterns, processes that

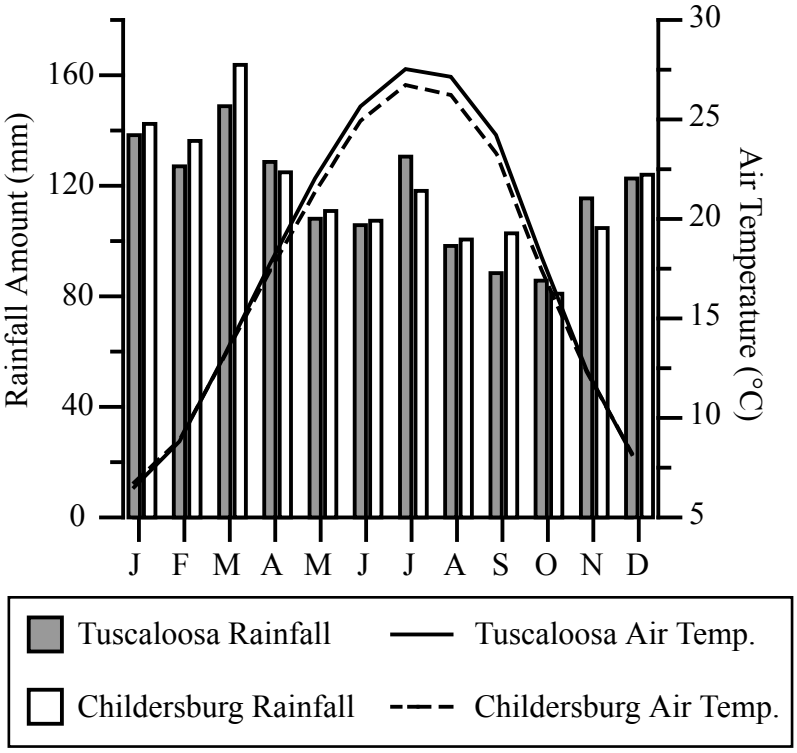


Fig. 2.3. Climographs of study sites for the period 1958-2004 (www.ncdc.noaa.gov).

have recently been addressed in a number of studies (e.g., Katz et al., 2003; Mo and Schemm, 2008, Portmann et al., 2009). The El Niño-Southern Oscillation (ENSO) and the position of the Bermuda High (BH) have been suggested as potential drivers of moisture flux (i.e., droughts and wet spells) for the Southeast for winter/early spring and summer/early fall months, respectively.

The influence of ENSO on southeastern USA weather has been explored in a number of studies (e.g., Ropelewski and Halpert, 1986; Kiladis and Diaz, 1989; Mo and Schemm, 2008). According to these studies and a review by Cane (2005), winter/early spring months in the Southeast tend to experience above average rainfall during an El Niño due to repositioning of the jet stream over this region (Fig. 2.4a). In contrast, strong La Niña phases tend to shift the storm tracks to a more northerly position in winter/early spring resulting in dryer than normal conditions for the Southeast (Fig. 2.4b).

The Bermuda High is a high-pressure system located over the northeast Atlantic Ocean during winter that drifts to the southwest and strengthens during summer (Katz et al., 2003). Consequently summer/early fall rainfall extremes in the Southeast are affected by the east-west position of the BH (Stahle and Cleaveland, 1992; Henderson and Vega, 1996). In general, the western edge of the BH is associated with strong landward funneling of moist tropical air from the Gulf of Mexico due to the clockwise flow of air around the high-pressure cell. Westward movement of the BH from its normal location allows for a steady supply of moisture fuelling convection style thunderstorms over central Alabama (Fig. 2.4c). Moreover, the BH position can enhance summer/early fall rainfall as tropical systems are blocked from the Atlantic Coast and steered into the Gulf of Mexico permitting frequent landfalls along the Gulf Coast. However, extended westward expansion of the BH shifts rainfall southwest and leaves the Southeast dry (Fig. 2.4d).

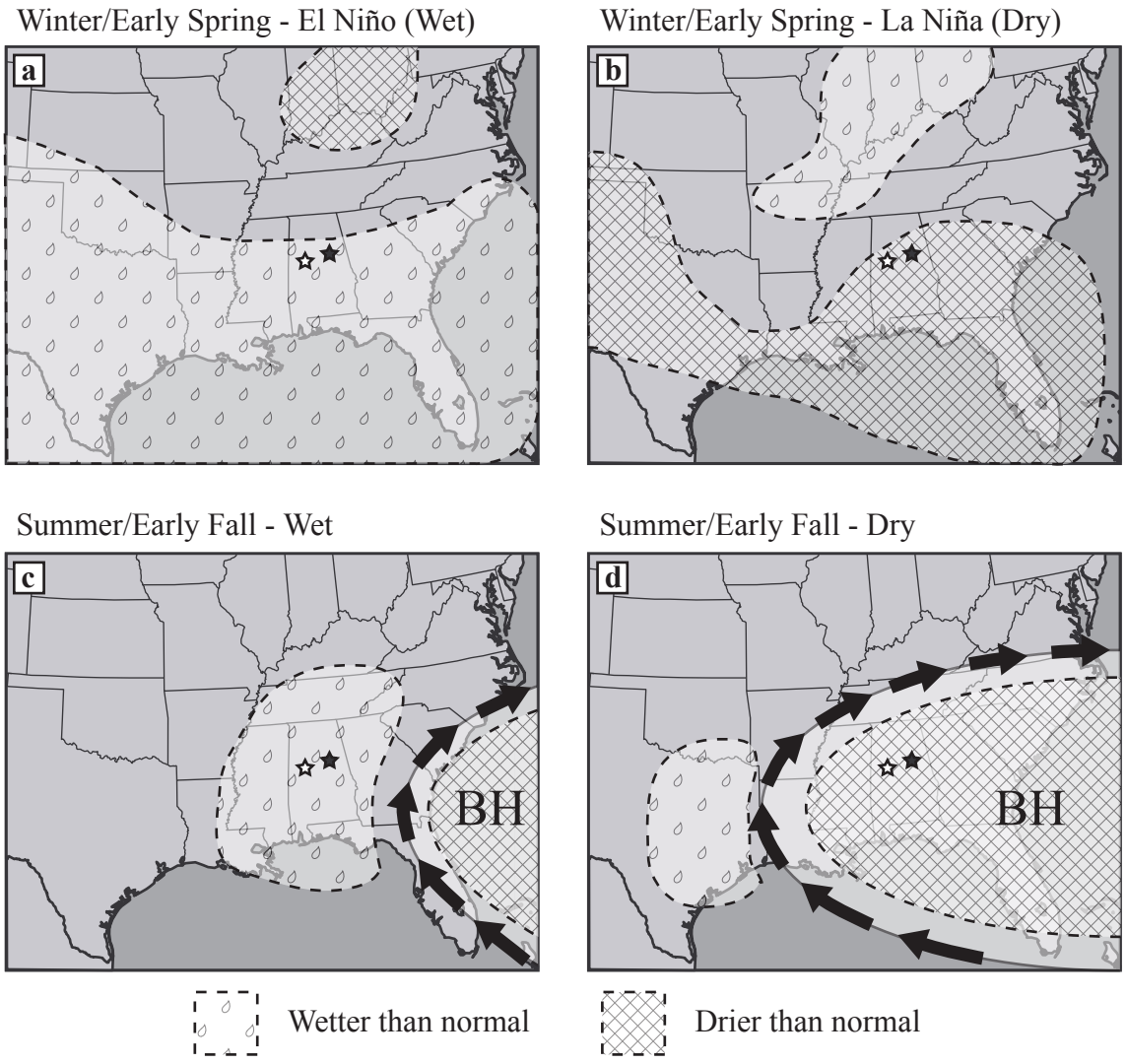


Fig. 2.4. Climate factors affecting the interannual rainfall variability in the study area. (a) Winter/early spring rainfall patterns (wet) across the Southeast during an El Niño event. (b) Same as (a) but for a La Niña event (dry). (c) Schematic illustration of the position of the Bermuda High in summer/early fall resulting in above normal rainfall in Alabama. (d) Schematic illustration of the position of the Bermuda High in summer/early fall resulting in below normal rainfall in Alabama (drought).

# 3. MATERIALS AND METHODS

## 3.1. Field Methods

The two IAEA stations in the Southeast that have monitored oxygen and hydrogen isotopes in rainwater are at Waco, TX and Hatteras in North Carolina (Fig. 2.1), both of which ceased sampling in 1976. Neither station is representative of Alabama rainfall; therefore, it was necessary to establish my own rainwater sampling station. Weekly-integrated rainwater was collected continuously over the period June 2005 to May 2008 using a standard 100-mm wide rain-gauge with 0.2 mm measurement increments. The gauge was checked each morning with collected water stored in clean Nalgene® bottles while the amount of rainfall was recorded. All rainwater falling during a single week (Monday to Sunday) was well-mixed and stored in the same bottle (smallest bottle used to limit headspace), and once analyzed it represented a weekly average for oxygen and hydrogen isotope data (see Appendix 2.1). To avoid post-sampling evaporation the bottle lids were tightened and wrapped with tape before storing in a dark cabinet at a cool and stable room temperature. Reported monthly averages for $\delta^{18}O$ and $\delta D$ are amount-weighted means with a range of 1 to 5 weeks incorporated depending on the number of weeks (n) on which rainfall occurred. Weekly variation in isotopic compositions contributing to the monthly weighted means is expressed as the standard error of the mean ($\sigma_m$) defined by:

$$\sigma_m = \sigma_{sd}/(n)^{1/2} \quad (1)$$

where, $\sigma_{sd}$ is the 1-sigma standard deviation and n is the number of weeks for which the isotopic composition was determined. Monthly mean surface air temperatures for Tuscaloosa were retrieved from a climatological station located within 6 km of this study's rain gauge (www.ncdc.noaa.gov).

Cave dripwaters at DeSoto Caverns were sampled at approximately 2-month intervals starting in March 2005 and ending in March 2008 (total of 19 collections). Drips 1 and 4 were sampled from the tips of two large stalactites, drips 2 and 3 from the tips of soda straws, and drip 5 from water flowing over a cave drapery (Fig. 2.2). Dripwater collection sites targeted drips thought to be continuous as they drained the 30-40 m thick overlying bedrock, as opposed to ephemeral drips from large fractures in portions of the cave with only 10 m of bedrock cover. Clean plastic bags were attached to the drip sources and left in place for at least 4 h in order to accumulate sufficient fluid for O and H determinations. Each water sample was then transferred into the appropriate size (15-, 50-, 125-ml) airtight glass bottle and filled completely to avoid headspace.

Drip flow rates were estimated by recording fluid volume accumulating over a fixed time span and the results are reported in μl/s. Supplementary dripwater flow-rate data were obtained using an automated drip rate data logger (MFR; www.driptych.com) placed under drip 4 from September 2006 to November 2008. The data logger records events per time interval based on drops of water impacting the acoustically-sensitive lid of the device as described by Collister and Mattey (2008). The device is capable of storing thousands of events allowing continuous monitoring of changes in drip rate through time. The logger recorded the number of drips occurring over 2-h intervals and the data were downloaded from the logger during each visit to the cave.

Water samples were also collected from a shallow pool, a deep pool (informally named the Confederate Well, and likely representing the top of the local water table), and a shallow (35 m) groundwater well located within 100 m of the cave entrance (Fig. 2.2). These waters were collected from March 2005 to March 2008, March 2006 to March 2008, and May 2006 to March 2008, respectively. Methods similar to collection and storage of dripwater samples were used throughout. Cave air temperature and relative humidity were monitored between March 13, 2006 to February 1, 2007 and March 10, 2008 to September 18, 2008 using Temp/RH data loggers. Precipitation amount and air temperature were obtained from a climatological station located within 7 km of DeSoto Caverns (www.ncdc.noaa.gov).

Monthly rates of potential evapotranspiration were calculated using methods suggested by Samani (2000), which estimates evapotranspiration using limited available climatic information, as was the case for this study. The simplified equation incorporates measured air temperature and solar radiation based on latitude, variables that account for 80% of evapotranspiration (Samani, 2000). Monthly water budget totals were calculated by subtracting estimated evapotranspiration amounts from rainfall amounts measured at the Childersburg climatological station.

### 3.2. Laboratory Methods

O and H isotope analyses of rainwater and cave dripwaters were performed using a modified Delta-plus CF-IRMS. Isotope ratios are reported in the conventional delta (δ) notation in per mil (‰). $^{18}O/^{16}O$ ratios were initially determined on $CO_2$ gas using the conventional $CO_2$-$H_2O$ equilibration method of Epstein and Mayeda (1953), and subsequently by $CO_2$-$H_2O$ equilibration using an automated GasBench II continuous flow system. The compatibility of the two methods

was tested using an internal water standard that yielded identical values within the analytical error (-9.4 ± 0.1‰ for n = 28, and -9.5 ± 0.1‰ for n = 31), respectively. An offline extraction system was used to derive $H_2$ gas from the water samples using the Zn reduction method modified after Kendall and Coplen (1985).

$\delta^{18}O$ and $\delta D$ values were normalized following methods of Coplen (1988) and are reported relative to the Vienna Standard Mean Ocean Water (VSMOW). The standard deviation of my measurements is ± 0.1 ‰ (1σ) for oxygen and ± 1.0 ‰ (1σ) for hydrogen based on sample repeats as well as internal and international standards.

## 4. RESULTS

### 4.1. Oxygen and Hydrogen Isotope Time-series in Rainfall

Weekly-integrated rainwater isotope data were acquired for 36 months over the period 2005-2008. During the first year of study monthly rainfall amounts ranged from a high of 228 mm in August 2005 to a low of 8.0 mm in October 2005 (Table 2.1). Six tropical systems (Arlene, Cindy, Dennis, Katrina, Rita, Tammy) and their associated rainfall reached this study's rain gauge during the unusually active hurricane season of 2005. These storms increased rainfall amounts for consecutive months (June, July, and August) to substantial excesses of up to 130 mm above the 30-year monthly mean (Fig. 2.5). In contrast, no tropical systems crossed central Alabama during 2006 and 2007 monitoring years. Rainfall amounts were near average during 2006 before drought conditions in the Southeast set in about January 2007. The region continued

Table 2.1. Summary of precipitation collection dates, rainfall amounts, weighted mean $\delta^{18}O$, weighted mean $\delta D$, and calculated weighted mean *d-excess* with corresponding 1$\sigma$ standard error of means and number of weeks (*n*) with rainfall each month. Summer, winter, and 3-year mean values are weighted means with 1$\sigma$ standard deviation and number of months (*n*) used for the calculations.

| Month | Rainfall (mm) | $\delta^{18}O$ (‰ VSMOW) | $\delta D$ (‰ VSMOW) | *d-excess* (‰) | *n* |
|---|---|---|---|---|---|
| J 2005 | 145.9 | -6.0±0.9 | -38.9±3.5 | 9.0±3.7 | 2 |
| J | 226.2 | -6.9±2.5 | -48.2±20.6 | 6.6±1.1 | 3 |
| A | 227.9 | -4.9±1.0 | -27.5±7.9 | 11.3±1.6 | 5 |
| S | 75.2 | -4.4±1.5 | -24.2±10.2 | 10.7±1.6 | 2 |
| O | 8.0 | -4.6±0.5 | -22.1±10.8 | 14.7±7.3 | 2 |
| N | 55.1 | -8.3±3.3 | -49.5±24.5 | 16.6±2.0 | 3 |
| D | 99.7 | -7.8±1.0 | -42.0±7.6 | 20.6±1.5 | 5 |
| J 2006 | 155.6 | -5.8±0.1 | -24.2±0.9 | 21.9±0.9 | 3 |
| F | 166.0 | -5.9±1.1 | -30.1±9.6 | 17.2±5.1 | 4 |
| M | 123.3 | -2.9±0.5 | -6.8±3.7 | 16.8±2.0 | 5 |
| A | 69.4 | -3.1±0.6 | -8.9±5.6 | 15.9±1.5 | 3 |
| M | 114.6 | -3.4±0.7 | -15.0±7.0 | 12.4±7.0 | 2 |
| J | 31.4 | -1.6±0.6 | -1.2±4.7 | 11.3±1.7 | 4 |
| J | 88.6 | -2.5±1.2 | -12.9±8.7 | 7.3±2.1 | 4 |
| A | 38.5 | -2.1±0.8 | -7.0±4.5 | 9.9±2.4 | 2 |
| S | 125.3 | -4.2±0.5 | -24.2±5.7 | 9.4±1.5 | 3 |
| O | 186.4 | -5.0±0.6 | -27.1±5.1 | 12.7±0.2 | 2 |
| N | 112.0 | -4.6±1.0 | -18.8±7.9 | 17.8±1.9 | 4 |
| D | 132.7 | -4.6±0.7 | -26.5±7.9 | 10.5±3.0 | 3 |
| J 2007 | 86.2 | -5.1±1.3 | -26.1±9.5 | 15.0±1.7 | 4 |
| F | 51.4 | -3.5±0.9 | -14.6±8.5 | 13.8±2.1 | 3 |
| M | 22.0 | -1.5±0.0 | -2.2±1.4 | 9.7±1.1 | 2 |
| A | 64.2 | -2.5±0.4 | -6.7±2.3 | 13.3±1.5 | 4 |
| M | 12.0 | -2.7±0.0 | -9.2±0.0 | 12.6±0.0 | 1 |
| J | 29.2 | -3.8±1.5 | -22.1±11.6 | 8.2±2.3 | 4 |
| J | 93.9 | -4.5±1.0 | -26.1±7.4 | 9.7±0.8 | 4 |
| A | 204.4 | -2.9±1.3 | -15.7±8.1 | 7.7±2.1 | 3 |
| S | 52.7 | -5.6±0.5 | -30.2±3.6 | 14.4±0.4 | 2 |
| O | 57.8 | -5.2±0.5 | -31.9±3.1 | 9.6±1.1 | 4 |
| N | 58.2 | -5.4±0.7 | -27.0±8.8 | 16.2±2.8 | 2 |
| D | 67.2 | -4.9±1.1 | -21.8±8.3 | 17.3±1.8 | 5 |
| J 2008 | 127.6 | -5.1±2.1 | -22.5±18.5 | 18.4±2.2 | 4 |
| F | 128.7 | -5.0±0.9 | -24.8±8.8 | 15.1±1.8 | 3 |
| M | 112.4 | -3.6±1.2 | -15.5±8.4 | 13.5±2.6 | 3 |
| A | 123.8 | -4.4±0.8 | -18.9±5.7 | 16.7±1.2 | 4 |
| M | 139.7 | -3.6±0.7 | -16.9±5.0 | 11.7±1.0 | 4 |
| Range (weekly data) | | 1.9 to -12.5 | 17.8 to -88.4 | 1.0 to 28.8 | 117 |
| Range (monthly data) | | -1.5 to -8.3 | -1.2 to -49.5 | 6.6 to 21.9 | 36 |
| Summer (Apr. to Oct.) | | -4.4±1.4 | -24.4±11.4 | 10.6±2.8 | 21 |
| Winter (Nov. to Mar.) | | -5.1±1.7 | -24.1±11.9 | 16.6±3.3 | 15 |
| 3-year mean | | -4.7±1.6 | -24.3±11.6 | 13.1±3.8 | 36 |

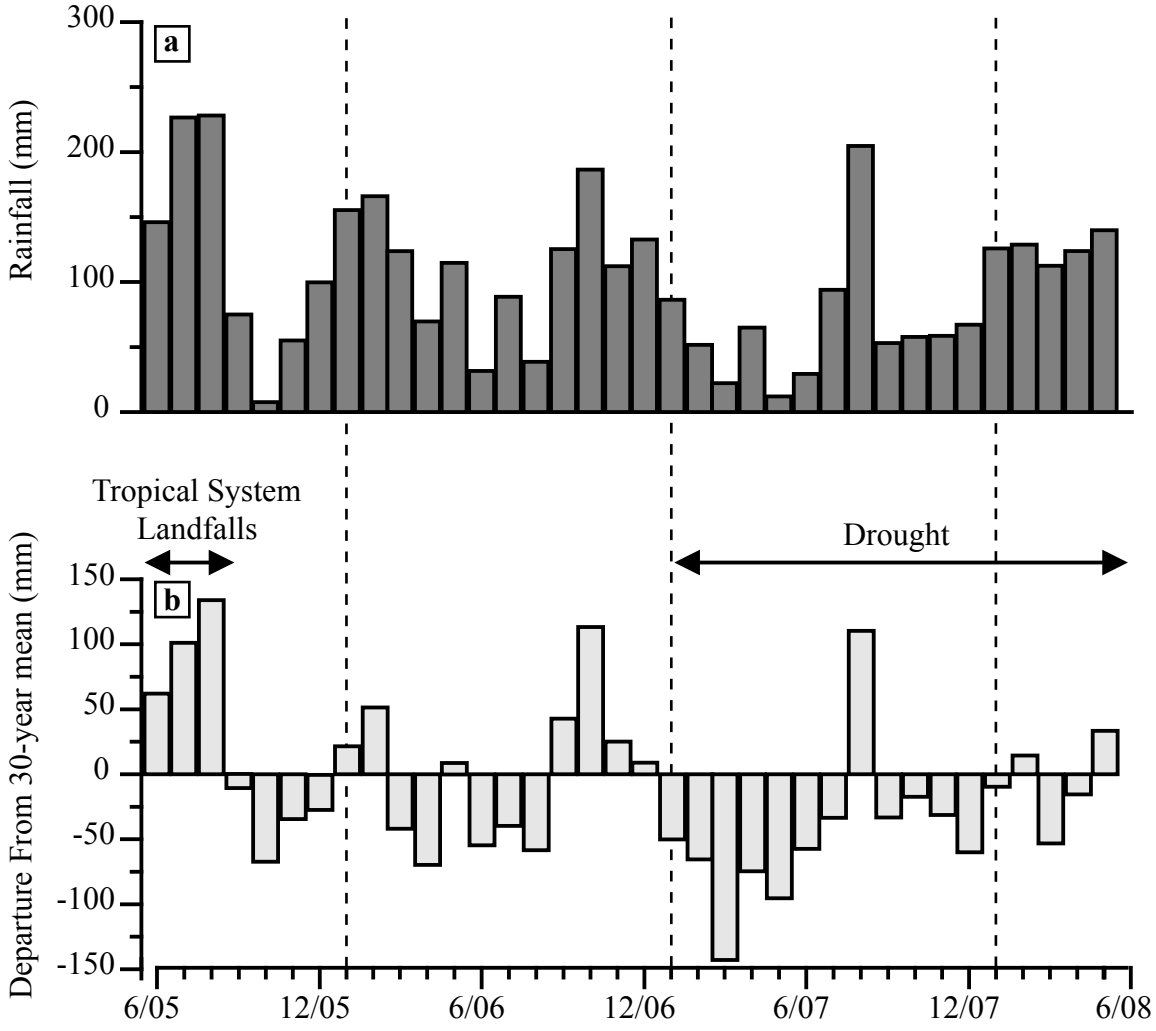


Fig. 2.5. Time-series of monthly rainfall amount from June 2005 to May 2008. (a) Rainfall data from the rain gauge station at the University of Alabama. (b) Monthly rainfall amount departure from 30-year (1950-1980) monthly mean values (www.ncdc.noaa.gov).

to linger under drought conditions during the remainder of the study with monthly rainfall deficits as low as 140 mm below the 30-year monthly mean (Fig. 2.5).

Air temperature in Tuscaloosa ranges from minima of 5-10 °C in winter to maxima of 30-32 °C in summer (Fig. 2.6a). There is no relationship ($r^2 = 0.01$) between monthly rainfall amounts and air temperature; however, there is significant interannual variability in the former and a trend toward reduced rainfall amounts from 2005 to 2008 (Fig. 2.6b). Weekly $\delta^{18}O$ and $\delta D$ values (n = 117) range from 1.9 to -12.5‰ and 17.8 to -88.4‰, respectively (Appendix 2.1) whereas weighted monthly mean values (n = 36) range from -1.5 to -8.3‰ ($\delta^{18}O$) and -1.2 to -49.5‰ ($\delta D$) (Table 2.1). The weighted annual (3-year) mean $\delta^{18}O$ and $\delta D$ values for all rainwater samples are -4.7‰ and -24.3‰, respectively. Winter rainwater (November to March) is more $^{18}O$-depleted (-5.1‰) relative to summer (April to October) rainwater (-4.4‰) but $\delta D$ values for winter (-24.1‰) and summer (-24.4‰) months are statistically indistinguishable. Rainwater associated with tropical systems has a weighted $\delta^{18}O$ mean value of -7.0‰ (n = 6) that is outside the range ($1\sigma$) of annual rainwater. There is evidence of an interannual trend toward $^{18}O$ and $^{2}H$ enrichments from 2005 to 2008 (Fig. 2.6c and d). Deuterium excess data (*d-excess* = $\delta D - 8\delta^{18}O$; Craig, 1961) exhibit seasonal amplitude changes of 10-20‰ with winter rainwater exhibiting higher *d-excess* values (up to 22‰) than summer (mean = 10‰) (Fig. 2.6e).

Neither the amount effect ($r^2 = 0.11$ for $\delta^{18}O$; $r^2 = 0.14$ for $\delta D$) nor the temperature effect ($r^2 = 0.13$ for $\delta^{18}O$; $r^2 = 0.02$ for $\delta D$) exert a significant control on rainwater monthly $\delta^{18}O$ and $\delta D$ values. The absence of such effects is consistent with other mid-latitude locations as described by Dansgaard (1964) and Rozanski et al. (1993). In contrast, monthly *d-excess* values exhibit strong seasonality and a significant negative correlation with monthly mean surface air temperatures ($r^2 = 0.59$) (Fig. 2.6e). The higher winter *d-excess* values likely result from a

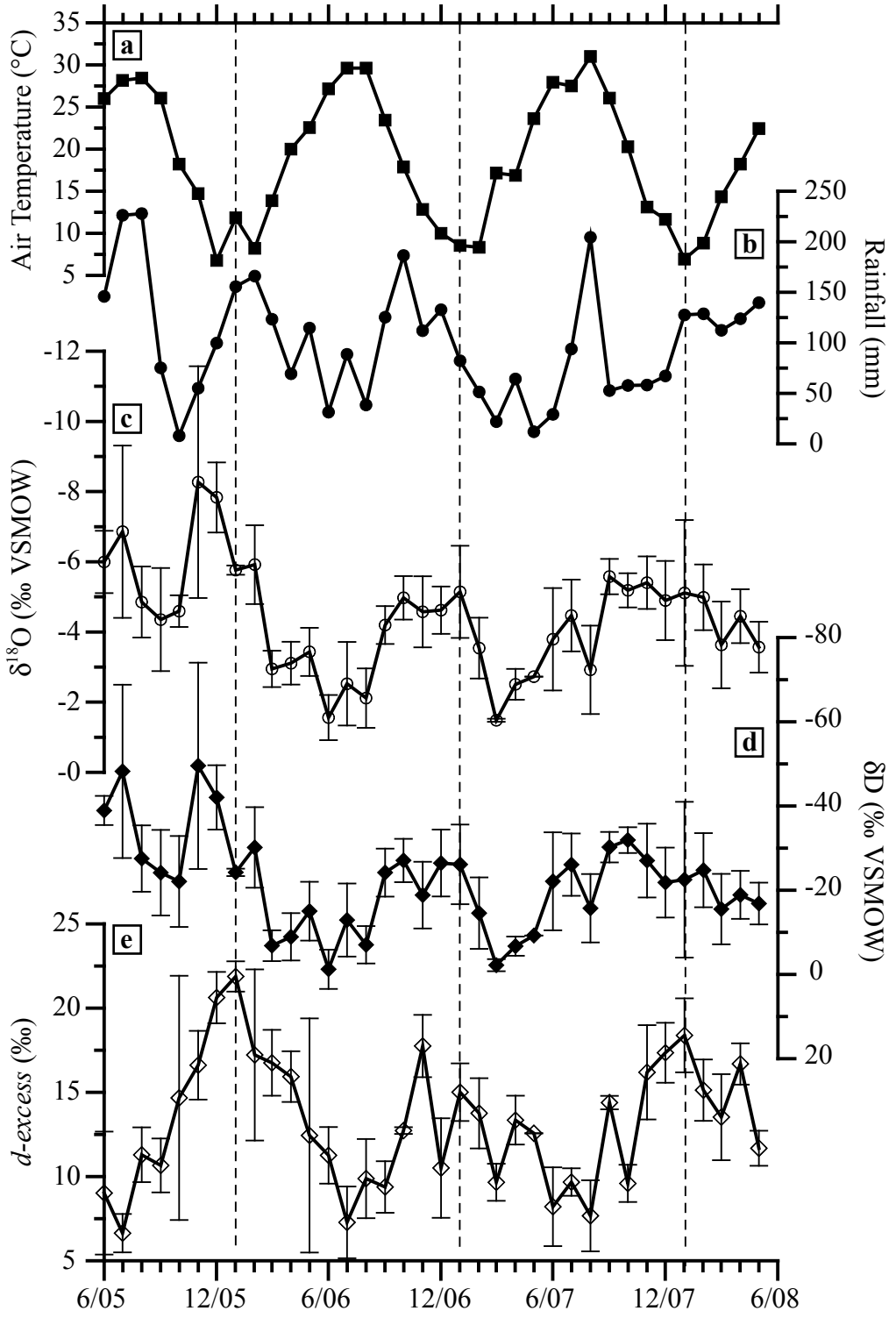


Fig. 2.6. (a) Monthly mean air temperature measured at the Tuscaloosa airport (www.ncdc.noaa.gov). (b) Monthly rainfall totals determined with this study's rain gauge. (c) Weighted monthly mean $\delta^{18}O$ values for rainwater measured in this study; bars are the standard error (1σ). (d) Same as (c) but for δD. (e) Same as (c) but for *d-excess*. Note that the *y*-axis for (c) and (d) is reversed.

reduced degree of evaporation from falling raindrops relative to summer months, a process described by Gat (1996) and observed in other North American IAEA data (Harvey, 2001).

For most natural waters, $\delta^{18}O$ and $\delta D$ values are positively correlated due to the fractionation processes occurring in the atmospheric part of the water cycle. The Rayleigh distillation process exerts the dominant control on this relationship (Craig, 1961; Dansgaard, 1964; Gat, 1980). $\delta^{18}O$ and $\delta D$ data typically plot along the Global Meteoric Water Line (GMWL) defined as $\delta D=8\delta^{18}O+10$ (Craig, 1961) but the slope and *y*-intercept (*d-excess*) values may be site-specific (Rozanski et al., 1993). Meteoric water lines representative of the Gulf Coast region (GCMWL) were derived from the weekly and monthly rainwater data using linear least-square regressions (IAEA, 1992) and are shown relative to the GMWL and meteoric water line for the IAEA station in Waco, TX (Fig. 2.7a and b):

$$\delta D=(7.11\pm 0.19)\delta^{18}O+(9.52\pm 0.88)\ ‰\ (r^2 = 0.92;\ \text{weekly data}) \quad (2)$$

$$\delta D =(7.03\pm 0.39)\delta^{18}O+(8.97\pm 1.79)\ ‰\ (r^2 = 0.91;\ \text{monthly data}) \quad (3)$$

**4.2. Dripwater at DeSoto Caverns: Drip Rates, Isotope Variability and Sources**

Humidity/air temperature data loggers deployed at DeSoto Caverns over two time intervals (March 2006-February 2007 and March 2008-September 2008) yielded a consistent relative humidity of >95% and a cave air temperature of 17.2 ± 0.1 °C, which is equal to the mean annual surface air temperature outside the cave (17.2 °C).

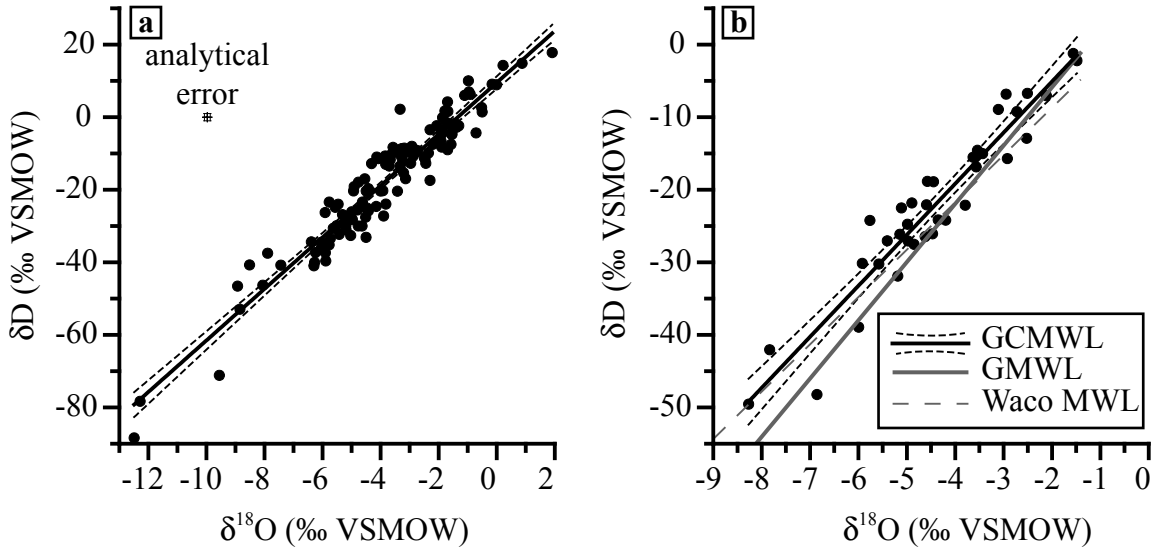


Fig. 2.7. Cross-plots of $\delta^{18}O$ vs. $\delta D$ for Tuscaloosa rainfall. The Gulf Coast Meteoric Water Line (GCMWL) is shown with 95% confidence intervals. (a) Weekly rainfall (n =117). (b) Monthly rainfall-amount weighted means (n = 36) with the Global Meteoric Water Line (GMWL) and meteoric water line for the IAEA station in Waco, TX shown for reference. See Table 2.1 for raw data and variance of calculated monthly means.

Drip flow rates vary notably among the collection sites; however, relative fluctuations in flow rates are mimicked through time at each site (Fig. 2.8a). Drip 2 became dry after the first sampling trip and will no longer be mentioned. In general, drip flow rates are higher (up to 100 µl/s) during early spring months (March-April) relative to the late fall/early winter months (October-November, down to 0.12 µl/s).

All drip sites monitored during this study can be classified as "seasonal drips" as described by Smart and Friederich (1986) based on observed maximum flow rates and variability through time. "Seasonal drips" are governed primarily by water excess above the cave so that seasonal changes in rainfall amounts and/or evapotranspiration effects exert a larger control on drip rates than short-lived rainfall events (Smart and Friederich, 1986; Baldini et al., 2006).

The water budget likely exerts the dominant control on drip flow rates based on the results of the automated high-resolution drip rate data logger (Fig. 2.9). A direct linkage between the drip rate time-series (Fig. 2.9c) and the rainfall amount (Fig. 2.9a) is not immediately obvious. The estimated monthly water budget (Fig. 2.9b), however, produces a much better match with the drip rate time-series when a lag time of 1-3 months is allowed (Fig. 2.9b and c).

Dripwater $\delta^{18}O$, $\delta D$, and *d-excess* values vary only slightly between the four drips and, unlike the rainwater data (Fig. 2.6), exhibit only weak seasonal variability and a slight decreasing trend over the 3-year study (Table 2.2 and Fig. 2.8). The excellent agreement observed among the dripwater data (Fig. 2.8b and d) and the coeval data acquired from cave pools (Table 2.3 and Fig. 2.10) suggests that evaporation in the cave is insignificant as testified by the congruency between the drips and evaporation-prone pools. Additional observations pertinent to this investigation are summarized below.

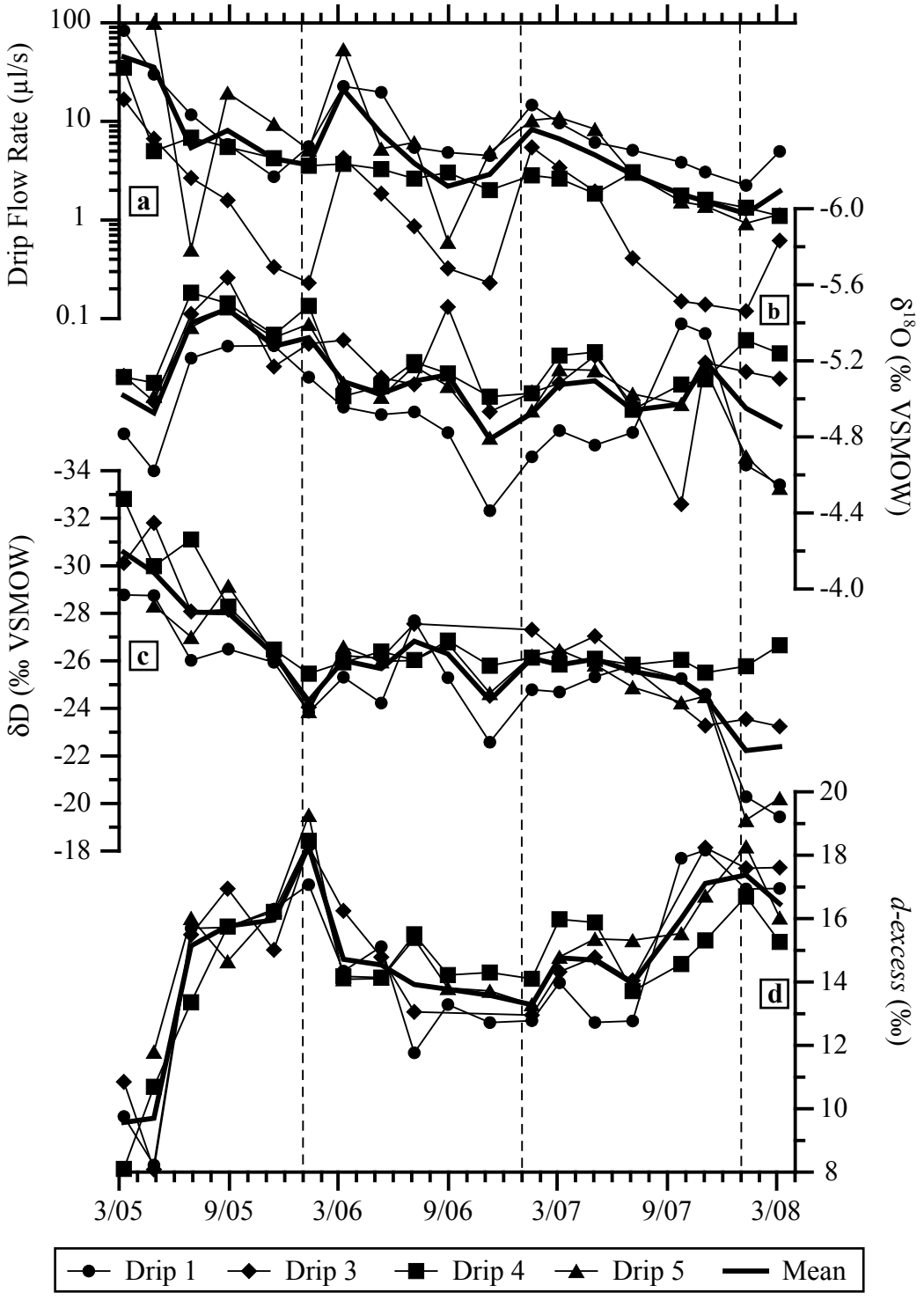


Fig. 2.8. Time-series of drip measurements at DeSoto Caverns. (a) Drip flow rates (µl/s) for each drip and mean values (bold line). (b) Same as (a) but for $\delta^{18}O$. (c) Same as (a) but for δD. (d) Same as (a) but for *d-excess*. Note that the *y*-axis for (b) and (c) is reversed.

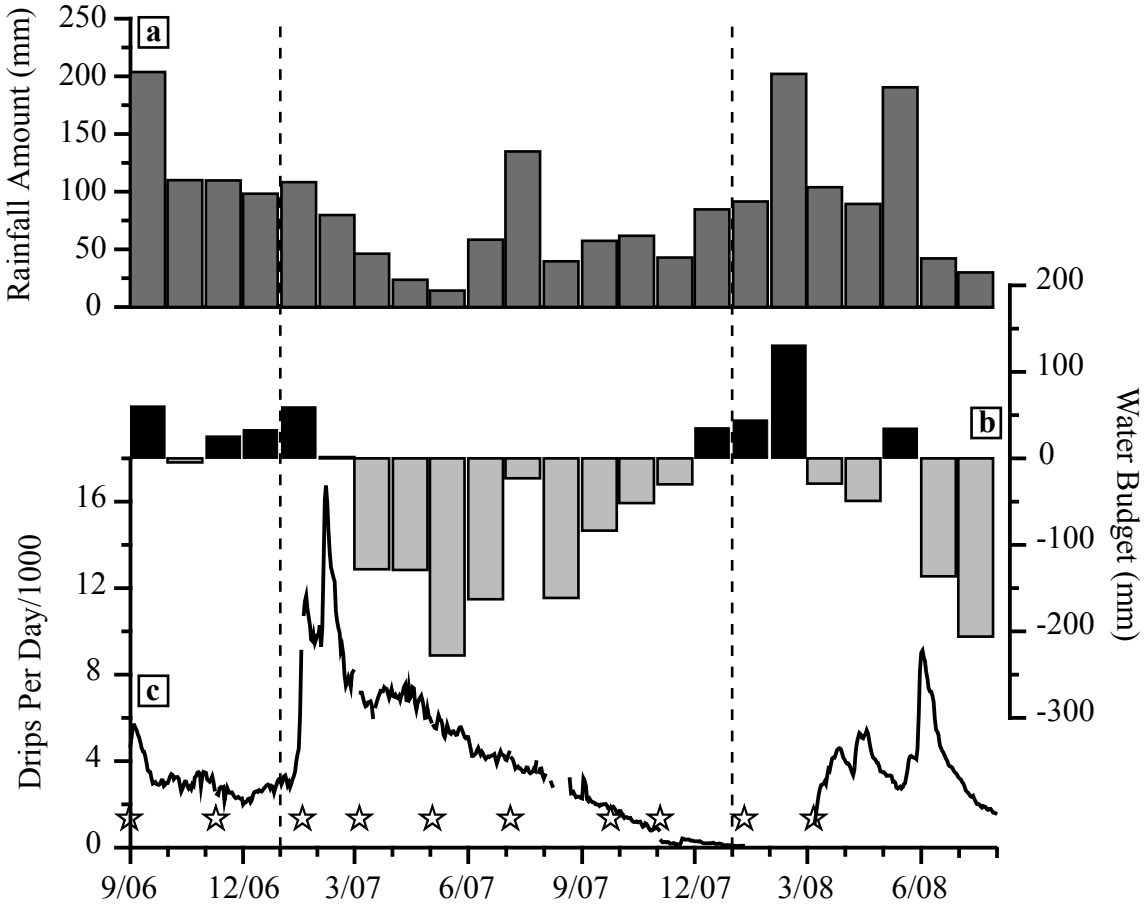


Fig. 2.9. Flow rates recorded by an automated data logger placed under drip 4 from September 2006 to November 2008 compared to coeval rainfall amounts and monthly water budget. (a) Monthly rainfall totals recorded 7 km from the DeSoto Caverns (www.ncdc.noaa.gov). (b) Monthly water budgets were calculated using potential evapotranspiration estimates following Samani (2000). (c) Variation in drips per day at drip 4 (gaps in curve represent missing data). Open stars indicate timing of water sampling trips to the cave.

Table 2.2. Summary of cave seepage measurements and their 1σ variability.

| | Drip Rate (μl/s) | *n* | $\delta^{18}O$ (‰ VSMOW) | *n* | δD (‰ VSMOW) | *n* | *d-excess* (‰) | *n* |
|---|---|---|---|---|---|---|---|---|
| Drip 1 | 12.9±18.7 | *19* | -4.9±0.3 | *19* | -25.0±2.4 | *19* | 14.3±2.7 | *19* |
| Drip 3 | 2.5±3.9 | *19* | -5.1±0.3 | *19* | -26.6±2.4 | *16* | 14.9±2.8 | *16* |
| Drip 4 | 4.8±7.5 | *19* | -5.2±0.2 | *19* | -27.0±2.1 | *19* | 14.5±2.2 | *19* |
| Drip 5 | 13.5±24.9 | *18* | -5.1±0.2 | *18* | -25.3±2.4 | *18* | 15.2±1.8 | *18* |
| Mean Value | 8.8±12.0 | *75* | -5.1±0.2 | *75* | -26.0±2.1 | *72* | 14.7±2.2 | *72* |

Table 2.3. Summary of groundwater isotope data collected at DeSoto Caverns. Error is 1σ variability.

| | $\delta^{18}O$ (‰ VSMOW) | *n* | δD (‰ VSMOW) | *n* | *d-excess* (‰) | *n* |
|---|---|---|---|---|---|---|
| Shallow Pool | -5.2±0.2 | *19* | -26.3±1.9 | *19* | 15.1±2.0 | *19* |
| Confederate Well | -4.8±0.3 | *13* | -24.1±1.3 | *13* | 14.3±2.3 | *13* |
| Shallow Well | -4.9±0.2 | *12* | -25.5±0.6 | *12* | 14.0±2.0 | *12* |
| Drip Water - Mean Value | -5.1±0.2 | *75* | -25.3±2.4 | *72* | 15.2±1.8 | *72* |

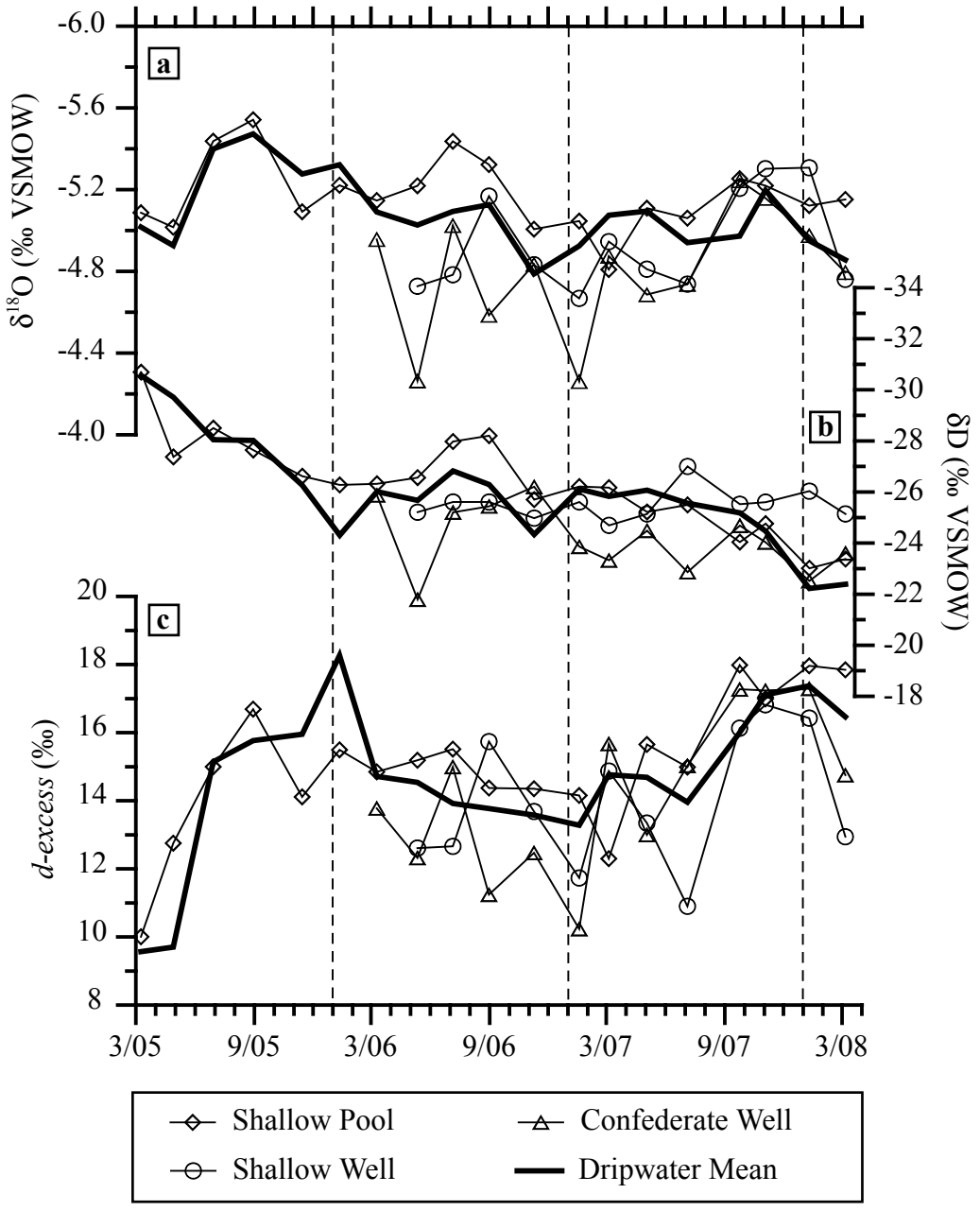


Fig. 2.10. Time-series of isotope determinations in cave pools and the groundwater well relative to the mean values of coeval drips (bold line). (a) $\delta^{18}O$; (b) $\delta D$; (c) *d-excess*.

(1) The prominent decline in drip flow rates (Fig. 2.8a) from 2005 to 2008 is compatible with the progressive onset of a regional drought (Fig. 2.6b). The water budget decline, causing the observed drip flow rates, is likely due to decreasing rainfall amounts rather than increased potential evapotranspiration.

(2) The small but noticeable $^{18}O$-enrichment time-trend from 2005 to 2008, attributed to the onset of regional drought conditions, is much better resolved in δD drip record that exhibits a 8.3 times higher $^{2}H$-enrichment over the same time interval (Fig. 2.8c), in agreement with the experimentally derived ratio of the equilibrium fractionation factors for $^{2}H$ and $^{18}O$ (8.2‰ at 25 ºC, Gat, 1980).

(3) The mean *d-excess* value for all drips over the course of the study is 14.7‰ with individual sampling date means (average of four drips on sampling date) ranging from 9.6‰ to 18.3‰ (Fig. 2.8d). The anomalously low *d-excess* values during the first two sampling trips of about 8‰ correlate well with the contemporaneous high drip flow rates (Fig. 2.8a). Most drip *d-excess* values range between the annual (13.1 ± 3.8‰, n = 36) and winter means (16.6 ± 3.3‰, n = 15) for local rainwater (Fig. 2.6e).

## 5. DISCUSSION

### 5.1. Relations Between Rainwater and Dripwater Isotopes

The deviation of the GCMWL from Craig's GMWL slope and *d-excess* values (Fig. 2.7) are attributed primarily to different rates of evaporation after condensation, and to humidity contrast

between the boundary layer and the surrounding atmosphere in the vapor source region, respectively (Clark and Fritz, 1997). For example, a slope close to a value of 8 is dictated by the ratio of the equilibrium fractionation factors for $^{2}H$ and $^{18}O$ but secondary evaporation during rainout forces the slope to values <8 (Dansgaard, 1964). High humidity during formation of moist air masses leads to *d-excess* (*y*-intercept) values <10 while greater humidity contrast between the vapor source and the dry atmosphere typically yields *d-excess* values in excess of 10 (Clark and Fritz, 1997).

The slopes of the GCMWL lines are slightly lower than that of GMWL whereas the *d-excess* values are statistically indistinguishable from that of the GMWL. GCMWL slope values < 8 ($7.03 \pm 0.39$ and $7.11 \pm 0.19$ for monthly and weekly data, respectively) are likely caused by seasonal differences in local evaporation intensity and are in good agreement with the Waco, TX MWL derived from rainfall sourced in tropical air masses from the warm Gulf of Mexico (Fig. 2.7).

With the exception of few outliers, dripwaters, cave pools, and shallow well isotope data plot within the GCMWL error envelope ($1\sigma$) thus confirming that the source is likely derived primarily from recent rainfall (Fig. 2.11). The substantial attenuation of dripwater relative to rainwater isotope variabilities suggests the occurrence of an interfacing "buffering" aquifer storage component (Fig. 2.12) whose size is larger than that of the aquifer above the portion of the cave with only 10 m of overlying bedrock. For example, the interannual transition from the "wet year " through the "normal year" and into the "drought year" leads to $^{18}O$ and $^{2}H$ enrichments of 1.4‰ and 11.6‰, respectively, in the rainwater isotope time-series (Fig. 2.12a and c). In contrast, coeval drip isotope time series record only 20% and 51%, respectively, of the $^{18}O$ and $^{2}H$ enrichments discerned in the rainwater time-trends (Fig. 2.12b and d).

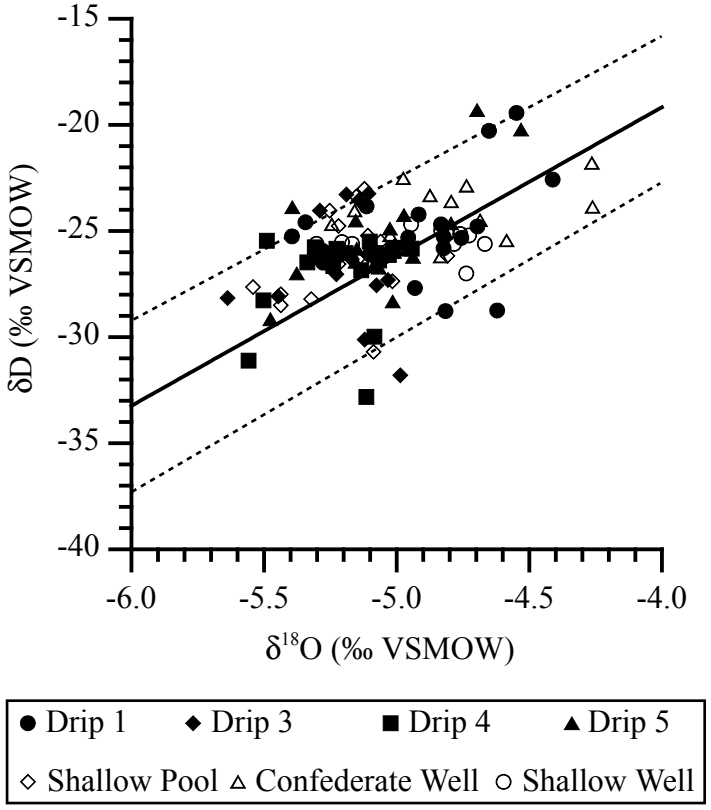


Fig. 2.11. Cross-plot of $\delta^{18}O$ vs. $\delta D$ for DeSoto Caverns dripwaters, pools, and the shallow well. With the exception of few outliers all samples fall within the error envelope (using equation #3) of the monthly Gulf Coast Meteoric Water Line (GCMWL).

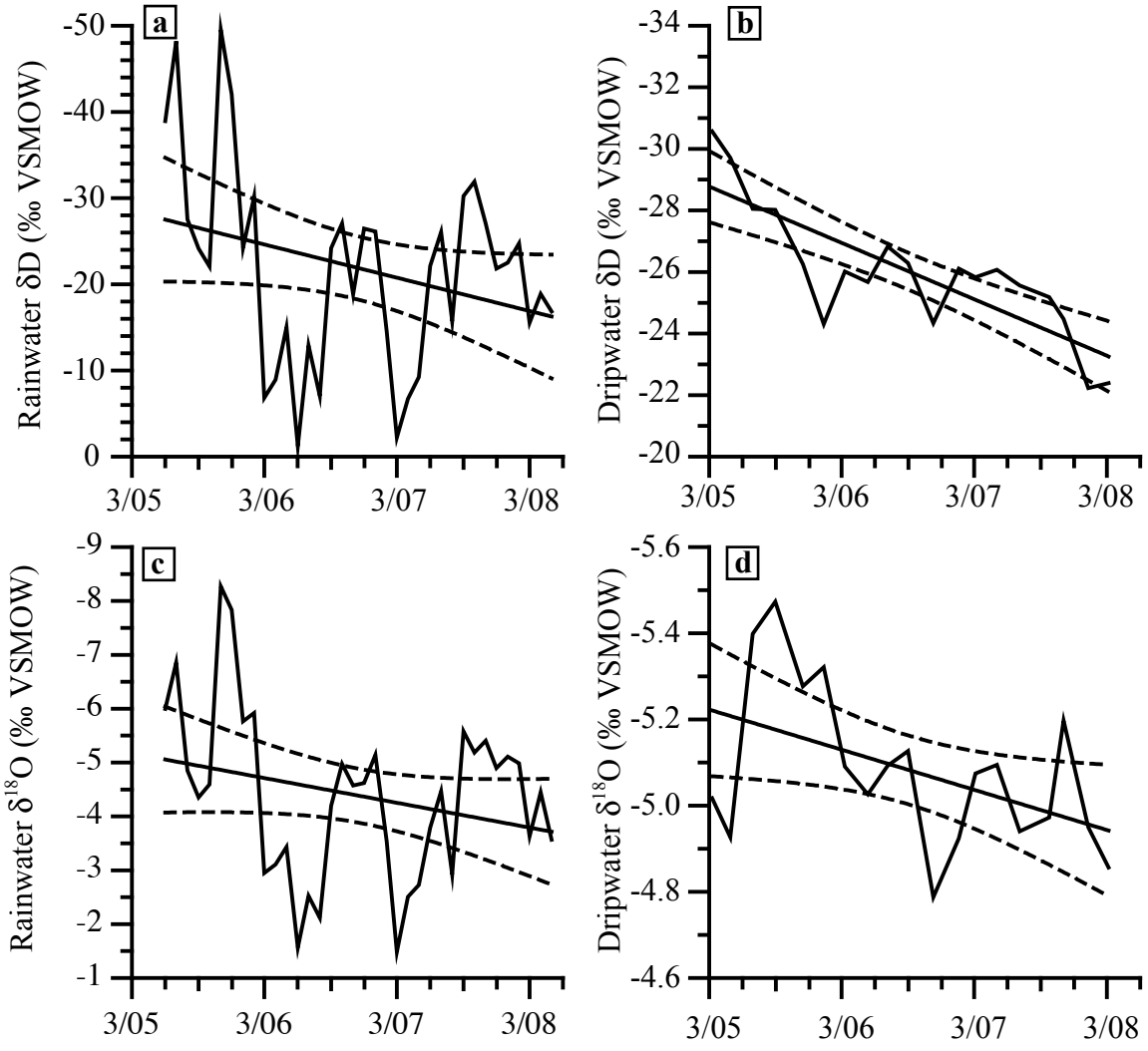


Fig. 2.12. Time trends of $^{18}O$ and $^{2}H$ enrichments in rainwater and dripwaters at DeSoto Caverns corresponding to the rainfall transition from a "wet" year (2005) through a "normal" year (2006) and into a "drought" year (2007-2008). Regression lines over the 3-year interval are shown with the 95% confidence interval. (a) Rainwater δD; (b) Dripwater δD; (c) Rainwater $\delta^{18}O$; (d) Dripwater $\delta^{18}O$. Maximum and mean $^{2}H$ and $^{18}O$ enrichment values over 3-years are as follows: (i) 25.3‰ and 11.6‰; 3.3‰ and 1.4‰ (rainwater); (ii) 7.6‰ and 5.9‰; 0.6‰ and 0.3‰ (dripwater). Dripwater $\delta^{18}O$ and δD variability is attenuated relative to rainwater isotope variability due to a relatively large aquifer storage component.

The occurrence of a well-mixed epikarst-storage compartment above the cave that dampens substantially the larger shifts discerned in the rainwater isotope time-series must be invoked in order to account for the observed rainwater-dripwater discrepancies. The inference of an epikarst storage component is supported by the following observations: (i) monthly $\delta^{18}O$ maximum amplitude in drips represents only 7% of the coeval monthly rainwater $\delta^{18}O$ maximum amplitude of 7.5‰ (November 2005 to June 2006), and (ii) mean $\delta^{18}O$ of the four drips (-5.1 ± 0.2‰, n = 75) matches that of the weighted $\delta^{18}O$ mean of local winter rainwater (-5.1 ± 1.7‰, n = 15) suggesting a greater fraction of winter rainwater reaching the cave ceiling. A rapid flushing of the epikarst-stored vadose waters by newly infiltrated winter rainfall-derived waters is corroborated by the evidence of anomalously low *d-excess* drip values (Fig. 2.8d) corresponding to anomalously high drip flow rates (Fig. 2.8a) that occurred at the start of the investigation.

Time trends of *d-excess* are sensitive indicators of post-rainfall evaporation (i.e., surface evaporation) during water flow in the vadose zone before re-emergence on the cave ceiling (Fairchild et al., 2006). Notwithstanding the weak seasonal variability in the vadose data, the overall 3-year trend in *d-excess* is consistent between the four drips (Fig. 2.8d), between the drips and cave pools and outside well (Fig. 2.10c) and between the drips and the rainwater (Fig. 2.6e) suggesting a tight coupling between the various compartments of the water cycle.

### 5.2. Rainwater Residence Time in the Epikarst

Drip water-derived oxygen isotopes in stalagmites often serve as proxies of past wet and dry episodes (e.g., McDermott, 2004; Fairchild et al., 2006). An understanding of the transmission of the rainwater isotope signal through the epikarst to the cave ceiling is therefore critical for

climate proxy signal calibration (Mattey et al., 2008; Lachniet, 2009). The drip rate data logger, placed under drip 4 (Fig. 2.2) for a period exceeding one year, helps to improve the understanding of rainwater residence time in the epikarst of DeSoto Caverns. The drip rate time series (Fig. 2.9) exhibit a prominent double-peak of 1 month duration that reached a maximum amplitude in mid-February 2007. A second triple-peak occurred over a 3-month period reaching maximum amplitude in mid-June 2008. A progressive decline in drip rate to almost complete cessation separates the two maxima (Fig. 2.9). The 1-3 month lag of the drip rate response to the water budget gives a realistic representation of the residence time of the rainwater in the 30-40 m thick epikarst at DeSoto Caverns.

### 5.3. Climate Controls of Rainfall Amount, Rainwater, and Cave Dripwater Isotope Variability

A rigorous assessment of linkages between the rainfall pattern and indices of atmosphere-ocean interactive systems (i.e., ENSO, BH) is not warranted at present because of the brevity of my time-series measurements. However, some possible couplings can be postulated from the available data. My 3-year study period overlapped with two ENSO events; an El Niño phase (September 2006 to early 2007) and a La Niña phase (June 2007 to March 2008) each of which varied in intensity but were never considered more than moderate in strength (Bell and Halpert, 2007; 2008). Greater than normal rainfall amounts were observed during the early 2006 winter El Niño phase, and dryer than normal conditions were witnessed during the majority of the 2007-08 winter which was associated with a La Niña event (Fig. 2.5). In both cases the resultant rainfall amounts recorded in the rain gauge corroborate the scenarios shown in Fig. 4a and b.

Above-normal rainfall during the summer/early fall of 2005 (Fig. 2.5) is attributed to the proximal position of the BH, which directed an unusually high number of tropical systems (six) into the study area (Virmani and Weisberg, 2006). The influence of the BH was also felt in the summer of 2007 when the dramatic westward shift of the BH (Fig. 2.4d) resulted in high rainfall amounts and flooding in portions of west Texas while drought conditions prevailed in much of the Southeast (Fig. 2.5). The annual trend of decreasing rainfall amounts, from an unusual "wet" year (2005), to a "normal" year (2006) to a "dry" year (2007-2008) observed in the rainfall data (Fig. 2.5) seem to reflect the influence of large-scale atmospheric circulation patterns during the course of this study.

Although rainfall amount and air temperature were not found to play significant roles in rainwater isotope variability observed in this study for monthly values, the role of large-scale atmospheric circulation pattern may better explain the magnitude of seasonal variability and interannual trends. Recent analysis of isotope data from the Global Network of Isotopes in Precipitation have shown that the degree of seasonal variability in $\delta^{18}O$ is strongly controlled by the geographical relationship to meridional circulation cells which, for the Northern Hemisphere, results in a zone with the lowest variability around 30° N (Feng et al., 2009). The down-welling air at this latitude picks up moisture from the GOM and transports it north bringing first-order Rayleigh distillation processes and rainfall to the collection site (33° N). Interannual variability of this zone, coupled with atmospheric circulation patterns associated with ENSO and the east-west position of the BH may partially explain the seasonal variations superimposed on interannual trends of $^{18}O$ and $^{2}H$ enrichments observed during this study (Fig. 2.6a and b). Therefore, the effects of large-scale atmospheric circulation pattern on seasonal rainfall amounts

and rainwater isotope compositions likely govern long-term trends in dripwater isotope compositions at DeSoto Caverns.

### 5.4. Implications for Paleoclimate Research in DeSoto Caverns

The rainwater-dripwater coeval isotope data reported here, viewed in the context of regional and global climate dynamics, have important implications in the application of oxygen isotopes as paleoclimate proxies in DeSoto speleothems. The 3-year (2005-2008) monitoring study points to seasonal and interannual stability of air temperature and relative humidity in the cave ambience that likely impedes significant kinetic evaporation effects. Under these conditions $\delta^{18}O$ values in the stalagmites are likely to be relatively free of kinetic isotope fractionation artifacts masking the paleoclimate signals. Because the seasonal isotope variability in dripwaters are substantially dampened relative to the one observed in the rainfall (Fig. 2.12), and because of the dripwater $\delta^{18}O$ bias toward winter rainwater $\delta^{18}O$ values, $\delta^{18}O$ assays in DeSoto stalagmites are unlikely to unravel paleo-seasonality and short-lived rainfall events (such as anomalously $^{18}O$-depleted hurricane-derived rainwater, Frappier et al., 2007). In contrast, annually resolved $\delta^{18}O$ time-series are likely to offer useful proxy records of interannual rainfall variability caused by droughts and/or anomalous wet years on the basis of documented dripwater $\delta^{18}O$ response to interannual trends in rainfall amounts and rainwater $\delta^{18}O$ (Fig. 2.6).

The results of this study suggest that conditions are promising for speleothems within DeSoto Caverns to serve as useful archives of paleoclimate information. Variations in speleothem $\delta^{18}O$ are therefore likely to record long-term changes in rainfall amounts attributed to past changes in regional atmospheric circulation patterns caused by ENSO and BH teleconnections. Extended

records of such processes acting in the Southeast and Gulf Coast would greatly enhance the understanding of past climate changes and improve global circulation models.

## 6. CONCLUSIONS

(1) Moderate to weak seasonality in $\delta^{18}O$ and $\delta D$ of Gulf Coast rainwater is attributed to a single major source of moisture (Gulf of Mexico), early stages of Rayleigh distillation, weak seasonality in rainfall amounts, and latitudinal position of the study site. In contrast, the strong seasonality discerned in *d-excess* whose values correlate with surface air temperature is ascribed to differences in the degree of evaporation from falling raindrops between summer and winter months. The slope and *y*-intercept of the GCMWL is similar to that of Waco, TX IAEA station, which depicts the Gulf of Mexico as the dominant moisture source.

(2) Flow rates of "seasonal drips" in the cave are primarily controlled by a 1-3 month water residence time and by the water budget in the epikarst as evapotranspiration reduces flow during fall and early winter months. The relatively large well-mixed reservoir above the cave attenuates individual storm events. The majority of vadose and shallow groundwater recharge is from winter rainfall.

(3) Isotope compositions of most dripwaters, pool waters, and well waters fall on, or near, the GCMWL and show little variation between sampling sites suggesting a tight coupling of the hydrologic system. The dampening effect caused by the thick overlying bedrock and relatively large epikarst-storage reservoir results in limited

seasonal variability (<0.5‰; $\delta^{18}O$) in dripwater isotope compositions despite substantial seasonal changes in flow rates.

(4) Interannual $^{18}O$ and $^{2}H$-enrichment trends in rainwater during the 3-year study are likely caused by coeval changes in global atmospheric circulation patterns (ENSO and Bermuda High).

(5) Stable air temperature, high humidity levels, and isotope compositions of dripwater mimicking that of local rainwater promote preservation of meaningful $\delta^{18}O$ variability encased within speleothems in DeSoto Caverns. Preserved $^{18}O$-enrichments and depletions through time will likely be that of interannual trends rather than seasonal or individual storm event isotope excursions.

(6) Speleothems within DeSoto Caverns have the potential of extending records of atmospheric circulation patterns into the past.

## ACKNOWLEDGMENTS

I thank Tim Lacy and Allen Mathis III for generously allowing free access to the cave for observations and sampling; students and faculty from the University of Alabama, too numerous to list, who joined me in field trips to the cave and provided assistance with sampling of rainwater and dripwater. This study is a part of the senior author's dissertation research at the University of Alabama. It was partially funded by the Gulf Coast Association of Geological Societies (GCAGS), Geological Society of America (GSA), Evolving Earth Foundation, John G. Newton Scholarship of the Alabama Geological Society, and multiple University of Alabama student research and travel grants. Valuable comments and insights from journal reviewers Dave Mattey and Lisa Baldini, an anonymous reviewer, Associate Editor Mira Bar-Matthews, and colleague David Kopaska-Merkel (Geological Survey of Alabama) greatly contributed to the improvement of this manuscript.

## REFERENCES


Ayalon A., Bar-Matthews M., and Sass E. (1998) Rainfall-recharge relationships within a karstic terrain in the Eastern Mediterranean semi-arid region, Israel: $\delta^{18}O$ and $\delta D$ characteristics. *J. Hydrol.* **207**, 18-31.

Baker A., Asrat A., Fairchild I. J., Leng M. J., Wynn P. M., Bryant C., Genty D., and Mohammed U. (2007) Analysis of the climate signal contained within $\delta^{18}O$ and growth rate parameters in two Ethiopian stalagmites. *Geochim. Cosmochim. Acta* **71**, 2975-2988.

Baldini J. U. I., McDermott F., and Fairchild I. J. (2006) Spatial variability in cave drip water hydrochemistry: Implications for stalagmite paleoclimate records. *Chem. Geol.* **235**, 390-404.

Bar-Matthews M., Ayalon A., Matthews A., Sass E., and Halicz L. (1996) Carbon and oxygen isotope study of the active water-carbonate system in a karstic Mediterranean cave: Implications for paleoclimate research in semiarid regions. *Geochim. Cosmochim. Acta* **60**(2), 337-347.

Bar-Matthews M., Ayalon A., Gilmour M., Matthews A., and Hawkesworth C. (2003) Sea-land oxygen isotopic relationships from planktonic foraminifera and speleothems in the Eastern Mediterranean region and their implication for paleorainfall during interglacial intervals *Geochim. Cosmochim. Acta* **67**(17), 3181-3199.

Bell G. D. and Halpert M. S. (2007) ENSO and the tropical Pacific. In *State of the climate in 2006* (ed. A. Arguez). Bulletin of the American Meteorological Society. pp. S44-S45.

Bell G. D. and Halpert M. S. (2008) ENSO and the tropical Pacific. In *State of the climate in 2007* (eds. D. H. Levinson and J. H. Lawrimore). Bulletin of the American Meteorological Society. pp. S63-S66.

Bryson R. A. and Hare F. K. (1974) The climates of North America. In *World survey of climatology*, **11** (eds. R. A. Bryson and F. K. Hare). Elsevier. pp. 321-356.

Cane M. A. (2005) The evolution of El Niño, past and future. *Earth Planet. Sci. Lett.* **230**, 227-240.

Clark I. D. and Fritz P. (1997) *Environmental isotopes in hydrogeology*. Lewis Publishers.

Collister C. and Mattey D. (2008) Controls on water drop volume at speleothem drip sites: An experimental study. *J. Hydrol.* **358**, 259-267.

Coplen T. B. (1988) Normalization of oxygen and hydrogen isotope data. *Chem. Geol.* **72**, 293-297.

Craig H. (1961) Isotopic variations in meteoric waters. *Science* **133**, 1702-1703.

Cruz F. W. J., Karmann I., Viana O. J., Burns S. J., Ferrari J. A., Vuille M., Sial A. N., and Moreira M. Z. (2005) Stable isotope study of cave percolation waters in subtropical Brazil: Implications for paleoclimate inferences from speleothems. *Chem. Geol.* **220**, 245-262.

Dansgaard W. (1964) Stable isotopes in precipitation. *Tellus* **16**, 436-468.

Downs J. L. M. (2005) *Childersburg Images of America*. Arcadia Publishing.

Epstein S. and Mayeda T. (1953) Variation in oxygen-18 content of water from natural sources. *Geochim. Cosmochim. Acta* **4**, 213-224.

Fairchild I. J., Smith C. L., Baker A., Fuller L., Spötl C., Mattey D., McDermott F., and E.I.M.F. (2006) Modification and preservation of environmental signals in speleothems. *Earth Sci. Rev.* **75**, 105-153.

Feng X., Faiia A. M., and Posmentier E. S. (2009) Seasonality of isotopes in precipitation: A global perspective. *J. Geophys. Res.* **114**, D08116, doi:10.1029/2008JD011279.

Frappier A., Sahagian D., Carpenter S. J., González L. A., and Frappier B. R. (2007) Stalagmite stable isotope record of recent tropical cyclone events. *Geology* **35**(2), 111-114.

Gat J. R. (1980) The isotopes of hydrogen and oxygen in precipitation. In *Handbook of Environmental Isotope* (eds. P. Fritz and J. C. Fontes). Elsevier. pp. 21-47.

Gat, J. R. (1996) Oxygen and hydrogen isotopes in the hydrologic cycle. *Annual Rev. Earth Planet Sci.* **24**, 225-262.

Harvey, F. E. (2001) Use of NADP archive samples to determine the isotope composition of precipitation: Characterizing the meteoric input function for use in ground water studies. *Ground Water* **39**(3), 380-390.

Henderson K. G. and Vega A. J. (1996) Regional precipitation variability in the southern United States. *Phys. Geogr.* **17**, 93-112.

Hendy C. H. (1971) The isotopic geochemistry of speleothems--I. The calculation of the effects of different modes of formation on the isotopic composition of speleothems and their applicability as palaeoclimatic indicators. *Geochim. Cosmochim. Acta* **35**, 801-824.

IAEA. (1992) Statistical treatment of data on environmental isotopes in precipitation. In *Technical Report Series No. 331*. International Atomic Energy Agency. pp. 781.

Katz R. W., Parlange M. B., and Tebaldi C. (2003) Stochastic modeling of the effects of large-scale circulation on daily weather in the southeastern U.S. *Clim. Change* **60**, 189-216.

Kendall C. and Coplen T. B. (1985) Multi-sample conversion of water to hydrogen by zinc for stable isotope determination. *Anal. Chem.* **57**(7), 1437-1440.

Kiladis G. N. and Diaz H. F. (1989) Global climate anomalies associated with extremes in the Southern Oscillation. *J. Clim.* **2**, 1069-1090.

Knight D. B. and Davis R. E. (2007) Climatology of tropical cyclone rainfall in the southeastern United States. *Phys. Geogr.* **28**(2), 126-147.

Lachniet M. S. (2009) Climatic and environmental controls on speleothem oxygen-isotope values. *Quat. Sci. Rev.* **28**, 412-432.

Maasch K. A. and Oglesby R. J. (1990) Meltwater cooling of the Gulf of Mexico: a GCM simulation of climatic conditions at 12 ka. *Paleoceanography* **5**, 977-996.

Mattey D., Lowry D., Duffet J., Fisher R., Hodge E., and Frisia S. (2008) A 53 year seasonally resolved oxygen and carbon isotope record from a modern Gibraltar speleothem: Reconstructed drip water and relationship to local precipitation. *Earth Planet. Sci. Lett.* **269**, 80-95.

McDermott F. (2004) Palaeo-climate reconstruction from stable isotope variations in speleothems: a review. *Quat. Sci. Rev.* **23**, 901-918.

Mo K. C. and Schemm J. E. (2008) Relationships between ENSO and drought over the southeastern United States. *Geophys. Res. Lett.* **35**, L15701, doi: 10.1029/2008GL034656.

Neff U., Burns S. J., Mangini A., Mudelsee M., Fleitmann D., and Matter A. (2001) Strong coherence between solar variability and the monsoon in Oman between 9 and 6 kyr ago. *Nature* **411**, 290-293.

Oglesby R. J., Maasch K. A., and Saltzman B. (1989) Glacial meltwater cooling of the Gulf of Mexico: GCM implications for Holocene and present-day climates. *Climate Dynam.* **3**, 115-133.

Portmann R. W., Solomon S., and Hegerl G. C. (2009) Spatial and seasonal patterns in climate change, temperatures, and precipitation across the United States. *PNAS* **106**(18), 7324-7329.

Rasmusson E. M. (1968) Atmospheric water vapor transport and the water balance of North America II. Large-scale water balance investigations. *Mon. Weather Rev.* **96**(10), 720-734.

Ropelewski C. F. and Halpert M. S. (1986) North American precipitation and temperature patterns associated with the El Niño/Southern Oscillation (ENSO). *Mon. Weather Rev.* **114**, 2352-2362.

Rozanski K., Araguás-Araguás L., and Gonfiantini R. (1993) Isotopic patterns in modern global precipitation. In *Climate change in continental isotopic records*. Geophysical Monograph 78, American Geophyiscal Union. pp. 1-36.

Samani Z. (2000) Estimating solar radiation and evapotranspiration using minimum climatological data. *J. Irrig. Drain. Eng.* **126**(4), 265-267.

Simpkins W. W. (1995) Isotopic composition of precipitation in central Iowa. *J. Hydrol.* **172**, 185-207.

Smart P. L. and Friederich H. (1986) Water movement and storage in the unsaturated zone of a maturely karstified aquifer, Mendip Hills, England. In *Proceedings of the Conference on Environmental Problems in Karst Terrains and Their Solutions*, pp. 57-87, National Water Wells Association, Bowling Green, KY.

Stahle D. W. and Cleaveland M. K. (1992) Reconstruction and analysis of spring rainfall over the southeastern U.S. for the past 1000 years. *Bulletin of the American Meteorological Society* **73**(12), 1947-1961.

Spötl C., Fairchild I. J., and Tooth A. F. (2005) Cave air control on dripwater geochemistry, Obir Caves (Austria): Implications for speleothem deposition in dynamically ventilated caves. *Geochim. Cosmochim. Acta* **69**(10), 2457-2468.

Virmani J. I. and Weisberg R. H. (2006) The 2005 hurricane season: An echo of the past or a harbinger of the future? *Geophys. Res. Lett.* **33**, doi:10.1029/2005GL025517.

Wang Y. J., Cheng H., Edwards R. L., An Z., Wu J., Shen C.-C., and Dorale J. A. (2001) A high-resolution absolute-dated Late Pleistocene monsoon record from Hulu Cave, China. *Science* **294**, 2345-2348.

CHAPTER 3

# CONTROLS ON DISSOLVED INORGANIC CARBON AND $\delta^{13}C$ IN CAVE WATERS FROM DESOTO CAVERNS: IMPLICATIONS FOR SPELEOTHEM $\delta^{13}C$ ASSESSMENTS

## ABSTRACT

Unraveling the factors controlling the carbon chemistry and flow within extant karst systems has important implications concerning the assessment of time-series $\delta^{13}C$ records of speleothems. Here I report the results of a 3-year study of total dissolved inorganic carbon (DIC) and $\delta^{13}C_{DIC}$ from cave waters at DeSoto Caverns (Southeastern USA) that offer valuable insight on carbon flow and the accompanied isotope fractionations from end-member sources to speleothems.

[DIC] and $\delta^{13}C_{DIC}$ values of cave waters entailing "fast" and "seasonal" drips range from 0.2 mM to 6.0 mM and 2.7 to -12.9 (‰ VPDB), respectively. [DIC] and $\delta^{13}C_{DIC}$ of drips show strong seasonal, albeit noisy, variability and are inversely related ($\delta^{13}C_{DIC} = -2.49[DIC] + 0.64$, $r^2 = 0.84$). A pool fed by multiple drips shows a bimodal $\delta^{13}C_{DIC}$ distribution with isotopically heavier mode during winter (-4‰ to -5 ‰ VPDB) relative to summer months (-9‰ to -10 ‰ VPDB). An interannual trend of decreasing water availability during the study period is not translated into a response of cave water carbon chemistry suggesting that rainfall amount may not be a significant controlling factor. Coupled cave air ventilation/stagnation and varying $CO_2$

fluxes through the soil horizon and epikarst exert the strongest influence on seasonal [DIC] and $\delta^{13}C_{DIC}$ variability. Isotopic equilibrium closely approximates the summer/early fall high [DIC] with relatively low $\delta^{13}C_{DIC}$ whereas kinetically enhanced isotopic fractionations are prominent during winter/early spring months at lower [DIC] and higher $^{13}C$-enrichments. The kinetically enhanced isotopic fractionation is greater by about a factor of two ($1000\ln\alpha = -6.7 \pm 0.3‰$) relative to the isotopic fractionation under equilibrium conditions (i.e., $1000\ln\alpha = -3.1‰$).

On the basis of $^{14}C$ mass balance and paired $^{14}C$-U/Th measurements I estimate that on average about ~23 % of C delivered annually by the drips to the aragonite stalagmites is derived from $^{14}C$-dead dolomite cap while the remainder of ~77 % is derived from $^{14}C$-live biomass. $\delta^{13}C$ measurements of aragonite (n = 12) sampled from the tips of active speleothems during the summer months are consistent with aragonite $\delta^{13}C$ values calculated on the basis of the pool summer/early fall data thus confirming the $\delta^{13}C$ seasonality bias in both drips and coeval aragonite. $\delta^{13}C$ values (n = 81) of an active stalagmite section spanning the last 200 years show a normal distribution with a mean of -7.1 ± 1.2‰ and a mode of -7‰ to -8‰ that are statistically indistinguishable from the mean and annual mode of the drips. Thus secular time-series $\delta^{13}C$ records of stalagmites at DeSoto Caverns with resolving power $>10^{-1}$ year will likely carry the imprints of drip annual means entailing climate-driven $\delta^{13}C$ seasonal biases.

# 1. INTRODUCTION

Speleothems are important continental paleoclimate archives because their chronology can be precisely established by radiometric methods and they preserve multiple proxies providing high-resolution climate records (Gascoyne, 1992; McDermott, 2004; Fairchild et al., 2006; Lachniet, 2009). Under favorable conditions, changes in mean annual temperature, rainfall variability, moisture sources and vegetation type are interpreted from measurable parameters including, but not limited to, $\delta^{18}O$, $\delta^{13}C$, intra- and interannual growth rates, trace elements, and the content of organic acids (Lauritzen, 2003). The focus of most paleoclimate reconstructions has been on speleothem $\delta^{18}O$ variability while changes in $\delta^{13}C$ received less attention because interpretations are confounded by the complexity of the carbon flow and isotope fractionations in the karst system (Cosford et al., 2009). $\delta^{13}C$ time-series could offer a valuable supplement to $\delta^{18}O$ assays if a better understanding of the karst carbon flow and the accompanying isotope fractionations is achieved using tracers of the carbon flow path under extant ambient cave conditions.

The most robust paleoclimate records derived from speleothems are those for which present-day cave monitoring programs precede/accompany the investigation of fossil deposits. Such an endeavor provides the opportunity to document the controls (i.e., rainfall amount, air temperature) on dripwater isotope chemistry and subsequently determine how ambient variability is entrained within the deposited speleothems. By necessity monitoring programs span multiple years in order to quantify seasonal and interannual variability affecting the cave environment (Baker and Brunsdon, 2003; Fuller et al., 2008). Full utilization of C isotopes has not been reached in part due to exclusion of present-day examination of the carbon system dynamics. Paleoclimate reconstructions are prone to incomplete utilization of the available data without a

high-resolution time-series of $\delta^{13}C$ in the drips and the spelean carbonates similar to the approach generally taken in the case of oxygen isotopes.

Here I report the results of a 3-year investigation of the carbon flow in cave waters from DeSoto Caverns, a karst system located in central Alabama, USA. This study complements a recent 3-year comprehensive investigation of oxygen and hydrogen isotope hydrology in rainfall and drips from DeSoto Caverns (Lambert and Aharon, 2010). The cave waters study examines the: (i) temporal and spatial variability of dripwater flow rates, dissolved inorganic carbon [DIC], and $\delta^{13}C$ of DIC ($\delta^{13}C_{DIC}$) in dripwaters and a control pool, and (ii) temporal relationships between flow rates and the carbon flow variability along the pathway from drips to the carbonate stalagmites. In addition, $\delta^{13}C$ assays from actively depositing speleothems bring insight to the relationship between dripwater and calcium carbonate forming in the ambient cave atmosphere.

The data and interpretations reported here will likely lead to a better understanding of $\delta^{13}C$ time-series as proxy climate records preserved in speleothems in general, and those in DeSoto Caverns specifically.

## 2. CARBON FLOW AND $\delta^{13}C$ SYSTEMATICS IN KARST SYSTEMS

Speleothems are carbonate cave deposits typically with calcite and/or aragonite mineralogy and are the product of dissolution of host carbonate bedrock above the cave followed by reprecipitation within the cave cavity. The speleothem deposition hinges on sequential 3-step reactions that include:

(i) soil-$CO_2$ mixing with percolating rainwater and forming weak carbonic acid:

$$CO_{2(g)} + H_2O_{(aq)} \rightarrow H_2CO_{3(aq)}, \quad (1)$$

(ii) dissolution of the carbonate bedrock by the weak acidic fluid:

$$H_2CO_{3(aq)} + CaCO_{3(s)} \rightarrow 2HCO_{3(aq)} + Ca^{2+}_{(aq)}, \quad (2)$$

(iii) $CO_2$ degassing in the cave chamber leading to supersaturation and carbonate precipitation:

$$2HCO_{3(aq)} + Ca^{2+}_{(aq)} \rightarrow CO_{2(g)} + CaCO_{3(s)} + H_2O_{(aq)}. \quad (3)$$

The $\delta^{13}C$ composition of the speleothems is therefore largely controlled by: (i) sources of C incorporated into the groundwater, (ii) the state of chemical equilibrium between vadose water and soil-$CO_2$, (iii) inorganic processes related to the dissolution of the bedrock (i.e., open vs. closed system), (iv) prior carbonate precipitation in the epikarst, (v) presence or absence of evaporation in the cave, and (vi) the extent and rate of $CO_2$ degassing from cave dripwater due to changes in drip flow rates or cave air $pCO_2$ (Cosford et al., 2009).

### 2.1. Karst Groundwater $\delta^{13}C_{DIC}$

Climate-controlled changes in groundwater $\delta^{13}C_{DIC}$ are of primary interest in paleoclimate reconstruction. The main carbon sources incorporated in the karst groundwater are derived via biological processes (plant root respiration and oxidation of organic debris by microbial

organisms) and the carbonate bedrock dissolution, with minor possible contributions from atmospheric $CO_2$ ($\delta^{13}C$ ~ -8‰ VPDB) (Hendy, 1971; Lauritzen, 2003; Cosford et al., 2009) (Fig. 3.1). Following the interaction with the bedrock, C is transported through the water karst system mainly in the form of bicarbonate ($HCO_3^-$), which is the dominant phase in dripwater DIC at pH levels that are typical of karst environments (e.g., 7.5 to 7.8, McDonald et al., 2007). According to the stoichiometry of equation (2) above, 50% of DIC carbon is derived from the bedrock although reported estimates based on radiocarbon mass balances are usually between 10% and 20% (Genty and Massault, 1997). The $\delta^{13}C$ value of carbonate bedrock, typically of marine origin, has a narrow $\delta^{13}C$ range (0‰ to 4‰ VPDB) while by comparison the $\delta^{13}C$ of the biological end-member is highly depleted in $^{13}C$ being a function of the plant photosynthetic pathway. Plants utilizing the Calvin cycle (C3 plants) exhibit a $\delta^{13}C$ range of -20‰ to -34‰ (average of -26‰) while C4 plants (Hatch-Slack pathway) have a range $\delta^{13}C$ of -9‰ to -16‰ (McDermott, 2004). Additionally, recent studies have demonstrated that $\delta^{13}C$ of plants using the C3 photosynthetic pathway are controlled by the degree of water availability such that higher rainfall amounts cause $^{13}C$ depletion while droughts lead to $^{13}C$ enrichments (Stewart et al., 1995; Ferrio et al., 2003). The $\delta^{13}C_{DIC}$ of karst groundwater is therefore partially governed by the mixing of source end-members, which also includes changes in the state (open vs. closed) of the inorganic dissolution processes (McDermott, 2004; McDermott et al., 2006; Cosford et al., 2009). For instance, where C3 plant cover dominates (generally denser biomass), the $\delta^{13}C_{DIC}$ at 15 °C is typically near -14‰ while a value around -7‰ is common in C4 environments (Salomons and Mook, 1986).

Before reaching the cave atmosphere via dripwater, groundwater $\delta^{13}C_{DIC}$ can be further affected by the degree of equilibration between soil-$CO_2$ and vadose water, as well as prior

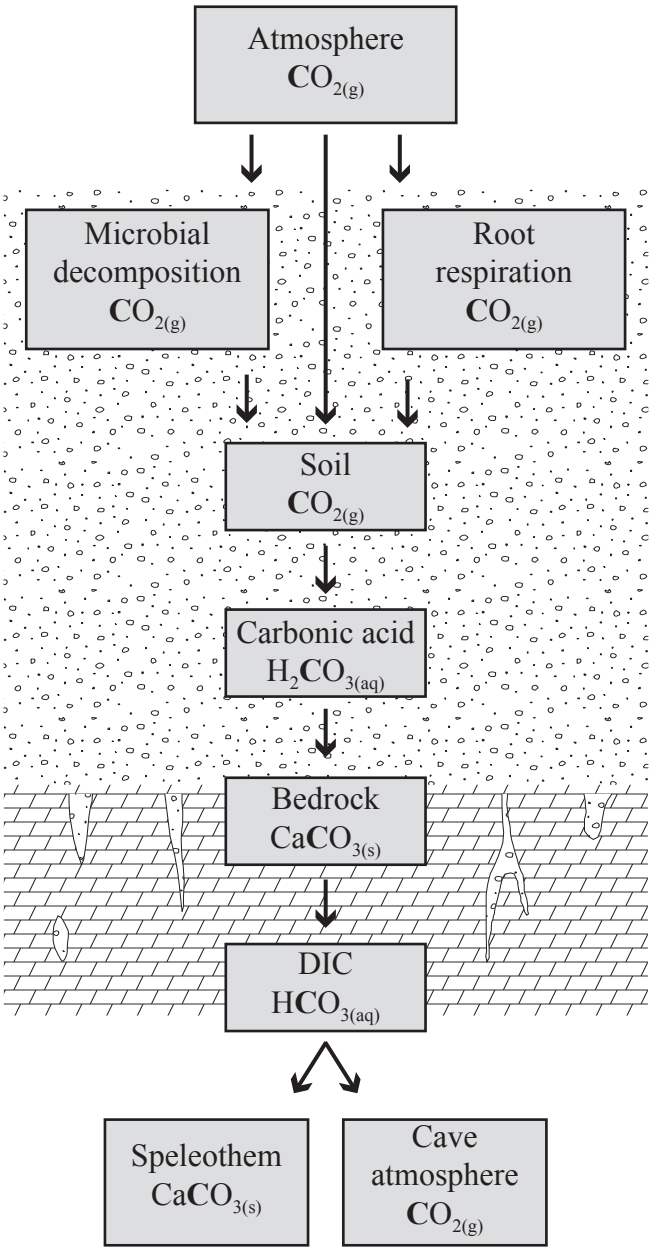


Fig. 3.1. Chart of carbon flow from sources to speleothem carbonate sink.

carbonate precipitation in the epikarst. Where vadose water percolation rates are relatively high, waters may not reach complete chemical equilibrium with the $^{13}C$-depleted soil-$CO_2$ and may retain a component of $^{13}C$-enriched atmospheric $CO_2$, resulting in elevated $\delta^{13}C_{DIC}$ (Baker et al., 1997). If groundwater percolation rates are low or the groundwater encounters macroporosity, calcium carbonate may precipitate leaving the remaining DIC enriched in $^{13}C$ (Baker et al., 1997). Variable temperature occurring in the flow path of C from source to dripwater DIC is an additional controlling factor of the isotope fractionation between carbon species (Fig. 3.1) and its magnitude is typically derived under the assumption of chemical and isotopic equilibria (Salomons and Mook, 1986).

## 2.2. Controls on Speleothem $\delta^{13}C$ within Cave Environments

The properties of the cave atmosphere dictate the final $\delta^{13}C$ of deposited speleothems in relation to the DIC source (Fig. 3.1). Upon groundwater's emergence at the cave ceiling, the $pCO_2$ of the water (typically $10^{-1.5}$ atm to $10^{-2.5}$ atm) is substantially greater than that of the cave atmosphere ($10^{-2.5}$ atm to $10^{-3.5}$ atm), which promotes degassing of $CO_2$ from the dripwater and precipitation of calcium carbonate as speleothems (Lauritzen, 2003). The rate and degree of degassing is influenced by dripwater flow rates and seasonal changes in $pCO_2$ of the cave atmosphere, both of which may alter the $\delta^{13}C$ of the speleothems (Spötl et al., 2005; Mattey et al., 2008a; Cosford et al., 2009). Slow drip rates, where the water is in contact with the speleothem surface for longer periods of time, allow for more complete degassing and deposition of isotopically heavier calcium carbonate (Bar-Matthews et al., 1996; Romanov et al., 2008). Recent studies have shown that seasonal changes in cave ventilation may affect $pCO_2$ levels

within certain caves to the extent that one season may experience "forced" degassing due to enhanced $pCO_{2DRIPWATER} - pCO_{2CAVE\ ATMOSPHERE}$ gradient, which results in $^{13}C$-enriched speleothem deposition (Spötl et al., 2005; Mattey et al., 2008a). Such ventilation control on speleothem $^{13}C$ has also been suggested to alter calcite/aragonite compositions for extended periods of time (Cosford et al., 2009). Similarly, supersaturation of calcite/aragonite in the dripwater can be driven by evaporation if the cave atmosphere has less than 100% relative humidity, which adds yet another potential kinetic effect that may affect speleothem $\delta^{13}C$ (Hendy, 1971).

Clearly, deciphering the controls on modern $\delta^{13}C$ variability is complex given the number of variables at play and the uncertainties present within the epikarst. Nonetheless, the role of parameters of interest can be identified by well-planned cave monitoring and by making reasonable assumptions that simplify the system.

## 3. STUDY SITE

Cave waters (drips and control pool) were acquired from DeSoto Caverns (Fig. 3.2; 33°18'26" N, 86°16'36" W), a cave within an Upper Ordovician-age dolomite karst system located near Childersburg, AL. The cave is roughly 150 m in length and has two continuous sections: (i) a large chamber (70 m long, 50 m wide, 36 m high) with approximately 10 m thick overlying bedrock, and (ii) smaller chambers in the back of the cave with substantially thicker (30 – 40 m) bedrock (Lambert and Aharon, 2010). The interior of the cave is ornately decorated with active and fossil speleothems that consist predominantly of aragonite.

The average monthly air temperatures outside the cave range from ~7 °C in January to ~27

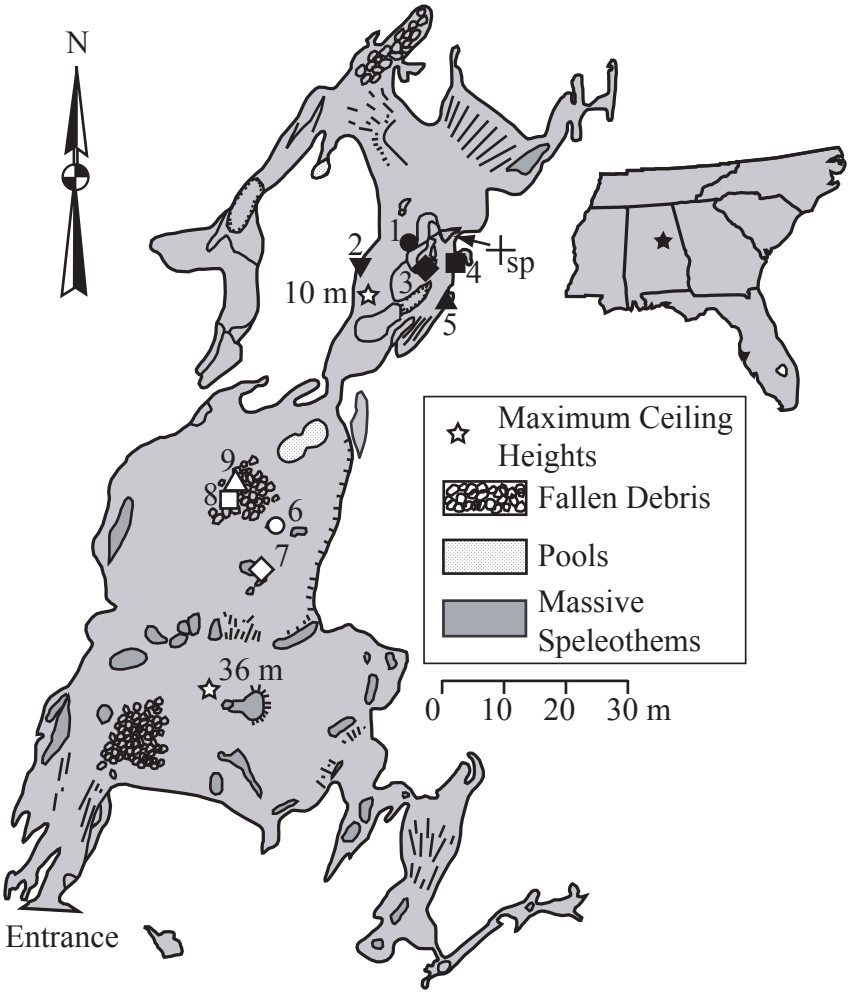


Fig. 3.2. Map (plan view) of DeSoto Caverns with water sampling locations and numbers (modified after Lambert and Aharon, 2010). Solid symbols indicate the location of "seasonal drips" while open symbols indicate "fast drips." The cross (+) indicates the location of the shallow pool (sp). Numbers next to open stars indicate the height of the chamber ceiling above the cave floor. Solid star on regional map indicates location of DeSoto Caverns.

°C in July. Rainfall is generally evenly distributed throughout the year with October (~80 mm) and March (~150 mm) being typically the driest and wettest months, respectively. The mean annual air temperature is 17.2 °C and the average annual total rainfall is 1417 mm based on 1958 to 2004 data (Lambert and Aharon, 2010). On a seasonal basis, increased evapotranspiration rates during summer months leads to a negative water budget whereas water is in excess during winter months and saturates the epikarst (Fig. 3.3a). The wide range of external air temperatures stands in sharp contrast to the practically invariable cave air temperature that varies by only 0.1 °C (1σ) annually (Fig. 3.3b; Lambert and Aharon, 2010).

The humid subtropical climate of central Alabama results in vegetation above the cave that is dominated by C3 plants (Cerling and Quade, 1993). These plants grow in a thin and poorly developed soil horizon and the vegetation type and quantity above the cave has not likely been drastically altered in modern times. A paleovegetation record (Delcourt et al., 1983) spanning the past 12 ka (kilo-annum) derived from nearby Cahaba Pond (35 km northwest) suggests notable climate-induced changes in plant communities in the past therefore making DeSoto Caverns a suitable study site for comparative paleoenvironmental reconstructions.

# 4. MATERIALS AND METHODS

## 4.1. Field Methods

Cave waters were sampled at approximately 2-month intervals from four drip sites and a permanent pool in the distal portion of DeSoto Caverns (Fig. 3.2) starting in March 2005 and ending in March 2008. The shallow pool integrates waters from multiple drips and offers a good

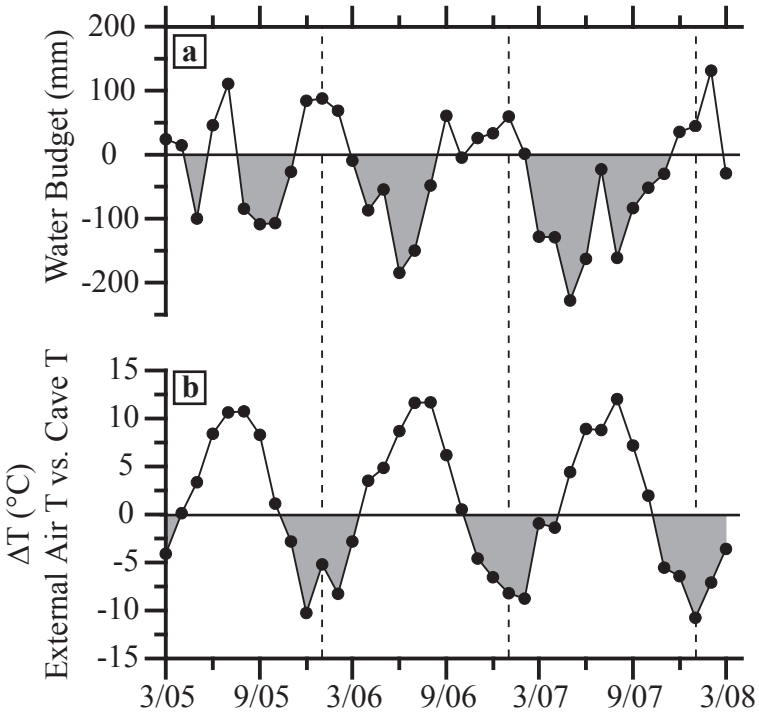


Fig. 3.3. (a) Estimated monthly water budget at DeSoto Caverns during the course of this study (modified from Lambert and Aharon, 2010). Shaded regions represent periods without significant water recharge. (b) External monthly air temperatures (www.ncdc.noaa.gov) normalized to the constant cave air temperature (~17.2 °C). Shaded regions depict intervals when outside air temperature is lower than the cave environment.

representation of seasonal changes in cave water chemistry. Drips 1 and 4 were sampled from the tips of two large stalactites, drips 2 and 3 from the tip of soda straws, and drip 5 from water flowing over a cave drapery on the perimeter of the cave. These drips have been classified by Lambert and Aharon (2010) as "seasonal drips" following the nomenclature of Smart and Friederich (1986). The dripwater flow rates are controlled partly by the water budget above the cave where water recharge is primarily during the winter months when the effects of evapotranspiration are minimal (Fig. 3.3a). A subsequent, twentieth sampling trip to the cave was made in June 2009 to collect dripwater (Drips 6-9, Fig. 3.2) emerging from fractures in the ceiling of the cave's largest chamber where the overburden is relatively thin (10 m) and the falling distance is >25 m. The rate of water issuing from these fractures is faster relative to the "seasonal drips" and their sampling was conducted for comparative purposes. These drips are referred qualitatively as "fast drips," although additional data would be needed for a proper classification. Dripwater flow rates were estimated by recording fluid volume accumulating in clean plastic bags over a fixed time span and the results are reported in µl/s. While in the cave, $HgCl_2$ was added to the collected water in order to prevent biological growth and transferred into the appropriate size airtight-glass bottle for storage before determination of [DIC] and corresponding $\delta^{13}C_{DIC}$.

In order to compare the $\delta^{13}C$ of aragonite ($\delta^{13}C_{AR}$) that is currently depositing in the cave with the $\delta^{13}C$ of the source bicarbonate, small sub-samples were removed using a stainless steel blade from the surface of eight actively forming speleothems. A pristine hand specimen of dolomite was removed from an outcrop directly above the cave in order to determine the $\delta^{13}C$ composition of the overlying bedrock.

## 4.2. Laboratory Methods

C isotopes and [DIC] measurements of cave waters as well as C isotopes of stalagmite-derived aragonite were carried out on a Gasbench on-line with a CF-IRMS (modified Delta-plus). [DIC] and $\delta^{13}C_{DIC}$ of cave waters were simultaneously derived from one sample aliquot (0.7 ml) using a method adapted from Spötl (2005). [DIC] are reported in millimoles/liter (mM), whereas $^{13}C/^{12}C$ ratios are reported in delta notation relative to Vienna Pee Dee Belemnite (VPDB) calibrated via the NBS-19 standard. Calibration curves, derived from an array of known DIC concentrations (0.2 mM – 5.0 mM of anhydrous $Na_2CO_3$ solution) relative to mass 44 beam intensity, governed reproducibility and accuracy of [DIC] measurements and maintained correlation coefficients better than $r^2 = 0.97$. $\delta^{13}C_{DIC}$ values of the internal $Na_2CO_3$ solution ($\delta^{13}C = -6.8 \pm 0.2‰$, n = 46) show good reproducibility and are within measurement error of the $Na_2CO_3$ powder analyzed independently ($\delta^{13}C = -7.2 \pm 0.2‰$, n = 13).

Extant aragonite samples were dried overnight in an oven at 50 °C and then ground to a powder and homogenized before the analysis. The dolomite bedrock sample was crushed to a powder and thoroughly blended with a Fisherbrand Touch Mixer. C isotopes of $CaCO_{3AR}$ were carried out on the CF-IRMS system by implementing methods similar to that described by Debajyoti and Skrzypek (2007). Carbon isotope values are expressed in per mil (‰) relative to the VPDB scale by use of the NBS-19 standard. Reproducibility for $\delta^{13}C$ assays are estimated to be ± 0.1‰ (1σ) based on multiple NBS-19 standard and sample repeats.

## 5. RESULTS

Dripwater flow rates vary notably among the individual "seasonal drips" although their interannual variability relative to each other is maintained over time (Fig. 3.4a and Appendix 3.1). Drip 2 became dry after the first sampling trip and will no longer be discussed. In general, dripwater flow rates are higher (up to 100 µl/s) during early spring months (March-April) relative to the late fall/early winter months (October-November; down to 0.12 µl/s). During the study central Alabama experienced an interannual trend of decreasing rainfall amounts characterized by extreme wet conditions (fall 2005) through periods of average rainfall (2006) to extreme drought (2007-08) (Lambert and Aharon, 2010). The progression of decreasing water recharge coupled with evapotranspiration processes is expressed as an overall interannual logarithmic decrease of dripwater flow rates over the 3-year period (Fig. 3.4a). The flow rates of the "fast drips" are substantially greater than those of the coevally sampled "seasonal drips" and range from 46 µl/s (drip 7) to 134 µl/s (drip 9). Water residence time above the cave has been estimated by Lambert and Aharon (2010) to be 1-3 months.

[DIC] and $\delta^{13}C_{DIC}$ values determined for individual "seasonal drips" and cave pool water are graphed in Fig. 3.4b and c (also, see Appendix 3.1). Seasonal changes in [DIC] and $\delta^{13}C_{DIC}$ are clearly discerned in both "seasonal drips" and the cave pool. However, it must be noted that drips data represent singular collections of a few hours of seepage whereas the pool integrates waters sourced in multiple drips that supply the pool for extended periods of time. These differences in time integration are likely to explain why dripwater [DIC] and $\delta^{13}C_{DIC}$ values exhibit "noisier" time-series relative to pool water values.

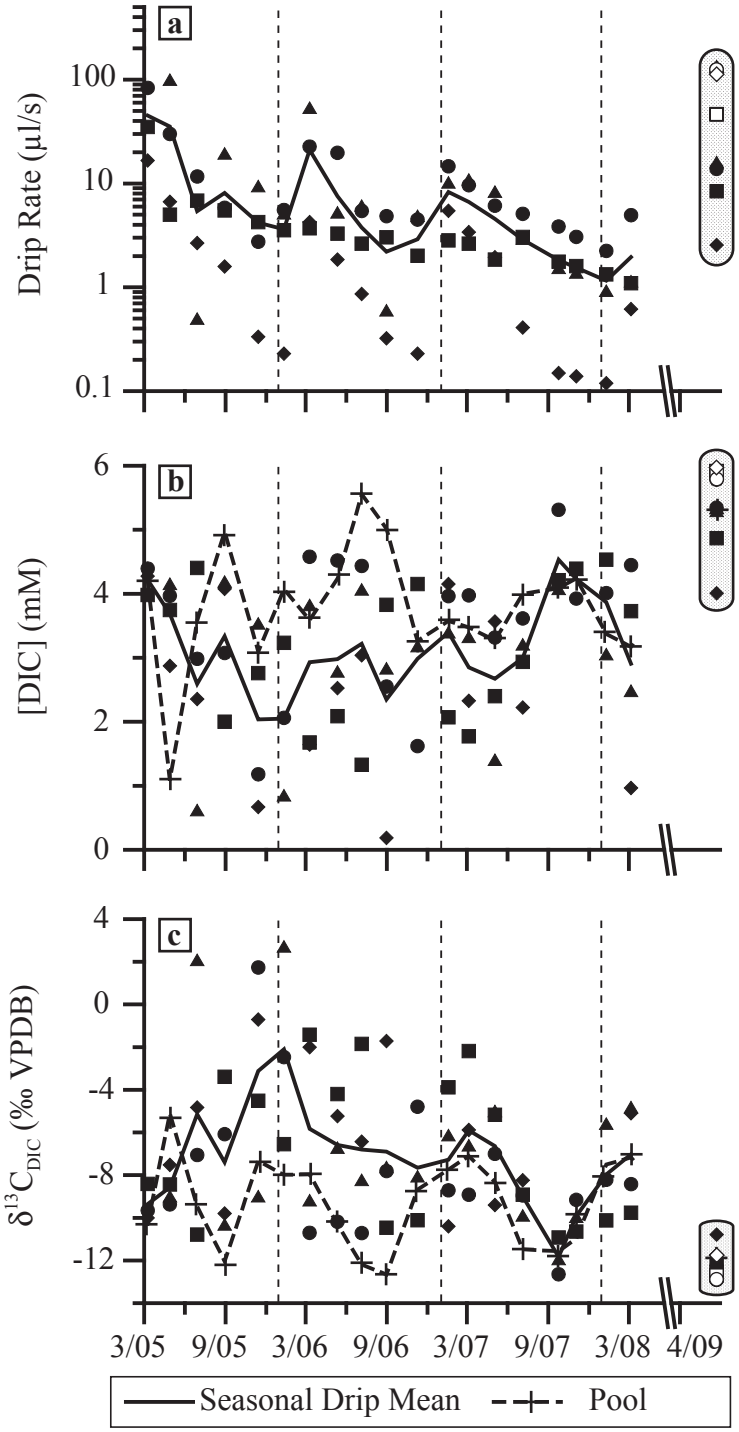


Fig. 3.4. Time-series of drip measurements at DeSoto Caverns. (a) Drip flow rates (µl/s) for individual drips and mean values (bold line). (b) [DIC] (mM) for individual drips with mean values (bold line) and pool (interrupted line). (c) Same as (b) but for $\delta^{13}C_{DIC}$. Refer to Fig. 3.2 for drip site locations and symbols. Pattern fields encompass "fast" and "seasonal drips" sampled at the end of June 2009.

Pool waters show a clear seasonal signal in both [DIC] and $\delta^{13}C_{DIC}$ with summer/fall months having higher [DIC] values and lower $\delta^{13}C_{DIC}$ (up to 5.6 mM and -12.7‰, respectively) relative to winter/early spring months when [DIC] is low and $\delta^{13}C_{DIC}$ is substantially more $^{13}C$-enriched (down to 1.1 mM and up to -5.1‰, respectively). Mean values for the drips (i.e., drips 1-5 for trip *n*) tend to mimic that of the pool water. Drip and pool water [DIC] and $\delta^{13}C_{DIC}$ values exhibit a highly significant negative correlation (Fig. 3.5; $r^2 = 0.84$, n = 98) with higher [DIC] being associated with more $^{13}C$-depleted values. "Fast drips" [DIC] range from 5.3 mM to 6.0 mM (Fig. 3.4b) while $\delta^{13}C_{DIC}$ values range from -11.7‰ to -12.9‰ (Fig. 3.4c; Table 3.1). [DIC] and $\delta^{13}C_{DIC}$ values of the "fast drips" fall on the lower end of the linear array (Fig. 3.5) suggesting that the inverse relation between [DIC] and $\delta^{13}C_{DIC}$ is independent of the drip type.

## 6. DISCUSSION

### 6.1. The Initial Composition of Dripwater $\delta^{13}C_{DIC}$

Time-series [DIC] and $\delta^{13}C_{DIC}$ drips data at DeSoto Caverns are likely the products of mixed carbon sources and isotopic fractionations, respectively, occurring during transport from sources to the cave environment sinks. If $\delta^{13}C$ of end-members sources are known and/or can be constrained then $\delta^{13}C_{DIC}$ of drips, prior to reaching the cave environment, can be predicted by modeling the modifications to their $^{13}C/^{12}C$ compositions as the carbon is transported through the aqueous phase. Admittedly complex, the interactions may be simplified by making some reasonable assumptions as follows: (i) C4-type vegetation is absent above the cave, (ii) direct contribution from atmospheric $CO_2$ is negligible and thus can be ignored (Cosford et al., 2009),

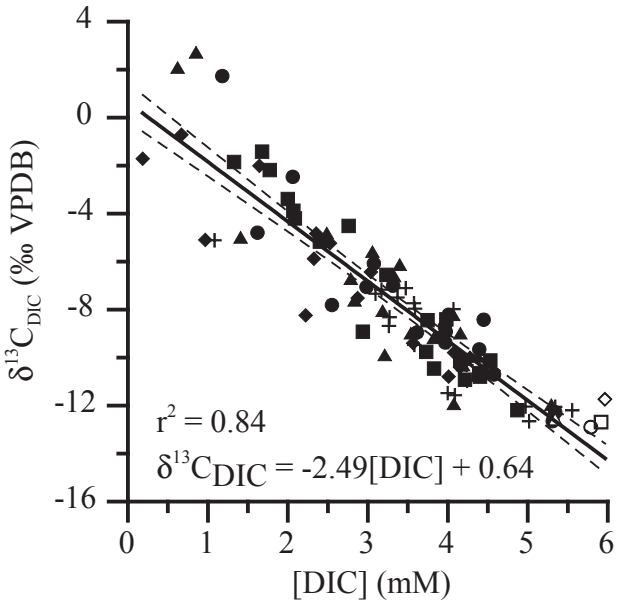


Fig. 3.5. [DIC] vs. $\delta^{13}C_{DIC}$ showing inverse relationship and corresponding 95% confidence intervals. Regression line is based on all cave waters collected in this study. Refer to Fig. 3.2 for drip site locations and symbols.

Table 3.1. Cave water measurements for the June 2009 sampling including "seasonal" and "fast" drips.

| Water Type | Drip Rate (µl/s) | DIC (mM) | $\delta^{13}C_{DIC}$ (‰ VPDB) |
|---|---|---|---|
| "Seasonal" | | | |
| Drip 1 | 13.8 | 5.3 | -12.3 |
| Drip 3 | 2.6 | 4.0 | -10.8 |
| Drip 4 | 8.4 | 4.9 | -12.2 |
| Drip 5 | 16.1 | 5.3 | -12.0 |
| | | | |
| "Fast" | | | |
| Drip 6 | 124.6 | 5.8 | -12.9 |
| Drip 7 | 112.4 | 6.0 | -11.7 |
| Drip 8 | 46.4 | 5.9 | -12.7 |
| Drip 9 | 134.0 | 5.3 | -12.6 |
| | | | |
| Shallow Pool | - | 5.3 | -12.1 |

(iii) chemical reactions accompanied by isotopic fractionations occur at a constant temperature of 17.2 °C which is that of the cave air, (iv) chemical and isotopic equilibrium is achieved during all reactions, (v) $[HCO^{-}_{3(aq)}] \gg [CO_{2(aq)}]$ at pH values of 7. 5 to 7.9 measured in selected drips, (vi) no prior carbonate precipitation takes place in the epikarst above the cave, and (vii) carbon source end-members at DeSoto Caverns have $\delta^{13}C$ values of -26.1‰ (Elkins, 2002) and +1.0‰ (this study) for the C3 biomass and dolomite bedrock, respectively.

The pathway of C from the biomass to caprock dissolution involves a number of isotopic fractionations along the way (Fig. 3.6). First, the $\delta^{13}C$ of respired soil-$CO_2$ is enriched in $^{13}C$ by 4.4‰ relative to the biomass source (Cerling et al., 1991). Second, soil-$CO_2$ in gas form enters the aqueous phase in the vadose zone, resulting in a weak carbonic acid ($H_2CO_3$) that is depleted in $^{13}C$ by about 1.1‰ relative to the $CO_2$ in gas phase (Vogel, 1970). Finally, equal $HCO_3^-$ fractions are produced by the reaction between the carbonic acid and dolomite bedrock interaction assuming that dolomite dissolution occurs in a closed system:

$$MgCa(CO_3)_{2(s)} + 2H_2CO_{3(aq)} \rightarrow Ca^{2+}_{(aq)} + Mg^{2+}_{(aq)} + 4HCO_{3(aq)} \quad (4)$$

The stoichiometry of equation (4) above dictates that half of the produced $HCO_3^-$ (in mol%) is derived from biomass with a $\delta^{13}C$ composition of about -14.0‰ while the other half is derived from dolomite with a $\delta^{13}C$ composition of about -3.1‰ using the isotopic fractionations from the source carbonic acid (+8.8‰, Mook et al., 1974) and the dolomite (-4.1‰, Aharon, 1988), respectively, at the ambient cave temperature of 17.2 °C (Fig. 3.6).

In natural systems however, bedrock dissolution is neither completely open nor closed but rather somewhere in between and likely changing in state throughout the year (Hendy, 1971;

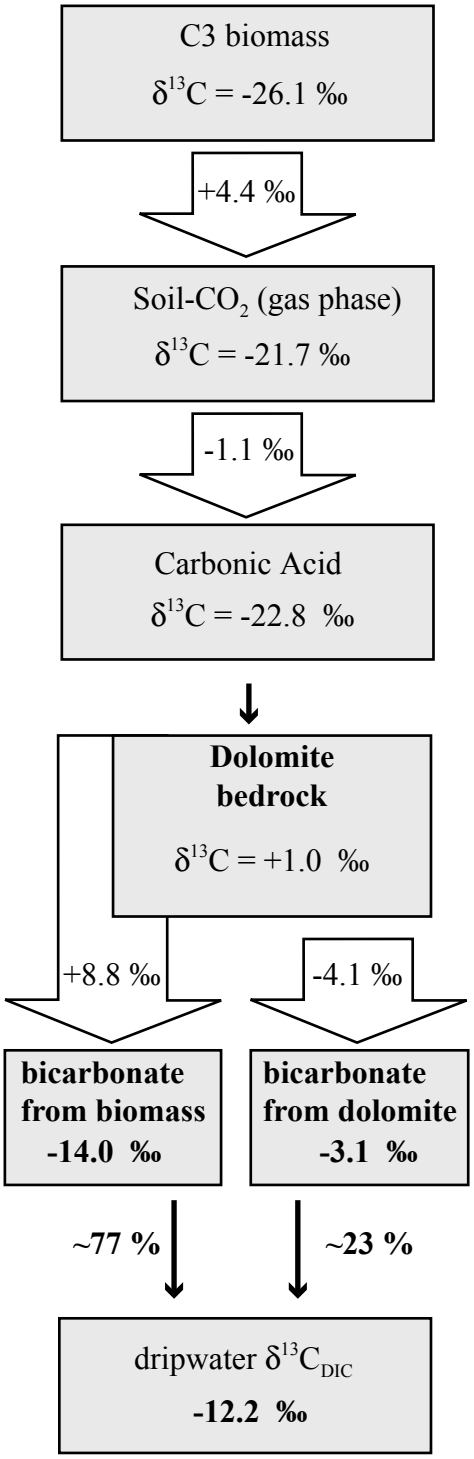


Fig. 3.6. Flow chart of C from C3 biomass and dolomite bedrock sources with associated isotopic fractionations between C species at 17.2 °C given within open arrows. Percent contribution of C from each source was estimated from a radiocarbon measurement of modern aragonite deposition in 2002 (see text).

Fairchild et al., 2006). A radiocarbon measurement of an actively forming aragonite layer sampled in 2002 from a stalagmite top (DSSG-1; Table 3.2) shows that $^{14}$C-dead dolomite contributes, on an annual average, ~23 % of C to the aragonite while the remainder of 77 % is derived from $^{14}$C-live biomass. The dead carbon percent (DCP) contribution to total C was obtained as follows:

$$DCP = \left(1 - \frac{PMC_m}{PMC_{atm}}\right) \times 100 \quad (5)$$

where, $PMC_m$ is the measured percent modern value of the stalagmite top (Table 3.2) and $PMC_{atm}$ is the contemporaneous atmospheric value (110.6 ± 1.6%; McGee et al., 2004; i.e., [1-(85.40/110.6)] x 100 = 22.8%).

Agreement between paired DCP-corrected $^{14}$C (cal yr) and U/Th ages confirms that the estimated ~23 % DCP value contributed annually remained constant at DeSoto over the past 24 ka (Table 3.2). Viewed this way the predicted $\delta^{13}C_{DIC}$ of dripwater entering the DeSoto cave environment is -12.2‰ using the material mass balance equation (6) below which accounts for fractional contributions of C from dolomite and biomass sources, respectively:

$$\delta^{13}C_{DIC} = \frac{\left(\delta^{13}C_{HCO3(dol)} \times \frac{12}{92.2} \times f_{dol}\right) + \left(\delta^{13}C_{HCO3(bio)} \times \frac{12}{62} \times (1 - f_{dol})\right)}{\left(\frac{12}{92.2} \times f_{dol}\right) + \left(\frac{12}{62} \times (1 - f_{dol})\right)} \quad (6)$$

Table 3.2. Paired $^{14}C$ and U/Th data from stalagmites DSSG-1 and DSSG-2 in DeSoto Caverns. Calibrated radiocarbon ages and errors (2σ) were calculated using CALIB 5.0.1 (Stuiver et al., 2005). Radiocarbon measurements were assayed at the NOSAMS facility, USA. U/Th data from Aharon et al. (2009).

| Stalagmite | DBT (mm) | PMC Measured (%) | $^{14}C$ Age Uncorrected (ka) | PMC[a] Corrected (%) | $^{14}C$ Age[b] Corrected (ka) | $^{14}C$ Age (Cal ka BP) | U/Th Age (Cal ka BP) |
|---|---|---|---|---|---|---|---|
| DSSG-1 | 0.5 | 85.40 ± 0.45 | 1.27 ± 0.04 | 110.59 ± 0.45 | -0.81 ± 0.04 | -0.05 ± 0.04 | 0.17 ± 0.18 |
| DSSG-1 | 44.0 | 73.76 ± 0.36 | 2.44 ± 0.04 | 95.52 ± 0.36 | 0.37 ± 0.04 | 0.52 ± 0.04 | 0.55 ± 0.03[c] |
| DSSG-2 | 0.5 | 29.28 ± 0.18 | 9.87 ± 0.05 | 37.92 ± 0.18 | 7.79 ± 0.05 | 8.54 ± 0.11 | 9.92 ± 2.05 |
| DSSG-2 | 62.9 | 21.98 ± 0.21 | 12.15 ± 0.08 | 28.46 ± 0.21 | 10.09 ± 0.08 | 11.66 ± 0.33 | 11.61 ± 0.052 |
| DSSG-2 | 171.8 | 16.60 ± 0.06 | 14.45 ± 0.08 | 21.50 ± 0.06 | 12.35 ± 0.08 | 14.41 ± 0.38 | 14.25 ± 0.56 |
| DSSG-2 | 366.1 | 5.90 ± 0.10 | 22.70 ± 0.13 | 7.64 ± 0.10 | 20.66 ± 0.13 | 24.88 ± 0.50 | 24.24 ± 0.15 |

(a) Calculated using: $PMC_{corr}$ (%) = $PMC_m$/[1-(dcp/100)], where DCP = 22.8 % (see text).
(b) Calculated using: $^{14}C\ Age_{corr}$ (ka) = {-8033 x [ln($PMC_{corr}$/100)]}/1000 (Aharon and Lambert, 2009).
(c) Extrapolated age between points.

where $f_{dol}$ = 0.23 (dolomite fraction) and $\delta^{13}C_{HCO_{3(dol)}}$ = -3.1‰; (1-$f_{dol}$) = 0.77 (fraction of biomass-derived C) and $\delta^{13}C_{HCO_{3(bio)}}$ = -14.0‰ (Fig. 3.6); (12/92.2) and (12/62) are the molar fractions of carbon in dolomite and biomass-derived carbonic acid, respectively.

### 6.2. Carbon Isotope Fractionations in the Cave Environment

The initial $\delta^{13}C_{DIC}$ value of -12.2‰ predicted by the model in Fig. 3.6 is in good agreement with the measured $\delta^{13}C_{DIC}$ values of the drips and pool during the summer/early fall months but substantially more $^{13}C$-depleted relative to drips sampled during the winter/early spring months (range -8‰ to -5‰ excluding the few outliers) (Fig. 3.4c and Appendix 3.1). The discrepancies are likely caused by isotope fractionations occurring subsequent to the drips emergence on the cave ceiling.

Drip DICs are in reality left over residuals after extraction of carbon from the system in the form of degassed $CO_2$ accompanied by transfer of $HCO_3^-$ to the aragonite owing to an increased carbonate saturation state (Spötl et al., 2005). Whether the isotope fractionations accompanying the degassing and carbonate deposition are controlled by equilibrium or kinetic processes are tested using a linear form of the Rayleigh equation (modified after Matthews and Kolodny, 1978 and Bar-Matthews et al., 1996):

$$\ln (\delta^{13}C_t + 1000) = \ln (\delta^{13}C_0 + 1000) + \ln f (\alpha - 1) \quad (7)$$

where, f is the fraction of [DIC] residuals in the drips and $\delta^{13}C_t$ and $\delta^{13}C_0$ are the isotopic compositions of the [DIC] residual at time (t) and initial (0). Following Bar-Matthews et al.

(1996) approach, fraction "f" is calculated by assuming that the drip with the highest [DIC] value emerging on the cave ceiling is representative of the initial DIC reservoir (6.0 mM); thus $f_0 = 1$ and $f_t = [DIC_t]/6.0$ (Fig. 3.7).

Were equilibrium isotope fractionations under a Raleigh distillation system dominant, the DeSoto data would line up along a line whose slope is defined by $1000\ln\alpha = -3.1‰$, assuming DIC is equally partitioned into $CaCO_3$ aragonite and slowly degassed $CO_2$ phases at 17.2 ºC:

$$Ca^{+2}_{(aq)} + 2HCO_{3(aq)} \rightarrow CaCO_{3(s)} + CO_{2(g)} + H_2O_{(aq)} \quad (8)$$

where, $1000\ln\alpha_{CO_2\text{-}HCO_3} = -8.8‰$ (Mook et al., 1974) and $1000\ln\alpha_{CaCO_{3(AR)}\text{-}HCO_3} = 2.7‰$ (Romanek et al., 1992). Instead, the drips and pool data form a linear array defined by a slope of $1000\ln\alpha = -6.7 \pm 0.3‰$, about twice as large as the thermodynamic effect. The results suggest that isotopic equilibrium closely approximates the summer/early fall high DICs with relatively low $\delta^{13}C_{DIC}$ whereas kinetically enhanced isotopic fractionations are prominent during winter/early spring months at lower DICs ($f = 0.7$ to 0.1) and higher $^{13}C$-enrichments. The intercept of the linear array formed by the drips at $f = 1$ yields an initial $\delta^{13}C_{DIC}$ value of $-11.8 \pm 0.3‰$ (Fig. 3.7) that is in good agreement with the initial $\delta^{13}C_{DIC}$ model estimate in Fig. 3.6.

### 6.3. Processes Controlling Drip [DIC] and $\delta^{13}C_{DIC}$ Variability

The time-series carbon chemistry assays at DeSoto raise questions concerning the factors controlling the [DIC] and $\delta^{13}C_{DIC}$ observations: (i) what controls the seasonal variability observed in both [DIC] and $\delta^{13}C_{DIC}$ (Fig. 3.4), (ii) what governs the inverse relation between

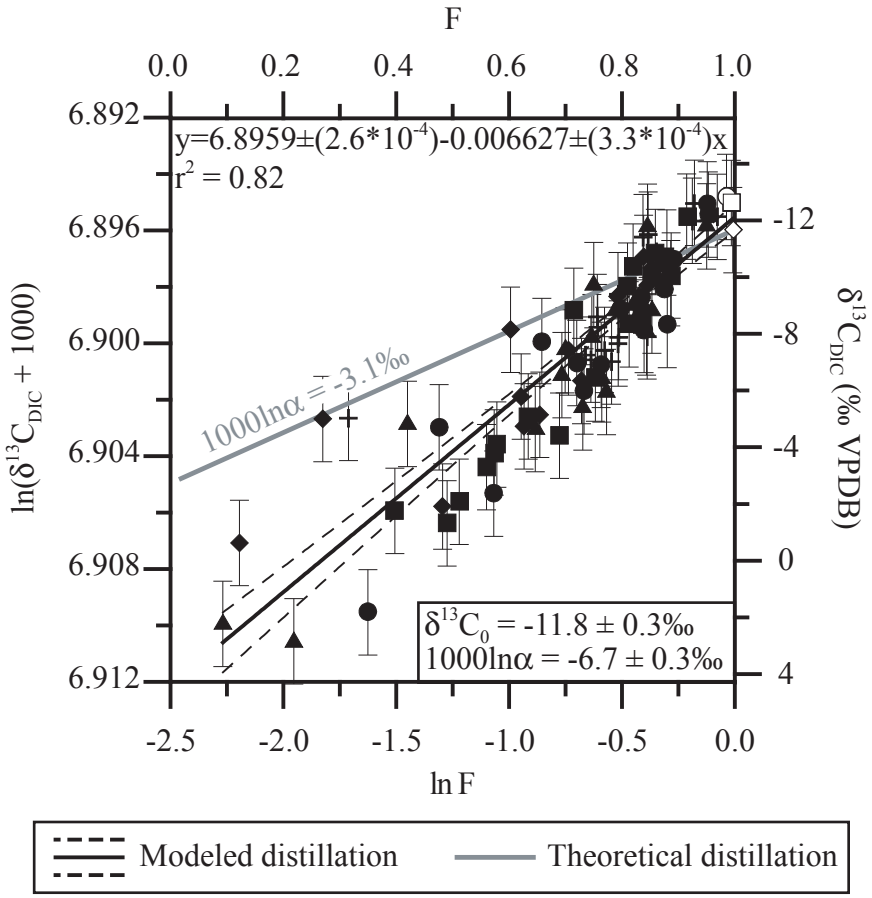


Fig. 3.7. Rayleigh distillation plot modeling the $\delta^{13}C$ fractionation caused by $CO_2$ degassing and carbonate precipitation using data from this study. See text for details regarding calculation of *x* and *y* variables. Note the disagreement between modeled fractionation (slope of linear fit with 95% CI) and theoretical fractionation (gray line). The uncertainties in "*y*" were estimated by means of the principle of maximum likelihood (Taylor, 1982). A single point, drip 3 on sampling trip 10, was an outlier and therefore not included in the plot. Refer to Fig. 3.2 for drip site locations and symbols.

[DIC] and $\delta^{13}C_{DIC}$ (Fig. 3.5), and (iii) why isotopic fractionations between residual [DIC] and degassed $CO_2$ seem to show distinct seasonal preferences?

Two principal factors are likely to control the observed seasonal geochemical variability: (i) differential loading of the infiltrating waters with soil-derived $CO_2$ (Epron et al., 2001), and (ii) density-driven ventilation of the cave chamber (Spötl et al., 2005; Mattey et al., 2008b). Under the regional subtropical climate regime (Fig. 3.3) infiltrating waters experience seasonal loading of $^{13}C$-depleted soil-$CO_2$. This is because higher summer temperatures are promoting plant respiration and oxidation of organic litter while biomass dormancy during the cold winter months accounts for impoverishment of soil-derived $CO_2$ fluxes (Epron et al., 2001). Consequently the net $CO_2$ flux from the epikarst to the cave air is higher in summer and lower in winter (Kowalczk and Froelich, 2010).

Temperature gradients of up to 10 °C between the outside air and the cave air (Fig. 3.3b) cause differential density gradients that control seasonally reversing airflows (Fig. 3.8). During the summer/early fall the cave air temperature is substantially lower than the outside temperature causing a negative pressure gradient. Summer cave air stagnation, produced by diminished reverse airflow (Fig. 3.8a), causes $CO_2$ to build up within the cave chamber as $CO_2$ is continuously delivered to the cave via infiltrating waters from the soil horizon and epikarst. The consequences of the cave air stagnation are anomalously high cave air $pCO_2$, sluggish drip-$CO_2$ degassing, and quasi-equilibrium isotope fractionations under Rayleigh conditions (Fig. 3.7). Conversely, the pressure gradient during the cold winter/early spring is reversed and cold, low $pCO_2$-air, descends from cave entrances that are topographically higher than the cave chambers thus enhancing cave ventilation (Fig. 3.8b). Substantially lower cave-air $pCO_2$ and greater

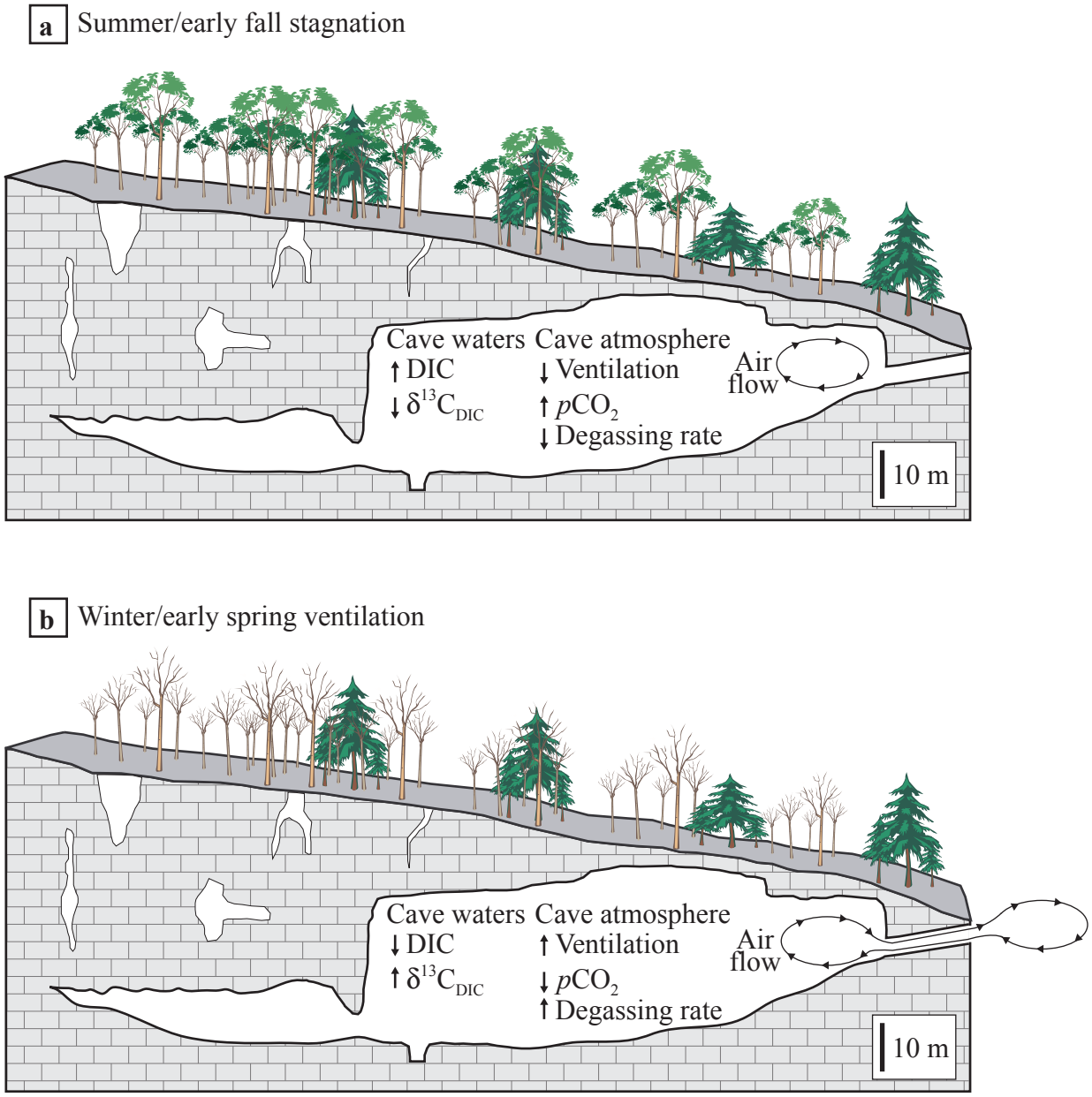


Fig. 3.8. Cross-section sketch of DeSoto Caverns showing seasonally controlled airflow and the ensuing relative changes in air composition and dripwater chemistry. Summer/early fall conditions (a) result in $^{13}C$-depleted DIC while winter/early spring conditions (b) promote $^{13}C$ enrichment of cave waters.

ventilation driving force leads to enhanced $CO_2$ degassing from DIC drips and accounts for the kinetically enhanced isotope fractionations (Fig. 3.7).

The model, indicating a seasonal coupling between $CO_2$ differential loading of the infiltrating waters and seasonally reversed air-flow (Fig. 3.8), is corroborated by the following observations of: (i) seasonal contrasts of up to 5 mM in drips and pool DICs between high summer/early fall and low winter/early spring values (Fig. 3.4b), (ii) inverse relation between $\delta^{13}C_{DIC}$ and [DIC] (Fig. 3.5), and (iii) quasi-equilibrium isotopic fractionations during the summer/early fall and kinetically enhanced isotopic fractionations during winter/early spring (Fig. 3.7) that cannot be explained simply by mixing of end-member carbon sources but require seasonal ventilation affecting the intensity of $CO_2$ forced degassing.

The impact of coupling between seasonal soil-$CO_2$ loading and seasonally reversing air flow on drips DICs and their $\delta^{13}C_{DIC,}$ cave air $pCO_2$ and $\delta^{13}C$ variability of degassed $CO_2$ has been documented in a number of recent studies in Harrison's Cave, Barbados (Mickler et al., 2004), Obir Caves, the Austrian Alps (Spötl et al., 2005) and Hollow Ridge Cave, the Florida Panhandle (Kowalczk and Froelich, 2010). The results of the monitoring investigation of the Hollow Ridge Cave (Kowalczk and Froelich, 2010) are particularly relevant to the study at DeSoto Caverns because of the cave's geographic proximity (Fig. 3.2), corresponding subtropical climate typical of the Gulf Coast region, and physical and air chemistry time-series data that complement the drips carbon chemistry time-series.

The following findings at Hollow Ridge Cave corroborate my data interpretations at DeSoto: (i) net $CO_2$ flux from the epikarst to the cave atmosphere is higher in summer relative to winter by a factor of 6, (ii) cave air $CO_2$ system shows continuous winter ventilation vis-à-vis summer stagnation, and (iii) cave air $pCO_2$ vary seasonally by about a factor of 10, between $10^{-3.4}$ atm in

winter to $10^{-2.4}$ atm in summer resulting from seasonal coupling of reversed density-driven flow and net $CO_2$ flux from the epikarst. In addition, the inverse relation observed between cave air $pCO_2$ and $\delta^{13}C_{AIR}$ at Hollow Ridge Cave (i.e., higher $pCO_2$ corresponding to more negative $\delta^{13}C_{AIR}$) mirrors the inverse relation observed between drip [DIC] and $\delta^{13}C_{DIC}$ at DeSoto (i.e., lower drip [DIC] corresponding to more positive $\delta^{13}C_{DIC}$ thus confirming the proposed impact of coupling between seasonally contrasting net soil $CO_2$ flux and forced $CO_2$ degassing from drips (Fig. 3.5). Viewed in context, the two independent data sets offer compelling evidence that seasonal drops and raises in cave air $pCO_2$ are the dominant cause of preferential loss of isotopically light $CO_2$ to the cave air, corresponding to kinetically enhanced $^{13}C$-enrichments in $\delta^{13}C_{DIC}$ of the residual DICs, whereas isotopically heavier $CO_2$ degassed into the cave air correspond to higher drip DICs and $^{13}C$-depletions in $\delta^{13}C_{DIC}$ approximating quasi-isotopic equilibrium fractionation values under Rayleigh distillation conditions (Fig. 3.7). An apparent absence of a relation documented between the observed logarithmic decline in drip flow rate time-series (Fig. 3.4a), reflecting an interannual drought (Fig. 3.3a), and the drips [DIC] and $\delta^{13}C_{DIC}$ time-series (Figs. 3.4b and c) suggests that the rainfall amount has an inconsequential effect on the drip carbon chemistry relative to the more prominent impact of net carbon flux, cave ventilation, and $CO_2$ degassing variability (Figs. 3.5 and 3.8), and by extension on the $\delta^{13}C$ imprints left by the drips in the speleothems. My data-based interpretations are consistent with the monitoring results of air chemistry time-series from the Hollow Ridge Cave (Kowalczk and Froelich, 2010) and are in agreement with Fairchild and McMillan's (2007) conclusions concerning the retrieval of seasonal processes on the basis of high-resolution stalagmite $\delta^{13}C$ time-series.

### 6.4. Implications for $\delta^{13}C$ Assessment in Speleothems

Processes governing the seasonal [DIC] and $\delta^{13}C$ variability of cave waters, identified in the preceding sections, have an important bearing on the interpretation of $\delta^{13}C$ time-series in speleothems as proxy records of climate-driven carbon flow changes in cave environments. Multi-year monitoring at bimonthly resolution yields meaningful but noisy carbon chemistries at individual drip level (Fig. 3.4). With the exception of isotope profiles at seasonal resolution via the ion microprobe (Orland et al., 2009), present mass spectrometry techniques yield time-series $\delta^{13}C$ records in speleothems that typically have interannual resolution. Thus resolving power disparity between monitored $\delta^{13}C_{DIC}$ and measured speleothem $\delta^{13}C_{AR}$ time-series makes unequivocal assessment of climate-driven controlling factors challenging.

Here I use a two-step approach in order to render useful insight on the factors controlling the interannual $\delta^{13}C$ time-series variability in DeSoto stalagmites. First, I compare the monthly distribution of $\delta^{13}C_{DIC}$ from the shallow pool with $\delta^{13}C$ of aragonite freshly deposited on top of active speleothems (Fig. 3.9a and b). Second, I compare present data with the $\delta^{13}C$ distribution in a 200-year long time-series of an active aragonitic stalagmite sampled at 2-year resolution (Aharon et al., 2009), assuming that present ambient cave conditions have not changed drastically in the past 200 years (Fig. 3.9c and Appendix 3.2). I opted for the shallow pool $\delta^{13}C$ time-series (Fig. 3.4c) instead of the individual drips because the former integrates a number of feeding drips and consequently is substantially less noisy than the latter. In order to facilitate the comparison I recalculated the drips $\delta^{13}C_{DIC}$ to aragonite $\delta^{13}C$ assuming an equilibrium fractionation of 2.7‰ (Romanek et al., 1992). The following observations emerge from the $\delta^{13}C$ histograms in Fig. 3.9.

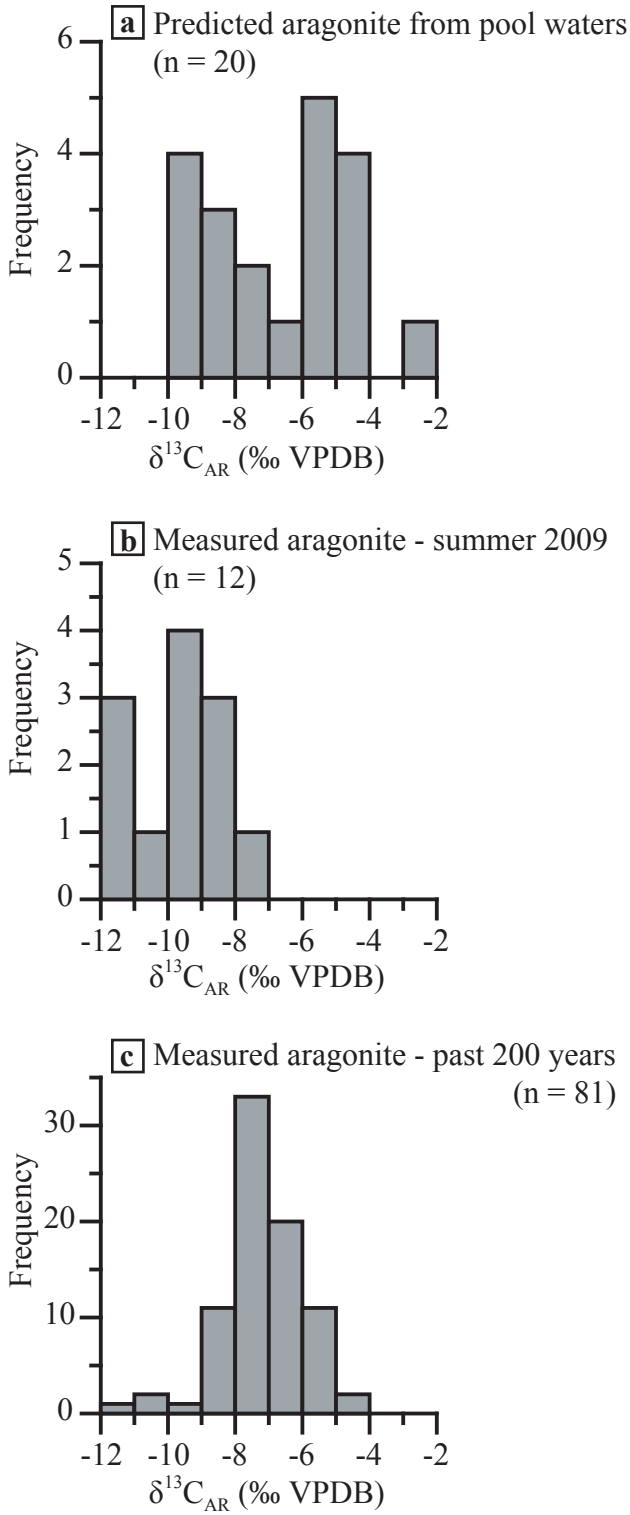


Fig. 3.9. (a) Bimodal distribution of predicted seasonal $\delta^{13}C_{AR}$ based on pool $\delta^{13}C_{DIC}$. (b) Measured$\delta^{13}C_{AR}$ representative of summer (2009) deposition (Table 3.3). (c) Interannually sampled $\delta^{13}C_{AR}$ representative of deposition within the cave over the past ~200 years (Aharon et al., 2009; Appendix 3.2).

(1) The multi-year pool record (n = 20) exhibits a clear bi-modal $\delta^{13}C$ distribution with one mode defined by summer/early fall samples ($mode_1$ = -9‰ to -10‰) and the other defined by winter/early spring samples ($mode_2$ = -4‰ to -5‰) (Fig. 3.9a). The bimodal $\delta^{13}C$ distribution confirms the seasonality model at DeSoto predicted on the basis of seasonal changes in $pCO_2$, $CO_2$ degassing rates, and soil-$CO_2$ fluxes (Fig. 3.8).

(2) The $\delta^{13}C$ of aragonites (n = 12) removed from the surface tips of speleothems during the summer of 2009 (Fig. 3.9b and Table 3.3) show a normal distribution with modal values of -9‰ to -10‰ that are consistent only with $mode_1$ of summer/early fall $\delta^{13}C_{AR}$ values (Fig. 3.9a) thus confirming the coupling between drips and coeval aragonite in their $\delta^{13}C$ seasonality bias.

(3) The $\delta^{13}C$ values (n = 81) of a stalagmite increment spanning the last 200 years show a normal distribution with a mean of -7.1 ± 1.2‰ and a mode of -7‰ to -8‰ (Fig. 3.9c) that are statistically indistinguishable from the mean (-6.6 ± 2.2‰) and annual mode (-6.5‰ to -7.5‰) of the pool. Thus time-series $\delta^{13}C$ records with resolving power >1 year are likely to record a transient mean that integrates the seasonal $\delta^{13}C$ modal changes.

Time-series $\delta^{13}C$ records from stalagmites have been interpreted as proxies of C3 and C4 plants climate-driven turnover above the cave (Dorale et al., 1998; Denniston et al., 2000;

Table 3.3. Carbon isotope compositions of active aragonite precipitation sampled at the end of June 2009.

| Corresponding Drip Type | $\delta^{13}C_{AR}$ (‰ VPDB) |
|---|---|
| seasonal | -11.0 |
| seasonal | -8.4 |
| seasonal | -9.7 |
| seasonal | -8.0 |
| seasonal | -9.3 |
| seasonal | -7.3 |
| fast | -10.0 |
| fast | -9.9 |
| fast | -12.0 |
| fast | -8.6 |
| fast | -11.4 |
| fast | -11.7 |

Cosford et al., 2009), shifts in soil-$CO_2$ inputs caused by changes in rainfall amounts (Yadava and Ramesh, 2005; Drysdale et al., 2006; Verheyden et al., 2008; Jo et al., 2010) and prior precipitation of calcite in the epikarst during dry periods (Johnson et al., 2006). Other studies have concluded that the dominant factor controlling the $\delta^{13}C$ values in stalagmites is $CO_2$ degassing in a Rayleigh distillation system with isotopic exchange between drip [DIC] and degassed $CO_2$ obeying either equilibrium (Bar-Matthews et al., 1996) or large kinetic fractionations (Mickler et al., 2006).

The comparisons in Fig. 3.9 demonstrate the importance of recognizing sampling method and seasonal signal integration (Fairchild et al., 2006). My observations argue in favor of a climate-driven shift in the balance between bimodal winter and summer carbon chemistries as the dominant factor governing the long-term changes in speleothem $\delta^{13}C$. Currently, I am unable to detangle the combined interannual effects of climate-related vegetation change, variable $CO_2$ flux, and alterations in cave air ventilation/degassing rates. The results confirm the importance of in-cave processes controlling the bimodal $\delta^{13}C$ seasonal distributions that are decoupled from above-cave processes (Spötl et al., 2005; Kowalczk and Froelich, 2010) and caution against a simplistic $\delta^{13}C$-vegetation-rainfall amount coupled interpretations.

## 7. CONCLUSIONS

(1) The state of cave air ventilation and differential loading of infiltrating waters with soil-derived $CO_2$ are the dominant controls on seasonal cave water chemistries within DeSoto Caverns. Summer/early fall air stagnation promotes slow degassing of $CO_2$ from cave waters accompanied by quasi-equilibrium isotopic fractionations.

Winter/early spring cave air ventilation promotes forced $CO_2$ degassing and kinetically enhanced rates of $^{13}C$-enrichment of residual [DIC]. Seasonally varying [DIC] concentrations are a function of increased summer $CO_2$ flux via root respiration and organic debris oxidation contrasting with winter drips from which bicarbonate is actively removed due to a higher carbonate saturation state. The combined effects of these processes result in a strong inverse relationship between [DIC] and $\delta^{13}C_{DIC}$.

(2) An interannual trend of decreasing rainfall amounts during the 3-year study is expressed as a logarithmic decrease of dripwater flow rates but has no significant effect on either [DIC] or $\delta^{13}C_{DIC}$ compositions. This implies rainfall amount plays little role in the carbon isotope composition of speleothems within the cave.

(3) Aragonite sampled during summer months suggests deposition is occurring near isotopic equilibrium with source waters. Furthermore, the annual distribution of predicted aragonite $\delta^{13}C$ compositions demonstrate how isotope profiles with interannual resolution integrate isotopically distinct seasonal deposition.

(4) Changes in vegetation alone cannot be used to interpret past variability in speleothem $\delta^{13}C$. One must use additional proxies archived within speleothems to decipher the effects of cave air ventilation, $CO_2$ flux, and changes in seasonal biases in aragonite deposition.

(5) Future monitoring of $CO_2$ levels and their $\delta^{13}C$ compositions coupled with drip [DIC] and $\delta^{13}C$ assays within DeSoto Caverns would assist in quantifying the air exchange with the external atmosphere and confirm the conjectures discussed in this study.

## ACKNOWLEDGMENTS

I thank Tim Lacy and Allen Mathis III for generously allowing free access to the cave for observations and sampling; students and faculty from the University of Alabama, too numerous to list, who joined me in field trips to the cave and provided assistance with sampling of cave waters. This study is a part of the senior author's dissertation research at the University of Alabama. It was partially funded by grants from the Gulf Coast Association of Geological Societies (GCAGS), Geological Society of America, Evolving Earth Foundation, John G. Newton Scholarship of the Alabama Geological Society, and multiple University of Alabama student research and travel grants.

## REFERENCES


Aharon P. (1988) A stable-isotope study of magnesites from the Rum Jungle uranium field, Australia: Implications for the origin of strata-bound massive magnesites. *Chem. Geol.* **69**, 127-145.

Aharon P. and Lambert W. J. (2009) Radiocarbon deficiencies of US Gulf Coast lakes compromise paleo-hurricane records. *Quat. Res.* **71**, 266-270.

Aharon P., Lambert W. J., and Hellstrom, J. (2009) Solar variability controls on rainfall in the last millennia: Evidence from a highly resolved stalagmite record from DeSoto Caverns (USA). *American Geophyiscal Union Fall Meeting*, San Francisco. #PP41B-1514 (abstc.).

Baker A., Ito E., Smart P. L., and McEwan R. F. (1997) Elevated and variable values of $^{13}C$ in speleothems in a British cave system. *Chem. Geol.* **136**, 263-270.

Baker A. and Brunsdon C. (2003) Non-linearities in drip water hydrology: an example from Stump Cross Caverns, Yorkshire. *J. Hydrol.* **277**, 151-163.

Bar-Matthews M., Ayalon A., Matthews A., Sass E., and Halicz L. (1996) Carbon and oxygen isotope study of the active water-carbonate system in a karstic Mediterranean cave: Implications for paleoclimate research in semiarid regions. *Geochim. Cosmochim. Acta* **60**(2), 337-347.

Cerling T. E. and Quade J. (1993) Stable carbon and oxygen isotopes in soil carbonates. In *Climate change in continental isotopic records*, Vol. 78 (eds. P. K. Swart, K. C. Lohmann, J. A. McKenzie, and S. M. Savin). American Union Geophysical Monograph. pp. 217-231

Cerling T. E., Solomon S., Quade J., and Bowman J. R. (1991) On the isotopic composition of carbon in soil carbon dioxide. *Geochem. Cosmochim. Acta* **55**, 3403-3405.

Cosford J., Qing H., Mattey D., Eglington B., and Zhang M. (2009) Climatic and local effects on stalagmite $\delta^{13}C$ values at Lianhua Cave, China. *Palaeogeogr. Palaeoclimatol. Palaeoecol.* **280**, 235-244.

Debajyoti P. and Skrzypek G. (2007) Assessment of carbonate-phosphoric acid analytical technique performed using GasBench II in continuous flow isotope ratio mass spectrometry. *Int. J. Mass Spectrom.* **262**, 180-186.

Delcourt H. R., Delcourt P. A., and Spiker E., C. (1983) A 12000-year record of forest history from Cahaba Pond, St. Clair County, Alabama. *Ecology* **64**(4), 874-887.

Denniston R. F., Gonzalez L., A., Asmerom Y., Reagan M. K., and Recelli-Snyder H. (2000) Speleothem carbon isotopic records of Holocene environments in the Ozark Highlands, USA. *Quat. Int. 1* **67**, 21-27.

Dorale J. A., Edwards R. L., Ito E., and González L. A. (1998) Climate and vegetation history of the midcontinent from 75 to 25 ka: A speleothem record from Crevice Cave, Missouri, USA. *Science* **282**, 1871-1874.

Drysdale R., Zanchetta G., Hellstrom J., Maas R., Fallick A., Pickett M., Cartwright I., and Piccini L. (2006) Late Holocene drought responsible for the collapse of Old World civilizations is recorded in an Italian cave flowstone. *Geology* **34**(2), 101-104.

Epron D., Dantec V. L., Dufrene E., and Granier A. (2001) Seasonal dynamics of soil carbon dioxide efflux and simulated rhizosphere respiration in a beech forest. *Tree Physiol.* **21**, 145-152.

Elkins J. T. (2002) Use of $\delta^{13}C$ values of soil organic matter found in speleothems as a new proxy for paleovegetation and interpreting paleoclimate. Ph.D. thesis, Univ. Georgia.

Fairchild I. J. and McMillan E. A. (2007) Speleothems as indicators of wet and dry periods. *Int. J. Speleol.* **36**(2), 69-74.

Fairchild I. J., Smith C. L., Baker A., Fuller L., Spötl C., Mattey D., McDermott F., and E.I.M.F. (2006) Modification and preservation of environmental signals in speleothems. *Earth Sci. Rev.* **75**, 105-153.

Ferrio J. P., Voltas J., and Araus J. L. (2003) Use of carbon isotope composition in monitoring environmental changes. *Manage. Environ. Qual.* **14**, 82-98.

Fuller L., Baker A., Fairchild I. J., Spötl C., Marca-Bell A., Rowe P., and Dennis P. F. (2008) Isotope hydrology of dripwaters in a Scottish cave and implications for stalagmite palaeoclimate research. *Hydro. Earth Syst. Sci.* **12**, 1065-1074.

Gascoyne M. (1992) Palaeoclimate Determination from Cave Calcite Deposits. *Quat. Sci. Rev.* **11**, 609-632.

Genty D. and Massault M. (1997) Bomb $^{14}C$ recorded in laminated speleothems - part 1: Dead carbon proportion calculation. *Radiocarbon* **39**, 33-48.

Hendy C. H. (1971) The isotopic geochemistry of speleothems--I. The calculation of the effects of different modes of formation on the isotopic composition of speleothems and their applicability as palaeoclimatic indicators. *Geochim. Cosmochim. Acta* **35**, 801-824.

Jo K.-n., Woo K. S., Cheng H., Edwards R. L., Wang Y., Kim R., and Jiang X. (2010) Textural and carbon isotopic evidence of monsoonal changes recorded in a composite-type speleothem from Korea since MIS 5a. *Quat. Res.* **74**, 100-112.

Johnson K. R., Hu C., Belshaw N. S., and Henderson G. M. (2006) Seasonal trace-element and stable-isotope variations in a Chinese speleothem: The potential for high-resolution paleomonsoon reconstruction. *Earth Planet. Sci. Lett.* **244**, 394-407.

Kowalczk A. J. and Froelich P. N. (2010) Cave air ventilation and $CO_2$ outgassing by radon-222 modeling: How fast do caves breathe? *Earth Planet. Sci. Lett.* **289**, 209-219.

Lachniet M. S. (2009) Climatic and environmental controls on speleothem oxygen-isotope values. *Quat. Sci. Rev.* **28**, 412-432.

Lauritzen S.-E. (2003) Reconstructing Holocene climate records from speleothems. In *Global climate change in the Holocene* (eds. A. Mackay, R. Battarbee, J. Birks, and F. Oldfield), Oxford Univ. Press. pp. 242-263.

Lambert W. J. and Aharon P. (2010) Oxygen and hydrogen isotopes of rainfall and dripwater at DeSoto Caverns (Alabama, USA): Key to understanding past climate variability of moisture transport from the Gulf of Mexico. *Geochem. Cosmochim. Acta* **74**, 846-861.

Mattey D., Lowry D., Duffet J., Fisher R., Hodge E., and Frisia S. (2008a) A 53 year seasonally resolved oxygen and carbon isotope record from a modern Gibraltar speleothem: Reconstructed drip water and relationship to local precipitation. *Earth Planet. Sci. Lett.* **269**, 80-95.

Mattey D., Latin J. P., and Ainsworth M. (2008b) Cave monitoring and calibration of a $\delta^{18}O$-climate transfer function for a Gibraltar speleothem. *PAGES News* **16**(3), 15-17.

Matthews A. and Kolodny Y. (1978) Oxygen isotope fractionation in decarbonation metamorphism: The mottled zone event. *Earth Planet. Sci. Lett.* **39**, 179-192.

McDermott F. (2004) Palaeo-climate reconstruction from stable isotope variations in speleothems: a review. *Quat. Sci. Rev.* **23**, 901-918.

McDermott F., Schwarcz H. P., and Rowe P. (2006) Isotopes in speleothem. In *Isotopes in Palaeoenvironmental Research* (ed. M. J. Leng), Springer. pp. 185-226.

McDonald J., Drysdale R., Hill D., Chisari R., and Wong H. (2007) The hydrochemical response of cave drip waters to sub-annual and inter-annual climate variability, Wombeyan Caves, SE Australia. *Chem. Geol.* **244**, 605-623.

McGee E. J., Gallagher D., Mitchell P. I., Baillie M., Brown D., and Keogh S. M. (2004) Recent chronologies for tree rings and terrestrial archives using $^{14}C$ bomb fallout history. *Geochem. Cosmochim. Acta* **68**(11), 2509-2516.

Mickler P. J., Banner J. L., Stern L., Asmerom Y., Edwards R. L., and Ito E. (2004) Stable isotope variations in modern tropical speleothems: Evaluating equilibrium vs. kinetic isotope effects. *Geochem. Cosmochim. Acta* **68**(21), 4381-4393.

Mickler P. J., Stern L. A., and Banner J. L. (2006) Large kinetic isotope effects in modern speleothems. *GSA Bulletin* **118**(1/2), 65-81; doi:10.1130/B25698.1.

Mook W. G., Bommerson J. C., and Staverman W. H. (1974) Carbon dioxide fractionation between dissolved bicarbonate and gaseous carbon dioxide. *Earth Planet. Sci. Lett.* **22**, 169-176.

Orland I. J., Bar-Matthews M., Kita N. T., Ayalon A., Matthews A., and Valley J. W. (2009) Climate deterioration in the East Mediterranean as revealed by ion microprobe analysis of a speleothem that grew from 2.2 to 0.9 ka in Soreq Cave, Israel. *Quat. Res.* **71**, 27-35.

Romanek C. S., Grossman E. L., and Worse J. W. (1992) Carbon isotopic fractionation in synthetic aragonite and calcite: Effects of temperature and precipitation rate. *Geochem. Cosmochim. Acta* **56**, 419-430.

Romanov D., Kaufmann G., and Dreybrodt W. (2008) $\delta^{13}C$ profiles along growth layers of stalagmites: Comparing theoretical and experimental results. *Geochim. Cosmochim. Acta* **72**, 438-448.

Salomons W. and Mook W. G. (1986) Isotope geochemistry of carbonates in the weathering zone. In *Handbook of environmental isotope geochemistry*, Vol. 2. The terrestrial environment (eds. P. Fritz and J. C. Fontes), Elevier. pp. 239-270.

Smart P. L. and Friederich H. (1986) Water movement and storage in the unsaturated zone of a maturely karstified aquifer, Mendip Hills, England. In *Proceedings of the Conference on Environmental Problems in Karst Terrains and Their Solutions*, National Water Wells Association, Bowling Green, KY. pp. 57-87.

Spötl C. (2005) A robust and fast method of sampling and analysis of $\delta^{13}C$ of dissolved inorganic carbon in ground waters. *Isot. Environ. Health Stud.* **41**(3), 217-221.

Spötl C., Fairchild I. J., and Tooth A. F. (2005) Cave air control on dripwater geochemistry, Obir Caves (Austria): Implications for speleothem deposition in dynamically ventilated caves. *Geochem. Cosmochim. Acta* **69**(10), 2457-2468.

Stewart G. R., Turnbull M. H., Schmidt S., and Erskine P. D. (1995) $^{13}C$ natural abundance in plant communities along a rainfall gradient: a biological integrator of water availability. *Aust. J.Plant Physiol.* **22**, 51-55.

Stuiver M, Reimer PJ, Reimer RW (2005) CALIB 5.0.2: Computer program for radiocarbon calibration. URL: http://calib.qub.ac.uk/calib/

Taylor J. R. (1982) *An introduction to error analysis: The study of uncertainties in physical measurements*, University Science Books, Mill Valley, CA.

Verheyden S., Nader F. H., Cheng H. J., Edwards R. L., and Swennen R. (2008) Paleoclimate

reconstruction in the Levant region from the geochemistry of a Holocene stalagmite from the Jeita cave, Lebanon. *Quat. Res.* **70**, 368-381.

Vogel J. C. (1970) Carbon-14 dating of groundwater. In *Isotope Hydrology*, IAEA. pp. 225-239.

Yadava M. G. and Ramesh R. (2005) Monsoon reconstruction from radiocarbon dated tropical Indian speleothems. *The Holocene* **15**(1), 48-59.

CHAPTER 4

# RAINFALL VARIABILITY IN THE SOUTHEAST USA ARCHIVED IN A STALAGMITE FROM DESOTO CAVERNS: IMPLICATIONS OF POLAR JET STREAM MIGRATION DURING THE LAST GLACIAL MAXIMUM AND DEGLACIATION INTERVALS

## ABSTRACT

This study presents a record of rainfall variability in the southeast United States from 31.9 to 11.3 ka BP on the basis of $\delta^{18}O$ and $\delta^{13}C$ measurements of a speleothem from DeSoto Caverns in central Alabama. The record shows that increased winter rainfall in the Southeast is associated with Northern Hemisphere cold phases (i.e., Heinrich events), which are attributed to a southward shift in the polar jet stream accompanied by frequent storm systems and increased contributions of $^{18}O$-depleted rainfall. Conversely, warm phases (i.e., Dansgaard-Oeschger events) are typically represented in the stalagmite record as $^{18}O$ enrichments caused by decreased winter rainfall. The chronology of the events identified in the record, which is based on U/Th (n = 44) and $^{14}C$ (n = 5) determinations, is in better agreement with the timing of glacial events identified in a similar speleothem record from the American Southwest (Fort Stanton Cave) than the chronology of the Greenland ice core GISP2 age model.

Variability of the polar jet stream's path across North America from the Last Glacial Maximum to the start of the Holocene is expressed as in-phase and anti-phase relationships

between winter rainfall amounts in the Southeast and Southwest regions. Between 32 - 22 ka and 17 - 13 ka, north-south migration of the polar jet stream affected winter rainfall in both locations as the Laurentide ice sheet promoted a strong jet stream across the North American South. Persistent infiltration of warm air from the Gulf of Mexico during the Younger Dryas pushed the polar jet northward resulting in dry winters over the Southeast and a hiatus of deposition for the DeSoto stalagmite. The establishment of near modern atmosphere circulation patterns just before the start of the Holocene greatly increased deposition rates of the stalagmite until increased infiltration rates inhibited dripwaters from depositing aragonite after ~11.3 ka. The study presented here fills an important gap in high-resolution continental paleoclimate data for North America and it offers critical data for general circulation models.

# 1. INTRODUCTION

Earth's oceans are the heartbeat for global climate with shifts in circulation patterns (heat transport) and ensuing sea surface temperature changes strongly influencing regional air temperatures and rainfall distribution (Broecker, 2000; Denton and Broecker, 2008). Future disruptions in circulation patterns, such as a shutdown of the thermohaline circulation system in the North Atlantic, are forthcoming; however, predicting the timing of such events and possible triggers of their occurrence by anthropogenic activities is highly debated (Manabe and Stouffer, 1993; Broecker, 1997). Great emphasis has been placed on global circulation models (e.g., COHMAP, 1988; Manabe and Stouffer, 1993) to predict the areas that will be significantly affected given various climate change scenarios. These models are improved when they incorporate past climate events that have been described regionally using climate archives (e.g., lake sediments, long-lived tree species, speleothems, etc.) allowing for confirmation of a model's accuracy or highlighting constraints needing adjustment. An area lacking such field-based climate reconstructions of sufficient temporal resolution is the southeast United States (Wurster, 2001). The Southeast is of great scientific importance as it is directly influenced by changes in northern moisture transport from the Gulf of Mexico (GOM), which is the major moisture source for much of eastern half of North America (Rasmusson, 1968; Bryson and Hare, 1974; Simpkins, 1995).

Paleoclimate reconstructions from ice cores (e.g., GISP2) in Greenland (Fig. 4.1) have revealed dramatic climate swings (many of which were likely caused by changes in ocean circulation) that affected the Northern Hemisphere over the past millennia (Alley et al., 1993; Alley, 2000a; Alley, 2004). Such events are particularly evident during the transition from the

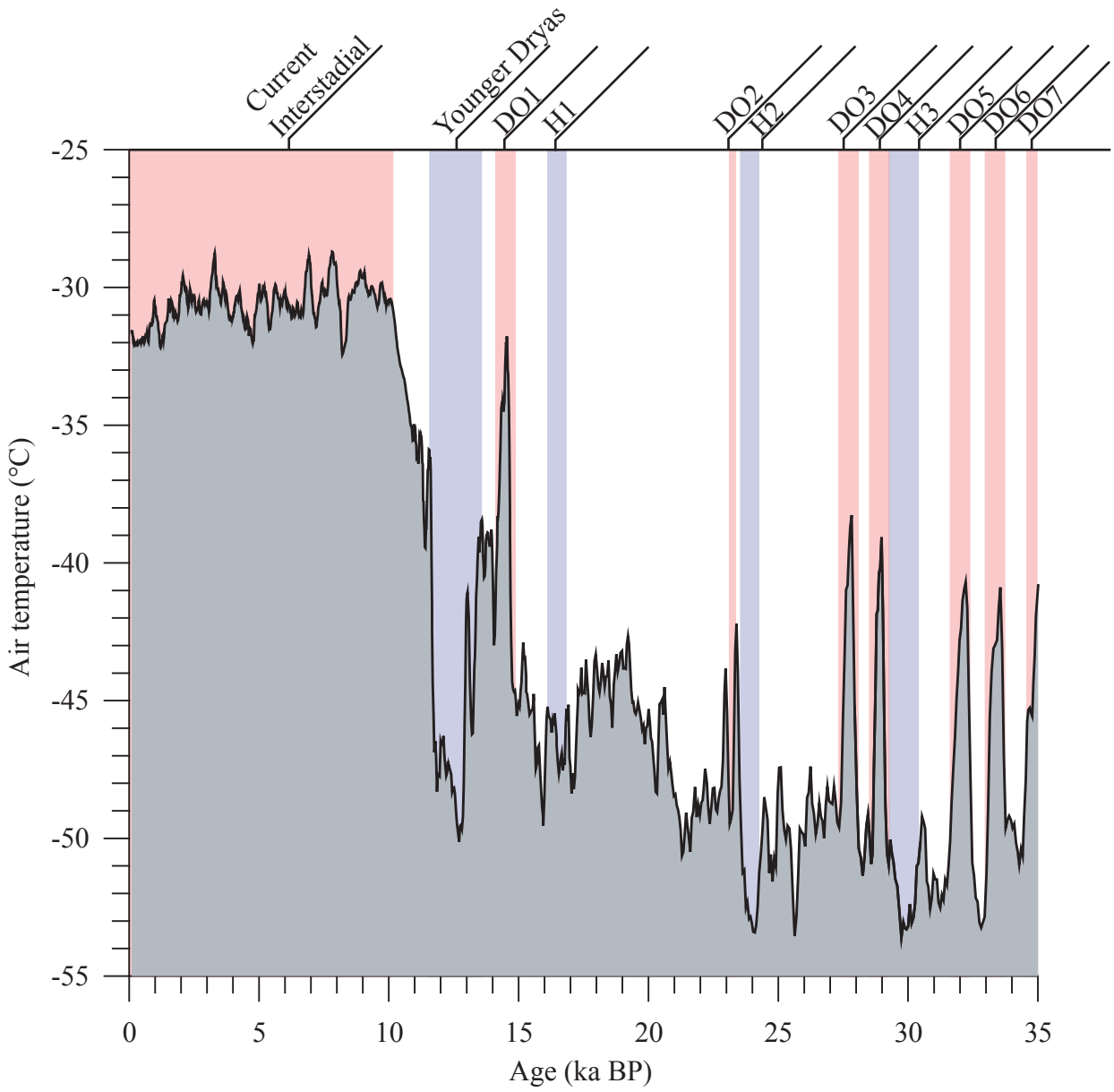


Fig. 4.1. Reconstructed air temperature over central Greenland during the past 35 ka as calculated from $\delta^{18}O$ of GISP2 ice cores (Alley, 2004). Timing and occurrence of cold-phase Heinrich events (H*n*) are based on the work of Hemming (2004). Also shown are prominent warm-phase Dansgaard-Oeschger (DO*n*) events (Heinrich, 1988b; Johnsen et al., 1992; Dansgaard et al., 1993). The Younger Dryas cold event has been suggested to be coeval with H0 (Andrews et al., 1995).

Last Glacial Maximum (LGM) to the current warm interstadial as the general warming trend was punctuated by a number of climate reversals, some of which may have changed phases in less than a decade (Flückiger, 2008). Deep-sea sediment cores taken in the North Atlantic further document periods of climate instability during the LGM as increased concentrations of ice rafted debris is evidence of periodically stronger glacial activity during enhanced cold phases (Heinrich, 1988a). These prominent cold phases, referred to as Heinrich events, often follow warm phases (Dansgaard-Oeschger events) identified from the ice core records (Fig. 4.1) (Johnsen et al., 1992). Although the expression of these events on continental environments is the strongest in the North Atlantic region (e.g., Europe), proxy evidence exists supporting nearly contemporaneous climate swings extending as far south as below the equator (Boës and Fagel, 2008).

In the Northern Hemisphere, scientists have used a vast array of climate archives to map the extent of climate events strongly expressed in the North Atlantic. Lake levels and pollen records give long records of past conditions but are hampered by low temporal resolution. Tree ring reconstructions provide seasonal resolution but their signal is biased toward the spring months and their length rarely exceeds the Holocene (Stahle and Cleaveland, 1992; Stahle and Cleaveland, 1994). Climate reconstructions based on proxy records preserved in speleothems have recently gained widespread attention due to the multiple proxies and accurate chronologies that can be obtained (see recent reviews by McDermott, 2004; Fairchild et al., 2006; Lachniet, 2009). I present here a high-resolution record of carbon and oxygen isotope ratios preserved within a stalagmite and interpret the results in light of paleoclimate conditions for the Southeast during the LGM and deglaciation interval. The stalagmite (DSSG-2) comes from DeSoto Caverns in

central Alabama and is an ideal study site as the karst system's water recharge intercepts moisture from the GOM as it is transported across the eastern half of North America.

## 2. STUDY SITE

### 2.1. DeSoto Caverns

DeSoto Caverns (Fig. 4.2; 33°18'26" N, 86°16'36" W) is a cave within an Upper Ordovician-age dolomite karst system. Its entrance is 170 m above sea level. Located in Childersburg, AL, the site is separated from the GOM by approximately 325 km of low elevation coastal plains. The cave, which is roughly 150 m in length, consists of a large chamber that is overlain by 10 m of bedrock and smaller chambers in the distal portion of the cave where bedrock is substantially thicker (30 – 40 m). Active speleothems within the cave are of aragonite mineralogy.

Stalagmites from within DeSoto Caverns were chosen for paleoclimate investigation because of the cave's proximity to the GOM, ease of accessibility and plethora of active and fossil speleothems. Additionally, the cave system has recently been the focus of thorough monitoring with respect to cave atmosphere conditions, dripwater flow rates, and dripwater chemistry (Lambert and Aharon, 2010; Lambert and Aharon, In Review).

### 2.2. Present-Day Climate

Currently, north central Alabama experiences a humid subtropical climate (Long, 1959).

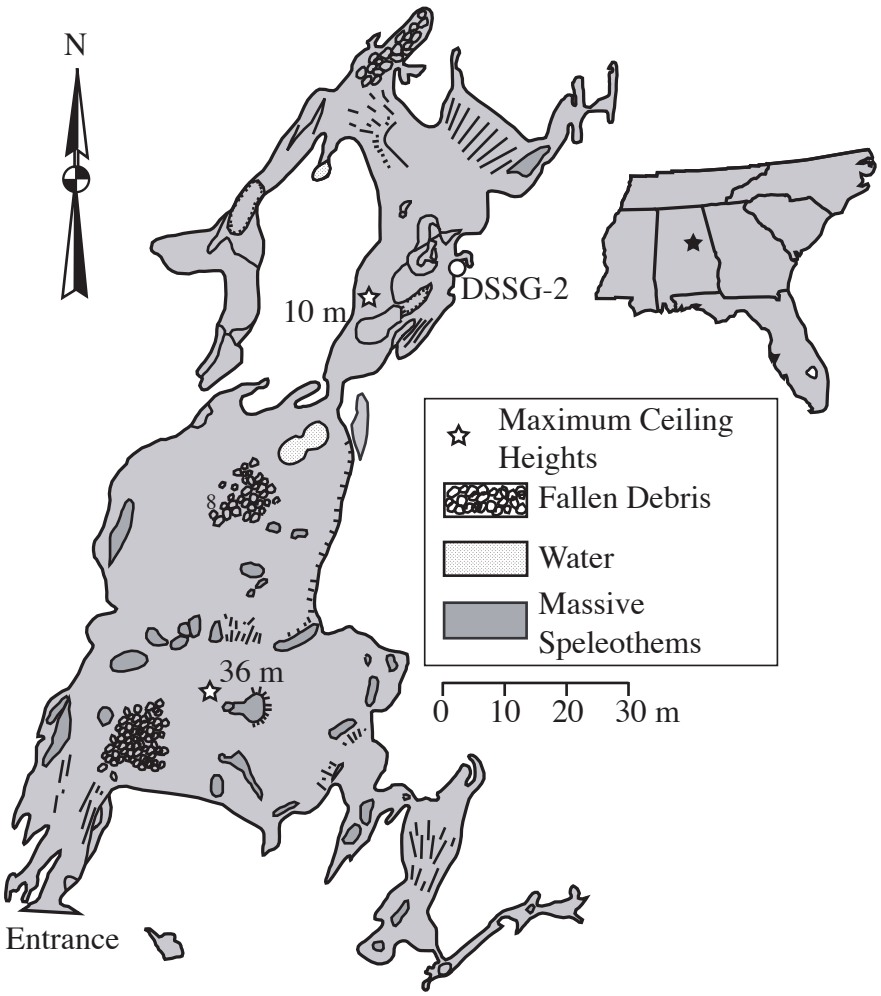


Fig. 4.2. Map (plan view) of DeSoto Caverns with location of stalagmite DSSG-2 (modified after Lambert and Aharon, 2010). Inset map gives approximate location of DeSoto Caverns within the southeast USA.

Outside of DeSoto Caverns the average monthly air temperatures range from ~7 °C in January to ~27 °C in July. Rainfall in Childersburg is generally evenly distributed throughout the year with October (~80 mm) and March (~150 mm) being typically the driest and wettest months, respectively. The mean annual air temperature is 17.2 °C and the average annual total rainfall is 1417 mm based on 1958 to 2004 data (www.ncdc.noaa.gov).

Typically, convection style thunderstorms deliver rainfall during the summer months while fall, winter, and spring rainfall often is associated with frontal systems that are driven west to east by the polar jet stream (PJS). Tropical systems (i.e., hurricanes, tropical storms, tropical depressions) add 40-60 mm of rainfall to north central Alabama each hurricane season (June-November; Knight and Davis, 2007); however, tropical system landfalls are stochastic in nature with large interannual variability.

Extended periods (interannual) of droughts and wet spells in the Southeast, including central Alabama, have been linked to changes in global atmospheric circulation patterns, processes that have recently been addressed in a number of studies (e.g., Katz et al., 2003; Mo and Schemm, 2008, Portmann et al., 2009) and reviewed by Lambert and Aharon (2010). In summary, summer rainfall amounts are highly dependant on the east-west position of the Bermuda High, which directs the path of tropical systems and either enhances or limits landward funneling of moisture from the GOM. Winter/early spring rainfall amounts are a function of the north-south position of the polar jet stream as rain-bearing storm systems are either driven across the Southeast or at a higher latitude, which reduces rainfall amounts for the Southeast.

## 2.3. Previous Work at DeSoto Caverns

Extensive monitoring of DeSoto Caverns was initiated in 2005 to describe the ambient conditions of the cave atmosphere and to characterize the controls on $\delta^{18}O$ and $\delta^{13}C$ variability of dripwater (Lambert and Aharon, 2010; Lambert and Aharon, In Review). This work was crucial to allow for proper interpretation of the proxy records archived in speleothems within the cave. Data loggers left in the cave found both the air temperature (17.2 °C) and relative humidity (>95 %) to be invariant throughout the year regardless of season, which is favorable for limiting unwanted noise from the isotope records. High rates of evapotranspiration reduce aquifer recharge during the summer months and result in seasonal variability in drip flow rates within the cave. Furthermore, a match of average dripwater $\delta^{18}O$ to average winter $\delta^{18}O$ of local rainfall is additional evidence of preferential winter recharge. Despite the seasonal variation in drip flow rates, the aquifer above the cave quickly homogenizes waters from individual storm events leading to dripwater $\delta^{18}O$ that responds to interannual trends in rainfall but not seasonal variation. These interannual trends in both rainfall and dripwater $\delta^{18}O$ are believed to be due to changes in atmospheric circulation; whereas the influence of monthly rainfall amounts and air temperature do not strongly affect present-day $\delta^{18}O$ compositions.

In contrast to the weak seasonality of dripwater $\delta^{18}O$, large seasonal variations (>10‰) were found in $\delta^{13}C$ of dissolved inorganic carbon feeding the deposition of the speleothems (Lambert and Aharon, In Review). Dominant controls over the dripwater $\delta^{13}C$ were determined to include the state of cave air ventilation and differential loading of infiltrating waters with soil-derived $CO_2$. Comparison with recently deposited aragonitic speleothems within the cave suggests climate-driven shifts in the balance between winter and summer carbon chemistries is the

dominant factor governing long-term changes in speleothem $\delta^{13}C$ (Lambert and Aharon, In Review). Therefore, the state of cave ventilation and soil-$CO_2$ flux at the time of past deposition must be considered when interpreting the $\delta^{13}C$ signal preserved within stalagmites of DeSoto Caverns.

## 3. MATERIALS AND METHODS

Stalagmite DSSG-2 was removed from the back portion of DeSoto Caverns in 2005 (Fig. 4.2). The stalagmite was chosen from this location because of the stable atmosphere deep within the cave (Lambert and Aharon, 2010) and because the water-supplying stalactite was <1 m above DSSG-2. Once in the laboratory, the stalagmite was halved vertically using a water-cooled saw with diamond blade to expose the central growth axis. However, before halving, the top ~10 cm was removed (horizontal cut) because the vertical growth of the stalagmite was not straight thus preventing a single pass from the saw blade to create equal halves. One half of DSSG-2 was set aside as an archive specimen and was untouched. The sample half was cut into slabs approximately 1 cm thick with the centermost slab (Fig. 4.3) dedicated for sampling for age dates, isotope assays, and mineralogical analysis by X-ray diffraction (XRD). A second slab, offset from the central growth axis by ~1 cm, provided material for thin-sections.

### 3.1. Petrography and XRD

A total of 8 large (50 mm x 75 mm) thin-sections were made to cover the entire length of DSSG-2. Typically, thin-sections were prepared with a thickness of 100-200 μm, which was


Fig. 4.3. Photograph of sectioned slab of stalagmite DSSG-2 from which materials were removed for radiometric dating and stable isotope analysis. The stalagmite was cut horizontally at ~10 cm DBT to allow proper vertical cuts.

conducive to observation of growth laminae; however, duplicate thin-sections of ~30 μm thickness were made of areas where petrographic inspection was desired. Crystal structure and growth patterns were viewed under transmitted and reflected light using a Nikon stereoscopic zoom microscope (model SMZ 800) equipped with a 2.0 megapixel digital camera (Spot Insight QE). Laminae thicknesses and other measurements on captured images were determined using digital software (Spot Advanced v. 4.0), which was calibrated against a transparent micrometer at varying degrees of magnification. Laminae counts and thicknesses could not be accounted for between the top two thin-sections and where the top of the stalagmite was cut horizontally (Fig. 4.3). For these missing intervals, the vertical length of lost material was calculated based on the saw blade thickness. An estimate of the number of missing bands was derived by taking the average band thickness for 20 mm above and below each saw cut. Mineral types observed microscopically were confirmed with by XRD patterns that were acquired by a Bruker D8 Advance diffractometer with a Vantec-1 detector.

### 3.2. Radiometric Age Determinations

Aliquots of material for $^{14}C$ and U/Th age determinations were removed along the central growth axis using a bench style drill with flexible shaft. A foot pedal controlled the speed of a 1-mm dental bit and allowed for precise removal of carbonate along growth layers of the same stratigraphic age. For $^{14}C$ samples, approximately 5 mg of drilled material was converted to $CO_2$ gas and sealed in glass vials before shipment to the National Ocean Sciences Accelerator Mass Spectrometry Facility in Woods Hole, MA. Reported $^{14}C$ ages were converted to calendar years using the Internet accessible CALIB 5.0.2 (Stuiver et al., 2005). U/Th age determinations were

carried out by using the parallel ion-counting capability of an MC-ICP-MS, which allows simultaneous measurement of the activity ratios of the desired elements from a single solution. Ages were corrected for detrital Th contamination using a value of 0.65 ± 0.30 for the initial $^{230}Th/^{232}Th$ activity for DeSoto Caverns samples therefore giving an absolute age relative to the date of measurement. To allow proper comparison to calibrated radiocarbon ages, U/Th ages were adjusted to years before present (yrs BP) relative to 1950 rather than date of measurement (e.g., 2006). Detailed discussion of U-series dating techniques used in this study can be found in Hellstrom (2006).

### 3.3. Stable Isotopes

Powdered material (50-100 μg) for stable isotope analysis was removed along the central growth axis of DSSG-2 by means of a New Wave Research/Merchantech micromill with sub-micron position control. Drilling increments were typically 300 μm but a second drilling profile at 100 μm was needed between 157-181 mm depth below top (DBT) to improve the sampling resolution where deposition rates were slow. A method of testing for isotopic equilibrium ("Hendy Test") during carbonate precipitation required micro-sampling within a single growth (annual) lamina in which case material was drilled directly from thin-sections using the Micromill's transmitted light source and software. C and O isotopic compositions of $CaCO_3$ were carried out on a GasBench-IRMS system by implementing methods similar to that described by Debajyoti and Skrzypek (2007). Both C and O isotope values are expressed in per mil (‰) relative to the Vienna Pee Dee Belemnite (VPDB) scale by use of the NBS-19 standard. Standard corrections to all measured carbonate $^{18}O$ compositions were made to account for

reaction temperature (50 °C). For aragonitic samples, an additional correction (-0.34‰) was needed to account for differences in acid-carbonate fractionations for sample aragonite and NBS-19 calcite materials (Kim et al., 2007). Reproducibility (1σ) for both $\delta^{13}C$ and $\delta^{18}O$ was calculated to be ± 0.1‰ based on NBS-19 and sample repeats.

## 4. RESULTS

### 4.1. Petrography

Typically stalagmites are calcitic in nature with aragonitic mineralogy being uncommon (Hill and Forti, 1986). Because of the important implications mineralogy type has on the geochemical properties of materials under analysis it was crucial to evaluate the mineralogy of the entire depositional history of DSSG-2. In general, much of the stalagmite can be described as pure white carbonate material; however, areas possessing a reddish-brown tint were also observed, typically in the lower and central portions of the sample (Fig. 4.3). When thin-sections were inspected under transmitted light, the white carbonate was found to be more opaque relative to the reddish-brown areas (generally translucent). Multiple XRD analyzes (n = 24) revealed the white (opaque) carbonate to be mostly aragonite while the reddish-brown (translucent) carbonate was predominantly calcite. Due to the optical characteristics of the two mineralogy types under both reflected and transmitted light sources, it was possible to map the general distribution of aragonite and calcite for DSSG-2 (Fig. 4.4).

It is feasible for both primary calcite and aragonite to be precipitated within the same speleothem (Railsback et al., 1994) or for secondary calcite to replace meta-stable aragonite

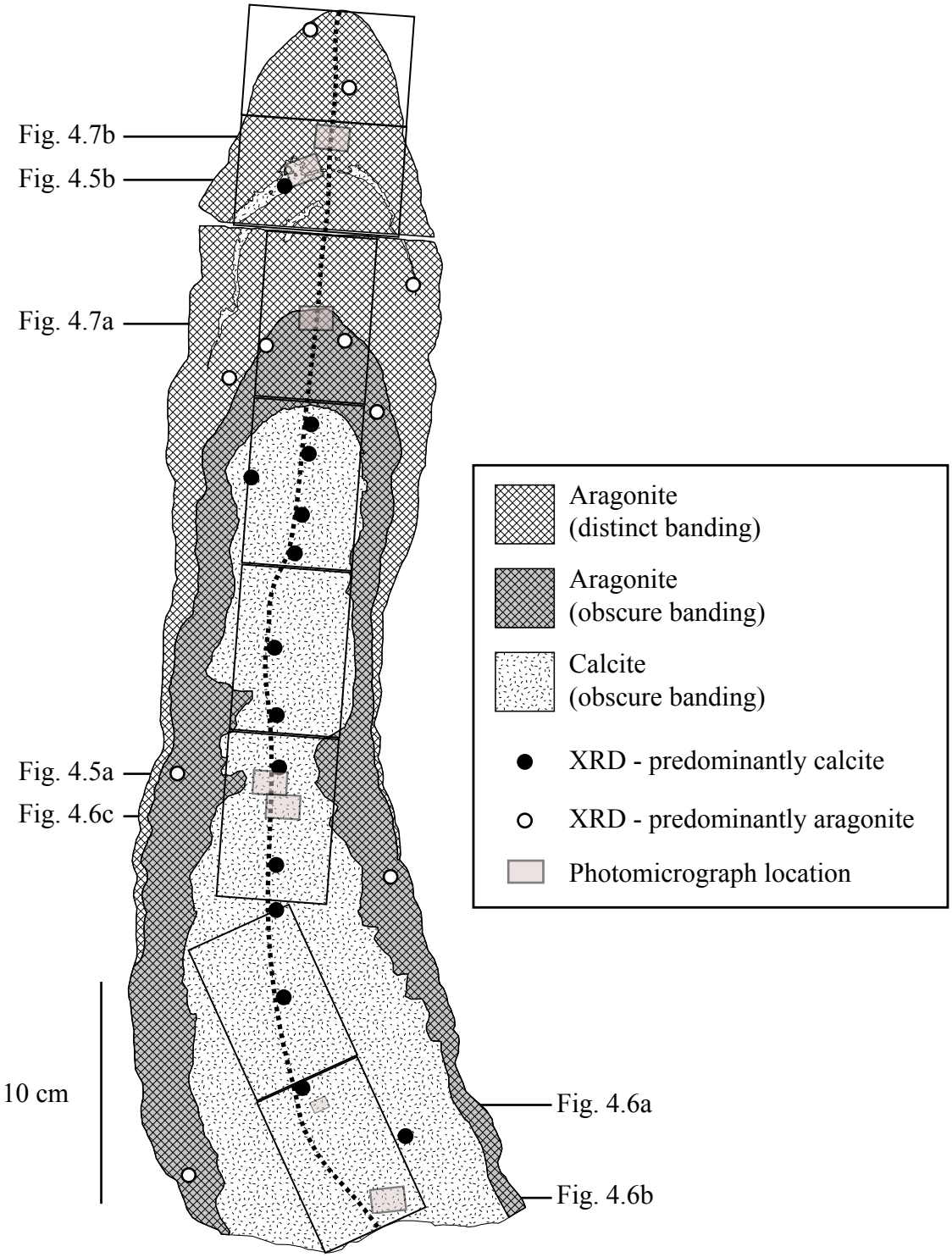


Fig. 4.4. Generalized distribution of areas of aragonite and calcite within DSSG-2 based on optical observations and XRD analysis (circles). Zones of various growth band prominence are also mapped. Open boxes show location of thin-sections used to describe mineralogy (different slab). Small gray boxes show approximate location of photomicrographs in Figs. 4.5-7. Dashed line marks profile for stable isotope sampling along central growth axis. The total length of the sampling axis is 54.7 cm.

(Frisia et al., 2002). Close examination of the petrographic relationships found in DSSG-2 suggests the majority of identified calcite has replaced the initially deposited aragonite; a process that has been observed is other cave environments (Martín-García, et al., 2009; Woo and Choi, 2006). Evidence for this process occurring in DeSoto Caverns is based on: (i) remnant aragonite crystal structures (i.e., radiating botryoids) found within areas of calcite (Fig. 4.5a), and (ii) numerous examples of aragonite laminae that are crosscut by calcite (Fig. 4.5b), a characteristic not found with primary deposition. The replacement appears to have been accomplished by neomorphism, a process where aragonite is replaced at a micron level allowing for the preservation of growth laminae and aragonite fabrics (Folk, 1965; Pingitore, 1976; Mazzullo, 1980). The secondary calcite displays two prominent crystal structures described here as: (i) sparry, with irregularly shaped crystals but generally of equal length in all directions (Fig. 4.6a), and (ii) columnar, having a more organized pattern of elongated crystals (Fig. 4.6b). In many cases the differing calcite crystal structures were intertwined with each other rather than separated by a clear boundary (Fig. 4.6c). The geochemical processes controlling aragonite replacement and varying secondary calcite crystallography are poorly understood and are beyond the scope of this research; although, the topic has been addressed by Cabrol and Coudray (1982) and Frisia et al. (2002).

Laminae found in DSSG-2 display two major depositional styles likely indicating different growth rate regimes with a sharp boundary separating the two at 136.7 mm DBT. The majority of growth laminae (136.7 mm – 547.4 mm) can be described as visible bundles encasing obscure and less visible bands whose thicknesses are typically <100 μm (Fig. 4.7a). Because of the large variations in laminae prominence and difficulty in resolving individual laminae optically, counting and detailed thicknesses of laminae below 136.7 mm was not possible. For the upper

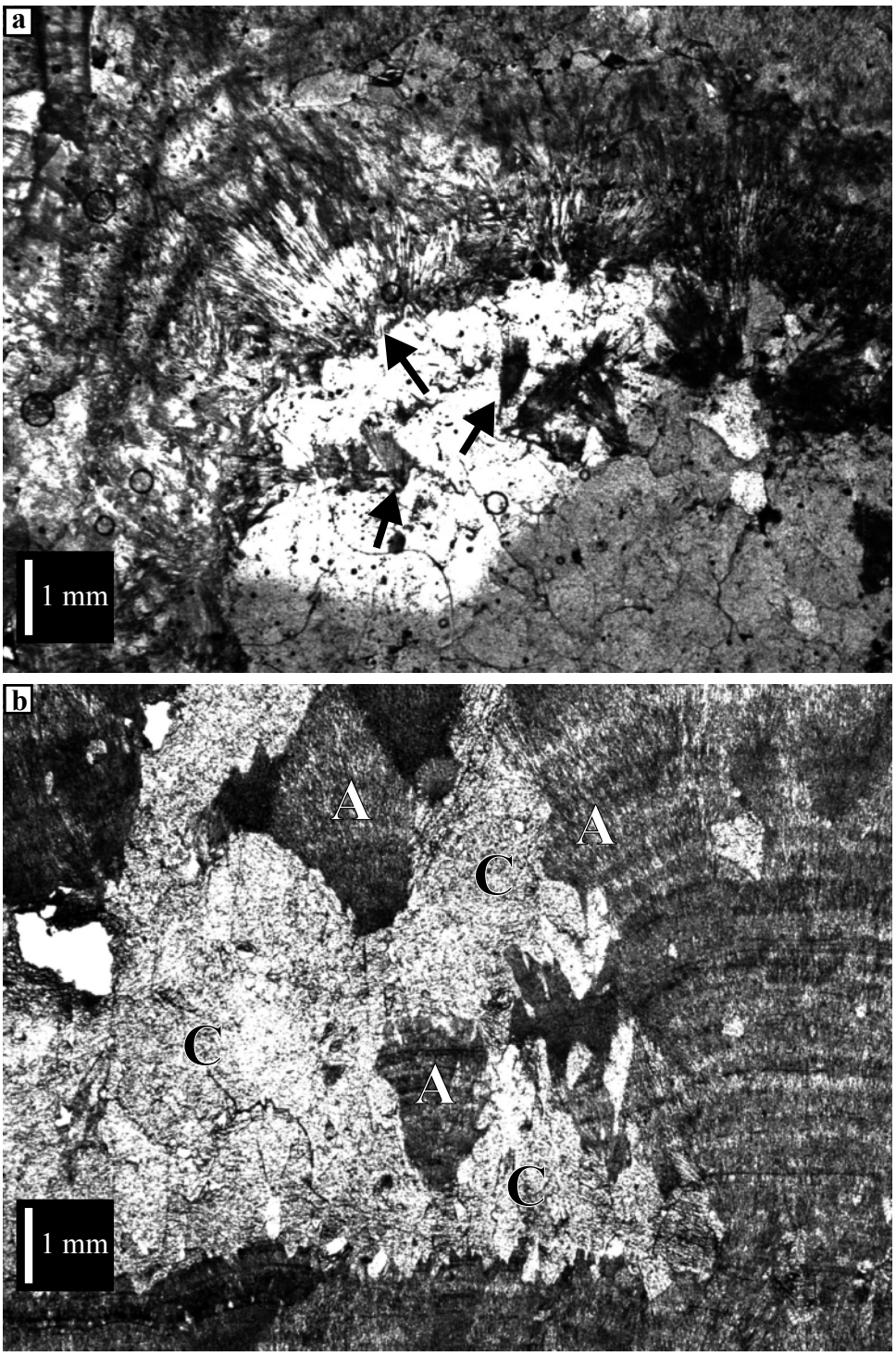


Fig. 4.5. (a) Relics of aragonite botryoids (black arrows) in calcite (10x; transmitted light). (b) Layered aragonite (A) cross-cut by secondary calcite (C) (10x; transmitted light). Refer to Fig. 4.4 for photomicrograph locations.

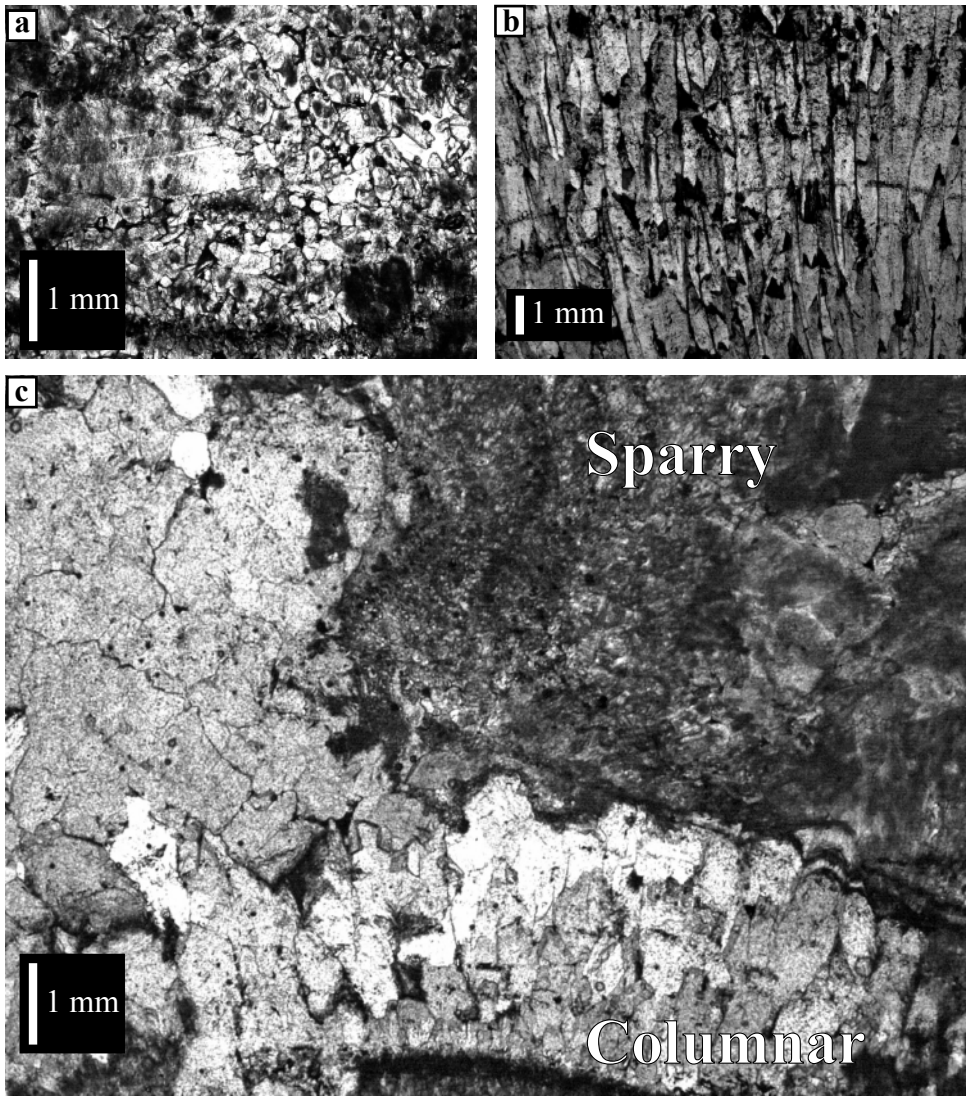


Fig. 4.6. Representative examples of (a) sparry (20x) and (b) columnar (10x) calcite crystals commonly found in DSSG-2 (transmitted light). (c) Complex nature of calcite crystal type distribution (10x; transmitted light). Refer to Fig. 4.4 for photomicrograph locations.

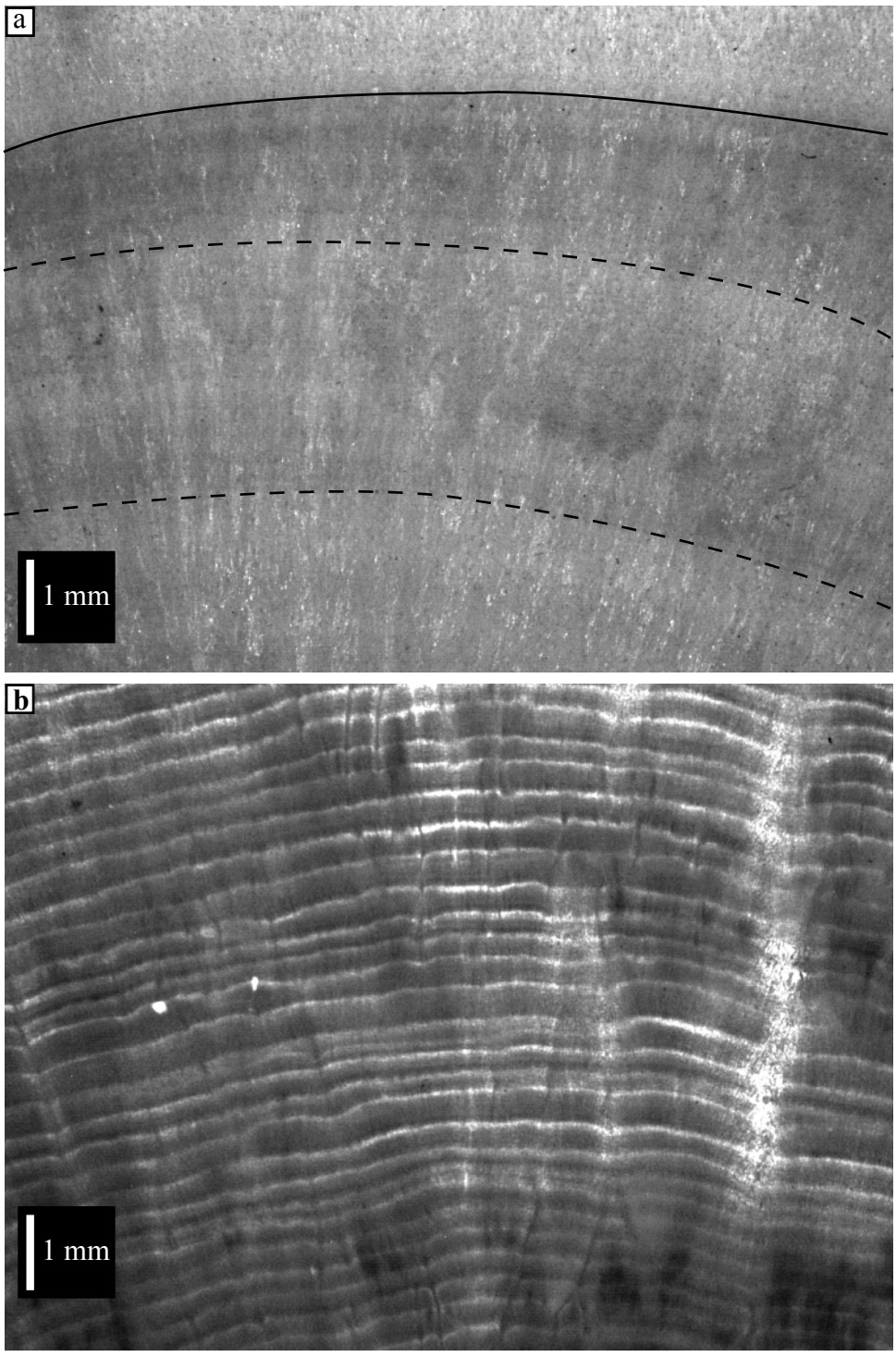


Fig. 4.7. Common growth styles observed in DSSG-2. (a) Visible bundles encasing obscure bands (10x; reflected light). Dashed lines divide bundles. The solid line indicates transition of growth styles. (b) Distinct banding common for the upper 136.7 mm of DSSG-2 (10x; transmitted light). Refer to Fig. 4.4 for photomicrograph locations.

portion of DSSG-2, growth laminae are very distinct with couplets of white and dark material whose total thicknesses are regular and typically between 200-300 μm (Fig. 4.7b).

### 4.2. Age Model

Development of a proper chronology for the deposition of stalagmites hinges on the application of multiple dating techniques to validate acceptance of an age model. In this study, I rely not only on densely spaced U/Th age determinations but also incorporate laminae counting (where possible) and radiocarbon to give age estimates that are independent of the U/Th system. Furthermore, close inspection of the thin-sections aided identifying possible hiatuses in growth. The results of this methodology suggests DSSG-2 was deposited between ~31.9 ka BP and 11.3 ka (kilo-annum) BP with a period of non-deposition occurring between ~12.9 ka BP and 11.9 ka BP.

All U/Th ages (44) are plotted in ka BP relative to sampling DBT in Fig. 4.8 and are listed in stratigraphic order along with their detailed geochemical compositions in Table 4.1. Concentrations of U ranged from 0.037 ppm to 4.944 ppm, although most (63 %) samples contained >1.0 ppm. Radiocarbon age calculations (n = 5; Table 4.2) must take into account mixing of $^{14}$C-dead carbon incorporated into the stalagmite, which gives falsely great ages, from the Ordovician dolomite above the cave. Here, I use a value of 23 % for the dead carbon percentage (DCP), which is based on the radiocarbon age (1270 $^{14}$C yrs BP) for modern deposition sampled in 2002 (Lambert and Aharon, In Review). Assuming the DCP has remained constant during the deposition of DSSG-2, this correction appears suitable as adjusted radiocarbon ages that have been converted to calendar years are identical within measurement

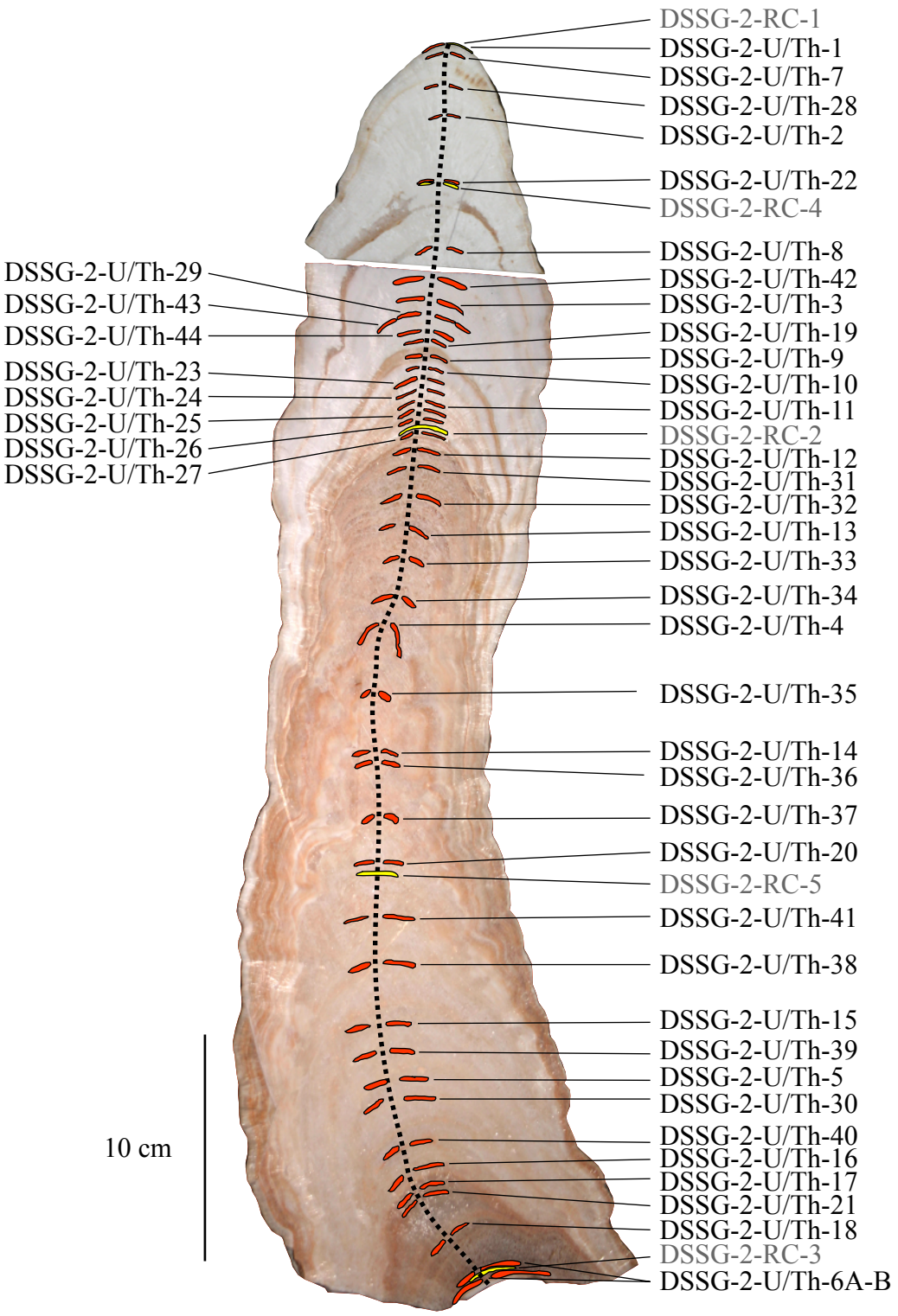


Fig. 4.8. U/Th (red) and radiocarbon (yellow) dates drilled in DSSG-2. The vertical dashed line represents the axis sampled for stable isotope ratios. Age date information is presented in Table 4.1 and Table 4.2 for U/Th and radiocarbon, respectively.

Table 4.1. U-series data and calculated ages for speleothem DSSG-2 from DeSoto Caverns.

| Sample DSSG-2- | Year meas | Depth (mm)[a] | U (ppm) | $^{234}U/^{238}U$ activity | $^{234}U/^{238}U$ activity (i) | $^{230}Th/^{238}U$ activity | Uncorrected Age (ka)[b] | $^{230}Th/^{232}Th$ activity | Corrected age (ka BP)[c] |
|---|---|---|---|---|---|---|---|---|---|
| U/Th-1 | 2006 | 0.5 | 1.146 | 1.760±0.004 | 1.786±0.004 | 0.186±0.0009 | 12.047±0.062 | 8 | 9.920±2.051[g] |
| U/Th-7 | 2007 | 4.0 | 2.253 | 1.731±0.003 | 1.755±0.003 | 0.174±0.0008 | 11.458±0.055 | 3942 | 11.395±0.060[d] |
| U/Th-28 | 2008 | 19.6 | 1.144 | 1.706±0.003 | 1.729±0.003 | 0.170±0.0007 | 11.335±0.050 | 479 | 11.260±0.062[d] |
| U/Th-2 | 2006 | 32.1 | 0.960 | 1.695±0.003 | 1.718±0.003 | 0.169±0.0013 | 11.319±0.086 | 1522 | 11.252±0.095[d] |
| U/Th-22 | 2008 | 61.7 | 4.805 | 1.681±0.003 | 1.704±0.003 | 0.172±0.0007 | 11.648±0.050 | 26731 | 11.606±0.052[d] |
| U/Th-8 | 2007 | 88.9 | 3.959 | 1.658±0.003 | 1.680±0.004 | 0.172±0.0014 | 11.804±0.099 | 19609 | 11.748±0.103[d] |
| U/Th-42 | 2009 | 109.3 | 2.984 | 1.669±0.003 | 1.693±0.003 | 0.175±0.0013 | 11.981±0.089 | 5870 | 11.919±0.095[d] |
| U/Th-3 | 2006 | 120.4 | 1.157 | 1.691±0.003 | 1.715±0.003 | 0.176±0.0008 | 11.876±0.059 | 979 | 11.801±0.067[d] |
| U/Th-29 | 2008 | 126.8 | 1.588 | 1.678±0.003 | 1.703±0.003 | 0.189±0.0011 | 12.898±0.080 | 46 | 12.699±0.115[g] |
| U/Th-43 | 2009 | 126.8 | 1.493 | 1.684±0.004 | 1.708±0.004 | 0.176±0.0016 | 11.940±0.109 | 2406 | 11.876±0.118[d] |
| U/Th-44 | 2009 | 129.7 | 1.240 | 1.696±0.004 | 1.720±0.036 | 0.176±0.0019 | 11.817±0.128 | 4689 | 11.753±0.135[d] |
| U/Th-19 | 2007 | 137.3 | 0.170 | 1.674±0.003 | 1.697±0.004 | 0.173±0.0019 | 11.756±0.131 | 386 | 11.661±0.141[d] |
| U/Th-9 | 2007 | 141.6 | 0.967 | 1.829±0.003 | 1.861±0.003 | 0.212±0.0011 | 13.297±0.069 | 146 | 13.115±0.144[e] |
| U/Th-10 | 2007 | 146.9 | 0.874 | 1.840±0.003 | 1.872±0.004 | 0.217±0.0013 | 13.547±0.084 | 961 | 13.471±0.092[f] |
| U/Th-23 | 2008 | 152.2 | 0.813 | 1.858±0.003 | 1.893±0.003 | 0.225±0.0010 | 13.900±0.065 | 395 | 13.815±0.087[f] |
| U/Th-24 | 2008 | 157.2 | 0.755 | 1.882±0.004 | 1.918±0.004 | 0.231±0.0014 | 14.077±0.089 | 222 | 13.958±0.127[f] |
| U/Th-11 | 2007 | 161.5 | 1.276 | 1.843±0.003 | 1.878±0.003 | 0.231±0.0008 | 14.394±0.056 | 96 | 14.132±0.226[f] |
| U/Th-25 | 2008 | 165.1 | 0.896 | 1.839±0.003 | 1.875±0.003 | 0.233±0.0009 | 14.561±0.061 | 469 | 14.484±0.076[f] |
| U/Th-26 | 2008 | 168.8 | 0.446 | 1.859±0.004 | 1.896±0.004 | 0.239±0.0016 | 14.810±0.101 | 39 | 14.254±0.557[f] |
| U/Th-27 | 2008 | 174.9 | 0.864 | 1.850±0.004 | 1.888±0.004 | 0.246±0.0015 | 15.352±0.097 | 90 | 15.089±0.256[e] |
| U/Th-12 | 2007 | 178.4 | 1.276 | 1.828±0.003 | 1.867±0.003 | 0.256±0.0011 | 16.214±0.073 | 37 | 15.569±0.612[e] |
| U/Th-31 | 2009 | 187.4 | 1.346 | 1.848±0.004 | 1.899±0.005 | 0.324±0.0023 | 20.660±0.160 | 180 | 20.439±0.217[g] |
| U/Th-32 | 2009 | 198.7 | 1.179 | 1.866±0.003 | 1.912±0.003 | 0.297±0.0017 | 18.615±0.113 | 296 | 18.471±0.149[g] |
| U/Th-13 | 2007 | 209.6 | 0.666 | 1.868±0.003 | 1.914±0.003 | 0.289±0.0018 | 18.056±0.117 | 39 | 17.356±0.631[f] |
| U/Th-33 | 2009 | 224.6 | 0.930 | 1.856±0.005 | 1.901±0.005 | 0.290±0.0024 | 18.280±0.161 | 220 | 18.102±0.208[f] |
| U/Th-34 | 2009 | 245.8 | 1.054 | 1.839±0.003 | 1.887±0.003 | 0.307±0.0015 | 19.615±0.101 | 313 | 19.474±0.142[e] |
| U/Th-4 | 2006 | 258.5 | 0.640 | 1.793±0.003 | 1.844±0.003 | 0.331±0.0010 | 21.880±0.073 | 34 | 20.952±0.885[f] |

| Sample DSSG-2 | Year meas | Depth (mm)[a] | U (ppm) | $^{234}U/^{238}U$ activity | $^{234}U/^{238}U$ activity (i) | $^{230}Th/^{238}U$ activity | Uncorrected Age (ka)[b] | $^{230}Th/^{232}Th$ activity | Corrected age (ka BP)[c] |
|---|---|---|---|---|---|---|---|---|---|
| U/Th-35 | 2009 | 285.3 | 2.274 | 1.771±0.003 | 1.821±0.003 | 0.332±0.0014 | 22.215±0.105 | 452 | 22.089±0.133[e] |
| U/Th-14 | 2007 | 314.3 | 2.343 | 1.776±0.003 | 1.834±0.003 | 0.380±0.0012 | 25.722±0.097 | 601 | 25.608±0.117[g] |
| U/Th-36 | 2009 | 317.3 | 2.446 | 1.767±0.003 | 1.819±0.004 | 0.332±0.0019 | 23.014±0.142 | 941 | 22.922±0.150[e] |
| U/Th-37 | 2009 | 336.7 | 1.796 | 1.719±0.003 | 1.768±0.004 | 0.335±0.0016 | 23.234±0.119 | 385 | 23.087±0.151[g] |
| U/Th-20 | 2007 | 362.8 | 2.411 | 1.647±0.003 | 1.693±0.003 | 0.335±0.0018 | 24.322±0.140 | 1313 | 24.241±0.152[e] |
| U/Th-41 | 2009 | 385.3 | 2.675 | 1.668±0.003 | 1.719±0.003 | 0.357±0.0020 | 25.756±0.161 | 1829 | 25.678±0.170[g] |
| U/Th-38 | 2009 | 400.0 | 2.257 | 1.684±0.003 | 1.735±0.004 | 0.355±0.0014 | 25.363±0.117 | 1073 | 25.269±0.128[f] |
| U/Th-15 | 2007 | 422.1 | 2.064 | 1.641±0.003 | 1.689±0.003 | 0.352±0.0020 | 25.863±0.159 | 270 | 25.676±0.214[f] |
| U/Th-39 | 2009 | 434.1 | 3.801 | 1.603±0.003 | 1.650±0.003 | 0.348±0.0014 | 26.207±0.118 | 696 | 26.094±0.139[e] |
| U/Th-5 | 2006 | 451.8 | 2.290 | 1.620±0.003 | 1.672±0.003 | 0.377±0.0017 | 28.321±0.140 | 1041 | 28.231±0.155[g] |
| U/Th-30 | 2008 | 457.9 | 4.424 | 1.618±0.003 | 1.670±0.003 | 0.379±0.0014 | 28.530±0.120 | 1411 | 28.489±0.135[g] |
| U/Th-40 | 2009 | 474.7 | 4.944 | 1.615±0.003 | 1.666±0.003 | 0.374±0.0017 | 28.176±0.141 | 1137 | 28.077±0.164[g] |
| U/Th-16 | 2007 | 490.4 | 2.139 | 1.630±0.003 | 1.683±0.003 | 0.381±0.0019 | 28.487±0.154 | 492 | 28.354±0.189[e] |
| U/Th-17 | 2007 | 496.0 | 0.159 | 1.660±0.003 | 1.733±0.004 | 0.491±0.0038 | 37.245±0.328 | 26 | 35.404±1.844[g] |
| U/Th-21 | 2007 | 499.9 | 0.051 | 1.577±0.009 | 1.632±0.010 | 0.406±0.0025 | 31.727±0.277 | 7 | 25.175±6.634[f] |
| U/Th-18 | 2007 | 522.1 | 0.044 | 1.550±0.004 | 1.605±0.005 | 0.420±0.0025 | 33.704±0.231 | 19 | 31.365±2.296[f] |
| U/Th-6 | 2007 | 540.9 | 0.037 | 1.576±0.014 | 1.640±0.015 | 0.465±0.0052 | 37.162±0.549 | 9 | 31.505±5.696[e] |

Note: All errors are 2σ.

(a) Depth below top (DBT) of DSSG-2.

(b) Two-sigma errors are propagated by monte-carlo simulation and can be considered symmetrical for young samples such as these.

(c) Ages recalculated to allow for the effect of detrital thorium, by assuming $^{230}Th/^{232}Th$ activity equal to 0.65 ± 30 at the time of formation. Corrected ages are reported relative to 1950 A.D. by accounting for the year of measurement.

(d) Ages used in linear regression fit for upper 136.7 mm of DSSG-2.

(e) Ages used as anchor points for final age model.

(f) Ages whose error overlaps with linerally extrapolated age.

(g) Ages not used in final age model.

Table 4.2. Radiocarbon data and calculated ages for speleothem DSSG-2 from DeSoto Caverns.

| Sample DSSG-2- | Depth (mm) | PMC (%) | $^{14}C$ (ka BP) | Corr. $^{14}C$ (ka BP) | Cal. years (ka) |
|---|---|---|---|---|---|
| RC-1 | 0.5 | 29.28±0.18 | 9.870±0.050 | 8.600±0.050 | 8.540±0.110 |
| RC-4 | 62.9 | 21.98±0.21 | 12.150±0.075 | 10.880±0.075 | 11.660±0.325 |
| RC-2 | 171.8 | 16.60±0.16 | 14.450±0.075 | 13.180±0.075 | 14.410±0.380 |
| RC-5 | 366.1 | 5.90±0.10 | 22.700±0.130 | 21.430±0.130 | 24.875±0.495 |
| RC-3 | 543.3 | 1.62±0.06 | 33.100±0.300 | 31.830±0.300 | 31.040±0.300 |

Note: Percent Modern Carbon (PMC). Correction was based on top of DSSG-1, which yielded an age of 1270 $^{14}C$ years BP. Corrected $^{14}C$ ages were converted to calendar years (A.D.) by the Internet accessible program CALIB 5.0.2 (Stuiver et al., 2005)

error of equal depth U/Th ages (Fig. 4.8). The uppermost U/Th age (DSSG-2-U/Th-1) and radiocarbon age (DSSG-2-RC-1), both of which included material from the dark surface of the fossil stalagmite, were not incorporated into the final age model as they likely suffer from contamination and yield inconsistent ages.

Two different approaches were used to create a final age/depth relationship for DSSG-2, with the chosen method dictated by the style of growth. The transition in growth style at 136.7 mm marks the location of a growth hiatus, discussed in detail below, and is the boundary between the two methods used in the age model. The upper section of the sample yielded U/Th ages suggesting a high rate of deposition (Fig. 4.9a) and lamina counting estimated a total of 449 light/dark couplets for this segment (Fig. 4.9b). Given the large number of age determinations spanning a brief period of time (Table 4.1), a linear regression ($r^2 = 0.74$) through the accepted U/Th ages and corresponding depths was warranted (Fig. 4.9b). This approach suggests the upper portion of DSSG-2 was deposited over a period spanning 579 ± 340 years. The agreement of the couplet counting with the U/Th age/depth relationship implies the laminae for this section are annual in nature. Sample DSSG-2-U/Th-29 at 126.8 mm DBT initially produced an age reversal; however, sample DSSG-2-U/Th-43 repeated this depth interval and yielded an age in the appropriate stratigraphic order (Fig. 4.9a).

Below the growth hiatus, linear regression was not feasible therefore ages were assigned to depth by integration between selected U/Th ages. Criteria for this approach included: (i) using as few U/Th ages as anchor points as possible, and (ii) by following the general trend of the overall growth rates for the lower section of DSSG-2. In many cases, a number of U/Th ages between anchor points gave the same age (within analytical error) for a given depth as the linearly integrated ages (Fig. 4.9a). Given the large number of U/Th age determinations, age reversals are

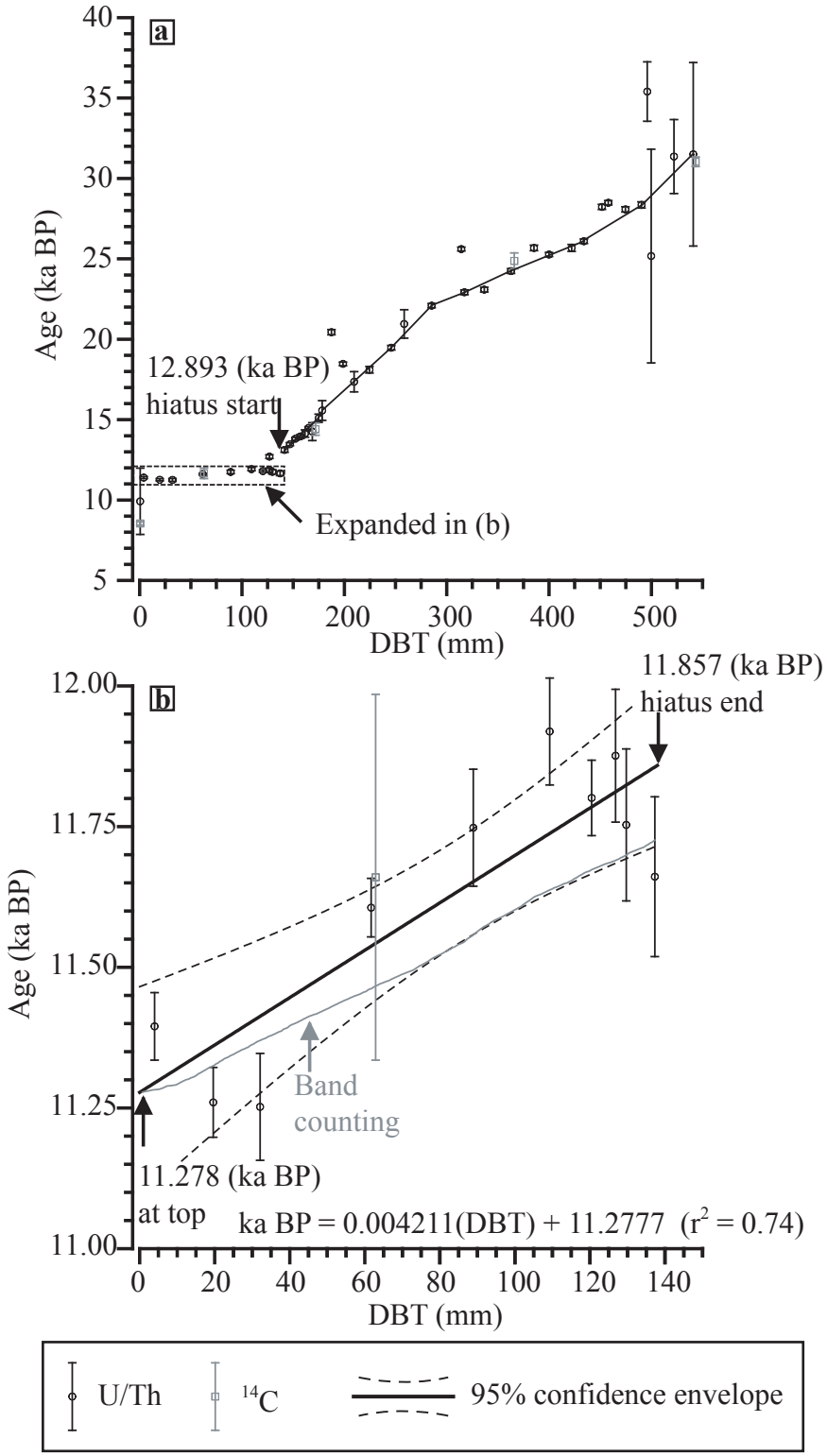


Fig. 4.9. (a) U/Th and radiocarbon ages (ka BP) plotted vs. DBT (mm) in DSSG-2. (b) Expanded view of upper 150 mm of DSSG-2. Solid line in (a) and (b) represents age/depth relationship used in the final age model. Gray line gives age estimate determined by band counting and assuming annual deposition. See text and Tables 4.1-2 for detailed description of age model. Error bars are 2σ. Note the age/depth relationship determined by band counting falls within the 95% confidence envelope based on U/Th ages.

likely to be inevitable and a few are observed with DSSG-2. These outlier ages cannot be explained by analytical error or detrital Th and may represent sections of the sample where the aragonite to calcite transformation took place in a partially open system, thus giving a falsely old age. Nevertheless, the large number of reliable U/Th ages and supporting $^{14}C$ ages gives an accurate account of the depositional history of DSSG-2.

The growth hiatus at 136.7 mm is obvious by the sharp break in U/Th ages and is easily recognized by the sharp change in growth patterns. However, a hiatus can only be dated by closely bracketed ages encompassing the boundary. I extrapolated the growth rates directly above and below the boundary to give ages of 12.893 ka BP and 11.857 ka BP for the start and end of the hiatus, respectively. Before this significant hiatus, growth rates were slow ranging from 7 μm/yr to 38 μm/yr assuming constant deposition between 31.910 ka BP and 12.893 ka BP (Fig. 4.10). Following the ~1000 year cessation of stalagmite growth, annual laminae were deposited at an average rate of 237 μm/yr before suddenly again ceasing deposition at 11.278 ka BP. The growth rates observed for much of DSSG-2 are significantly slower than Holocene age stalagmites (100-250 μm/yr) from the cave that are currently under investigation (Aharon et al., 2009). The slow deposition of DSSG-2 during the LGM and the initial deglaciation intervals may be a function of lower temperatures and decreased soil-$CO_2$ availability, factors that have been suggested to control deposition rates of speleothems (Baker et al., 1998; Kaufmann, 2003).

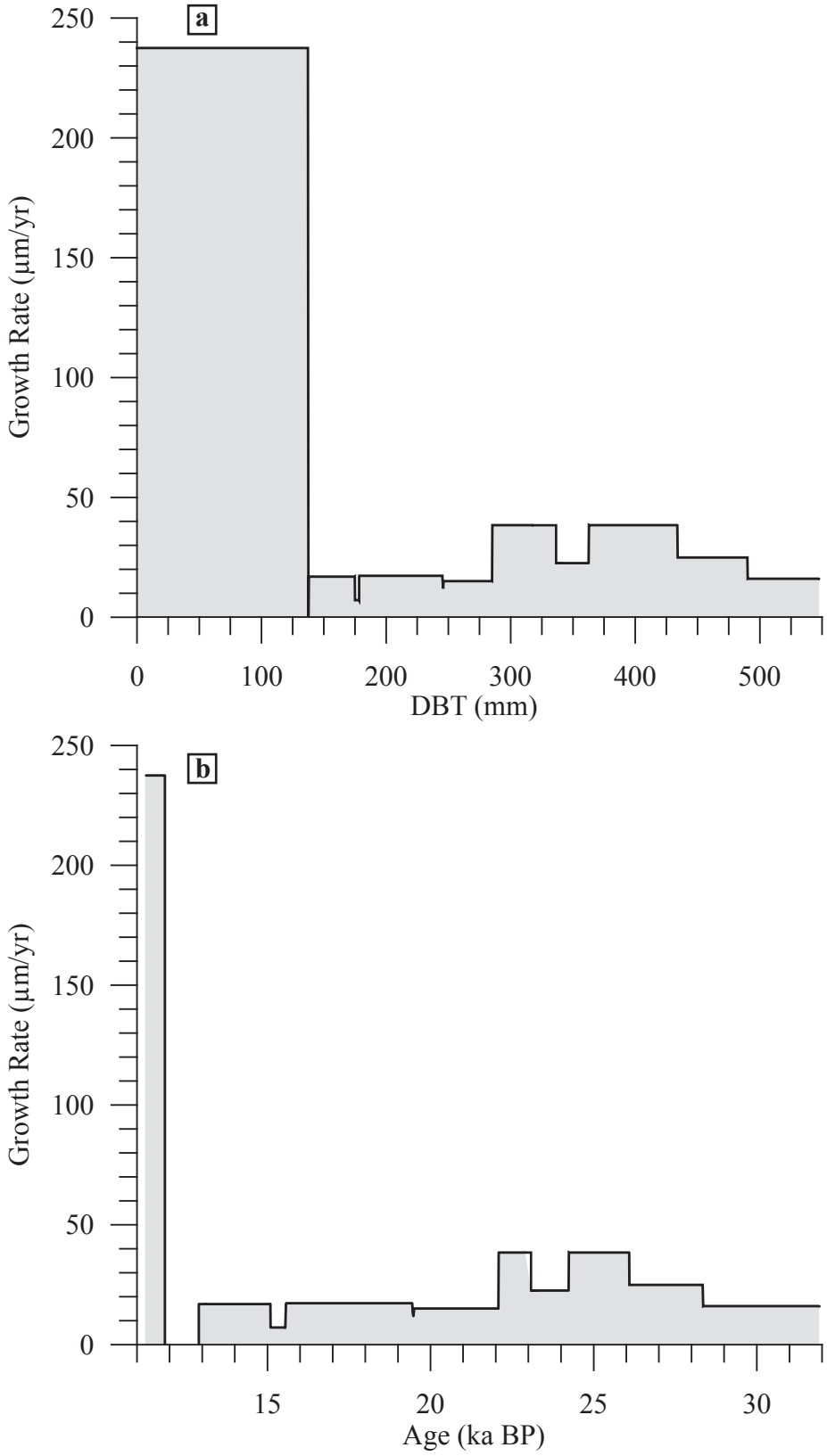


Fig. 4.10. Growth rates in µm/yr for DSSG-2 against DBT (a) and age (b).

## 4.3. Stable Isotopes

### *4.3.1. Isotopic Equilibrium*

Monitoring studies at DeSoto Caverns suggest present-day ambient conditions (>95 % relative humidity) of the cave atmosphere are favorable for $CaCO_3$ precipitation that is at or near isotopic equilibrium with source waters (Lambert and Aharon, 2010). To determine the state of isotopic equilibrium during past deposition, the isotopic variation along individual growth lamina as well as the relationship between $\delta^{13}C$ and $\delta^{18}O$ through time must be examined as described by Hendy (1971). Conditions indicative of kinetic fractionation during past $CaCO_3$ precipitation are as follows: (i) an increase in carbonate $\delta^{18}O$ values with distance away from the central growth axis, (ii) positive covariation between $\delta^{13}C$ and $\delta^{18}O$ along a growth layer, and (iii) $\delta^{13}C/\delta^{18}O$ covariation along the central growth axis (Hendy, 1971). "Hendy Tests" were performed at 33.5 mm (HT-1) and 153.0 mm (HT-2) DBT and show no significant covariation between $\delta^{13}C$ and $\delta^{18}O$ with $r^2$ values of 0.05 (n = 15) and 0.48 (n = 14) for HT-1 and HT-2, respectively (Fig. 4.11). A single point from the center portion of HT-2 was excluded as both $\delta^{13}C$ and $\delta^{18}O$ values were anonymously positive. Enrichments in $^{18}O$ toward the flanks of the sample were not observed and $\delta^{18}O$ showed little variation along individual layers with $1\sigma$ standard deviations of 0.3‰ for HT-1 and 0.2‰ for HT-2 (Fig. 4.11). The isotope data for DSSG-2 also pass the third "Hendy Test" criteria as covariation between $\delta^{13}C$ and $\delta^{18}O$ along the central growth axis is absent ($r^2 = 0.01$; n = 1992).

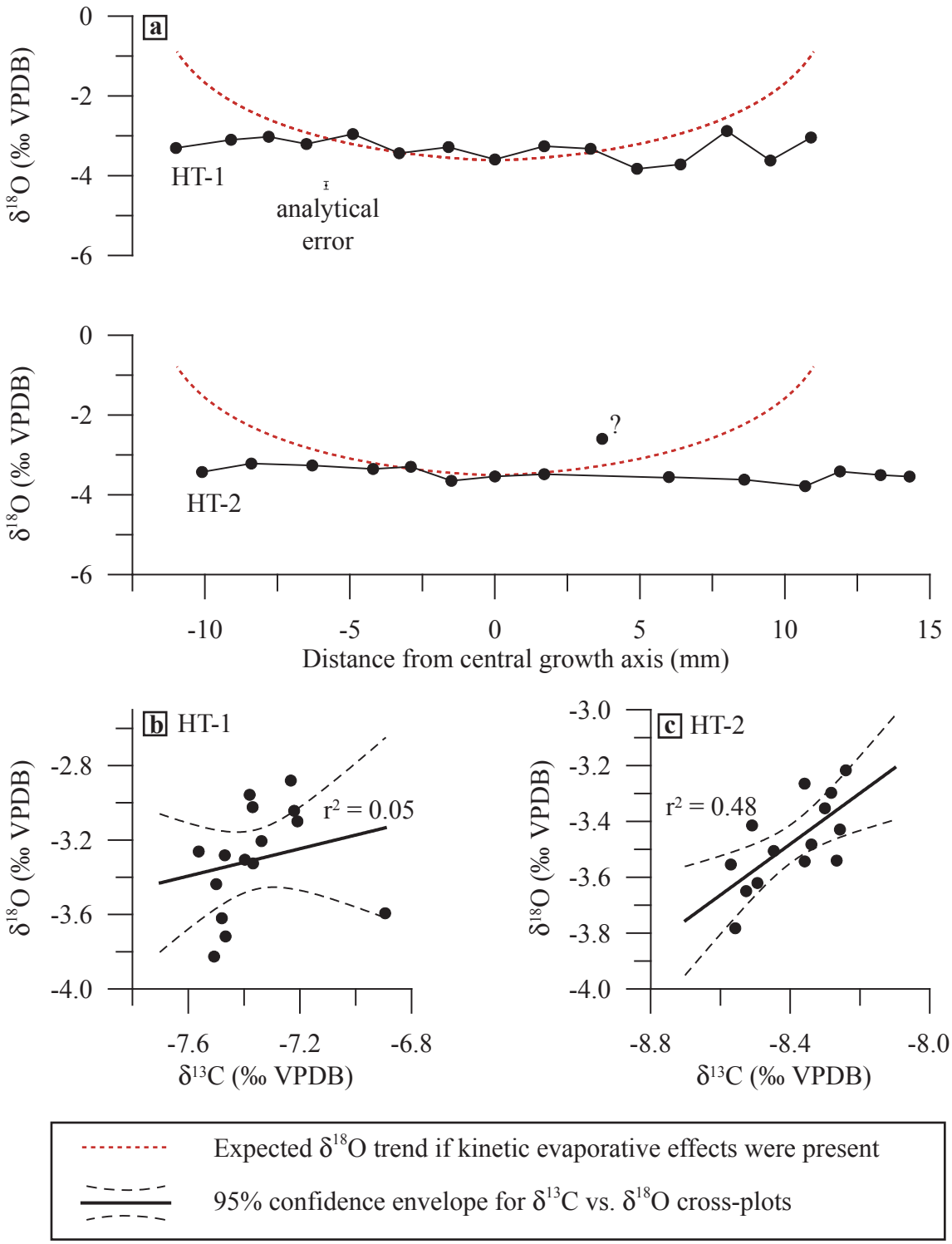


Fig. 4.11. "Hendy Tests" for DSSG-2 sampled from individual growth layers at 33.5 (HT-1) and 153.0 mm DBT (HT-2). (a) Variation in $\delta^{18}O$ from the central growth axis for HT-1 and HT-2. Note the absence of a significant relationship between $\delta^{13}C$ and $\delta^{18}O$ for HT-1 (b) and HT-2 (c). A single outlier shown in (a) was not incorporated into plot (c).

*4.3.2. Aragonite-Calcite Transformation*

The effect of neomorphism on the proxy records entrained within speleothems has yet to be resolved. Studies by Frisia et al. (2002), Bar-Matthews et al. (1991), Woo and Choi (2006), and Martín-García et al. (2009) have stressed the importance of neomorphism in aragonite-bearing caves and the need to undertake detailed petrographic and geochemical studies before using diagenetically altered speleothems as paleoclimate archives. Martín-García et al. (2009) found that secondary calcite with relics of aragonite crystalline structure possessed isotopic compositions very similar to those of primary aragonite. It is unclear, however, if their comparisons are that of stratigraphically-equal lamina that underwent partial inversion to calcite.

To ascertain if secondary calcite within DSSG-2 (Fig. 4.4) preserves meaningful isotope compositions, a series of experiments were designed to determine potential isotope offsets and degree of signal retention. Five test areas (Fig. 4.12) in DSSG-2 and DSSG-5 (a cored stalagmite within the cave) were selected where material could be drilled from stratigraphically equal annual lamina that had experienced partial inversion to calcite thereby giving a direct comparison of primary aragonite and secondary calcite isotope compositions. With respect to $^{13}C/^{12}C$ compositions, $\delta^{13}C$ of secondary calcite was equal (within analytical error) of aragonite when the calcite displayed sparry crystalline structure (Appendix 4.1). Interestingly, in locations where calcite had columnar structure the calcite was ~1.8 ± 0.3‰ depleted in $^{13}C$ than aragonite. For $\delta^{18}O$, the secondary calcite was depleted in $^{18}O$ compared to aragonite by 0.3 ± 0.1‰ regardless of crystalline structure (Appendix 4.1). The $^{13}C$ depletion of 1.8‰ for calcite relative to aragonite based on these tests is equal to an experimental calcite-aragonite fractionation value of 1.7 ± 0.4‰ (Romanek et al., 1992). Experiments by Tarutani et al. (1969) regarding $\delta^{18}O$

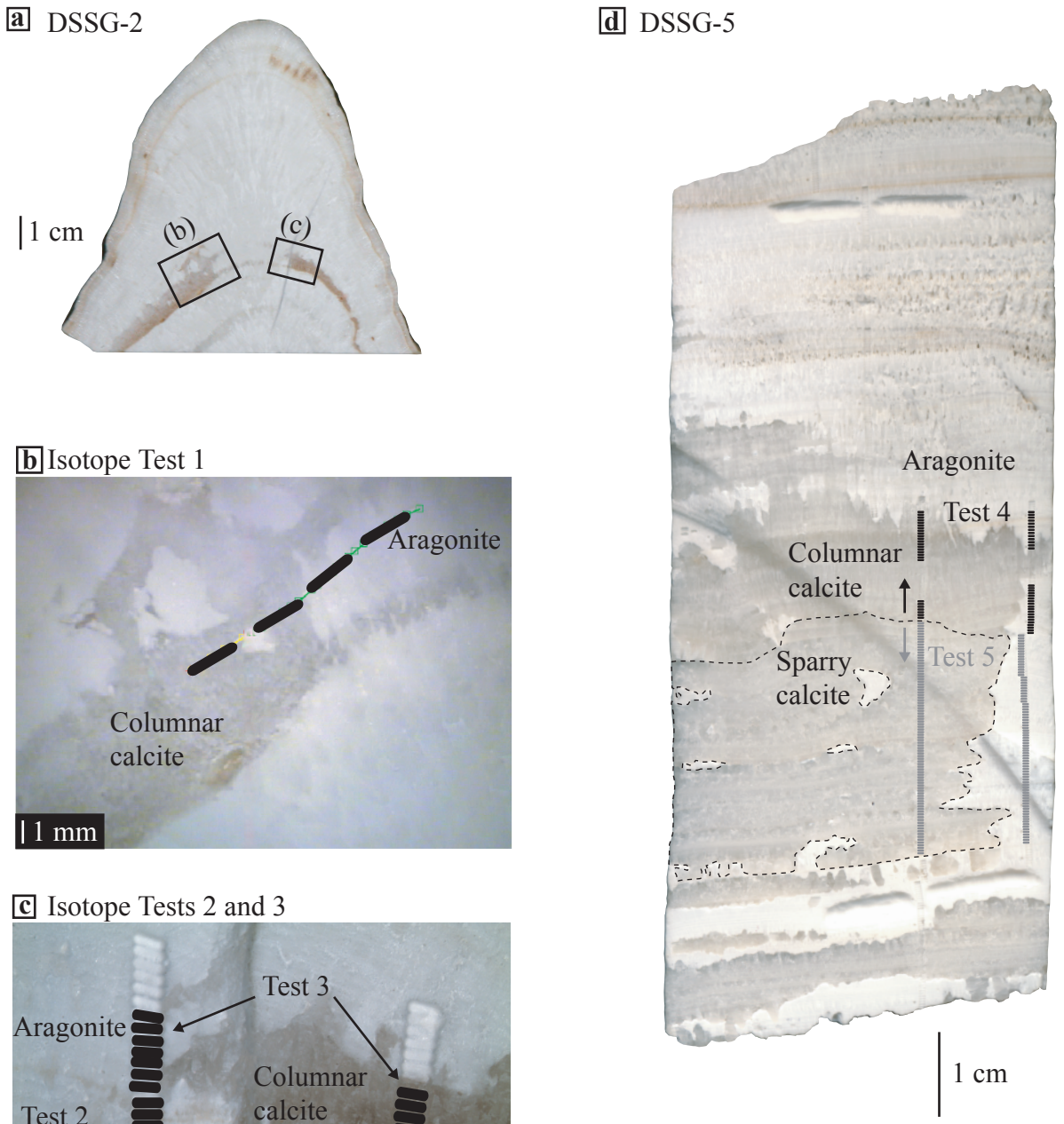


Fig. 4.12. Sampling locations for aragonite/calcite isotope comparisons. (a) Upper portion of DSSG-2 showing locations of Tests 1 (b) and 2-3 (c). (d) Sampling in DSSG-5 provided isotope offsets for both columnar calcite (Test 4) and sparry calcite (Test 5). See Appendix 4.1 for isotope data and calculated offsets.

suggest calcite should be $^{18}O$ depleted by 0.6 ± 0.2‰ relative to coeval aragonite, which is slightly different than the average offset (0.3‰) calculated by the tests in DSSG-2 and DSSG-5. Additional data would be needed to further evaluate the small discrepancy between $\delta^{18}O$ fractionation values calculated by experiments and values observed in this study.

To properly calculate the isotopic composition when the speleothem was initially deposited as aragonite, 0.3‰ must be added to $\delta^{18}O$ compositions obtained from secondary calcite. Because of the intertwining nature of secondary calcite crystal structures and the inability to properly map these zones at the scale of isotope sampling, it is inadvisable to interpret variations in $\delta^{13}C$ obtained from calcite in DSSG-2 as climatic in origin due to the varying degree of diagenetic effects on the $^{13}C/^{12}C$ compositions.

*4.3.3. DSSG-2 Isotope Profiles*

The isotopic compositions measured from the central growth axis of DSSG-2 are plotted against DBT in Fig. 4.13 (Appendix 4.2). All $\delta^{18}O$ values drilled in calcite (below 181.2 mm DBT) have been corrected for the effect of neomorphism (Fig. 4.13a). In general, the $^{18}O/^{16}O$ composition during the depositional history of DSSG-2 remained fairly constant and hovers around -3.3 ± 0.4‰ (n = 1992). An overall shift toward $^{18}O$-enriched values is noted around 170 ± 10 mm and corresponds well with the aragonite section displaying obscure banding (Figs. 4.4 and 13). Superimposed on the gradual sinusoid $\delta^{18}O$ variation are abrupt shifts between samples of >1‰. Compositions for $\delta^{13}C$ at all depths are shown although variations observed in the calcitic portion of DSSG-2 are likely due to both climatic and diagenetic effects. Within the aragonite displaying obscure banding, $\delta^{13}C$ trends toward $^{13}C$-depleted values as the material

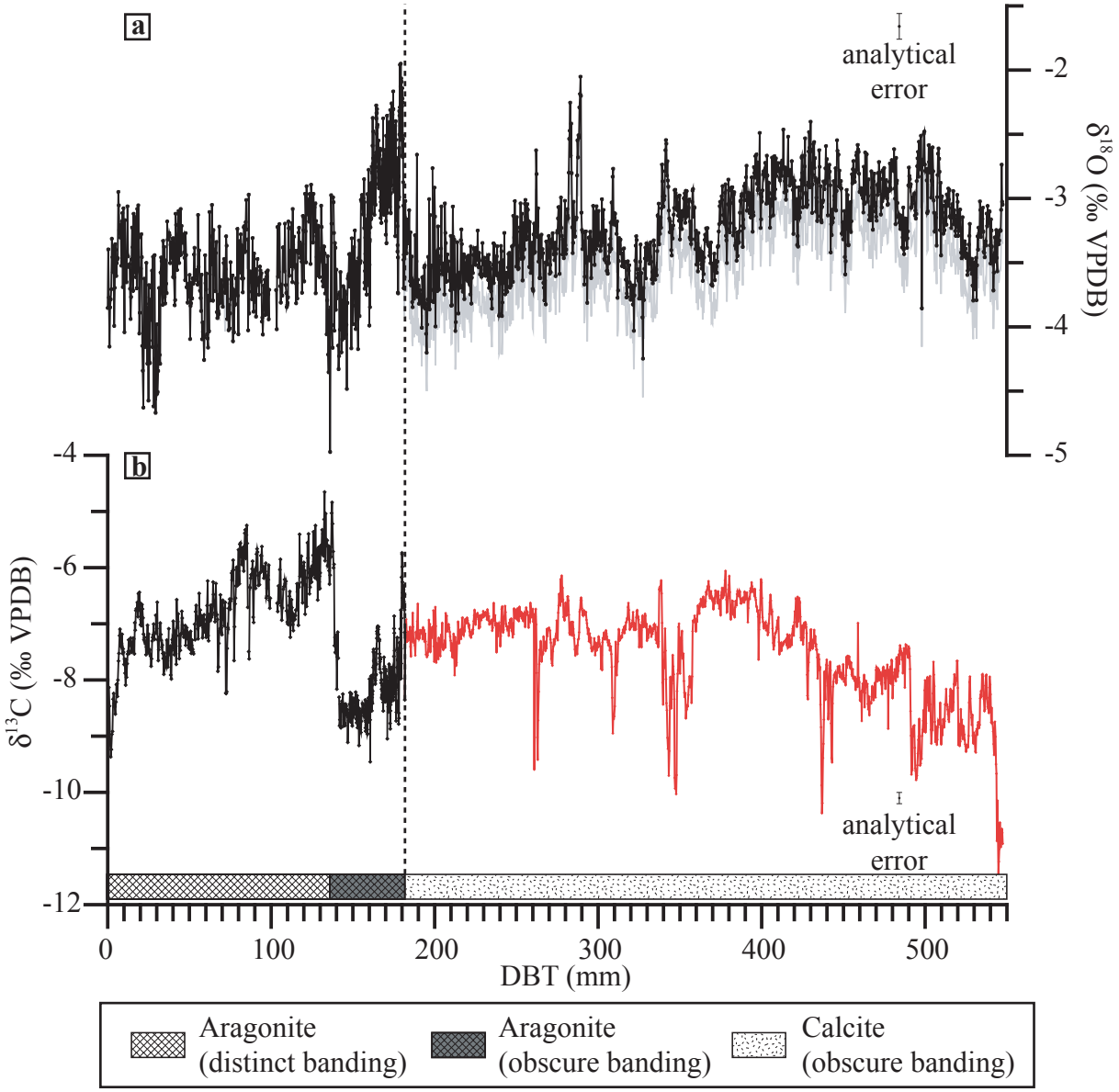


Fig. 4.13. Stable isotope compositions (black lines) for oxygen (a) and carbon (b) against DBT along the central growth axis of DSSG-2. Refer to Fig. 4.4 for profile location. Vertical dashed line is DBT of transition to calcite. Gray line in oxygen plot is raw data uncorrected inversion to calcite. Red line in carbon plot is data collected in calcite and likely affected by diagenetic alteration (see text). Error bars are 1σ.

was deposited (Fig. 4.13b). A sharp shift of ~3‰ to $^{13}C$-enriched values correlates with crossing the depositional hiatus at 136.7 mm DBT. During the deposition of the distinct annual aragonite bands, $\delta^{13}C$ compositions oscillate between samples but trend toward depleted values while $\delta^{18}O$ do not drift significantly over the same interval.

When comparing $\delta^{18}O$ compositions that record changes in meteoric water over long time periods, it has been suggested such data should be adjusted to account for variations in the $\delta^{18}O$ composition of the oceanic moisture source (Grootes, 1993). On the contrary, within the international speleothem literature, the necessity of a correction has received mixed reviews because of competing factors (e.g., lower sea-surface temperatures) that may offset the effects of an $^{18}O$-enriched oceanic source during glacial periods (Lachniet, 2009). Here, $\delta^{18}O$ compositions both uncorrected and corrected for source water $\delta^{18}O$ are shown for comparison against time (Fig. 4.14a) by implementing the age model developed from the accepted U/Th ages (Fig. 4.6). Approximate global sea levels during the deposition of DSSG-2 are taken from the sea level history proposed by Peltier and Fairbanks (2006) allowing DSSG-2 $\delta^{18}O$ values to be corrected by subtracting 0.011‰ per 1 m sea level drop according to Fairbanks (1989). When adjusting the $\delta^{18}O$ to compensate for the sea level effect, $\delta^{18}O$ continues to display minimal variability during the 21 ka-long record but has a mean of -4.3 ± 0.4‰ if assuming a $^{18}O$-enriched moisture source for paleo-rainfall. The $\delta^{13}C$ values are independent of sea level changes and give robust compositions between ~15.7 ka BP and 11.3 ka BP (Fig. 4.14b).

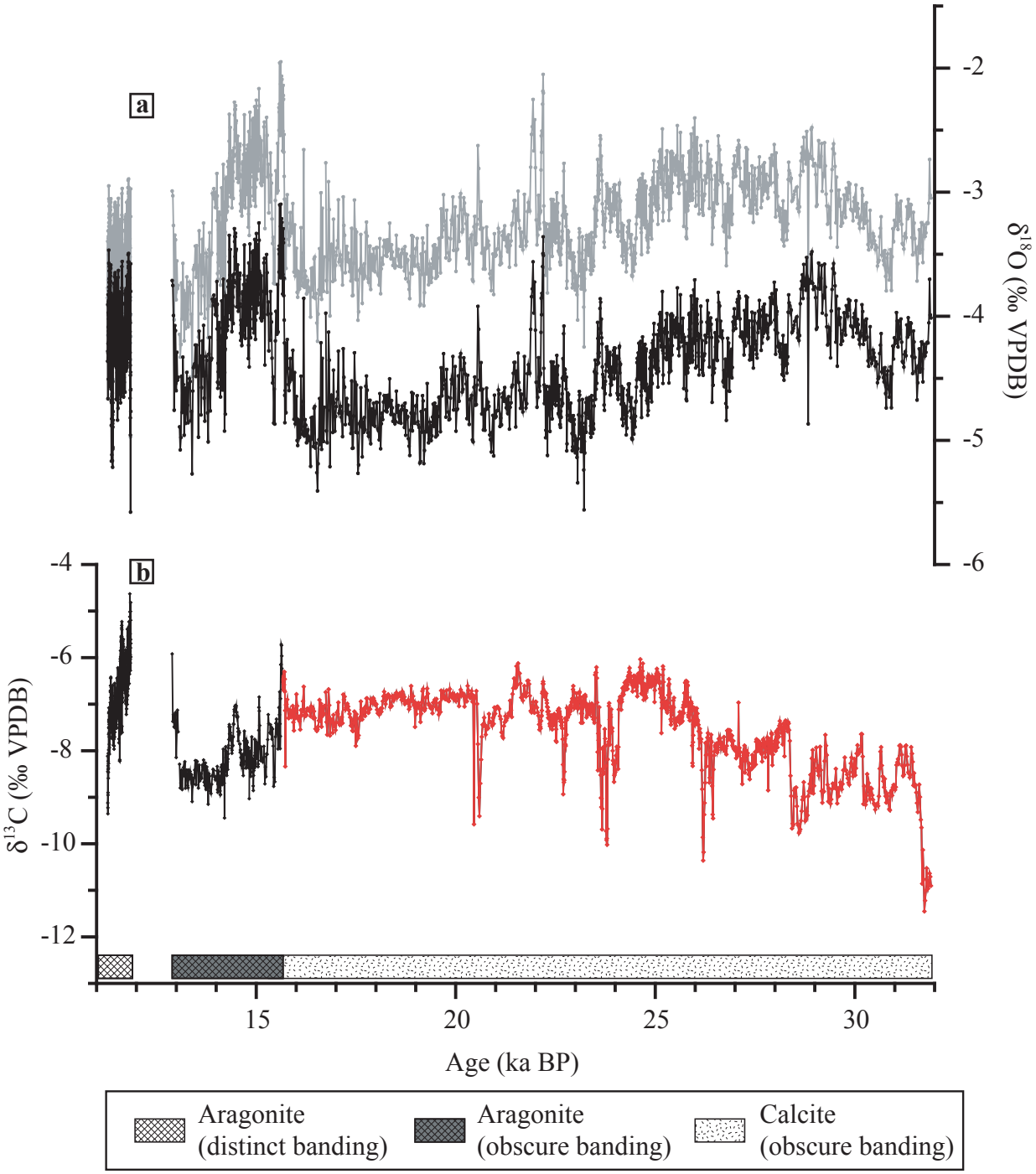


Fig. 4.14. Stable isotope compositions for oxygen (a) and carbon (b) against age based on the age model in Fig. 4.9 and described in text. Black line in oxygen plot represents data corrected for changing $\delta^{18}O$ of oceanic moisture source. Red line in carbon plot is data collected in calcite and possibly affected by diagenetic alteration. Refer to Fig. 4.4 for profile location.

# 5. DISCUSSION

The oxygen isotope composition in DSSG-2 provides a history of winter rainfall variability at DeSoto Caverns (Lambert and Aharon, 2010), which can be interpreted in light of changing atmospheric circulation patterns. During the LGM, the PJS's path across North America was different relative to today (Fig. 4.15) and greatly affected paleo-rainfall distribution (COHMAP, 1988). Proxy data and global circulation models suggest the PJS was split during the winter by the 3-km thick Laurentide ice sheet into a weak northern and strong southern branch (Fig. 4.15b). The southerly position of the PJS along the western North Hemisphere and its increased strength have been suggested in a number of studies to be the primary factors in the formation of pluvial lakes of the southwest USA due to the increased frequency of rain-bearing storm systems (Kutzbach and Wright, 1985; Menking et al., 2004).

A recent investigation of a speleothem (FS-2) from Fort Stanton Cave (33°31'27" N, 105°27'33" W) in New Mexico has provided a high-resolution record of the temperature-dependent north-south migration of the PJS over the Southwest between 55.9 ka BP and 11.4 ka BP (Asmerom et al., 2010), a period dominated by glacial conditions. Variations in $\delta^{18}O$ in the FS-2 stalagmite were attributed to changing contributions of $^{18}O$-depleted moisture from the Pacific Ocean such that $^{18}O$-depleted winter rainfall was limited when warmer conditions drove the PJS north. Asmerom et al. (2010) identified $^{18}O$-depletions associated with each of the six Heinrich events (H*n*) and the Younger Dryas cold phase with $^{18}O$-depletions representing each cold event in the GISP2 ice core record. During the same time span (55.9-11.4 ka BP), 14 Dansgaard-Oeschger warm events (DO*n*) were identified in both the GISP2 and NM records as $^{18}O$-enrichments. Although the NM cave is positioned 1800 km west of DeSoto Caverns, FS-2 is

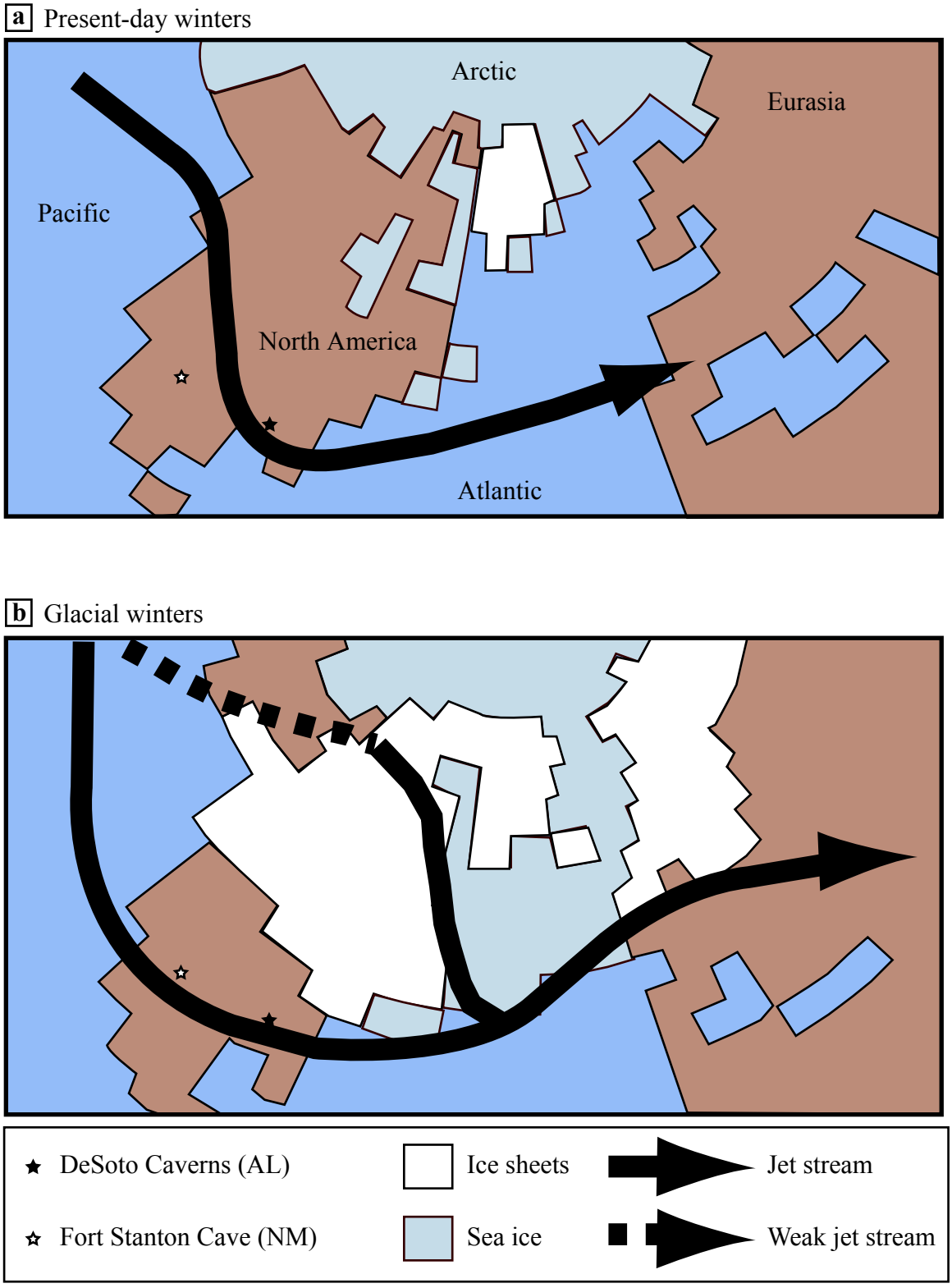


Fig. 4.15. Average position of the polar jet stream during present-day winters (a) and during winters of the Last Glacial Maximum (b). Note the split of the jet stream caused by the Laurentide ice sheet during peak glacial conditions. Map modified after COHMAP (1988).

an adequate choice for comparison with DSSG-2 because both caves are at 33 °N and winter rainfall variability is affected by the position and intensity of the PJS (Fig. 4.15).

The $\delta^{18}O$ records (Fig. 4.16) produced by the NM and AL studies display different absolute values and degrees of variability due to their respective moisture source(s). DSSG-2 $\delta^{18}O$ averages -3.3‰ (without ice volume correction) and varies between -5.0‰ and -1.9‰ because the cave receives most of its moisture from the nearby GOM (Fig. 4.16c). For the same time interval, FS-2 is on average (-8.0‰) significantly more $^{18}O$-depleted relative to DSSG-2 and displays a ~6‰ range (-11.3‰ to -5.5‰) in $^{18}O$ composition (Fig. 4.16b). The FS-2 record is more $^{18}O$-depleted than DSSG-2 because the site receives significant winter rainfall where moisture is sourced from the Pacific Ocean (-11‰; Yapp, 1985) and travels a minimum 1100 km to the cave, further depleting the rainfall in $^{18}O$ due to Rayleigh fractionation processes (Rozanski et al., 1993). The large amplitude shifts in the FS-2 record are the result of changing contributions of moisture from the Pacific Ocean during winter and GOM during summer months, with the GOM moisture (-2‰; Yapp, 1985) being $^{18}O$-enriched. Furthermore, the two records are dissimilar in sampling resolution where the FS-2 stalagmite averages ~44 years (9-165 year range) between data points while the DSSG-2 record averages ~10 years (1-25 year range).

Reliable comparison of long-term trends (i.e., >5 ka) in the two records is complicated by poorly constrained factors that modify the $\delta^{18}O$ signals, which include: (i) uncertainties associated with ice volume correction (Lachniet, 2009), (ii) changes in air temperature within the respective caves, depleting the stalagmites in $^{18}O$ by 0.24‰ for every degree (°C) increase (O'Neil et al., 1969), and (iii) the changing distance moisture must travel from source (i.e., GOM) to study site due to varying sea level (Rozanski et al., 1993). Here I will focus on relative

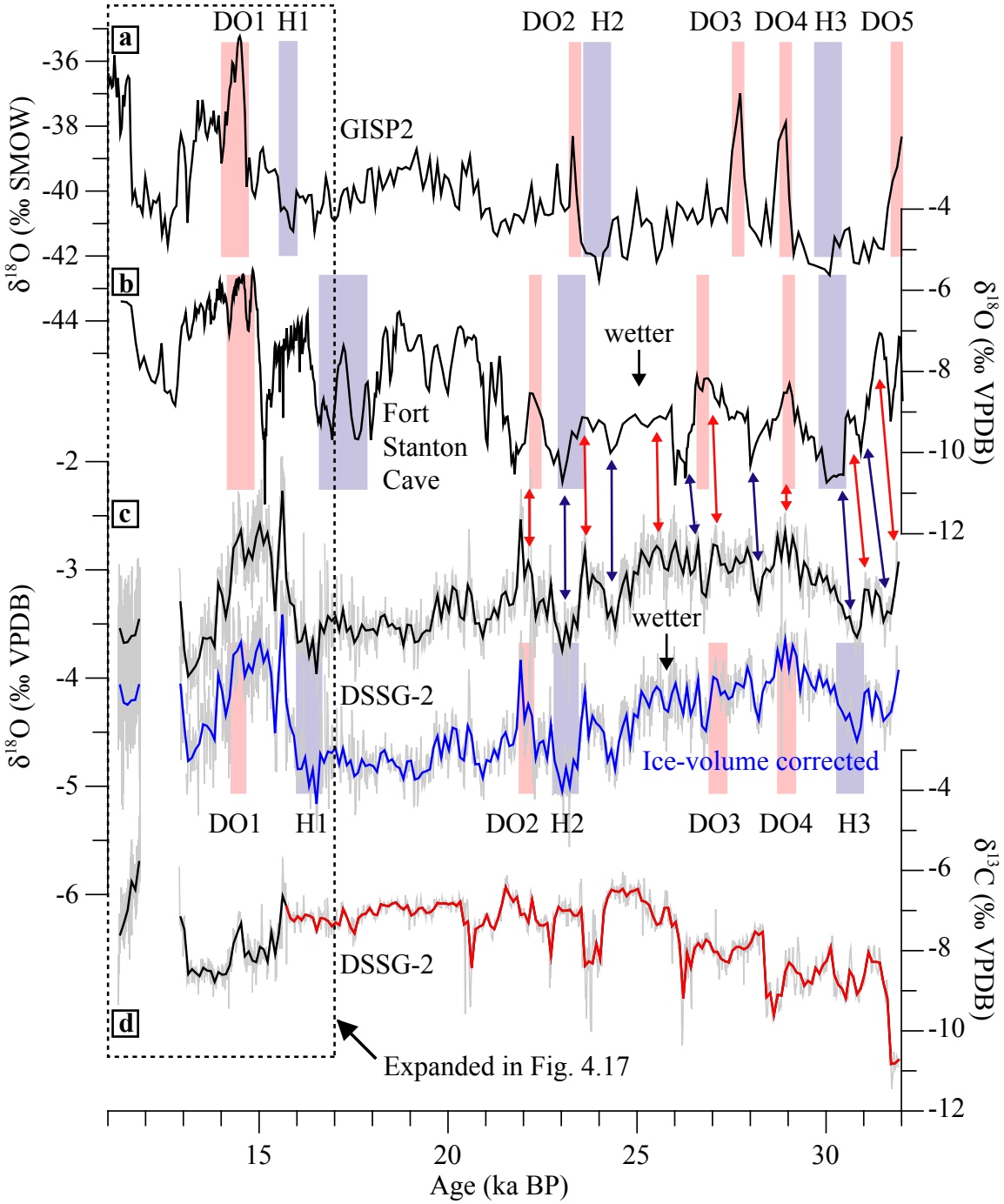


Fig. 4.16. Comparison of GISP2 ice core $\delta^{18}O$ record (a) with stalagmite $\delta^{18}O$ records from Fort Stanton Cave (b) and DeSoto Caverns (c) for the 32-11 ka interval. $\delta^{13}C$ data (d) from DSSG-2 considered to be "suspect" due to post-depositional alteration are in red. The $\delta^{18}O$ profile for DSSG-2 is shown with (blue) and without (black) ice-volume correction. $\delta^{18}O$ and $\delta^{13}C$ profiles from DSSG-2 have been averaged at 100-year intervals with raw data in gray. Timing of H*n* events for the GISP2 record is based on Hemming (2004), while DO*n* events are based on Heinrich (1988b), Johnsen et al. (1992), and Dansgaard et al. (1993). Approximate timing of H*n* and DO*n* events from the Fort Stanton Cave record were taken from Asmerom et al. (2010).

$\delta^{18}O$ excursions related to millennial-scale events that are less prone to the before-mentioned complicating factors.

### 5.1. Heinrich and Dansgaard-Oeschger Events

For better comparison with the GISP2 and FS-2 proxy records, $\delta^{18}O$ and $\delta^{13}C$ profiles from DSSG-2 were averaged at 100-year intervals between 31.9 ka BP and 11.3 ka BP (Fig. 4.16). At millennial-scale resolution, $\delta^{18}O$ variability of DSSG-2 shows a remarkable coherency with most of FS-2 record implying the PJS (Fig. 15b) also influenced Southeast rainfall patterns. The relationship is weakest between ~22 ka BP and 17 ka BP as well as from 13 ka BP until 11.3 ka BP when both stalagmites stopped depositing within approximately 100 years of each other (11.4 ka BP; FS-2), suggesting different atmospheric conditions affecting the regions during these times.

From the Southwest stalagmite record spanning the 31.9-11.3 ka BP interval, Asmerom et al. (2010) identified three of the more prominent $^{18}O$-depletions with Heinrich events 1-3 and four significant $^{18}O$-enrichments with Dansgaard-Oeschger events 1-4 (Fig. 4.16b). Overall, the timing of the events identified in the FS-2 record is in good agreement with the GISP2 chronology; however, slight discrepancies were attributed to uncertainties with the age model applied to the ice cores rather than the well-dated (68 U/Th dates) FS-2 stalagmite (Asmerom et al., 2010). From the DSSG-2 $\delta^{18}O$ record I identify Heinrich events 1-3 and Dansgaard-Oeschger events 1-4 based on $^{18}O$ depletions and enrichments, respectively. The Pacific Ocean is not a significant source of moisture for Southeast rainfall (Rasmusson, 1968; Bryson and Hare, 1974;

Simpkins, 1995); therefore, $\delta^{18}O$ variability in DSSG-2 is controlled by changing contributions of $^{18}O$-depleted winter rainfall from the GOM (Lambert and Aharon, 2010).

Supporting evidence for my interpretation of rainfall variability in the Southeast comes from 60-ka long pollen records derived from sediment cores extracted from Lake Tulane in central Florida (Grimm et al., 1993; Grimm et al., 2006). In the study, sharp increases in the abundance of *Pinus* (pine) pollen, a wet climate species, correlated with Heinrich events while *Quercus* (oak) pollen during Dansgaard-Oeschger phases suggested dryer conditions.

### 5.2. Deglaciation Events

In Greenland the transition from the cold LGM to the warm Holocene was punctuated by a number of significant climate reversals that are easily recognized in the GISP-2 core (Fig. 17a). The two most prominent events are the Bølling-Allerød (BA) interstadial (14.50-12.94 ka BP; Jouzel et al., 2001) and the Younger Dryas (YD) stadial (12.94–11.64 ka BP; Alley et al., 1993). The BA was characterized by near present-day warmth and its influence was not restricted to the North Atlantic region (Shakun and Carlson, 2010). In some locations evidence exists for a brief cold period, known as the Older Dryas (Fig. 17a), that is typically a century or two in duration centered around 14.1 ka BP, thus dividing the BA interval. The YD is by far the most discussed climate event during deglacial times in scientific literature (see review by Peteet, 1995) because of the sudden return to near full glacial conditions (within a decade; Alley, 2000b) and the rapid return to the general trend of warming that characterized the start of the Holocene.

The BA has been recognized in the Southwest a period of warmth and drier conditions in the FS-2 stalagmite (Fig. 17b; Asmerom et al., 2010) as well as a number of other proxy records in

the area (Polyak et al., 2004; Wagner et al., 2010). Conversely, it has been inferred that the more southerly PJS during the YD brought wet conditions to the Southwest (Polyak et al., 2004). Cessation of growth following the YD in FS-2 (Asmerom et al., 2010) and other regional stalagmites (Polyak et al., 2004) has been attributed to the onset of present-day moisture-limiting climatic conditions characterized by drier winters (northern PJS position; Fig. 15a) and increased evapotranspiration during summer months.

The initiation of warmer and drier winter conditions, based on $^{18}O$-enrichments in FS-2 and DSSG-2 (Fig. 4.17; 50-year smooth), appears to precede the start of the BA as defined by the GISP2 chronology. The discrepancies are in part based on errors associated with each proxy record's age model; however, the possibility of warmer conditions prevailing in lower latitudes sooner than in Greenland cannot be ignored. Although multiple oscillations in $\delta^{18}O$ can be correlated between the DSSG-2 and FS-2 records during the overall period of warmth (Fig. 4.17) suggesting the PJS position was still a controlling factor at both sites, the DSSG-2 record better matches the overall trend of the GISP2 record and may be due to an overall progression toward wetter conditions in the Southeast from 15 ka BP to 13 ka BP. Although not recognized by Asmerom et al. (2010), the Older Dryas is expressed in both sites as $^{18}O$-depletions representing slightly wetter conditions during the relatively dry BA warm period (Fig. 4.17).

I interpret the start of the YD as the beginning of dramatic changes in the PJS across North America and divergence from the coupled relationship between winter rainfall variability in the Southwest and Southeast study sites. The YD is expressed at DeSoto Caverns as extremely dry winters resulting in a hiatus of deposition for DSSG-2 during the interval 12.893 ka BP to 11.857 ka BP (Figs. 4.9 and 17). This is in stark contrast to the extreme wet conditions of the Southwest during the cold period (Polyak et al., 2004). I hypothesize that during YD winters the PJS

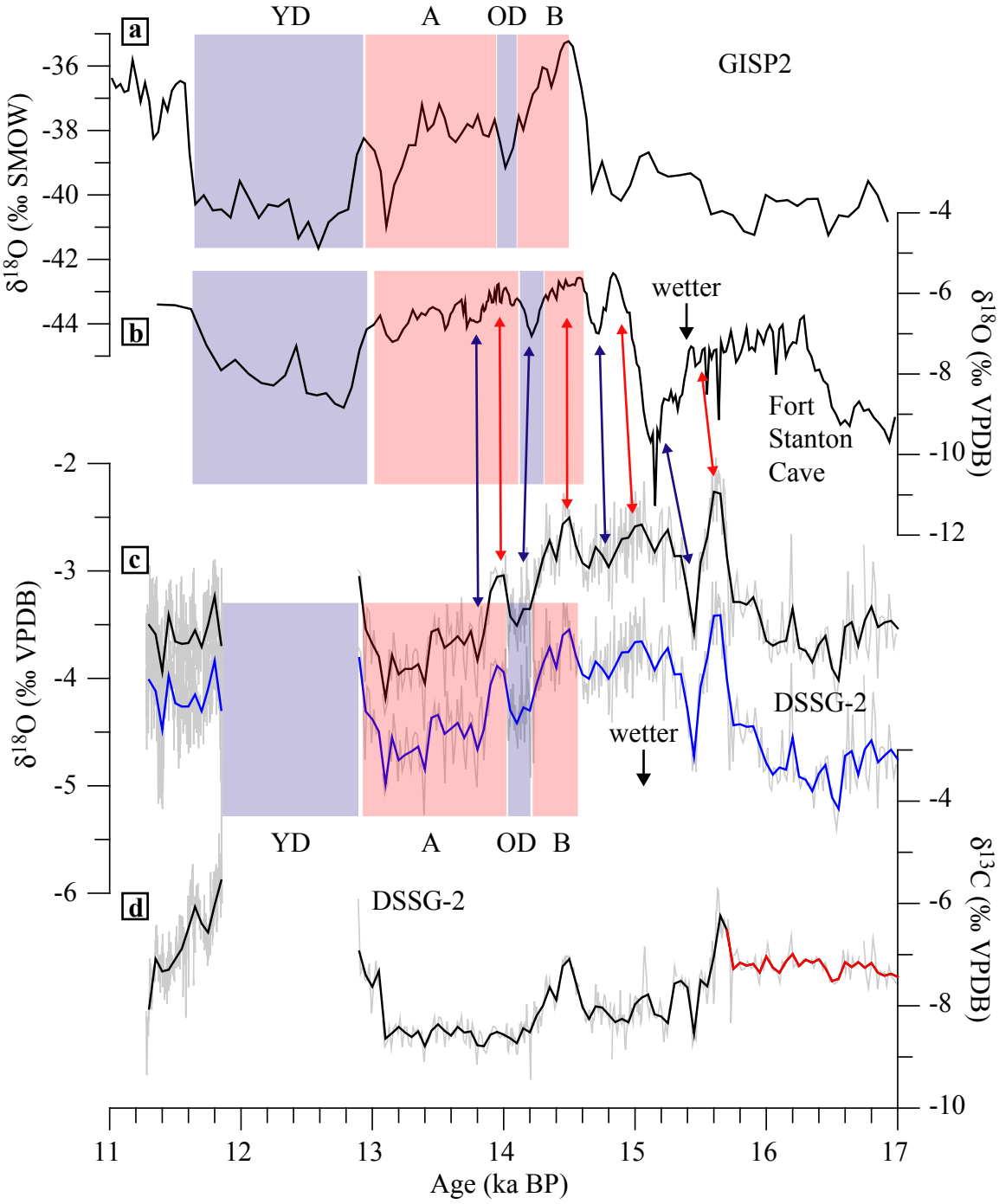


Fig. 4.17. Comparison of GISP2 ice core $\delta^{18}O$ record (a) with stalagmite $\delta^{18}O$ records from Fort Stanton Cave (b) and DeSoto Caverns (c) for the 17-11 ka interval. $\delta^{13}C$ data (d) from DSSG-2 considered to be "suspect" due to post-depositional alteration are in red. The $\delta^{18}O$ profile for DSSG-2 is shown with (blue) and without (black) ice-volume correction. $\delta^{18}O$ and $\delta^{13}C$ profiles from DSSG-2 have been averaged at 50-year intervals with raw data in gray. See text for timing of deglaciation events in GISP2 record. YD = Younger Dryas, A = Allerød; OD = Older Dryas; B = Bølling.

entered North America centered across the American Southwest and exited the continent at a higher latitude (Great Lakes area), a PJS trajectory that is the inverse the present-day path (Fig. 4.15a).

Support for dry/drought conditions in the eastern half of the United States during the YD is based on recent studies from Big Eddy archaeological site (23CE426), southwestern Missouri (Dorale et al., 2010), Tampa Bay, Florida (Willard et al., 2007), and from the Southern High Plains, Texas (Holliday, 2000). Arid conditions for southwestern Missouri during the YD were inferred from increased dominance of C4-type vegetation, based on $\delta^{13}C$ of organic material removed from a soil profile, in response to less precipitation as opposed to increased air temperatures (Dorale et al., 2010). Two-step drying in central Florida during the YD was evidenced by pollen assemblages extracted from a sediment core (MD02-2579) collected from Tampa Bay on the West Coast of the Florida Peninsula (Willard et al., 2007). Furthermore, dry conditions appeared to be prevalent in the Southern High Plains of Texas as indicated by increased eolian activity (wind erosion, eolian deposition) during the YD (Holliday, 2000).

A more northern position of the winter PJS across the eastern US is supported by a model, recently proposed by Yu and Wright (2001), of the distribution of the major air masses during the YD. Their model contends that arctic air was trapped behind the Laurentide ice sheet and allowed warm air from the Gulf of Mexico to infiltrate deep into the interior of eastern North America (Fig. 4.18). The boundary between the cold air mass to the north and the infiltrating warm air mass would define the location of the PJS. The dominance of the warm air mass had an ameliorating effect on the climate with winters not having the low temperature extremes found today therefore supporting temperate fauna (e.g., ash, oak, and elm) at higher than expected latitudes as well as weakening the signal of the YD in much of the North America interior (Yu

Model of air mass dominance during Younger Dryas

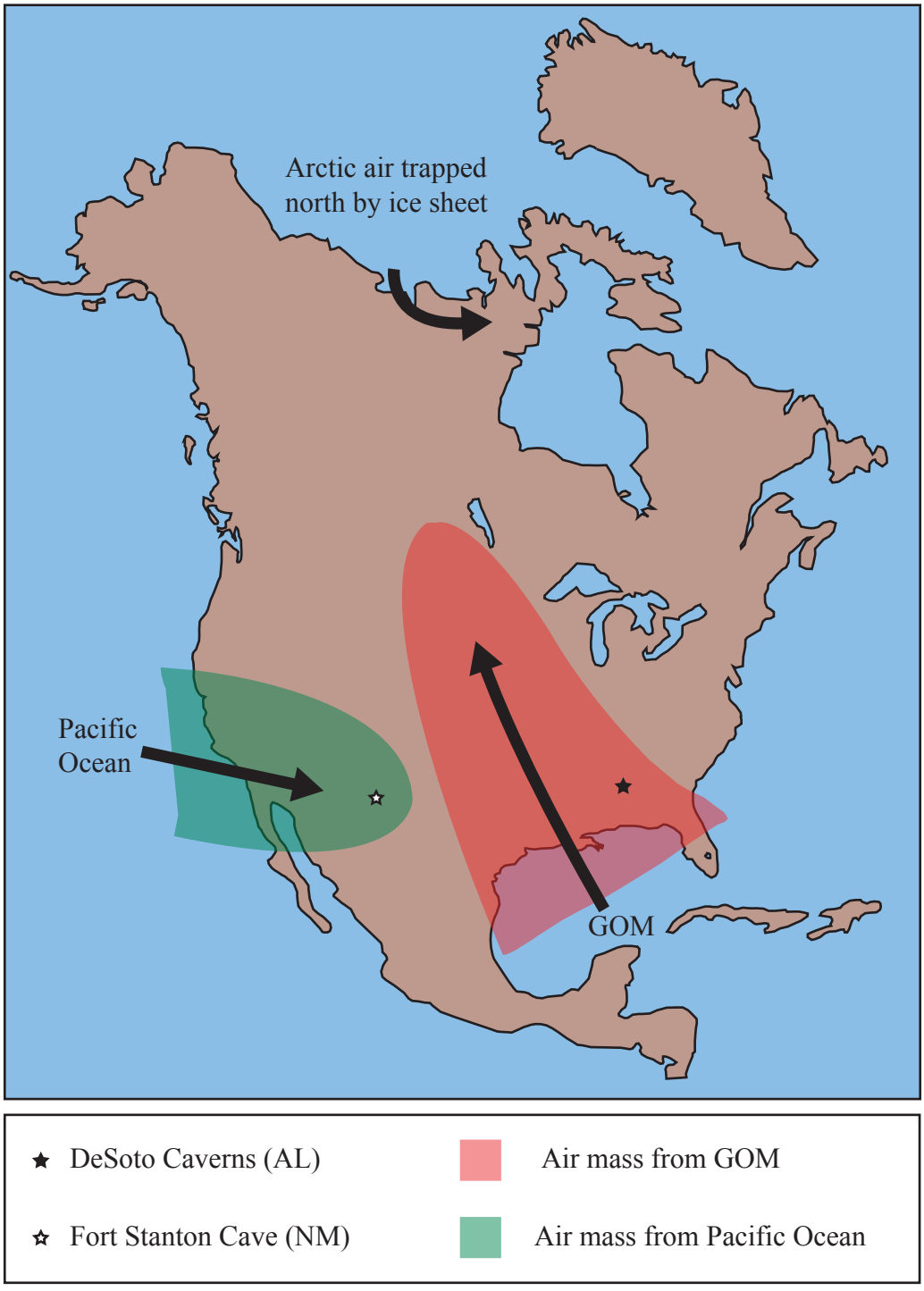


Fig. 4.18. Hypothesized distribution of major air masses over North America during the Younger Dryas (modifed after Yu and Wright, 2001). The model suggests warm air from the Gulf of Mexico had an ameliorating effect on winter air temperatures. The scenario may explain dry winters in the Southeast.

and Wright, 2001). Warmer than expected sea surface temperatures in the GOM during the onset of the YD may have further helped to ameliorate Southeast winters (Flower et al., 2004). The atmospheric configuration proposed here would result in less rainfall in the Southeast as storm tracks would be diverted north and the Southeast would experience warm but dry winters as the cold fronts needed to initiate rainfall would not frequent the region. Summers in the Southeast may have been wetter than YD winters but not to the extent that recharge exceeded evapotranspiration, thus limiting infiltration into the aquifer above DeSoto Caverns and preventing deposition of DSSG-2.

Immediately following the YD, deposition of DSSG-2 shifted from obscure banding to distinct annual couplets whose growth rate was an order of magnitude greater than previously observed in the stalagmite (Figs. 4.7 and 10). This boost in growth rates is attributed to an overall increase in rainfall, enhanced $CO_2$ flux through the epikarst via dripwater, and strong seasonality in ventilation of the cave chamber. Annual rainfall amounts approaching totals found today would increase the delivery of $CO_2$ transport into the cave via dripwater (Kowalczk and Froelich, 2010) creating a strong $pCO_2$ gradient between dripwaters and the cave atmosphere. This situation would drive the dripwaters toward saturation with respect to aragonite and promote rapid carbonate deposition (Spötl et al., 2005). Amplified seasonality in cave ventilation best explains the couplet nature of the distinct bands where seasonal crystal structure is a function of $CO_2$ degassing rates and ensuing aragonite deposition rates (Baker et al., 2008; Boch and Spötl, 2008; Mattey et al., 2008). The strong $pCO_2$ gradient and amplified ventilation of the cave chamber likely kinetically enhanced the $^{13}C$ enrichment of cave waters as evidenced by post YD deposition displaying the most $^{13}C$-enriched aragonite (Fig. 4.17d) observed in DSSG-2 (Lambert and Aharon, In Review).

The increased rainfall in the Southeast following the YD can be attributed to warmer summers around the peak of summer insolation (COHMAP, 1988) and the establishment of the PJS near its current path (Fig. 4.13a). Whereas drier conditions in the Southwest ceased deposition of stalagmites around 11 ka BP (Polyak et al., 2004), increased rainfall at DeSoto Caverns may have altered water flow paths and rates through the epikarst such that seepage waters emerging from the stalactite above DSSG-2 were no longer primed chemically for aragonite deposition after ~11.3 ka BP. A similar pattern of rapid aragonite deposition (up to 185 μm/yr) followed by a cessation of growth (~10.9 ka) observed in another stalagmite (DSSG-3; Appendix 4.3) within DeSoto Caverns (Fig. 4.19) supports the hypothesis of amplified seasonality followed by changing water chemistries.

## 6. CONCLUSIONS

(1) Relics of botryoidal structures and crosscutting relationships of mineralogy types are evidence that calcite identified within DSSG-2 is secondary in nature and replaced primary aragonite by the process of neomorphism.

(2) Secondary calcite displays two common crystal structures, columnar and sparry. Calcite with sparry crystalline structure preserves the $\delta^{13}C$ signature from the primary aragonite while columnar calcite was $^{13}C$-depleted by 1.8 ± 0.3‰ relative to contemporaneous aragonite. With regard to oxygen isotopes, the secondary calcite was depleted in $^{18}O$ compared to aragonite by 0.3 ± 0.1‰ regardless of columnar or sparry crystalline structures.

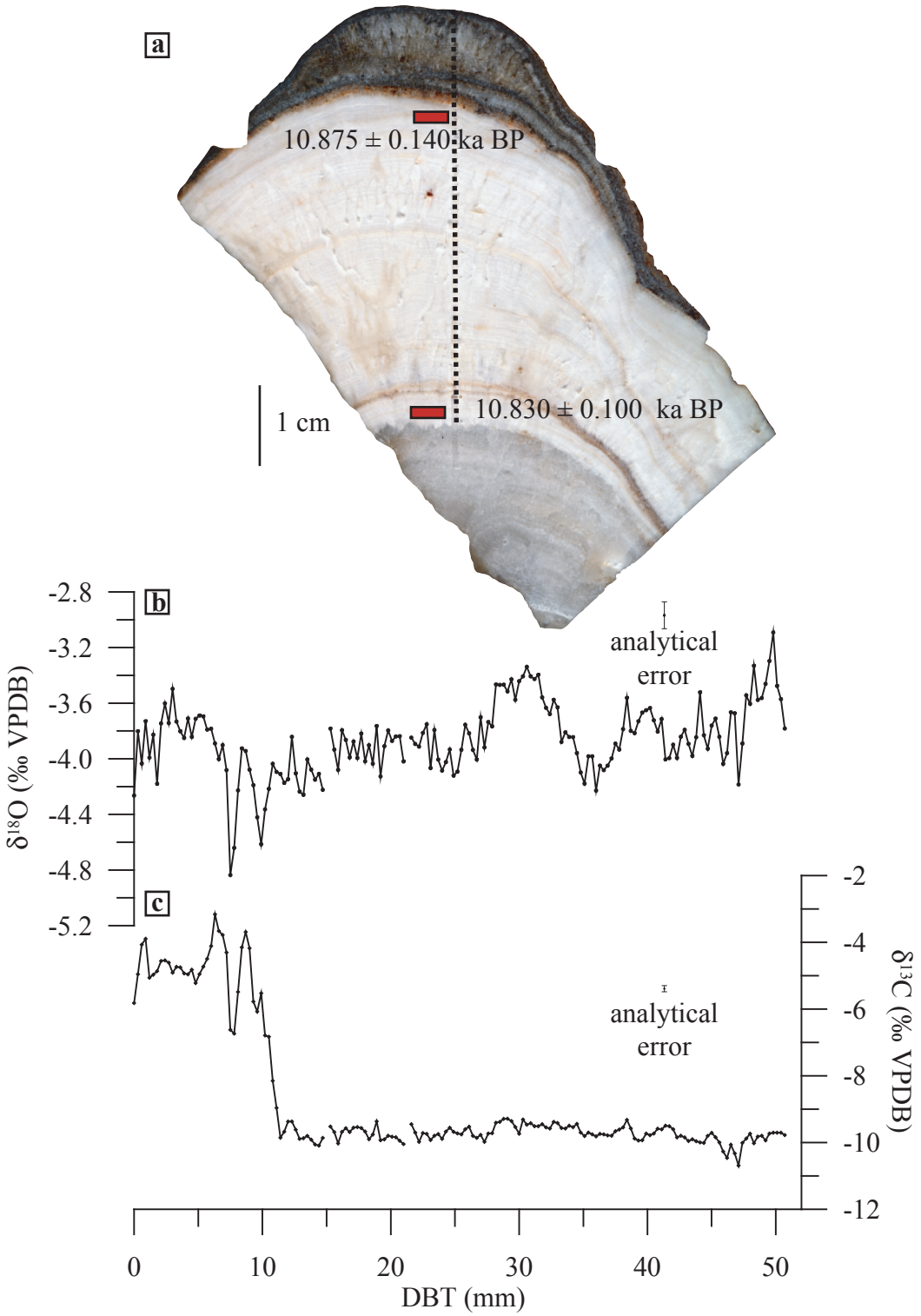


Fig. 4.19. (a) Locations of U/Th age dates and sampling profile for stable-istope ratios from DSSG-3. Stable-isotope compositions for oxygen (b) and carbon (c) against DBT along the central growth axis. $\delta^{18}O$ data do not incorporate changes in $\delta^{18}O$ of oceanic moisture source. See Appendix 4.3 for stable isotope data.

(3) Aragonite deposition of DSSG-2 occurred between 31.9 ka BP and 11.3 ka BP with a hiatus in growth occurring between 12.9 ka BP and 11.9 ka BP based on the age model developed using multiple dating techniques. Couplet counting and radiometric dating show that distinct bands deposited after 11.9 ka BP are annual in nature.

(4) The results from "Hendy Tests" suggest that DSSG-2 was deposited in isotopic quasi-equilibrium with its source waters. Therefore, kinetic effects have not played a role in the transmission of signals from dripwaters to speleothems.

(5) The Southeast experienced wet winter conditions during the Heinrich cold events and dry winters during the Dansgaard-Oeschger warm events. The rainfall variability was likely controlled by the north-south migration of the polar jet stream.

(6) Following a progressive trend toward wetter conditions through the relatively dry Bølling-Allerød, the deposition of DSSG-2 ceased during the Younger Dryas because of exceptionally dry winters and inadequate groundwater recharge during summer months. Decreased winter rainfall was caused by perseverance of warm air from the Gulf of Mexico across the interior of eastern North America, which resulted in infrequent collisions of warm and cold air masses required to induce rainfall over the Southeast.

(7) Changes in the path of the polar jet stream across North America have resulted in in-phase and anti-phase relationships between rainfall distribution across the Southeast and Southwest. The areas were both affected strongly (in-phase) by the polar jet stream position between 32 - 22 ka BP and 17 - 13 ka BP. During the Younger Dryas, the polar jet stream cut across the Southwest and exited the continent in the Great Lakes region. Following the Younger Dryas, the polar jet stream migrated toward the

position observed today with dry conditions in the Southwest and wet conditions in the Southeast.

(8) The high-resolution record of rainfall variability and polar jet stream migration interpreted from isotope profiles of DSSG-2 provides much needed data for general circulation models.

## ACKNOWLEDGMENTS

I thank Tim Lacy and Allen Mathis III for generously allowing free access to the cave for observations and sampling of speleothems. I thank Jim Donahoe (University of Alabama) for his assistance with XRD analysis. Dr. John Hellstrom (University of Melbourne) played a vital role in the development of the age model for the stalagmite under investigation. This study is a part of the senior author's dissertation research at the University of Alabama. It was partially funded by the Gulf Coast Association of Geological Societies (GCAGS student grants), Geological Society of America, Evolving Earth Foundation, John G. Newton Scholarship of the Alabama Geological Society, and multiple University of Alabama student research and travel grants.

## REFERENCES


Aharon P., Lambert W. J., and Hellstrom J. (2009) Solar variability controls on rainfall in the last millennia: Evidence from a highly resolved stalagmite record from DeSoto Caverns (USA). *American Geophyiscal Union Fall Meeting*, San Francisco. #PP41B-1514 (abstc.).

Alley R. B. (2000a) Ice-core evidence of abrupt climate changes. *PNAS* **97**(4), 1331-1334.

Alley R. B. (2000b) The Younger Dryas cold interval as viewed from central Greenland. *Quat. Sci. Rev.* **19**, 213-226.

Alley R. B. (2004) GISP2 Ice Core Temperature and Accumulation Data. IGBP PAGES/World Data Center for Paleoclimatology Data Contribution Series #2004-013. NOAA/NGDC Paleoclimatology Program, Boulder CO, USA.

Alley R. B., Meese D. A., Shuman C. A., Gow A. J., Taylor K. C., Grootes P. M., White J. W. C., Ram M., Waddington E. D., Mayewski P. A., and Zielinski G. A. (1993) Abrupt increase in Greenland snow accumulation at the end of the Younger Dryas event. *Nature* **362**, 527-529.

Andrews J. T., Jennings A. E., Kerwin M. W., Kirby M., Manley W., Miller G. H., Bond G., and MacLean B. (1995) A Heinrich-like event, H-0 (DC-0): Source(s) for detrital Carbonate in the North Atlantic during the Younger Dryas chronozone. *Palaeogeography* **10**, 943-952.

Asmerom Y., Polyak V. J., and Burns S. J. (2010) Variable winter moisture in the southwestern United States linked to rapid glacial climate shifts. *Nat. Geosci.* **3**, 114-117.

Bar-Matthews M., Matthews A., and Ayalon A. (1991) Environmental Controls of Speleothem Mineralogy in a Karstic Dolomitic Terrain (Soreq Cave, Israel). *J. Geol.* **99**, 189-207.

Baker A., Genty D., Dreybrodt W., Barnes W. L., Mockler N. J., and Grapes J. (1998) Testing theoretically predicted stalagmite growth rate with recent annually laminated samples: Implications for past stalagmite deposition. *Geochim. Cosmochim. Acta* **62**(3), 393-404.

Baker A., Smith C. L., Jex C., Fairchild I. J., Genty D., and Fuller L. (2008) Annually laminated speleothems: A review. *Int. J. Speleol.* **37**(3), 193-206.

Boch R. and Spötl C. (2008) The origin of lamination in stalagmites from Katerloch Cave, Austria: Towards a seasonal proxy. *PAGES News* **16**(3), 21-22.

Boës X. and Fagel N. (2008) Timing of the late glacial and Younger Dryas cold reversal in southern Chile varved sediments. *J. Paleolim.* **39**, 267-281.

Broecker W. S. (1997) Thermohaline circulation, the achilles heel of our climate system: Will man-made $CO_2$ upset the current balance? *Science* **278**, 1582-1588.

Broecker W. S. (2000) Abrupt climate change: causal constraints provided by the paleoclimate record. *Earth Sci. Rev.* **51**, 137-154.

Bryson R. A. and Hare F. K. (1974) The climates of North America. In *World survey of climatology*, Vol. 11 (eds. R. A. Bryson and F. K. Hare). Elsevier. pp. 321-356.

Cabrol P. and Coundray J. (1982) Climatic fluctuations influence in the genesis and diagenesis of carbonate speleothems in southwestern France. *Nat. Speleol. Soc.* **44**, 112-117.

COHMAP members. (1988) Climatic changes of the last 18,000 Years: Observations and model simulations. *Science* **241**, 1043-1052.

Dansgaard W., Johnsen S. J., Clausen H. B., Dahl-Jensen D., Gundestrup N., Hammer C. U., Hvidberg C. S., Steffensen J. P., Sveinbjörnsdóttir Á. E., Jouzel J., and Bond G. (1993) Evidence for general instability of past climate from a 250-kyr ice-core record. *Nature* **364**, 218-220.

Debajyoti P. and Skrzypek G. (2007) Assessment of carbonate-phosphoric acid analytical technique performed using GasBench II in continuous flow isotope ratio mass spectrometry. *Int. J. Mass Spec.* **262**, 180-186.

Denton G. H. and Broecker W. S. (2008) Wobbly ocean conveyor circulation during the Holocene? *Quat. Sci. Rev.* **27**, 1939-1950.

Dorale J. A., Wozniak L. A., Bettis III E. A., Carpenter S. J., Mandel R. D., Hajic E. R., Lopinot N. H., and Ray J. H. (2010) Isotopic evidence for Younger Dryas aridity in the North American midcontinent. *Geology* **38**(6), 519-522.

Fairbanks R. G. (1989) A 17,000-year glacio-eustatic sea level record: Influence of glacial melting rates on the Younger Dryas event and deep-ocean circulation. *Nature* **342**, 637-642.

Fairchild I. J., Smith C. L., Baker A., Fuller L., Spötl C., Mattey D., McDermott F., and E.I.M.F. (2006) Modification and preservation of environmental signals in speleothems. *Earth Sci. Rev.* **75**, 105-153.

Flower B. P., Hastings D. W., Hill H. W., and Quinn T. M. (2004) Phasing of deglacial warming and Laurentide Ice Sheet meltwater in the Gulf of Mexico. *Geology* **32**(7), 597-600, doi:10.1130/G2064.1.

Flückiger J. (2008) Did you say "Fast?" *Science* **321**, 650-651.

Folk R. L. (1965) Some aspects of recrystallization in ancient limestones. In *Dolomitization and Limestone Diagenesis - A Symposium* (eds. L. C. Pray and R. C. Murray). Society of

Economic Paleontologists and Mineralologists, Special Publication 13. pp. 14-48.

Frisia S., Borsato A., Fairchild I. J., McDermott F., and Selmo E. M. (2002) Aragonite-calcite relationships in speleothems (Grotte de Clamouse, France): Environment, fabrics, and carbonate chemistry. *J. Sed. Res.* **72**(5), 687-699.

Grimm E. C., Jacobson G. L. J., Watts W. A., Hansen B. C. S., and Maasch K. A. (1993) A 50,000-year record of climate oscillations from Florida and its temporal correlation with the Heinrich Events. *Science* **261**(5118), 198-200; doi:10.1126/science.261.5118.198.

Grimm E. C., Watts W. A., Jacobson G. L. J., Hansen B. C. S., Almquist H. R., and Dieffenbacher-Krall A. C. (2006) Evidence for warm wet Heinrich events in Florida. *Quat. Sci. Rev.* **25**, 2197-2211.

Grootes P. M. (1993) Interpreting continental oxygen isotope records. In *Climate change in continental isotope records* (eds. P. K. Swart, K. C. Lohmann, J. McKenzie, and S. Savin). American Geophysical Union. pp. 37-46.

Heinrich H. (1988a) Discovery and description of six layers rich in ice-rafted debris in the sediment cores from the Dreizack seamount in the northeastern Atlantic. *Quat. Res.* **29**, 142-152.

Heinrich H. (1988b) Origin and consequences of cyclic ice rafting in the northeast Atlantic Ocean during the past 13,000 yr. *Quat. Res.* **29**, 142-153.

Hellstrom J. (2006) U–Th dating of speleothems with high initial $^{230}$Th using stratigraphical constraint. *Quat. Geochronol.* **1**, 289-295.

Hemming S. R. (2004) Heinrich events: Massive late Pleistocene detritus layers of the North Atlantic and their global climate impact. *Rev. Geophys.* **42**, 1-43.

Hendy C. H. (1971) The isotopic geochemistry of speleothems--I. The calculation of the effects of different modes of formation on the isotopic composition of speleothems and their applicability as palaeoclimatic indicators. *Geochim. Cosmochim. Acta* **35**, 801-824.

Hill C. A. and Forti P. (1986) *Cave minerals of the world*. Alabama National Speleological Society.

Holliday V. T. (2000) Folsom drought and episodic drying on the Southern High Plains from 10,900–10,200 14C yr B.P. *Quat. Res.* **53**, 1-12.

Johnsen S. J., Clausen H. B., Dansgaard W., Fuhrer K., Gundestrup N., Hammer C. U., Iversen P., Jouzel J., Stauffer B., and Steffensen J. P. (1992) Irregular glacial interstadials recorded in a new Greenland ice core. *Nature* **359**, 311-313.

Jouzel J., Masson V., Cattani O., Falourd S., Stievenard M., Stenni B., Longinelli A., Johnsen S.

J., Steffensen J. P., Petit J. R., Schwander J., Souchez R., and Barkov N. I. (2001) A new 21 ky high resolution East Antarctic climate record. *Geophys. Res. Lett.* **28**(16), 3199-3202.

Katz R. W., Parlange M. B., and Tebaldi C. (2003) Stochastic modeling of the effects of large-scale circulation on daily weather in the southeastern U.S. *Clim. Change* **60**, 189-216.

Kaufmann G. (2003) Stalagmite growth and palaeo-climate: the numerical perspective. *Earth Planet. Sci. Lett.* **214**, 251-266.

Kim S.-T., Mucci A., and Taylor B. E. (2007) Phosphoric acid fractionation factors for calcite and aragonite between 25 and 75 °C: Revisited. *Chem. Geol.* **246**, 135-146.

Knight D. B. and Davis R. E. (2007) Climatology of tropical cyclone rainfall in the southeastern United States. *Phys. Geogr.* **28**(2), 126-147.

Kowalczk A. J. and Froelich P. N. (2010) Cave air ventilation and $CO_2$ outgassing by radon-222 modeling: How fast do caves breathe? *Earth Planet. Sci. Lett.* **289**, 209-219.

Kutzbach J. E. and Wright H. E. (1985) Simulation of the climate of 18,000 years B.P.: Results for the North American/North Atlantic/European sector and comparison with the geological record of North America. *Quat. Sci. Rev.* **4**, 147-187.

Lambert W. J. and Aharon P. (2010) Oxygen and hydrogen isotopes of rainfall and dripwater at DeSoto Caverns (Alabama, USA): Key to understanding past climate variability of moisture transport from the Gulf of Mexico. *Geochem. Cosmochim. Acta* **74**, 846-861.

Lachniet M. S. (2009) Climatic and environmental controls on speleothem oxygen-isotope values. *Quat. Sci. Rev.* **28**, 412-432.

Long A. R. (1959) The Climate of Alabama. In *United States National Oceanic and Atmospheric Administration 1974. Volume 1: Eastern states plus Puerto Rico and the United States Virgin Islands.* Water Information Center. pp. 1-14.

Manabe S. and Stouffer R. J. (1993) Century-scale effects of increased atmospheric $CO_2$ on the ocean-atmosphere system. *Nature* **364**, 215-218.

Martín-García R., Alonso-Zarza A. M., and Martín-Pérez A. (2009) Loss of primary texture and geochemical signatures in speleothems due to diagenesis: evidences from Castañar Cave, Spain. *Sediment. Geol.* **221**, 141-149.

Mattey D., Latin J. P., and Ainsworth M. (2008) Cave monitoring and calibration of a $\delta^{18}O$-climate transfer function for a Gibraltar speleothem. *PAGES News* **16**(3), 15-17.

Mazzullo S. J. (1980) Calcite pseudospar replacive of marine acicular aragonite, and implications for aragonite cement diagenesis. *J. Sediment. Petrol.* **50**, 409-422.

McDermott F. (2004) Palaeo-climate reconstruction from stable isotope variations in speleothems: a review. *Quat. Sci. Rev.* **23**, 901-918.

Menking K. M., Anderson R. Y., Shafike N. G., Syed K. H., and Allen B. D. (2004) Wetter or colder during the Last Glacial Maximum? Revisiting the pluvial lake question in southwestern North America. *Quat. Res.* **62**, 280-288.

Mo K. C. and Schemm J. E. (2008) Relationships between ENSO and drought over the southeastern United States. *Geophys. Res. Lett.* **35**, L15701, doi: 10.1029/2008GL034656.

O'Neil J. R., Clayton R. N., and Mayeda T. K. (1969) Oxygen isotope fractionation in divalent metal carbonates. *J. Chem. Phys.* **51**(12), 5547-5558.

Peltier W. R. and Fairbanks R. G. (2006) Global glacial ice volume and Last Glacial Maximum duration from an extended Barbados sea level record. *Quat. Sci. Rev.* **25**, 3322-3337.

Peteet D. (1995) Global Younger Dryas? *Quat. Int.* **28**, 93-104.

Pingitore N. E. (1976) Vadose and phreatic diagenesis: Processes, products and their recognition in corals. *J. Sediment. Petrol.* **46**, 985-1006.

Polyak V. J., Rasmussen J. B. T., and Asmerom Y. (2004) Prolonged wet period in the southwestern United States through the Younger Dryas. *Geology* **32**(1), 5-8.

Portmann R. W., Solomon S., and Hegerl G. C. (2009) Spatial and seasonal patterns in climate change, temperatures, and precipitation across the United States. *PNAS* **106**(18), 7324-7329.

Railsback L. B., Brook G. A., Chen J., Kalin R., and Fleisher C. J. (1994) Environmental Controls on the Petrology of a Late Holocene Speleothem from Botswana with Annual Layers of Aragonite and Calcite. *J. Sediment. Res.* **A64**(1), 147-155.

Rasmusson E. M. (1968) Atmospheric water vapor transport and the water balance of North America II. Large-scale water balance investigations. *Mon. Weather Rev.* **96**(10), 720-734.

Romanek C. S., Grossman E. L., and Worse J. W. (1992) Carbon isotopic fractionation in synthetic aragonite and calcite: Effects of temperature and precipitation rate. *Geochem. Cosmochim. Acta* **56**, 419-430.

Rozanski K., Araguás-Araguás L., and Gonfiantini R. (1993) Isotopic patterns in modern global precipitation. In *Climate change in continental isotopic records*. Geophysical Monograph 78, American Geophyiscal Union. pp. 1-36.

Shakun J. D. and Carlson A. E. (2010) A global perspective on Last Glacial Maximum to Holocene climate change. *Quat. Sci. Rev.* **29**, 1801-1816.

Simpkins W. W. (1995) Isotopic composition of precipitation in central Iowa. *J. Hydrol.* **172**, 185-207.

Spötl C., Fairchild I. J., and Tooth A. F. (2005) Cave air control on dripwater geochemistry, Obir Caves (Austria): Implications for speleothem deposition in dynamically ventilated caves. *Geochim. Cosmochim. Acta* **69**(10), 2457-2468.

Stahle D. W. and Cleaveland M. K. (1992) Reconstruction and analysis of spring rainfall over the southeastern U.S. for the past 1000 years. *Bull. Am. Meteorol. Soc.* **73**(12), 1947-1961.

Stahle D. W. and Cleaveland M. K. (1994) Tree-ring reconstructed rainfall over the southeastern U.S.A. during the Medieval Warm Period and Little Ice Age. *Clim. Change* **26**, 199-212.

Stuiver M, Reimer PJ, Reimer RW (2005) CALIB 5.0.2: Computer program for radiocarbon calibration. URL: http://calib.qub.ac.uk/calib/

Tarutani T., Clayton R. N., and Mayeda T. (1969) The effect of polymorphism and magnesium substitution on oxygen isotope fractionation between calcium carbonate and water. *Geochem. Cosmochim. Acta* **33**, 987-996.

Wagner J. D. M., Cole J. E., Beck J. W., Patchett J. W., Patchett P. J., Henderson G. M., and Barnett H. R. (2010) Moisture variability in the southwestern United States linked to abrupt glacial climate change. *Nat. Geosci.* **3**, 110-113.

Willard D. A., Bernhardt C. E., Brooks G. R., Cronin T. M., Edgar T., and Larson R. (2007) Deglacial climate variability in central Florida, USA. *Palaeogeogr. Palaeoclimatol. Palaeoecol.* **251**, 366-382.

Woo K. S. and Choi D. W. (2006) Calcitization of aragonite speleothems in limestone caves in Korea: Diagenetic process in a semiclosed system. In *Perspectives on karst geomorphology, hydrology, and geochemistry - A tribute to Derek C. Ford and William B. White* (eds. R. S. Harmon and C. Wicks). Geological Society of America Special Paper 404. pp. 297-306.

Wurster C. M. and Patterson W. P. (2001) Late Holocene climate change for the eastern interior United States: evidence from high-resolution $\delta^{18}O$ values of sagittal otoliths. *Palaeogeogr. Palaeoclimatol. Palaeoecol.* **170**, 81-100.

Yapp C. J. (1985) D/H variations of meteoric waters in Albuquerque, New Mexico, U.S.A. *J. Hydrol.* **76**(1-2), 63-84.

Yu Z. and Wright Jr. H. E. (2001) Response of interior North America to abrupt climate oscillations in the North Atlantic region during the last deglaciation. *Earth Sci. Rev.* **52**, 333-369.

CHAPTER 5

# CONCLUSIONS

This work provides valuable insights into the dominant controls of $\delta^{18}O$ and $\delta^{13}C$ of cave waters of DeSoto Caverns, which allowed proper interpretation of paleoclimate conditions affecting the Southeast between 31.9 ka BP and 11.3 ka BP. High rates of evapotranspiration during summer/early fall months limit aquifer recharge to winter/early spring months, an observation that is confirmed by the match between mean cave water $\delta^{18}O$ and mean winter $\delta^{18}O$ of recharging rainfall. Decreasing rainfall amounts over interannual time spans is related to changes in atmospheric circulation patterns (i.e., ENSO and Bermuda High) and is expressed by overall enrichments in $^{18}O$ and $^{2}H$ of rainfall and decreasing drip flow rates of infiltrating cave waters. Seasonal variability in $\delta^{18}O$ and $\delta D$ of rainfall are not transmitted through the cave waters due to mixing within the karst aquifer; however, attenuated interannual $^{18}O$ and $^{2}H$ enrichment trends are observed in the cave waters. Changes in speleothem $\delta^{18}O$ in DeSoto Caverns are biased toward winter rainfall variability and provide the opportunity for extending records of atmospheric circulation patterns into the past.

Unlike dripwater $\delta^{18}O$, the $\delta^{13}C$ of dissolved inorganic carbon of cave waters have strong seasonal variations with measured summer values near the predicted value of -12.2‰ and winter

waters $^{13}C$-enriched by >10‰. Seasonal variations in DIC and $\delta^{13}C_{DIC}$ were found to be modulated by the state of cave air ventilation and differential loading of infiltrating waters with soil-derived $CO_2$. Summer/early fall air stagnation within DeSoto Caverns promotes slow degassing of $CO_2$ from cave waters accompanied by quasi-equilibrium isotopic fractionations. Winter/early spring cave air ventilation promotes forced $CO_2$ degassing and kinetically enhanced rates of $^{13}C$-enrichment of residual DIC. Seasonally varying DIC concentrations are a function of increased summer $CO_2$ flux via root respiration and organic debris oxidation contrasting with winter drips from which bicarbonate is actively removed due to an increased carbonate saturation state. Therefore, variations in speleothem $\delta^{13}C$ are not simply a reflection of biological activity above the cave but are also the result of changing seasonal biases in $CO_2$ flux and the state of cave air ventilation.

Dramatic climate swings (i.e., Heinrich and Dansgaard-Oeschger events) during the Last Glacial Maximum and deglaciation intervals (31.9-11.3 ka BP) were expressed as periods of increased and decreased winter rainfall during cold and warm events, respectively. These variations were attributed to north-south migration of the polar jet stream and were manifested in the stalagmite as $^{18}O$-depletions due to increased contribution of $^{18}O$-depleted winter rainfall from the Gulf of Mexico. My data suggest the onset of the Younger Dryas cold phase, which was coeval with a period of non-deposition in the DeSoto stalagmite, marked the start of significant changes in the polar jet stream's path across North America. A mean position of the polar jet stream around the Great Lakes allowed warm air from the Gulf of Mexico to infiltrate much of the eastern interior of North America, which resulted in infrequent collisions of warm and cold air masses needed to induce rainfall over the Southeast. Following the Younger Dryas dry spell, migration of the polar jet stream toward its current position allowed the establishment of near

modern rainfall conditions, which promoted an order of magnitude increase in ($^{13}$C-enriched) aragonite deposition rates before the new flow regime through the epikarst prohibited deposition after 11.3 ka BP. This new high-resolution record of winter rainfall variability and jet stream migration is of great importance to the scientific community and will aid in better predicting the Southeast's response to future climate change.

REFERENCES


Alexandrov V. and Hoogenboom G. (2000) Vulnerability and adaptation assessments of agricultural crops under climate change in the Southeastern USA. *Theor. Appl. Climatol.* **67**, 45-63.

Bar-Matthews M., Ayalon A., Gilmour M., Matthews A., and Hawkesworth C. (2003) Sea-land oxygen isotopic relationships from planktonic foraminifera and speleothems in the Eastern Mediterranean region and their implication for paleorainfall during interglacial intervals *Geochim. Cosmochim. Acta* **67**(17), 3181-3199.

Baker A., Asrat A., Fairchild I. J., Leng M. J., Wynn P. M., Bryant C., Genty D., and Mohammed U. (2007) Analysis of the climate signal contained within $\delta^{18}O$ and growth rate parameters in two Ethiopian stalagmites. *Geochim. Cosmochim. Acta* **71**, 2975-2988.

Baker A., Smith C. L., Jex C., Fairchild I. J., Genty D., and Fuller L. (2008) Annually laminated speleothems: a review. *Int. J. Speleol.* **37**(3), 193-206.

Bryson R. A. and Hare F. K. (1974) The climates of North America. In *World survey of climatology*, Vol. 11 (eds. R. A. Bryson and F. K. Hare). Elsevier. pp. 321-356.

Cane M. A. (2005) The evolution of El Niño, past and future. *Earth Planet. Sci. Lett.* **230**, 227-240.

Cruz F. W. J., Karmann I., Viana O. J., Burns S. J., Ferrari J. A., Vuille M., Sial A. N., and Moreira M. Z. (2005) Stable isotope study of cave percolation waters in subtropical Brazil: Implications for paleoclimate inferences from speleothems. *Chem. Geol.* **220**, 245-262.

Delcourt P. A. (1980) Goshen Springs: Late Quaternary Vegetation Record for Southern Alabama. *Ecology* **61**(2), 371-386.

Delcourt H. R., Delcourt P. A., and Spiker E., C. (1983) A 12000-year record of forest history from Cahaba Pond, St. Clair County, Alabama. *Ecology* **64**(4), 874-887.

Dixon B. L. and Segerson K. (1999) Impacts of increased climate variability on the profitability of Midwest agriculture. *J. Agr. Appl. Econ.* **31**(3), 537-549.

Fairchild I. J., Smith C. L., Baker A., Fuller L., Spötl C., Mattey D., McDermott F., and E.I.M.F. (2006) Modification and preservation of environmental signals in speleothems. *Earth Sci. Rev.* **75**, 105-153.

Hinrichsen D. (1998) *Coastal Waters of the World: Trends, Threats, and Strategies*. Island Press.

Katz R. W., Parlange M. B., and Tebaldi C. (2003) Stochastic modeling of the effects of large-scale circulation on daily weather in the southeastern U.S. *Clim. Change* **60**, 189-216.

Knight D. B. and Davis R. E. (2007) Climatology of tropical cyclone rainfall in the southeastern United States. *Phys. Geogr.* **28**(2), 126-147.

Lachniet M. S. (2009) Climatic and environmental controls on speleothem oxygen-isotope values. *Quat. Sci. Rev.* **28**, 412-432.

Long A. R. (1959) The Climate of Alabama. In *United States National Oceanic and Atmospheric Administration 1974. Volume 1: Eastern states plus Puerto Rico and the United States Virgin Islands*. Water Information Center. pp. 1-14.

McDermott F. (2004) Palaeo-climate reconstruction from stable isotope variations in speleothems: a review. *Quat. Sci. Rev.* **23**, 901-918.

Neff U., Burns S. J., Mangini A., Mudelsee M., Fleitmann D., and Matter A. (2001) Strong coherence between solar variability and the monsoon in Oman between 9 and 6 kyr ago. *Nature* **411**, 290-293.

Pirie R. L., de Loë R. C., and Kreutzwiser R. (2004) Drought planning and water allocation: An assessment of local capacity in Minnesota. *J. Environ. Manage.* **73**, 25-38.

Rasmusson E. M. (1968) Atmospheric water vapor transport and the water balance of North America II. Large-scale water balance investigations. *Mon. Weather Rev.* **96**(10), 720-734.

Rosen M. R., Bright J., Carran P., Stewart M. K., and Reeves R. (1999) Estimating rainfall recharge and soil water residence times in Pukekohe, New Zealand, by combining geophysical, chemical and isotopic methods. *Ground Water* **37**(6), 836-844.

Rosenzweig C., Iglesias A., Yang X. B., Epstein P. R., and Chivian E. (2001) Climate change and extreme weather events: Implications for food production, plant diseases, and pests. *Global Clim. Hum. Health* **2**(2), 90-104.

Simpkins W. W. (1995) Isotopic composition of precipitation in central Iowa. *J. Hydrol.* **172**, 185-207.

Stahle D. W. and Cleaveland M. K. (1992) Reconstruction and analysis of spring rainfall over the southeastern U.S. for the past 1000 years. *Bull. Am. Meteorol. Soc.* **73**(12), 1947-1961.

Stahle D. W. and Cleaveland M. K. (1994) Tree-ring reconstructed rainfall over the southeastern U.S.A. during the Medieval Warm Period and Little Ice Age. *Clim. Change* **26**, 199-212.

Watts W. A. (1980) The Late Quaternary vegetation history of the Southeastern United States. *Annu. Rev. Ecol. Syst.* **11**, 387-409.

Yin Z.-Y. (1994) Moisture condition in the South-eastern USA and teleconnection patterns. *Int. J. Climatol.* **14**, 947-967.

## APPENDIX 2.1.

(WEEKLY TUSCALOOSA RAINFALL WATER ISOTOPE DATA)

Summary of weekly precipitation collection dates, rainfall amounts, measured $\delta^{18}O$, measured $\delta D$, and calculated *d-excess* (*d-excess*=$\delta D - 8\delta^{18}O$).

| Week | Dates of Sampling (mm/dd-mm/dd) | Year | Rainfall (mm) | $\delta^{18}O$ (‰ VSMOW) | $\delta D$ (‰ VSMOW) | *d-excess* (‰) |
|---|---|---|---|---|---|---|
| 1 | 5/30-6/5 | 2005 | 69.1 | -7.4 | -48.5 | 10.3 |
| 2 | 6/6-6/12 | 2005 | 122.9 | -6.3 | -40.0 | 10.2 |
| 3 | 6/13-6/19 | 2005 | 0.0 | - | - | - |
| 4 | 6/20-6/26 | 2005 | 0.0 | - | - | - |
| 5 | 6/27-7/3 | 2005 | 23.0 | -4.5 | -33.1 | 2.9 |
| 6 | 7/4-7/10 | 2005 | 145.5 | -9.6 | -71.2 | 5.3 |
| 7 | 7/11-7/17 | 2005 | 4.2 | -2.4 | -12.7 | 6.8 |
| 8 | 7/18-7/24 | 2005 | 0.0 | - | - | - |
| 9 | 7/25-7/31 | 2005 | 76.5 | -2.0 | -6.6 | 9.2 |
| 10 | 8/1-8/7 | 2005 | 33.0 | -3.9 | -27.2 | 3.9 |
| 11 | 8/8-8/14 | 2005 | 110.7 | -5.0 | -26.3 | 13.7 |
| 12 | 8/15-8/21 | 2005 | 2.3 | 0.0 | 8.9 | 9.0 |
| 13 | 8/22-8/28 | 2005 | 5.8 | -1.9 | -4.7 | 10.6 |
| 14 | 8/29-9/4 | 2005 | 76.1 | -5.4 | -32.3 | 11.1 |
| 15 | 9/5-9/11 | 2005 | 0.0 | - | - | - |
| 16 | 9/12-9/18 | 2005 | 3.2 | -1.5 | -4.7 | 7.6 |
| 17 | 9/19-9/25 | 2005 | 72.0 | -4.5 | -25.0 | 10.8 |
| 18 | 9/26-10/2 | 2005 | 0.0 | - | - | - |
| 19 | 10/3-10/9 | 2005 | 4.1 | -5.0 | -32.6 | 7.6 |
| 20 | 10/10-10/16 | 2005 | 0.0 | - | - | - |
| 21 | 10/17-10/23 | 2005 | 0.0 | - | - | - |
| 22 | 10/24-10/30 | 2005 | 0.0 | - | - | - |
| 23 | 10/31-11/6 | 2005 | 3.9 | -4.1 | -11.0 | 22.1 |
| 24 | 11/7-11/13 | 2005 | 0.7 | -0.9 | 6.3 | 13.6 |
| 25 | 11/14-11/20 | 2005 | 31.5 | -5.5 | -29.9 | 14.2 |
| 26 | 11/21-11/27 | 2005 | 22.9 | -12.3 | -78.3 | 20.0 |
| 27 | 11/28-12/4 | 2005 | 18.4 | -4.9 | -20.3 | 19.1 |
| 28 | 12/5-12/11 | 2005 | 10.6 | -7.9 | -37.5 | 25.6 |
| 29 | 12/12-12/18 | 2005 | 42.0 | -8.8 | -52.9 | 17.9 |
| 30 | 12/19-12/25 | 2005 | 24.6 | -8.9 | -46.6 | 24.9 |
| 31 | 12/26-1/1 | 2005/6 | 4.1 | -4.3 | -12.8 | 21.7 |
| 32 | 1/2-1/8 | 2006 | 0.0 | - | - | - |
| 33 | 1/9-1/15 | 2006 | 40.3 | -5.9 | -26.3 | 21.0 |
| 34 | 1/16-1/22 | 2006 | 93.2 | -5.8 | -23.4 | 22.8 |
| 35 | 1/23-1/29 | 2006 | 22.1 | -5.5 | -24.0 | 19.7 |
| 36 | 1/30-2/5 | 2006 | 44.8 | -4.6 | -30.0 | 7.1 |
| 37 | 2/6-2/12 | 2006 | 27.0 | -8.5 | -40.7 | 27.4 |
| 38 | 2/13-2/19 | 2006 | 18.5 | -3.3 | 2.2 | 28.8 |
| 39 | 2/20-2/26 | 2006 | 75.7 | -6.4 | -34.4 | 16.7 |
| 40 | 2/27-3/5 | 2006 | 4.1 | -1.5 | -3.4 | 8.8 |

| Week | Dates of Sampling (mm/dd-mm/dd) | Year | Rainfall (mm) | $\delta^{18}O$ (‰ VSMOW) | δD (‰ VSMOW) | *d-excess* (‰) |
|---|---|---|---|---|---|---|
| 41 | 3/6-3/12 | 2006 | 23.1 | -3.6 | -8.3 | 20.3 |
| 42 | 3/13-3/19 | 2006 | 21.2 | -3.3 | -8.7 | 17.6 |
| 43 | 3/20-3/26 | 2006 | 61.6 | -3.1 | -9.5 | 15.5 |
| 44 | 3/27-4/2 | 2006 | 13.3 | -1.0 | 10.0 | 17.8 |
| 45 | 4/3-4/9 | 2006 | 27.4 | -3.7 | -11.7 | 17.6 |
| 46 | 4/10-4/16 | 2006 | 0.0 | - | - | - |
| 47 | 4/17-4/23 | 2006 | 26.9 | -3.3 | -13.5 | 13.2 |
| 48 | 4/24-4/30 | 2006 | 15.1 | -1.7 | 4.2 | 17.8 |
| 49 | 5/1-5/7 | 2006 | 19.7 | -2.3 | -3.5 | 14.9 |
| 50 | 5/8-5/14 | 2006 | 94.9 | -2.3 | -17.4 | 1.0 |
| 51 | 5/15-5/21 | 2006 | 0.0 | - | - | - |
| 52 | 5/22-5/28 | 2006 | 0.0 | - | - | - |
| 53 | 5/29-6/4 | 2006 | 2.5 | 0.9 | 14.9 | 7.9 |
| 54 | 6/5-6/11 | 2006 | 2.2 | -1.4 | -2.8 | 8.3 |
| 55 | 6/12-6/18 | 2006 | 13.1 | -1.7 | 1.6 | 15.0 |
| 56 | 6/19-6/25 | 2006 | 13.6 | -1.9 | -6.6 | 8.7 |
| 57 | 6/26-7/2 | 2006 | 0.0 | - | - | - |
| 58 | 7/3-7/9 | 2006 | 7.6 | 1.9 | 17.8 | 2.5 |
| 59 | 7/10-7/16 | 2006 | 0.0 | - | - | - |
| 60 | 7/17-7/23 | 2006 | 20.4 | -1.7 | -1.5 | 12.4 |
| 61 | 7/24-7/30 | 2006 | 47.1 | -3.8 | -24.0 | 6.6 |
| 62 | 7/31-8/6 | 2006 | 13.5 | -1.7 | -9.0 | 4.6 |
| 63 | 8/6-8/13 | 2006 | 36.6 | -2.2 | -7.5 | 10.1 |
| 64 | 8/14-8/20 | 2006 | 1.9 | -0.5 | 1.4 | 5.4 |
| 65 | 8/21-8/27 | 2006 | 0.0 | - | - | - |
| 66 | 8/28-9/3 | 2006 | 0.0 | - | - | - |
| 67 | 9/4-9/10 | 2006 | 8.6 | -3.0 | -12.7 | 11.0 |
| 68 | 9/11-9/17 | 2006 | 15.8 | -2.8 | -8.9 | 13.8 |
| 69 | 9/18-9/24 | 2006 | 100.9 | -4.5 | -27.6 | 8.5 |
| 70 | 9/25-10/1 | 2006 | 0.0 | - | - | - |
| 71 | 10/2-10/8 | 2006 | 0.0 | - | - | - |
| 72 | 10/9-10/15 | 2006 | 0.0 | - | - | - |
| 73 | 10/16-10/22 | 2006 | 159.0 | -4.8 | -25.6 | 12.8 |
| 74 | 10/23-10/29 | 2006 | 27.4 | -6.0 | -35.8 | 12.4 |
| 75 | 10/30-11/5 | 2006 | 27.3 | -3.8 | -10.7 | 20.0 |
| 76 | 11/6-11/12 | 2006 | 49.1 | -5.6 | -24.8 | 19.7 |
| 77 | 11/13-11/19 | 2006 | 23.2 | -5.2 | -29.1 | 12.5 |
| 78 | 11/20-11/26 | 2006 | 0.0 | - | - | - |
| 79 | 11/27-12/3 | 2006 | 12.4 | -1.1 | 6.0 | 14.8 |
| 80 | 12/4-12/10 | 2006 | 0.0 | - | - | - |
| 81 | 12/11-12/17 | 2006 | 14.3 | -3.8 | -13.0 | 17.6 |
| 82 | 12/18-12/24 | 2006 | 47.8 | -5.9 | -39.6 | 7.5 |

| Week | Dates of Sampling (mm/dd-mm/dd) | Year | Rainfall (mm) | $\delta^{18}O$ (‰ VSMOW) | δD (‰ VSMOW) | *d-excess* (‰) |
|---|---|---|---|---|---|---|
| 83 | 12/25-12/31 | 2006 | 70.6 | -3.9 | -20.3 | 11.1 |
| 84 | 1/1-1/7 | 2007 | 18.0 | -3.2 | -15.3 | 10.3 |
| 85 | 1/8-1/14 | 2007 | 0.0 | - | - | - |
| 86 | 1/15-1/21 | 2007 | 23.7 | -2.1 | -2.4 | 14.2 |
| 87 | 1/22-1/28 | 2007 | 3.6 | -5.2 | -29.9 | 11.7 |
| 88 | 1/29-2/4 | 2007 | 36.9 | -8.1 | -46.3 | 18.1 |
| 89 | 2/5-2/11 | 2007 | 5.6 | -4.2 | -24.6 | 8.6 |
| 90 | 2/12-2/18 | 2007 | 8.3 | -5.9 | -37.4 | 9.9 |
| 91 | 2/19-2/25 | 2007 | 37.5 | -2.9 | -8.0 | 15.4 |
| 92 | 2/26-3/4 | 2007 | 19.2 | -1.5 | -1.8 | 9.9 |
| 93 | 3/5-3/11 | 2007 | 0.0 | - | - | - |
| 94 | 3/12-3/18 | 2007 | 2.8 | -1.6 | -4.7 | 7.7 |
| 95 | 3/19-3/25 | 2007 | 0.0 | - | - | - |
| 96 | 3/26-4/1 | 2007 | 4.4 | -1.9 | -3.6 | 11.6 |
| 97 | 4/2-4/8 | 2007 | 4.3 | -2.9 | -10.8 | 12.3 |
| 98 | 4/9-4/15 | 2007 | 23.5 | -1.4 | -1.8 | 9.6 |
| 99 | 4/16-4/22 | 2007 | 0.0 | - | - | - |
| 100 | 4/23-4/29 | 2007 | 32.0 | -3.3 | -10.2 | 16.5 |
| 101 | 4/30-5/6 | 2007 | 0.0 | - | - | - |
| 102 | 5/7-5/13 | 2007 | 0.0 | - | - | - |
| 103 | 5/14-5/20 | 2007 | 12.0 | -2.7 | -9.2 | 12.6 |
| 104 | 5/21-5/27 | 2007 | 0.0 | - | - | - |
| 105 | 5/28-6/3 | 2007 | 1.2 | 0.2 | 14.3 | 12.5 |
| 106 | 6/4-6/10 | 2007 | 0.0 | - | - | - |
| 107 | 6/11-6/17 | 2007 | 3.3 | -0.7 | -4.3 | 1.4 |
| 108 | 6/18-6/24 | 2007 | 15.3 | -6.3 | -41.0 | 9.4 |
| 109 | 6/25-7/1 | 2007 | 9.4 | -1.3 | -2.4 | 8.1 |
| 110 | 7/2-7/8 | 2007 | 52.5 | -4.4 | -25.8 | 9.6 |
| 111 | 7/9-7/15 | 2007 | 30.8 | -5.2 | -31.0 | 10.5 |
| 112 | 7/16-7/22 | 2007 | 8.4 | -3.1 | -17.0 | 8.2 |
| 113 | 7/23-7/29 | 2007 | 2.2 | -0.5 | 2.6 | 6.8 |
| 114 | 7/30-8/5 | 2007 | 0.0 | - | - | - |
| 115 | 8/6-8/12 | 2007 | 0.0 | - | - | - |
| 116 | 8/13-8/19 | 2007 | 123.4 | -1.6 | -7.5 | 5.1 |
| 117 | 8/20-8/26 | 2007 | 19.0 | -2.5 | -11.1 | 8.9 |
| 118 | 8/27-9/2 | 2007 | 62.0 | -5.7 | -33.4 | 12.4 |
| 119 | 9/3-9/9 | 2007 | 0.0 | - | - | - |
| 120 | 9/10-9/16 | 2007 | 49.9 | -5.6 | -30.6 | 14.4 |
| 121 | 9/17-9/23 | 2007 | 2.8 | -4.6 | -23.4 | 13.6 |
| 122 | 9/24-9/30 | 2007 | 0.0 | - | - | - |
| 123 | 10/1-10/7 | 2007 | 1.6 | -3.4 | -20.4 | 7.0 |
| 124 | 10/8-10/14 | 2007 | 3.6 | -5.0 | -28.2 | 11.6 |

| Week | Dates of Sampling (mm/dd-mm/dd) | Year | Rainfall (mm) | $\delta^{18}O$ (‰ VSMOW) | δD (‰ VSMOW) | *d-excess* (‰) |
|---|---|---|---|---|---|---|
| 125 | 10/15-10/21 | 2007 | 27.2 | -4.8 | -30.0 | 8.2 |
| 126 | 10/22-10/28 | 2007 | 25.4 | -5.8 | -35.2 | 11.0 |
| 127 | 10/29-11/4 | 2007 | 0.0 | - | - | - |
| 128 | 11/5-11/11 | 2007 | 0.0 | - | - | - |
| 129 | 11/12-11/18 | 2007 | 24.8 | -4.5 | -17.0 | 19.4 |
| 130 | 11/19-11/25 | 2007 | 33.4 | -6.0 | -34.5 | 13.8 |
| 131 | 11/26-12/2 | 2007 | 4.2 | -1.8 | 1.7 | 16.0 |
| 132 | 12/3-12/9 | 2007 | 1.2 | -1.0 | 7.0 | 14.6 |
| 133 | 12/10-10/16 | 2007 | 2.1 | -2.5 | -11.5 | 8.3 |
| 134 | 12/17-12/23 | 2007 | 29.4 | -7.4 | -40.8 | 18.7 |
| 135 | 12/24-12/30 | 2007 | 30.3 | -3.2 | -8.5 | 16.9 |
| 136 | 12/31-1/6 | 2007/8 | 0.0 | - | - | - |
| 137 | 1/7-1/13 | 2008 | 37.6 | -3.7 | -13.5 | 16.2 |
| 138 | 1/14-1/20 | 2008 | 16.2 | -12.5 | -88.4 | 11.5 |
| 139 | 1/21-1/27 | 2008 | 11.6 | -4.9 | -19.2 | 20.1 |
| 140 | 1/28-2/3 | 2008 | 62.2 | -4.1 | -11.4 | 21.2 |
| 141 | 2/4-2/10 | 2008 | 12.6 | -3.3 | -11.4 | 14.7 |
| 142 | 2/11-2/17 | 2008 | 47.9 | -3.6 | -10.4 | 18.8 |
| 143 | 2/18-2/24 | 2008 | 68.2 | -6.2 | -37.3 | 12.6 |
| 144 | 2/25-3/2 | 2008 | 0.0 | - | - | - |
| 145 | 3/3-3/9 | 2008 | 81.8 | -4.4 | -19.7 | 15.7 |
| 146 | 3/10-3/16 | 2008 | 23.8 | -1.9 | -8.2 | 6.9 |
| 147 | 3/17-3/23 | 2008 | 0.0 | - | - | - |
| 148 | 3/24-3/30 | 2008 | 6.8 | -0.2 | 9.1 | 10.4 |
| 149 | 3/31-4/6 | 2008 | 39.0 | -4.5 | -20.4 | 15.6 |
| 150 | 4/7-4/13 | 2008 | 16.8 | -1.9 | -0.1 | 14.8 |
| 151 | 4/14-4/20 | 2008 | 31.6 | -4.8 | -17.9 | 20.2 |
| 152 | 4/21-4/27 | 2008 | 36.4 | -5.3 | -26.9 | 15.7 |
| 153 | 4/28-5/4 | 2008 | 20.8 | -5.0 | -26.1 | 13.9 |
| 154 | 5/5-5/11 | 2008 | 34.9 | -1.9 | -4.1 | 10.8 |
| 155 | 5/12-5/18 | 2008 | 79.8 | -4.0 | -20.4 | 11.7 |
| 156 | 5/19-5/25 | 2008 | 0.0 | - | - | - |
| 157 | 5/26-6/1 | 2008 | 4.2 | -2.4 | -9.9 | 8.9 |

**APPENDIX 3.1.**

(CAVE WATER CHEMISTRY)

DeSoto Caverns drip and pool water measurements.

| Date | Drip Rate (µl/s) | $\delta^{13}C$ (‰ VPDB) | DIC (mM) | Drip Rate (µl/s) | $\delta^{13}C$ (‰ VPDB) | DIC (mM) | Drip Rate (µl/s) | $\delta^{13}C$ (‰ VPDB) | DIC (mM) | Drip Rate (µl/s) | $\delta^{13}C$ (‰ VPDB) | DIC (mM) |
|---|---|---|---|---|---|---|---|---|---|---|---|---|
| | | Drip 1 | | | Drip 3 | | | Drip 4 | | | Drip 5 | |
| 3/9/05 | 83.3 | -9.7 | 4.4 | 16.7 | -10.0 | 4.3 | 35.0 | -8.4 | 4.0 | - | - | - |
| 4/28/05 | 30.0 | -9.4 | 4.0 | 6.7 | -7.5 | 2.9 | 5.0 | -8.4 | 3.7 | 100.0 | -9.0 | 4.2 |
| 6/29/05 | 11.7 | -7.1 | 3.0 | 2.7 | -4.8 | 2.4 | 6.8 | -10.8 | 4.4 | 0.5 | 2.1 | 0.6 |
| 8/30/05 | 5.8 | -6.1 | 3.1 | 1.6 | -9.8 | 4.1 | 5.5 | -3.4 | 2.0 | 19.5 | -10.3 | 4.2 |
| 11/14/05 | 2.7 | 1.7 | 1.2 | 0.3 | -0.7 | 0.7 | 4.2 | -4.5 | 2.8 | 9.4 | -9.0 | 3.5 |
| 1/11/06 | 5.6 | -2.5 | 2.1 | 0.2 | - | - | 3.6 | -6.6 | 3.2 | 5.2 | 2.7 | 0.9 |
| 3/10/06 | 22.6 | -10.7 | 4.6 | 4.2 | -2.0 | 1.6 | 3.7 | -1.4 | 1.7 | 53.7 | -9.2 | 3.8 |
| 5/12/06 | 19.7 | -10.2 | 4.5 | 1.9 | -5.2 | 2.5 | 3.3 | -4.2 | 2.1 | 5.3 | -6.7 | 2.8 |
| 7/6/06 | 5.4 | -10.7 | 4.4 | 0.9 | -6.4 | 3.0 | 2.6 | -1.8 | 1.3 | 6.1 | -8.2 | 4.1 |
| 8/31/06 | 4.8 | -7.8 | 2.6 | 0.3 | -1.7 | 0.2 | 3.0 | -10.5 | 3.8 | 0.6 | -7.6 | 2.8 |
| 11/9/06 | 4.5 | -4.8 | 1.6 | 0.2 | - | - | 2.0 | -10.1 | 4.2 | 4.9 | -8.0 | 3.2 |
| 1/18/07 | 14.6 | -8.7 | 4.0 | 5.4 | -10.4 | 4.2 | 2.8 | -3.9 | 2.1 | 10.2 | -6.1 | 3.4 |
| 3/5/07 | 9.6 | -8.9 | 4.0 | 3.4 | -5.9 | 2.3 | 2.6 | -2.2 | 1.8 | 10.9 | -6.6 | 3.3 |
| 5/3/07 | 6.1 | -7.0 | 3.3 | 1.9 | -9.4 | 3.6 | 1.9 | -5.2 | 2.4 | 8.3 | -5.0 | 1.4 |
| 7/5/07 | 5.1 | -9.0 | 3.6 | 0.4 | -8.2 | 2.2 | 3.1 | -8.9 | 2.9 | 2.9 | -9.9 | 3.2 |
| 9/24/07 | 3.8 | -12.6 | 5.3 | 0.1 | - | - | 1.8 | -10.9 | 4.2 | 1.5 | -11.9 | 4.1 |
| 11/3/07 | 3.1 | -9.2 | 3.9 | 0.1 | - | - | 1.6 | -10.6 | 4.4 | 1.4 | -9.9 | 4.4 |
| 1/10/08 | 2.2 | -8.2 | 4.0 | 0.1 | - | - | 1.3 | -10.1 | 4.5 | 0.9 | -5.6 | 3.1 |
| 3/6/08 | 5.0 | -8.4 | 4.4 | 0.6 | -5.1 | 1.0 | 1.1 | -9.8 | 3.7 | 1.1 | -4.8 | 2.5 |
| 6/23/09 | 13.8 | -12.3 | 5.3 | 2.6 | -10.8 | 4.0 | 8.4 | -12.2 | 4.9 | 16.1 | -12.0 | 5.3 |

| Date | $\delta^{13}C$ (‰ VPDB) | DIC (mM) | | | | Drip Rate (µl/s) | $\delta^{13}C$ (‰ VPDB) | DIC (mM) |
|---|---|---|---|---|---|---|---|---|
| | Pool | | | Fast Drips | | | | |
| 3/9/05 | -10.3 | 4.2 | Trip 20 | 6-23-09 | Drip 6 | 124.6 | -12.9 | 5.8 |
| 4/28/05 | -5.1 | 1.1 | Trip 20 | 6-23-09 | Drip 7 | 112.4 | -11.7 | 6.0 |
| 6/29/05 | -9.5 | 3.6 | Trip 20 | 6-23-09 | Drip 8 | 46.4 | -12.7 | 5.9 |
| 8/30/05 | -12.0 | 5.0 | Trip 20 | 6-23-09 | Drip 9 | 134.0 | -12.6 | 5.3 |
| 11/14/05 | -7.3 | 3.1 | | | | | | |
| 1/11/06 | -8.0 | 4.1 | | | | | | |
| 3/10/06 | -8.0 | 3.6 | | | | | | |
| 5/12/06 | -10.3 | 4.2 | | | | | | |
| 7/6/06 | -12.2 | 5.6 | | | | | | |
| 8/31/06 | -12.7 | 5.0 | | | | | | |
| 11/9/06 | -8.7 | 3.3 | | | | | | |
| 1/18/07 | -7.7 | 3.6 | | | | | | |
| 3/5/07 | -7.1 | 3.5 | | | | | | |
| 5/3/07 | -8.3 | 3.3 | | | | | | |
| 7/5/07 | -11.5 | 4.0 | | | | | | |
| 9/24/07 | -11.6 | 4.1 | | | | | | |
| 11/3/07 | -11.0 | 4.2 | | | | | | |
| 1/10/08 | -7.5 | 3.4 | | | | | | |
| 3/6/08 | -7.2 | 3.2 | | | | | | |
| 6/23/09 | -12.1 | 5.3 | | | | | | |

**APPENDIX 3.2.**

(DSSG-1 STABLE ISOTOPE DATA)

$\delta^{13}C$ data for DeSoto Caverns stalagmite DSSG-1 (Aharon et al., 2009).

| Depth Below Top (mm) | Year AD | $\delta^{13}C$ (‰ VPDB) |
|---|---|---|
| 0.1 | 2000 | -11.0 |
| 0.2 | 1997 | -10.6 |
| 0.3 | 1995 | -10.3 |
| 0.4 | 1992 | -9.6 |
| 0.5 | 1990 | -6.8 |
| 0.6 | 1987 | -6.6 |
| 0.7 | 1985 | -6.8 |
| 0.8 | 1982 | -6.9 |
| 0.9 | 1980 | -7.1 |
| 1.0 | 1977 | -7.6 |
| 1.1 | 1975 | -7.6 |
| 1.2 | 1972 | -7.5 |
| 1.3 | 1970 | -6.9 |
| 1.4 | 1967 | -7.5 |
| 1.5 | 1965 | -7.3 |
| 1.6 | 1962 | -6.8 |
| 1.7 | 1960 | -7.2 |
| 1.8 | 1957 | -7.3 |
| 1.9 | 1955 | -7.2 |
| 2.0 | 1952 | -7.0 |
| 2.1 | 1950 | -6.7 |
| 2.2 | 1948 | -6.7 |
| 2.3 | 1945 | -6.4 |
| 2.4 | 1943 | -6.2 |
| 2.5 | 1940 | -6.8 |
| 2.6 | 1938 | -7.0 |
| 2.7 | 1935 | -7.8 |
| 2.8 | 1933 | -7.4 |
| 2.9 | 1930 | -7.3 |
| 3.0 | 1928 | -7.8 |
| 3.1 | 1925 | -6.8 |
| 3.2 | 1923 | -6.4 |
| 3.3 | 1920 | -6.6 |
| 3.4 | 1918 | -7.6 |
| 3.5 | 1915 | -7.6 |
| 3.6 | 1913 | -7.1 |
| 3.7 | 1910 | -7.2 |
| 3.8 | 1908 | -7.3 |
| 3.9 | 1905 | -7.0 |
| 4.0 | 1903 | -7.3 |
| 4.1 | 1900 | -7.2 |
| 4.2 | 1898 | -6.7 |
| 4.3 | 1896 | -6.0 |
| 4.4 | 1893 | -6.5 |

| Depth Below Top (mm) | Year AD | $\delta^{13}C$ (‰ VPDB) |
|---|---|---|
| 4.5 | 1891 | -6.7 |
| 4.6 | 1888 | -7.0 |
| 4.7 | 1886 | -7.3 |
| 4.8 | 1883 | -7.0 |
| 4.9 | 1881 | -7.3 |
| 5.0 | 1878 | -7.8 |
| 5.1 | 1876 | -8.6 |
| 5.2 | 1873 | -8.7 |
| 5.3 | 1871 | -8.3 |
| 5.4 | 1868 | -8.2 |
| 5.5 | 1866 | -8.5 |
| 5.6 | 1863 | -8.7 |
| 5.7 | 1861 | -8.7 |
| 5.8 | 1858 | -8.0 |
| 5.9 | 1856 | -8.0 |
| 6.0 | 1853 | -8.1 |
| 6.1 | 1851 | -7.9 |
| 6.2 | 1848 | -8.2 |
| 6.3 | 1846 | -7.6 |
| 6.4 | 1844 | -7.6 |
| 6.5 | 1841 | -7.6 |
| 6.6 | 1839 | -7.0 |
| 6.7 | 1836 | -6.6 |
| 6.8 | 1834 | -6.1 |
| 6.9 | 1831 | -5.8 |
| 7.0 | 1829 | -5.4 |
| 7.1 | 1826 | -5.2 |
| 7.2 | 1824 | -5.2 |
| 7.3 | 1821 | -5.4 |
| 7.4 | 1819 | -5.5 |
| 7.5 | 1816 | -4.9 |
| 7.6 | 1814 | -4.9 |
| 7.7 | 1811 | -5.3 |
| 7.8 | 1809 | -5.5 |
| 7.9 | 1806 | -5.6 |
| 8.0 | 1804 | -5.7 |
| 8.1 | 1801 | -5.9 |
| 4.3 | 1896 | -6.0 |

**APPENDIX 4.1.**

(ARAGONITE-CALCITE ISOTOPE COMPARISONS)

Carbon and oxygen isotope determinations used to calculate the offsets between primary aragonite ($\delta^{13}C_{AR}$; $\delta^{18}O_{AR}$) and coeval secondary columnar ($\delta^{13}C_{CC}$; $\delta^{18}O_{CC}$) and sparry calcites ($\delta^{13}C_{SC}$; $\delta^{18}O_{SC}$). Offsets represent difference between secondary minerals relative to their primary compositions ($\Delta\delta^{13}C_{AR-C}$; $\Delta\delta^{18}O_{AR-C}$). All values are in ‰ (VPDB). Errors are 1σ. Data are from stalagmites DSSG-2 and DSSG-5.

| $\delta^{13}C_{AR}$ | $\delta^{13}C_{CC}$ | $\delta^{13}C_{SC}$ | $\delta^{18}O_{AR}$ | $\delta^{18}O_{CC}$ | $\delta^{18}O_{SC}$ | $\Delta\delta^{13}C_{AR-C}$ | $\Delta\delta^{18}O_{AR-C}$ |
|---|---|---|---|---|---|---|---|
| Test 1: Sampled horizontally along annual band in DSSG-2 | | | | | | | |
| -6.67 | | | -3.65 | | | | |
| -6.40 | | | -3.38 | | | | |
| | -8.63 | | | -3.82 | | | |
| | -8.77 | | | -3.61 | | | |
| Test 1 means and standard devations | | | | | | | |
| -6.54 | -8.70 | | -3.52 | -3.72 | | 2.17 | 0.20 |
| ± 0.19 | ± 0.10 | | ± 0.19 | ± 0.15 | | ± 0.22 | ± 0.24 |
| | | | | | | | |
| Test 2: Sampled horizontally along annual band in DSSG-2 | | | | | | | |
| -6.76 | | | -3.71 | | | | |
| -7.36 | | | -3.88 | | | | |
| | -8.75 | | | -4.12 | | | |
| | -8.87 | | | -3.97 | | | |
| Test 2 means and standard deviations | | | | | | | |
| -7.06 | -8.81 | | -3.80 | -4.05 | | 1.75 | 0.25 |
| ± 0.42 | ± 0.08 | | ± 0.12 | ± 0.11 | | ± 0.43 | ± 0.16 |
| | | | | | | | |
| Test 3: Sampled vertically across multiple annual bands in DSSG-2 | | | | | | | |
| -7.52 | | | -3.46 | | | | |
| -7.28 | | | -3.51 | | | | |
| -7.21 | | | -3.79 | | | | |
| -6.95 | | | -3.40 | | | | |
| -7.23 | | | -3.71 | | | | |
| -7.82 | | | -3.77 | | | | |
| -7.70 | | | -3.58 | | | | |
| -7.50 | | | -3.67 | | | | |
| -7.33 | | | -3.82 | | | | |
| -7.18 | | | -3.78 | | | | |
| -6.80 | | | -3.55 | | | | |
| -6.96 | | | -3.77 | | | | |
| -6.56 | | | -3.43 | | | | |
| -6.98 | | | -3.74 | | | | |
| -7.48 | | | -4.02 | | | | |
| | -8.63 | | | -3.55 | | | |
| | -9.10 | | | -3.95 | | | |
| | -9.12 | | | -4.13 | | | |
| | -9.17 | | | -4.17 | | | |
| | -8.85 | | | -3.92 | | | |

| $\delta^{13}C_{AR}$ | $\delta^{13}C_{CC}$ | $\delta^{13}C_{SC}$ | $\delta^{18}O_{AR}$ | $\delta^{18}O_{CC}$ | $\delta^{18}O_{SC}$ | $\Delta\delta^{13}C_{AR\text{-}C}$ | $\Delta\delta^{18}O_{AR\text{-}C}$ |
|---|---|---|---|---|---|---|---|
| | -8.96 | | | -3.89 | | | |
| | -9.01 | | | -4.03 | | | |
| | -9.08 | | | -4.17 | | | |
| | -8.83 | | | -4.18 | | | |
| | -8.71 | | | -4.03 | | | |
| | -8.81 | | | -4.25 | | | |
| Test 3 means and standard deviations | | | | | | | |
| -7.23 | -8.93 | | -3.67 | -4.02 | | 1.70 | 0.36 |
| ± 0.34 | ± 0.18 | | ± 0.17 | ± 0.20 | | ± 0.39 | ± 0.26 |
| | | | | | | | |
| Test 4: Sampled vertically across multiple annual bands in DSSG-5 | | | | | | | |
| -7.56 | | | -3.49 | | | | |
| -8.05 | | | -3.49 | | | | |
| -7.29 | | | -3.26 | | | | |
| -7.86 | | | -3.47 | | | | |
| -7.28 | | | -3.50 | | | | |
| -7.44 | | | -3.71 | | | | |
| -7.19 | | | -3.79 | | | | |
| -7.44 | | | -3.66 | | | | |
| -7.50 | | | -3.53 | | | | |
| -7.27 | | | -3.52 | | | | |
| -7.25 | | | -3.55 | | | | |
| -7.79 | | | -3.70 | | | | |
| -8.17 | | | -3.45 | | | | |
| -7.17 | | | -3.50 | | | | |
| -7.28 | | | -3.60 | | | | |
| -6.98 | | | -3.58 | | | | |
| -7.12 | | | -3.36 | | | | |
| -7.27 | | | -3.49 | | | | |
| -7.15 | | | -3.46 | | | | |
| -7.79 | | | -3.58 | | | | |
| -7.09 | | | -3.36 | | | | |
| | -7.70 | | | -3.2 | | | |
| | -7.66 | | | -3.2 | | | |
| | -8.28 | | | -3.7 | | | |
| | -8.39 | | | -3.4 | | | |
| | -9.76 | | | -3.9 | | | |
| | -9.70 | | | -4.1 | | | |
| | -9.56 | | | -3.7 | | | |
| | -9.62 | | | -3.8 | | | |
| | -9.53 | | | -4.0 | | | |
| | -9.59 | | | -4.2 | | | |
| | -9.45 | | | -4.3 | | | |
| | -9.66 | | | -4.3 | | | |
| | -9.81 | | | -4.1 | | | |

| $\delta^{13}C_{AR}$ | $\delta^{13}C_{CC}$ | $\delta^{13}C_{SC}$ | $\delta^{18}O_{AR}$ | $\delta^{18}O_{CC}$ | $\delta^{18}O_{SC}$ | $\Delta\delta^{13}C_{AR\text{-}C}$ | $\Delta\delta^{18}O_{AR\text{-}C}$ |
|---|---|---|---|---|---|---|---|
| | -9.84 | | | -4.1 | | | |
| | -9.64 | | | -4.1 | | | |
| | -9.91 | | | -4.4 | | | |
| | -10.11 | | | -4.0 | | | |
| | -10.11 | | | -4.3 | | | |
| | -10.04 | | | -3.9 | | | |
| | -8.87 | | | -4.1 | | | |
| | -8.55 | | | -4.0 | | | |
| | -8.40 | | | -3.9 | | | |
| | -8.68 | | | -3.9 | | | |
| | -8.42 | | | -3.7 | | | |
| | -8.76 | | | -4.0 | | | |
| | -8.90 | | | -3.9 | | | |
| Test 4 means and standard deviations | | | | | | | |
| -7.43 | -9.19 | | -3.53 | -3.93 | | 1.76 | 0.40 |
| ± 0.33 | ± 0.74 | | ± 0.12 | ± 0.31 | | ± 0.81 | ± 0.33 |
| | | | | | | | |
| Test 5: Sampled vertically across multiple annual bands in DSSG-5 | | | | | | | |
| -7.60 | -3.24 | | | | | | |
| -6.93 | -2.94 | | | | | | |
| -7.19 | -3.02 | | | | | | |
| -7.35 | -3.29 | | | | | | |
| -6.80 | -3.09 | | | | | | |
| -6.95 | -3.18 | | | | | | |
| -7.18 | -3.03 | | | | | | |
| -7.18 | -2.79 | | | | | | |
| -6.90 | -2.72 | | | | | | |
| -6.84 | -2.62 | | | | | | |
| -7.28 | -2.83 | | | | | | |
| -7.17 | -2.87 | | | | | | |
| -7.06 | -2.85 | | | | | | |
| -7.12 | -2.91 | | | | | | |
| -6.55 | -2.71 | | | | | | |
| -6.86 | -2.76 | | | | | | |
| -7.15 | -3.00 | | | | | | |
| -6.96 | -3.01 | | | | | | |
| -6.72 | -2.91 | | | | | | |
| -6.49 | -2.83 | | | | | | |
| -6.94 | -2.91 | | | | | | |
| -6.83 | -2.93 | | | | | | |
| -6.94 | -3.00 | | | | | | |
| -6.82 | -3.14 | | | | | | |
| -6.95 | -2.96 | | | | | | |
| -6.72 | -2.95 | | | | | | |
| -6.32 | -2.99 | | | | | | |

| $\delta^{13}C_{AR}$ | $\delta^{13}C_{CC}$ | $\delta^{13}C_{SC}$ | $\delta^{18}O_{AR}$ | $\delta^{18}O_{CC}$ | $\delta^{18}O_{SC}$ | $\Delta\delta^{13}C_{AR-C}$ | $\Delta\delta^{18}O_{AR-C}$ |
|---|---|---|---|---|---|---|---|
| -7.33 | -3.28 | | | | | | |
| -6.97 | -3.25 | | | | | | |
| -7.03 | -3.39 | | | | | | |
| -7.19 | -3.46 | | | | | | |
| -7.23 | -3.31 | | | | | | |
| -6.99 | -2.90 | | | | | | |
| -7.27 | -3.05 | | | | | | |
| -7.51 | -2.90 | | | | | | |
| -7.32 | -3.06 | | | | | | |
| -6.88 | -2.93 | | | | | | |
| -7.11 | -3.16 | | | | | | |
| -7.24 | -3.24 | | | | | | |
| -7.63 | -3.44 | | | | | | |
| -7.43 | -3.14 | | | | | | |
| -6.80 | -2.91 | | | | | | |
| -7.13 | -2.89 | | | | | | |
| -7.28 | -2.72 | | | | | | |
| -7.39 | -2.91 | | | | | | |
| -7.38 | -2.94 | | | | | | |
| -7.68 | -3.15 | | | | | | |
| -6.85 | -3.03 | | | | | | |
| -7.31 | -3.07 | | | | | | |
| -7.23 | -3.02 | | | | | | |
| -7.08 | -3.03 | | | | | | |
| -7.80 | -3.16 | | | | | | |
| -6.89 | -3.00 | | | | | | |
| -7.45 | -3.16 | | | | | | |
| -6.95 | -3.11 | | | | | | |
| -6.64 | -3.00 | | | | | | |
| -7.44 | -3.00 | | | | | | |
| -7.84 | -3.00 | | | | | | |
| -8.06 | -2.86 | | | | | | |
| -7.30 | -2.84 | | | | | | |
| -7.04 | -2.80 | | | | | | |
| -7.02 | -2.77 | | | | | | |
| -7.64 | -2.82 | | | | | | |
| -7.31 | -2.87 | | | | | | |
| -7.69 | -2.74 | | | | | | |
| -7.81 | -2.89 | | | | | | |
| -7.47 | -2.93 | | | | | | |
| -7.18 | -2.71 | | | | | | |
| -8.03 | -2.82 | | | | | | |
| -7.44 | -2.79 | | | | | | |
| -7.78 | -2.71 | | | | | | |
| -7.48 | -2.71 | | | | | | |

| $\delta^{13}C_{AR}$ | $\delta^{13}C_{CC}$ | $\delta^{13}C_{SC}$ | $\delta^{18}O_{AR}$ | $\delta^{18}O_{CC}$ | $\delta^{18}O_{SC}$ | $\Delta\delta^{13}C_{AR\text{-}C}$ | $\Delta\delta^{18}O_{AR\text{-}C}$ |
|---|---|---|---|---|---|---|---|
| -7.09 | -2.68 | | | | | | |
| -6.77 | -2.67 | | | | | | |
| -6.76 | -2.66 | | | | | | |
| -7.26 | -2.76 | | | | | | |
| -7.28 | -2.56 | | | | | | |
| -7.68 | -2.78 | | | | | | |
| -7.54 | -2.95 | | | | | | |
| -7.62 | -2.88 | | | | | | |
| -6.96 | -2.78 | | | | | | |
| -7.43 | -3.05 | | | | | | |
| -7.33 | -2.90 | | | | | | |
| -7.66 | -3.04 | | | | | | |
| -7.57 | -3.04 | | | | | | |
| -7.51 | -2.97 | | | | | | |
| -7.16 | -2.96 | | | | | | |
| -7.14 | -3.02 | | | | | | |
| -7.83 | -3.36 | | | | | | |
| -7.83 | -3.14 | | | | | | |
| -7.55 | -3.27 | | | | | | |
| | | -7.93 | | | -3.62 | | |
| | | -7.78 | | | -3.32 | | |
| | | -7.68 | | | -3.52 | | |
| | | -7.76 | | | -3.64 | | |
| | | -7.64 | | | -3.62 | | |
| | | -7.63 | | | -3.54 | | |
| | | -7.62 | | | -3.46 | | |
| | | -7.33 | | | -3.11 | | |
| | | -7.33 | | | -3.56 | | |
| | | -7.23 | | | -3.32 | | |
| | | -7.35 | | | -3.57 | | |
| | | -7.23 | | | -3.37 | | |
| | | -6.97 | | | -3.43 | | |
| | | -7.05 | | | -3.19 | | |
| | | -7.24 | | | -3.25 | | |
| | | -7.14 | | | -3.58 | | |
| | | -6.94 | | | -3.34 | | |
| | | -7.04 | | | -3.41 | | |
| | | -7.18 | | | -3.71 | | |
| | | -7.10 | | | -3.71 | | |
| | | -7.05 | | | -3.48 | | |
| | | -7.08 | | | -3.54 | | |
| | | -7.05 | | | -3.33 | | |
| | | -6.97 | | | -3.82 | | |
| | | -6.96 | | | -3.48 | | |

| $\delta^{13}C_{AR}$ | $\delta^{13}C_{CC}$ | $\delta^{13}C_{SC}$ | $\delta^{18}O_{AR}$ | $\delta^{18}O_{CC}$ | $\delta^{18}O_{SC}$ | $\Delta\delta^{13}C_{AR\text{-}C}$ | $\Delta\delta^{18}O_{AR\text{-}C}$ |
|---|---|---|---|---|---|---|---|
| | | -6.95 | | | -3.27 | | |
| | | -6.99 | | | -3.50 | | |
| | | -7.15 | | | -3.45 | | |
| | | -7.10 | | | -3.32 | | |
| | | -7.13 | | | -3.60 | | |
| | | -7.34 | | | -3.91 | | |
| | | -7.40 | | | -3.39 | | |
| | | -7.31 | | | -3.61 | | |
| | | -7.29 | | | -3.37 | | |
| | | -7.21 | | | -3.50 | | |
| | | -7.38 | | | -3.37 | | |
| | | -7.36 | | | -3.47 | | |
| | | -7.25 | | | -3.71 | | |
| | | -7.25 | | | -3.49 | | |
| | | -7.32 | | | -3.36 | | |
| | | -7.38 | | | -3.10 | | |
| | | -7.35 | | | -3.29 | | |
| | | -7.42 | | | -3.35 | | |
| | | -7.47 | | | -3.15 | | |
| | | -7.43 | | | -3.47 | | |
| | | -7.53 | | | -3.68 | | |
| | | -7.52 | | | -3.53 | | |
| | | -7.56 | | | -3.69 | | |
| | | -7.20 | | | -3.60 | | |
| | | -7.12 | | | -3.33 | | |
| | | -7.11 | | | -3.46 | | |
| | | -7.17 | | | -3.58 | | |
| | | -7.59 | | | -3.64 | | |
| | | -7.51 | | | -3.67 | | |
| | | -7.60 | | | -3.30 | | |
| | | -7.42 | | | -3.25 | | |
| | | -7.47 | | | -3.39 | | |
| | | -7.63 | | | -3.72 | | |
| | | -7.64 | | | -3.26 | | |
| | | -7.60 | | | -3.72 | | |
| | | -7.65 | | | -3.70 | | |
| | | -7.69 | | | -3.55 | | |
| | | -7.69 | | | -3.61 | | |
| | | -7.65 | | | -3.77 | | |
| | | -7.26 | | | -3.27 | | |
| | | -7.59 | | | -3.60 | | |
| | | -7.54 | | | -3.57 | | |
| | | -7.45 | | | -3.48 | | |
| | | -7.45 | | | -3.76 | | |
| | | -7.37 | | | -3.45 | | |

| $\delta^{13}C_{AR}$ | $\delta^{13}C_{CC}$ | $\delta^{13}C_{SC}$ | $\delta^{18}O_{AR}$ | $\delta^{18}O_{CC}$ | $\delta^{18}O_{SC}$ | $\Delta\delta^{13}C_{AR\text{-}C}$ | $\Delta\delta^{18}O_{AR\text{-}C}$ |
|---|---|---|---|---|---|---|---|
| | | -7.42 | | | -3.55 | | |
| | | -7.57 | | | -3.80 | | |
| | | -7.49 | | | -3.80 | | |
| | | -7.54 | | | -3.40 | | |
| | | -7.40 | | | -3.44 | | |
| | | -7.68 | | | -3.24 | | |
| | | -7.13 | | | -2.97 | | |
| | | -7.52 | | | -3.63 | | |
| | | -7.55 | | | -3.39 | | |
| | | -7.72 | | | -3.92 | | |
| | | -7.77 | | | -4.23 | | |
| | | -7.60 | | | -4.04 | | |
| | | -7.53 | | | -3.60 | | |
| | | -7.45 | | | -3.29 | | |
| | | -7.66 | | | -3.37 | | |
| | | -7.42 | | | -3.03 | | |
| | | -7.50 | | | -3.51 | | |
| Test 5 means and standard deviations | | | | | | | |
| -7.22 | -2.97 | -7.39 | | | -3.50 | 0.16 | 0.53 |
| ± 0.36 | ± 0.19 | ± 0.23 | | | ± 0.22 | ± 0.43 | ± 0.29 |
| | | | | | | | |
| Columnar calcite offsets | | | | | | | |
| | | | | | | **1.84** | **0.30** |
| | | | | | | **± 0.28** | **± 0.09** |
| | | | | | | | |
| Sparry calcite offsets | | | | | | | |
| | | | | | | **0.16** | **0.53** |
| | | | | | | **± 0.43** | **± 0.29** |

**APPENDIX 4.2.**

(DSSG-2 STABLE ISOTOPE DATA)

| Depth (mm) | Age (ka BP) | $\delta^{13}C$ (‰ VPDB) | $\delta^{18}O$ (‰ VPDB) | $\delta^{18}O$ (‰ VPDB) Calcite Corr. | $\delta^{18}O$ (‰ VPDB) Sea Level Corr. |
|---|---|---|---|---|---|
| 0.0 | 11.278 | -8.1 | -3.9 | -3.9 | -4.4 |
| 0.4 | 11.279 | -8.4 | -3.4 | -3.4 | -3.9 |
| 0.7 | 11.281 | -9.1 | -3.8 | -3.8 | -4.3 |
| 1.1 | 11.282 | -9.4 | -4.2 | -4.2 | -4.7 |
| 1.4 | 11.284 | -9.2 | -3.8 | -3.8 | -4.4 |
| 1.8 | 11.285 | -9.0 | -3.8 | -3.8 | -4.3 |
| 2.2 | 11.287 | -8.9 | -3.7 | -3.7 | -4.2 |
| 2.5 | 11.288 | -8.3 | -3.3 | -3.3 | -3.8 |
| 2.9 | 11.290 | -8.2 | -3.5 | -3.5 | -4.0 |
| 3.3 | 11.291 | -8.4 | -3.6 | -3.6 | -4.1 |
| 3.6 | 11.293 | -8.5 | -3.4 | -3.4 | -3.9 |
| 4.0 | 11.294 | -8.6 | -4.0 | -4.0 | -4.5 |
| 4.3 | 11.296 | -8.4 | -3.7 | -3.7 | -4.2 |
| 4.6 | 11.297 | -8.1 | -3.4 | -3.4 | -3.9 |
| 4.9 | 11.298 | -8.1 | -3.4 | -3.4 | -3.9 |
| 5.2 | 11.300 | -8.3 | -3.6 | -3.6 | -4.1 |
| 5.5 | 11.301 | -8.0 | -3.5 | -3.5 | -4.0 |
| 5.9 | 11.302 | -7.6 | -3.5 | -3.5 | -4.0 |
| 6.2 | 11.304 | -7.5 | -3.5 | -3.5 | -4.0 |
| 6.5 | 11.305 | -7.2 | -2.9 | -2.9 | -3.5 |
| 6.8 | 11.306 | -7.1 | -3.1 | -3.1 | -3.6 |
| 7.1 | 11.308 | -7.4 | -3.2 | -3.2 | -3.8 |
| 7.4 | 11.309 | -7.4 | -3.3 | -3.3 | -3.8 |
| 7.7 | 11.310 | -7.3 | -3.3 | -3.3 | -3.8 |
| 8.0 | 11.312 | -7.2 | -3.2 | -3.2 | -3.7 |
| 8.4 | 11.313 | -7.5 | -3.5 | -3.5 | -4.0 |
| 8.7 | 11.314 | -7.4 | -3.2 | -3.2 | -3.7 |
| 9.0 | 11.316 | -7.5 | -3.1 | -3.1 | -3.6 |
| 9.3 | 11.317 | -7.7 | -3.7 | -3.7 | -4.2 |
| 9.6 | 11.318 | -7.6 | -3.1 | -3.1 | -3.6 |
| 9.9 | 11.319 | -7.9 | -3.5 | -3.5 | -4.0 |
| 10.2 | 11.321 | -8.1 | -4.0 | -4.0 | -4.6 |
| 10.5 | 11.322 | -7.6 | -3.2 | -3.2 | -3.7 |
| 10.9 | 11.323 | -7.9 | -3.5 | -3.5 | -4.0 |
| 11.2 | 11.325 | -7.7 | -3.5 | -3.5 | -4.0 |
| 11.5 | 11.326 | -7.5 | -3.7 | -3.7 | -4.2 |
| 11.8 | 11.327 | -7.5 | -3.4 | -3.4 | -4.0 |
| 12.1 | 11.329 | -7.3 | -3.1 | -3.1 | -3.6 |
| 12.4 | 11.330 | -7.5 | -3.5 | -3.5 | -4.0 |
| 13.0 | 11.333 | -7.4 | -3.5 | -3.5 | -4.1 |
| 13.4 | 11.334 | -7.2 | -3.5 | -3.5 | -4.0 |
| 13.7 | 11.335 | -7.5 | -3.7 | -3.7 | -4.2 |

| Depth (mm) | Age (ka BP) | $\delta^{13}C$ (‰ VPDB) | $\delta^{18}O$ (‰ VPDB) | $\delta^{18}O$ (‰ VPDB) Calcite Corr. | $\delta^{18}O$ (‰ VPDB) Sea Level Corr. |
|---|---|---|---|---|---|
| 14.0 | 11.337 | -7.5 | -3.9 | -3.9 | -4.5 |
| 14.3 | 11.338 | -7.4 | -3.8 | -3.8 | -4.3 |
| 14.6 | 11.339 | -7.3 | -3.5 | -3.5 | -4.0 |
| 14.9 | 11.341 | -7.2 | -3.2 | -3.2 | -3.8 |
| 15.2 | 11.342 | -7.3 | -3.4 | -3.4 | -3.9 |
| 15.5 | 11.343 | -7.5 | -3.7 | -3.7 | -4.2 |
| 15.9 | 11.344 | -7.0 | -3.1 | -3.1 | -3.6 |
| 16.2 | 11.346 | -7.1 | -3.6 | -3.6 | -4.1 |
| 16.5 | 11.347 | -6.7 | -3.1 | -3.1 | -3.7 |
| 16.8 | 11.348 | -6.7 | -3.4 | -3.4 | -3.9 |
| 17.1 | 11.350 | -6.7 | -3.6 | -3.6 | -4.1 |
| 17.4 | 11.351 | -6.6 | -3.2 | -3.2 | -3.7 |
| 17.7 | 11.352 | -6.9 | -3.7 | -3.7 | -4.2 |
| 18.1 | 11.354 | -6.4 | -3.1 | -3.1 | -3.6 |
| 18.4 | 11.355 | -6.7 | -3.6 | -3.6 | -4.1 |
| 18.7 | 11.356 | -6.4 | -3.1 | -3.1 | -3.6 |
| 19.0 | 11.358 | -6.6 | -3.3 | -3.3 | -3.8 |
| 19.3 | 11.359 | -7.0 | -4.1 | -4.1 | -4.6 |
| 19.6 | 11.360 | -6.9 | -3.9 | -3.9 | -4.4 |
| 19.9 | 11.362 | -7.0 | -3.6 | -3.6 | -4.1 |
| 20.2 | 11.363 | -6.6 | -3.5 | -3.5 | -4.1 |
| 20.6 | 11.364 | -6.7 | -3.3 | -3.3 | -3.8 |
| 20.9 | 11.366 | -6.9 | -3.5 | -3.5 | -4.0 |
| 21.2 | 11.367 | -7.2 | -4.1 | -4.1 | -4.7 |
| 21.5 | 11.368 | -7.3 | -4.3 | -4.3 | -4.9 |
| 21.8 | 11.369 | -7.2 | -4.6 | -4.6 | -5.2 |
| 22.1 | 11.371 | -7.3 | -4.1 | -4.1 | -4.7 |
| 22.4 | 11.372 | -7.3 | -3.6 | -3.6 | -4.2 |
| 22.7 | 11.373 | -7.5 | -4.2 | -4.2 | -4.7 |
| 23.0 | 11.375 | -7.4 | -3.8 | -3.8 | -4.3 |
| 23.4 | 11.376 | -7.2 | -3.8 | -3.8 | -4.4 |
| 23.7 | 11.377 | -7.0 | -3.5 | -3.5 | -4.0 |
| 24.0 | 11.379 | -7.5 | -3.9 | -3.9 | -4.4 |
| 24.3 | 11.380 | -7.2 | -4.3 | -4.3 | -4.8 |
| 24.6 | 11.381 | -7.4 | -3.9 | -3.9 | -4.4 |
| 24.9 | 11.383 | -7.4 | -4.6 | -4.6 | -5.1 |
| 25.2 | 11.384 | -7.5 | -3.7 | -3.7 | -4.2 |
| 25.5 | 11.385 | -7.6 | -4.1 | -4.1 | -4.6 |
| 25.9 | 11.387 | -7.7 | -4.3 | -4.3 | -4.8 |
| 26.2 | 11.388 | -7.6 | -3.8 | -3.8 | -4.3 |
| 26.5 | 11.389 | -7.3 | -3.9 | -3.9 | -4.5 |
| 26.8 | 11.391 | -7.2 | -3.7 | -3.7 | -4.2 |
| 27.1 | 11.392 | -7.2 | -3.6 | -3.6 | -4.1 |

| Depth (mm) | Age (ka BP) | $\delta^{13}C$ (‰ VPDB) | $\delta^{18}O$ (‰ VPDB) | $\delta^{18}O$ (‰ VPDB) Calcite Corr. | $\delta^{18}O$ (‰ VPDB) Sea Level Corr. |
|---|---|---|---|---|---|
| 27.4 | 11.393 | -7.0 | -4.2 | -4.2 | -4.7 |
| 27.7 | 11.394 | -7.1 | -3.5 | -3.5 | -4.0 |
| 28.0 | 11.396 | -7.3 | -4.6 | -4.6 | -5.2 |
| 28.7 | 11.398 | -6.8 | -3.4 | -3.4 | -4.0 |
| 29.0 | 11.400 | -7.2 | -4.2 | -4.2 | -4.8 |
| 29.3 | 11.401 | -7.1 | -4.7 | -4.7 | -5.2 |
| 29.6 | 11.402 | -6.6 | -4.3 | -4.3 | -4.9 |
| 29.9 | 11.404 | -7.3 | -4.0 | -4.0 | -4.5 |
| 30.2 | 11.405 | -7.6 | -4.5 | -4.5 | -5.1 |
| 30.5 | 11.406 | -7.4 | -4.5 | -4.5 | -5.1 |
| 30.8 | 11.408 | -7.2 | -4.3 | -4.3 | -4.9 |
| 31.2 | 11.409 | -7.2 | -4.1 | -4.1 | -4.7 |
| 31.5 | 11.410 | -7.0 | -3.7 | -3.7 | -4.2 |
| 31.8 | 11.412 | -7.2 | -4.2 | -4.2 | -4.8 |
| 32.1 | 11.413 | -7.3 | -4.3 | -4.3 | -4.8 |
| 32.4 | 11.414 | -7.4 | -3.6 | -3.6 | -4.1 |
| 32.7 | 11.415 | -7.4 | -3.5 | -3.5 | -4.0 |
| 33.0 | 11.417 | -7.5 | -3.5 | -3.5 | -4.0 |
| 33.3 | 11.418 | -7.6 | -3.7 | -3.7 | -4.3 |
| 33.6 | 11.419 | -7.9 | -3.8 | -3.8 | -4.4 |
| 33.9 | 11.421 | -7.5 | -3.3 | -3.3 | -3.9 |
| 34.2 | 11.422 | -7.6 | -3.6 | -3.6 | -4.2 |
| 34.5 | 11.423 | -7.7 | -3.4 | -3.4 | -3.9 |
| 34.8 | 11.424 | -7.7 | -3.8 | -3.8 | -4.3 |
| 35.1 | 11.426 | -7.7 | -3.8 | -3.8 | -4.4 |
| 35.5 | 11.427 | -7.3 | -3.5 | -3.5 | -4.0 |
| 35.8 | 11.428 | -7.6 | -3.7 | -3.7 | -4.2 |
| 36.1 | 11.430 | -7.8 | -3.7 | -3.7 | -4.3 |
| 36.4 | 11.431 | -7.5 | -3.2 | -3.2 | -3.7 |
| 36.7 | 11.432 | -7.1 | -3.3 | -3.3 | -3.9 |
| 37.3 | 11.435 | -7.5 | -3.3 | -3.3 | -3.9 |
| 37.6 | 11.436 | -7.4 | -3.3 | -3.3 | -3.8 |
| 37.9 | 11.437 | -7.9 | -3.3 | -3.3 | -3.8 |
| 38.2 | 11.439 | -8.0 | -3.5 | -3.5 | -4.1 |
| 38.5 | 11.440 | -7.5 | -3.4 | -3.4 | -3.9 |
| 38.8 | 11.441 | -7.3 | -3.3 | -3.3 | -3.9 |
| 39.1 | 11.442 | -7.3 | -3.5 | -3.5 | -4.0 |
| 39.4 | 11.444 | -6.9 | -3.3 | -3.3 | -3.9 |
| 39.7 | 11.445 | -7.4 | -3.3 | -3.3 | -3.9 |
| 40.0 | 11.446 | -7.5 | -3.6 | -3.6 | -4.2 |
| 40.3 | 11.448 | -7.1 | -3.3 | -3.3 | -3.9 |
| 40.6 | 11.449 | -7.1 | -3.6 | -3.6 | -4.2 |
| 40.9 | 11.450 | -7.5 | -3.8 | -3.8 | -4.4 |

| Depth (mm) | Age (ka BP) | $\delta^{13}C$ (‰ VPDB) | $\delta^{18}O$ (‰ VPDB) | $\delta^{18}O$ (‰ VPDB) Calcite Corr. | $\delta^{18}O$ (‰ VPDB) Sea Level Corr. |
|---|---|---|---|---|---|
| 41.2 | 11.451 | -7.7 | -3.8 | -3.8 | -4.4 |
| 41.6 | 11.453 | -6.6 | -3.1 | -3.1 | -3.7 |
| 41.9 | 11.454 | -7.0 | -3.2 | -3.2 | -3.8 |
| 42.2 | 11.455 | -6.9 | -3.4 | -3.4 | -3.9 |
| 42.5 | 11.457 | -6.8 | -3.6 | -3.6 | -4.1 |
| 42.8 | 11.458 | -7.2 | -3.3 | -3.3 | -3.8 |
| 43.1 | 11.459 | -7.6 | -3.5 | -3.5 | -4.1 |
| 43.4 | 11.460 | -7.4 | -3.1 | -3.1 | -3.7 |
| 43.7 | 11.462 | -7.5 | -3.5 | -3.5 | -4.1 |
| 44.0 | 11.463 | -7.2 | -3.3 | -3.3 | -3.9 |
| 44.3 | 11.464 | -7.2 | -3.4 | -3.4 | -4.0 |
| 44.6 | 11.466 | -6.8 | -3.1 | -3.1 | -3.6 |
| 44.9 | 11.467 | -6.9 | -3.4 | -3.4 | -4.0 |
| 45.2 | 11.468 | -7.0 | -3.2 | -3.2 | -3.8 |
| 45.5 | 11.469 | -7.1 | -3.3 | -3.3 | -3.8 |
| 45.8 | 11.471 | -7.2 | -3.3 | -3.3 | -3.9 |
| 46.1 | 11.472 | -7.2 | -3.3 | -3.3 | -3.9 |
| 46.4 | 11.473 | -7.1 | -3.3 | -3.3 | -3.9 |
| 46.7 | 11.475 | -7.0 | -3.4 | -3.4 | -4.0 |
| 47.0 | 11.476 | -7.4 | -3.5 | -3.5 | -4.0 |
| 47.3 | 11.477 | -7.2 | -3.6 | -3.6 | -4.2 |
| 47.7 | 11.478 | -7.1 | -3.3 | -3.3 | -3.8 |
| 48.0 | 11.480 | -7.2 | -3.4 | -3.4 | -4.0 |
| 48.3 | 11.481 | -7.1 | -3.7 | -3.7 | -4.3 |
| 48.6 | 11.482 | -7.2 | -3.7 | -3.7 | -4.3 |
| 48.9 | 11.484 | -7.4 | -3.8 | -3.8 | -4.4 |
| 49.2 | 11.485 | -7.1 | -3.7 | -3.7 | -4.2 |
| 49.5 | 11.486 | -7.4 | -3.8 | -3.8 | -4.3 |
| 49.8 | 11.487 | -7.4 | -3.7 | -3.7 | -4.3 |
| 50.1 | 11.489 | -7.1 | -3.6 | -3.6 | -4.2 |
| 50.4 | 11.490 | -7.5 | -4.1 | -4.1 | -4.7 |
| 50.7 | 11.491 | -7.4 | -3.8 | -3.8 | -4.4 |
| 51.0 | 11.493 | -7.3 | -3.8 | -3.8 | -4.4 |
| 51.3 | 11.494 | -7.4 | -3.7 | -3.7 | -4.2 |
| 51.6 | 11.495 | -7.5 | -3.8 | -3.8 | -4.4 |
| 51.9 | 11.496 | -7.5 | -3.6 | -3.6 | -4.2 |
| 52.5 | 11.499 | -7.0 | -3.7 | -3.7 | -4.2 |
| 52.8 | 11.500 | -7.3 | -3.4 | -3.4 | -4.0 |
| 53.1 | 11.501 | -6.8 | -3.4 | -3.4 | -4.0 |
| 53.4 | 11.503 | -6.7 | -3.6 | -3.6 | -4.2 |
| 53.8 | 11.504 | -6.8 | -3.6 | -3.6 | -4.2 |
| 54.1 | 11.505 | -6.9 | -3.6 | -3.6 | -4.2 |
| 54.4 | 11.507 | -7.1 | -3.6 | -3.6 | -4.1 |

| Depth (mm) | Age (ka BP) | $\delta^{13}C$ (‰ VPDB) | $\delta^{18}O$ (‰ VPDB) | $\delta^{18}O$ (‰ VPDB) Calcite Corr. | $\delta^{18}O$ (‰ VPDB) Sea Level Corr. |
|---|---|---|---|---|---|
| 54.7 | 11.508 | -7.2 | -3.6 | -3.6 | -4.1 |
| 55.0 | 11.509 | -7.0 | -3.7 | -3.7 | -4.2 |
| 55.3 | 11.510 | -6.4 | -3.1 | -3.1 | -3.7 |
| 55.6 | 11.512 | -7.0 | -3.5 | -3.5 | -4.1 |
| 55.9 | 11.513 | -6.7 | -3.4 | -3.4 | -4.0 |
| 56.2 | 11.514 | -6.9 | -3.7 | -3.7 | -4.2 |
| 56.5 | 11.516 | -7.0 | -3.7 | -3.7 | -4.3 |
| 56.8 | 11.517 | -6.8 | -3.8 | -3.8 | -4.4 |
| 57.1 | 11.518 | -6.9 | -3.9 | -3.9 | -4.5 |
| 57.4 | 11.519 | -7.2 | -3.6 | -3.6 | -4.2 |
| 57.7 | 11.521 | -7.1 | -4.1 | -4.1 | -4.7 |
| 58.0 | 11.522 | -6.9 | -4.0 | -4.0 | -4.5 |
| 58.3 | 11.523 | -6.8 | -4.0 | -4.0 | -4.6 |
| 58.6 | 11.525 | -7.1 | -4.1 | -4.1 | -4.7 |
| 58.9 | 11.526 | -7.1 | -4.3 | -4.3 | -4.8 |
| 59.2 | 11.527 | -7.0 | -4.1 | -4.1 | -4.7 |
| 59.6 | 11.528 | -7.2 | -3.4 | -3.4 | -4.0 |
| 59.9 | 11.530 | -6.9 | -3.7 | -3.7 | -4.2 |
| 60.2 | 11.531 | -6.7 | -3.7 | -3.7 | -4.3 |
| 60.5 | 11.532 | -6.2 | -3.6 | -3.6 | -4.2 |
| 60.8 | 11.534 | -7.2 | -4.1 | -4.1 | -4.6 |
| 61.1 | 11.535 | -7.3 | -4.1 | -4.1 | -4.7 |
| 61.4 | 11.536 | -6.9 | -4.2 | -4.2 | -4.7 |
| 61.7 | 11.537 | -6.8 | -3.8 | -3.8 | -4.3 |
| 62.0 | 11.539 | -6.9 | -4.0 | -4.0 | -4.6 |
| 62.3 | 11.540 | -6.7 | -3.1 | -3.1 | -3.7 |
| 62.6 | 11.541 | -6.8 | -3.8 | -3.8 | -4.4 |
| 62.9 | 11.543 | -6.9 | -3.5 | -3.5 | -4.1 |
| 63.2 | 11.544 | -6.8 | -3.5 | -3.5 | -4.1 |
| 63.5 | 11.545 | -6.6 | -3.3 | -3.3 | -3.9 |
| 63.8 | 11.546 | -6.2 | -3.1 | -3.1 | -3.6 |
| 64.1 | 11.548 | -6.5 | -3.5 | -3.5 | -4.1 |
| 64.4 | 11.549 | -6.6 | -3.8 | -3.8 | -4.4 |
| 64.7 | 11.550 | -6.8 | -3.2 | -3.2 | -3.8 |
| 65.0 | 11.551 | -6.9 | -3.6 | -3.6 | -4.2 |
| 65.3 | 11.553 | -6.8 | -3.5 | -3.5 | -4.1 |
| 65.6 | 11.554 | -6.3 | -3.4 | -3.4 | -4.0 |
| 65.9 | 11.555 | -6.8 | -3.7 | -3.7 | -4.3 |
| 66.2 | 11.556 | -6.8 | -3.4 | -3.4 | -4.0 |
| 66.5 | 11.558 | -6.9 | -3.3 | -3.3 | -3.9 |
| 66.8 | 11.559 | -7.8 | -3.9 | -3.9 | -4.5 |
| 67.1 | 11.560 | -7.7 | -3.9 | -3.9 | -4.5 |
| 67.4 | 11.561 | -7.3 | -3.7 | -3.7 | -4.3 |

| Depth (mm) | Age (ka BP) | $\delta^{13}C$ (‰ VPDB) | $\delta^{18}O$ (‰ VPDB) | $\delta^{18}O$ (‰ VPDB) Calcite Corr. | $\delta^{18}O$ (‰ VPDB) Sea Level Corr. |
|---|---|---|---|---|---|
| 67.7 | 11.563 | -7.1 | -3.9 | -3.9 | -4.5 |
| 68.0 | 11.564 | -7.1 | -3.9 | -3.9 | -4.5 |
| 68.3 | 11.565 | -6.5 | -3.2 | -3.2 | -3.8 |
| 68.6 | 11.566 | -7.1 | -3.8 | -3.8 | -4.4 |
| 68.9 | 11.568 | -7.1 | -3.8 | -3.8 | -4.4 |
| 69.2 | 11.569 | -7.2 | -3.8 | -3.8 | -4.4 |
| 69.5 | 11.570 | -6.6 | -3.6 | -3.6 | -4.2 |
| 69.8 | 11.571 | -6.6 | -3.7 | -3.7 | -4.3 |
| 70.1 | 11.573 | -6.9 | -3.7 | -3.7 | -4.3 |
| 70.4 | 11.574 | -6.9 | -3.8 | -3.8 | -4.4 |
| 70.7 | 11.575 | -7.0 | -3.7 | -3.7 | -4.3 |
| 71.0 | 11.577 | -6.7 | -3.5 | -3.5 | -4.1 |
| 71.3 | 11.578 | -6.6 | -3.5 | -3.5 | -4.1 |
| 71.6 | 11.579 | -8.2 | -3.9 | -3.6 | -4.2 |
| 71.9 | 11.580 | -8.2 | -4.0 | -3.7 | -4.3 |
| 72.2 | 11.582 | -8.2 | -3.9 | -3.6 | -4.1 |
| 72.5 | 11.583 | -7.4 | -3.6 | -3.3 | -3.9 |
| 72.8 | 11.584 | -7.0 | -3.7 | -3.4 | -4.0 |
| 73.1 | 11.585 | -7.1 | -3.9 | -3.9 | -4.5 |
| 73.4 | 11.587 | -6.7 | -3.6 | -3.6 | -4.2 |
| 73.7 | 11.588 | -6.6 | -3.9 | -3.9 | -4.4 |
| 74.0 | 11.589 | -6.5 | -4.0 | -4.0 | -4.6 |
| 74.3 | 11.590 | -6.7 | -3.8 | -3.8 | -4.4 |
| 74.6 | 11.592 | -6.6 | -4.0 | -4.0 | -4.6 |
| 74.9 | 11.593 | -6.5 | -3.9 | -3.9 | -4.5 |
| 75.2 | 11.594 | -6.1 | -3.5 | -3.5 | -4.1 |
| 75.5 | 11.595 | -6.2 | -3.8 | -3.8 | -4.4 |
| 75.8 | 11.597 | -6.0 | -3.7 | -3.7 | -4.3 |
| 76.1 | 11.598 | -5.8 | -3.7 | -3.7 | -4.3 |
| 76.4 | 11.599 | -6.0 | -3.6 | -3.6 | -4.2 |
| 76.7 | 11.600 | -7.6 | -4.1 | -4.1 | -4.7 |
| 77.0 | 11.602 | -7.0 | -3.7 | -3.7 | -4.3 |
| 77.2 | 11.603 | -6.6 | -4.0 | -4.0 | -4.6 |
| 77.5 | 11.604 | -6.5 | -3.8 | -3.8 | -4.4 |
| 77.8 | 11.606 | -6.3 | -3.7 | -3.7 | -4.3 |
| 78.1 | 11.607 | -6.0 | -3.8 | -3.8 | -4.4 |
| 78.4 | 11.608 | -6.2 | -3.6 | -3.6 | -4.2 |
| 78.7 | 11.609 | -6.3 | -3.7 | -3.7 | -4.3 |
| 79.0 | 11.611 | -6.0 | -3.7 | -3.7 | -4.3 |
| 79.3 | 11.612 | -5.7 | -3.2 | -3.2 | -3.8 |
| 79.6 | 11.613 | -6.0 | -3.8 | -3.8 | -4.3 |
| 79.9 | 11.614 | -6.3 | -4.1 | -4.1 | -4.6 |
| 80.2 | 11.616 | -5.6 | -3.5 | -3.5 | -4.1 |

| Depth (mm) | Age (ka BP) | $\delta^{13}C$ (‰ VPDB) | $\delta^{18}O$ (‰ VPDB) | $\delta^{18}O$ (‰ VPDB) Calcite Corr. | $\delta^{18}O$ (‰ VPDB) Sea Level Corr. |
|---|---|---|---|---|---|
| 80.5 | 11.617 | -5.5 | -3.3 | -3.3 | -3.9 |
| 80.8 | 11.618 | -5.8 | -3.6 | -3.6 | -4.2 |
| 81.1 | 11.619 | -5.6 | -3.4 | -3.4 | -4.0 |
| 81.4 | 11.621 | -5.9 | -3.3 | -3.3 | -3.9 |
| 81.7 | 11.622 | -5.9 | -3.4 | -3.4 | -4.0 |
| 82.0 | 11.623 | -5.6 | -3.6 | -3.6 | -4.2 |
| 82.3 | 11.624 | -5.6 | -3.4 | -3.4 | -4.0 |
| 82.6 | 11.626 | -6.0 | -3.7 | -3.7 | -4.3 |
| 82.9 | 11.627 | -5.7 | -3.6 | -3.6 | -4.2 |
| 83.2 | 11.628 | -5.4 | -3.2 | -3.2 | -3.8 |
| 83.5 | 11.629 | -5.3 | -3.2 | -3.2 | -3.8 |
| 83.8 | 11.631 | -5.8 | -3.4 | -3.4 | -4.0 |
| 84.1 | 11.632 | -5.4 | -3.4 | -3.4 | -4.0 |
| 84.4 | 11.633 | -5.2 | -3.2 | -3.2 | -3.8 |
| 84.7 | 11.635 | -5.5 | -3.3 | -3.0 | -3.6 |
| 85.0 | 11.636 | -6.7 | -3.5 | -3.2 | -3.8 |
| 85.6 | 11.638 | -7.5 | -3.6 | -3.3 | -3.9 |
| 85.9 | 11.640 | -7.6 | -4.0 | -4.0 | -4.6 |
| 86.2 | 11.641 | -6.3 | -3.0 | -3.0 | -3.6 |
| 86.5 | 11.642 | -6.3 | -3.9 | -3.9 | -4.5 |
| 86.8 | 11.643 | -6.2 | -3.6 | -3.6 | -4.2 |
| 87.1 | 11.645 | -6.1 | -3.6 | -3.6 | -4.2 |
| 87.4 | 11.646 | -6.1 | -3.6 | -3.6 | -4.2 |
| 87.7 | 11.647 | -6.0 | -3.6 | -3.6 | -4.2 |
| 88.0 | 11.648 | -5.9 | -3.7 | -3.7 | -4.3 |
| 88.3 | 11.650 | -6.9 | -3.8 | -3.8 | -4.4 |
| 88.6 | 11.651 | -7.0 | -3.3 | -3.3 | -3.9 |
| 88.9 | 11.652 | -6.1 | -3.7 | -3.7 | -4.3 |
| 89.2 | 11.653 | -6.1 | -3.9 | -3.9 | -4.5 |
| 89.5 | 11.655 | -6.0 | -3.4 | -3.4 | -4.0 |
| 89.8 | 11.656 | -6.4 | -3.8 | -3.8 | -4.4 |
| 90.1 | 11.657 | -6.0 | -3.6 | -3.6 | -4.1 |
| 90.4 | 11.658 | -5.7 | -3.7 | -3.7 | -4.3 |
| 90.7 | 11.660 | -5.6 | -3.9 | -3.9 | -4.5 |
| 91.0 | 11.661 | -5.7 | -3.6 | -3.6 | -4.2 |
| 91.3 | 11.662 | -6.1 | -3.7 | -3.7 | -4.3 |
| 91.6 | 11.663 | -6.3 | -3.5 | -3.5 | -4.1 |
| 92.2 | 11.666 | -6.3 | -3.6 | -3.6 | -4.2 |
| 92.5 | 11.667 | -6.1 | -3.7 | -3.7 | -4.3 |
| 92.8 | 11.669 | -6.1 | -3.6 | -3.6 | -4.2 |
| 93.1 | 11.670 | -5.8 | -3.5 | -3.5 | -4.1 |
| 93.4 | 11.671 | -5.8 | -3.6 | -3.6 | -4.2 |
| 93.7 | 11.672 | -5.6 | -3.6 | -3.6 | -4.2 |

| Depth (mm) | Age (ka BP) | $\delta^{13}C$ (‰ VPDB) | $\delta^{18}O$ (‰ VPDB) | $\delta^{18}O$ (‰ VPDB) Calcite Corr. | $\delta^{18}O$ (‰ VPDB) Sea Level Corr. |
|---|---|---|---|---|---|
| 94.0 | 11.674 | -6.0 | -3.6 | -3.6 | -4.2 |
| 94.3 | 11.675 | -6.0 | -4.0 | -4.0 | -4.5 |
| 94.6 | 11.676 | -6.0 | -3.9 | -3.9 | -4.5 |
| 94.9 | 11.677 | -6.2 | -4.1 | -4.1 | -4.7 |
| 95.2 | 11.679 | -6.0 | -3.9 | -3.9 | -4.5 |
| 95.5 | 11.680 | -6.1 | -3.7 | -3.7 | -4.3 |
| 95.8 | 11.681 | -6.0 | -3.7 | -3.7 | -4.3 |
| 96.1 | 11.682 | -5.9 | -3.6 | -3.6 | -4.2 |
| 96.4 | 11.684 | -6.5 | -3.9 | -3.9 | -4.5 |
| 96.7 | 11.685 | -6.5 | -3.8 | -3.8 | -4.4 |
| 97.0 | 11.686 | -6.3 | -3.6 | -3.6 | -4.2 |
| 97.3 | 11.687 | -6.1 | -3.6 | -3.6 | -4.2 |
| 97.6 | 11.689 | -6.2 | -3.9 | -3.9 | -4.5 |
| 97.9 | 11.690 | -5.9 | -3.6 | -3.6 | -4.2 |
| 98.2 | 11.691 | -6.6 | -3.7 | -3.7 | -4.3 |
| 98.5 | 11.692 | -6.7 | -3.9 | -3.9 | -4.5 |
| 98.8 | 11.694 | -6.5 | -3.7 | -3.7 | -4.3 |
| 103.0 | 11.711 | -6.6 | -3.7 | -3.7 | -4.3 |
| 103.4 | 11.713 | -6.8 | -4.0 | -4.0 | -4.6 |
| 103.8 | 11.715 | -6.3 | -3.2 | -3.2 | -3.8 |
| 104.2 | 11.717 | -6.6 | -3.6 | -3.6 | -4.2 |
| 104.7 | 11.718 | -6.0 | -3.6 | -3.6 | -4.2 |
| 105.1 | 11.720 | -5.8 | -3.2 | -3.2 | -3.8 |
| 105.5 | 11.722 | -6.7 | -3.7 | -3.7 | -4.3 |
| 105.9 | 11.724 | -6.9 | -3.8 | -3.8 | -4.4 |
| 106.3 | 11.725 | -6.7 | -3.7 | -3.7 | -4.3 |
| 106.8 | 11.727 | -6.4 | -3.8 | -3.8 | -4.4 |
| 107.2 | 11.729 | -6.3 | -3.4 | -3.4 | -4.0 |
| 107.6 | 11.731 | -6.2 | -3.4 | -3.4 | -4.0 |
| 108.0 | 11.733 | -6.3 | -3.6 | -3.6 | -4.2 |
| 108.4 | 11.734 | -6.2 | -3.2 | -3.2 | -3.8 |
| 108.8 | 11.736 | -6.8 | -3.7 | -3.7 | -4.3 |
| 109.3 | 11.738 | -6.9 | -3.7 | -3.7 | -4.3 |
| 109.5 | 11.739 | -7.0 | -3.8 | -3.8 | -4.4 |
| 109.8 | 11.740 | -7.0 | -3.8 | -3.8 | -4.4 |
| 110.0 | 11.741 | -6.8 | -3.8 | -3.8 | -4.4 |
| 110.3 | 11.742 | -6.7 | -3.8 | -3.8 | -4.4 |
| 110.6 | 11.743 | -6.5 | -3.2 | -3.2 | -3.8 |
| 110.8 | 11.744 | -6.4 | -3.2 | -3.2 | -3.8 |
| 111.1 | 11.745 | -7.2 | -3.6 | -3.6 | -4.2 |
| 111.3 | 11.747 | -7.0 | -3.4 | -3.4 | -4.0 |
| 111.6 | 11.748 | -6.9 | -3.5 | -3.5 | -4.1 |
| 111.9 | 11.749 | -6.6 | -3.5 | -3.5 | -4.1 |

| Depth (mm) | Age (ka BP) | $\delta^{13}C$ (‰ VPDB) | $\delta^{18}O$ (‰ VPDB) | $\delta^{18}O$ (‰ VPDB) Calcite Corr. | $\delta^{18}O$ (‰ VPDB) Sea Level Corr. |
|---|---|---|---|---|---|
| 112.1 | 11.750 | -6.7 | -3.5 | -3.5 | -4.1 |
| 112.4 | 11.751 | -6.8 | -3.2 | -3.2 | -3.8 |
| 112.6 | 11.752 | -7.0 | -3.2 | -3.2 | -3.8 |
| 112.9 | 11.753 | -7.1 | -3.7 | -3.7 | -4.2 |
| 113.2 | 11.754 | -6.8 | -3.1 | -3.1 | -3.7 |
| 113.4 | 11.755 | -6.8 | -3.4 | -3.4 | -4.0 |
| 113.7 | 11.756 | -6.9 | -3.5 | -3.5 | -4.1 |
| 113.9 | 11.758 | -6.9 | -3.3 | -3.3 | -3.9 |
| 114.2 | 11.759 | -6.8 | -3.5 | -3.5 | -4.1 |
| 114.5 | 11.760 | -6.7 | -3.5 | -3.5 | -4.1 |
| 114.7 | 11.761 | -6.7 | -3.4 | -3.4 | -4.0 |
| 115.0 | 11.762 | -6.7 | -3.7 | -3.7 | -4.3 |
| 115.2 | 11.763 | -6.3 | -3.8 | -3.8 | -4.4 |
| 115.5 | 11.764 | -6.4 | -3.5 | -3.5 | -4.1 |
| 115.8 | 11.765 | -6.3 | -3.7 | -3.7 | -4.3 |
| 116.0 | 11.766 | -7.0 | -3.8 | -3.8 | -4.4 |
| 116.3 | 11.767 | -6.3 | -3.4 | -3.4 | -4.0 |
| 116.5 | 11.768 | -6.3 | -3.4 | -3.4 | -4.0 |
| 116.8 | 11.770 | -5.4 | -3.3 | -3.3 | -3.9 |
| 117.1 | 11.771 | -6.1 | -3.2 | -3.2 | -3.8 |
| 117.3 | 11.772 | -5.9 | -3.3 | -3.3 | -3.9 |
| 117.6 | 11.773 | -6.1 | -3.4 | -3.4 | -4.0 |
| 117.8 | 11.774 | -5.8 | -3.5 | -3.5 | -4.1 |
| 118.1 | 11.775 | -6.0 | -3.4 | -3.4 | -4.0 |
| 118.4 | 11.776 | -6.2 | -3.4 | -3.4 | -4.0 |
| 118.6 | 11.777 | -6.6 | -3.5 | -3.5 | -4.1 |
| 118.9 | 11.778 | -6.0 | -3.7 | -3.7 | -4.3 |
| 119.1 | 11.779 | -6.0 | -3.4 | -3.4 | -4.0 |
| 119.4 | 11.781 | -5.9 | -3.1 | -3.1 | -3.7 |
| 119.7 | 11.782 | -6.3 | -3.2 | -3.2 | -3.8 |
| 119.9 | 11.783 | -6.0 | -3.1 | -3.1 | -3.7 |
| 120.2 | 11.784 | -6.8 | -3.6 | -3.6 | -4.2 |
| 120.7 | 11.786 | -6.3 | -3.0 | -3.0 | -3.6 |
| 121.0 | 11.787 | -6.7 | -3.3 | -3.3 | -3.9 |
| 121.4 | 11.789 | -6.2 | -3.5 | -3.5 | -4.1 |
| 121.7 | 11.790 | -5.5 | -2.9 | -2.9 | -3.5 |
| 122.0 | 11.791 | -5.8 | -3.1 | -3.1 | -3.7 |
| 122.3 | 11.793 | -5.4 | -3.1 | -3.1 | -3.7 |
| 122.6 | 11.794 | -6.1 | -3.1 | -3.1 | -3.7 |
| 122.9 | 11.795 | -6.4 | -3.0 | -3.0 | -3.6 |
| 123.2 | 11.796 | -6.3 | -3.2 | -3.2 | -3.8 |
| 123.5 | 11.798 | -6.0 | -3.0 | -3.0 | -3.6 |
| 123.8 | 11.799 | -6.2 | -3.0 | -3.0 | -3.6 |

| Depth (mm) | Age (ka BP) | $\delta^{13}C$ (‰ VPDB) | $\delta^{18}O$ (‰ VPDB) | $\delta^{18}O$ (‰ VPDB) Calcite Corr. | $\delta^{18}O$ (‰ VPDB) Sea Level Corr. |
|---|---|---|---|---|---|
| 124.1 | 11.800 | -6.2 | -3.5 | -3.5 | -4.1 |
| 124.4 | 11.801 | -6.0 | -2.9 | -2.9 | -3.5 |
| 124.7 | 11.803 | -6.1 | -3.0 | -3.0 | -3.6 |
| 125.0 | 11.804 | -5.8 | -3.1 | -3.1 | -3.7 |
| 125.3 | 11.805 | -5.3 | -3.1 | -3.1 | -3.7 |
| 125.6 | 11.807 | -5.9 | -3.3 | -3.3 | -3.9 |
| 125.9 | 11.808 | -6.1 | -3.0 | -3.0 | -3.6 |
| 126.2 | 11.809 | -6.2 | -3.1 | -3.1 | -3.7 |
| 126.5 | 11.810 | -5.2 | -3.1 | -3.1 | -3.7 |
| 126.8 | 11.812 | -5.9 | -3.3 | -3.3 | -3.9 |
| 127.0 | 11.813 | -5.7 | -3.0 | -3.0 | -3.6 |
| 127.2 | 11.814 | -6.1 | -3.7 | -3.7 | -4.3 |
| 127.5 | 11.814 | -6.2 | -3.2 | -3.2 | -3.8 |
| 127.7 | 11.815 | -6.0 | -3.3 | -3.3 | -3.9 |
| 127.9 | 11.816 | -6.6 | -3.5 | -3.5 | -4.1 |
| 128.1 | 11.817 | -5.8 | -3.3 | -3.3 | -3.9 |
| 128.3 | 11.818 | -5.6 | -3.2 | -3.2 | -3.8 |
| 128.6 | 11.819 | -6.4 | -3.6 | -3.6 | -4.2 |
| 128.8 | 11.820 | -6.2 | -3.2 | -3.2 | -3.8 |
| 129.0 | 11.821 | -6.1 | -3.2 | -3.2 | -3.8 |
| 129.2 | 11.822 | -6.4 | -3.5 | -3.5 | -4.1 |
| 129.4 | 11.823 | -6.1 | -3.5 | -3.5 | -4.1 |
| 129.7 | 11.824 | -5.6 | -3.6 | -3.6 | -4.2 |
| 130.0 | 11.825 | -5.6 | -3.5 | -3.5 | -4.1 |
| 130.3 | 11.826 | -5.6 | -3.5 | -3.5 | -4.1 |
| 130.6 | 11.828 | -5.3 | -3.1 | -3.1 | -3.7 |
| 130.9 | 11.829 | -5.7 | -3.2 | -3.2 | -3.8 |
| 131.2 | 11.830 | -5.4 | -3.4 | -3.4 | -4.0 |
| 131.5 | 11.831 | -5.8 | -3.6 | -3.6 | -4.2 |
| 131.8 | 11.833 | -5.1 | -3.7 | -3.7 | -4.3 |
| 132.1 | 11.834 | -4.6 | -3.4 | -3.4 | -4.0 |
| 132.4 | 11.835 | -5.9 | -3.4 | -3.4 | -4.0 |
| 132.7 | 11.837 | -5.0 | -3.4 | -3.4 | -4.0 |
| 133.0 | 11.838 | -5.6 | -3.7 | -3.7 | -4.3 |
| 133.3 | 11.839 | -5.5 | -3.5 | -3.5 | -4.1 |
| 133.6 | 11.840 | -5.5 | -3.7 | -3.7 | -4.3 |
| 133.9 | 11.842 | -6.0 | -4.1 | -4.1 | -4.7 |
| 134.2 | 11.843 | -5.9 | -3.8 | -3.8 | -4.4 |
| 134.5 | 11.844 | -5.6 | -3.4 | -3.4 | -4.1 |
| 134.9 | 11.846 | -6.0 | -4.2 | -4.2 | -4.8 |
| 135.2 | 11.847 | -6.3 | -4.4 | -4.4 | -5.0 |
| 135.5 | 11.848 | -6.1 | -3.9 | -3.9 | -4.5 |
| 135.8 | 11.849 | -5.6 | -4.0 | -4.0 | -4.6 |

| Depth (mm) | Age (ka BP) | $\delta^{13}C$ (‰ VPDB) | $\delta^{18}O$ (‰ VPDB) | $\delta^{18}O$ (‰ VPDB) Calcite Corr. | $\delta^{18}O$ (‰ VPDB) Sea Level Corr. |
|---|---|---|---|---|---|
| 136.1 | 11.851 | -5.8 | -5.0 | -5.0 | -5.6 |
| 136.4 | 11.852 | -5.0 | -3.8 | -3.8 | -4.4 |
| 136.7 | 11.853 | -4.8 | -3.0 | -3.0 | -3.6 |
| 137.0 | 11.855 | -5.2 | -3.2 | -3.2 | -3.8 |
| 137.3 | 11.856 | -5.7 | -4.0 | -4.0 | -4.6 |
| 137.6 | 11.857 | -6.0 | -4.2 | -4.2 | -4.8 |
| 137.9 | 12.893 | -5.9 | -3.0 | -3.0 | -3.7 |
| 138.1 | 12.910 | -7.4 | -3.0 | -3.0 | -3.8 |
| 138.4 | 12.927 | -7.2 | -3.3 | -3.3 | -4.0 |
| 138.7 | 12.944 | -7.5 | -4.0 | -4.0 | -4.8 |
| 139.0 | 12.960 | -7.5 | -3.3 | -3.3 | -4.1 |
| 139.3 | 12.977 | -7.2 | -3.4 | -3.4 | -4.1 |
| 139.6 | 12.994 | -8.1 | -3.9 | -3.9 | -4.6 |
| 139.9 | 13.011 | -7.6 | -3.6 | -3.6 | -4.3 |
| 140.1 | 13.028 | -7.1 | -3.8 | -3.8 | -4.5 |
| 140.4 | 13.044 | -7.6 | -3.8 | -3.8 | -4.5 |
| 141.0 | 13.078 | -8.3 | -4.1 | -4.1 | -4.9 |
| 141.3 | 13.095 | -8.8 | -4.3 | -4.3 | -5.1 |
| 141.6 | 13.115 | -8.7 | -4.2 | -4.2 | -5.0 |
| 141.8 | 13.128 | -8.4 | -3.7 | -3.7 | -4.5 |
| 142.1 | 13.145 | -8.8 | -4.0 | -4.0 | -4.8 |
| 142.4 | 13.161 | -8.4 | -3.6 | -3.6 | -4.3 |
| 142.7 | 13.178 | -8.4 | -3.8 | -3.8 | -4.6 |
| 143.0 | 13.195 | -8.5 | -4.2 | -4.2 | -5.0 |
| 143.2 | 13.211 | -8.2 | -3.8 | -3.8 | -4.6 |
| 143.5 | 13.228 | -8.8 | -4.1 | -4.1 | -4.9 |
| 143.8 | 13.244 | -8.4 | -4.0 | -4.0 | -4.8 |
| 144.1 | 13.261 | -8.4 | -3.7 | -3.7 | -4.5 |
| 144.4 | 13.277 | -8.7 | -3.9 | -3.9 | -4.7 |
| 144.6 | 13.294 | -8.8 | -4.1 | -4.1 | -4.9 |
| 144.9 | 13.311 | -8.4 | -3.8 | -3.8 | -4.5 |
| 145.2 | 13.327 | -8.5 | -3.7 | -3.7 | -4.5 |
| 145.5 | 13.344 | -8.4 | -3.7 | -3.7 | -4.5 |
| 145.8 | 13.360 | -8.6 | -4.1 | -4.1 | -4.8 |
| 146.0 | 13.377 | -8.5 | -4.0 | -4.0 | -4.8 |
| 146.3 | 13.393 | -9.1 | -4.5 | -4.5 | -5.3 |
| 146.6 | 13.410 | -8.7 | -3.8 | -3.8 | -4.6 |
| 146.9 | 13.426 | -8.7 | -3.6 | -3.6 | -4.4 |
| 147.2 | 13.442 | -8.6 | -3.6 | -3.6 | -4.4 |
| 147.4 | 13.458 | -8.4 | -3.6 | -3.6 | -4.4 |
| 147.7 | 13.474 | -8.2 | -3.4 | -3.4 | -4.2 |
| 148.0 | 13.490 | -8.7 | -3.7 | -3.7 | -4.5 |
| 148.2 | 13.506 | -8.2 | -3.4 | -3.4 | -4.2 |

| Depth (mm) | Age (ka BP) | $\delta^{13}C$ (‰ VPDB) | $\delta^{18}O$ (‰ VPDB) | $\delta^{18}O$ (‰ VPDB) Calcite Corr. | $\delta^{18}O$ (‰ VPDB) Sea Level Corr. |
|---|---|---|---|---|---|
| 148.5 | 13.521 | -8.2 | -3.6 | -3.6 | -4.4 |
| 148.8 | 13.537 | -8.4 | -3.6 | -3.6 | -4.4 |
| 149.0 | 13.553 | -8.8 | -4.2 | -4.2 | -5.0 |
| 149.3 | 13.569 | -8.3 | -3.3 | -3.3 | -4.1 |
| 149.6 | 13.585 | -8.7 | -3.6 | -3.6 | -4.4 |
| 149.8 | 13.601 | -8.6 | -3.5 | -3.5 | -4.3 |
| 150.1 | 13.616 | -8.5 | -4.0 | -4.0 | -4.8 |
| 150.4 | 13.632 | -8.6 | -3.8 | -3.8 | -4.6 |
| 150.6 | 13.648 | -8.3 | -3.4 | -3.4 | -4.2 |
| 150.9 | 13.664 | -8.4 | -3.7 | -3.7 | -4.5 |
| 151.2 | 13.680 | -8.2 | -3.2 | -3.2 | -4.1 |
| 151.4 | 13.696 | -8.7 | -3.8 | -3.8 | -4.7 |
| 151.7 | 13.711 | -8.7 | -4.0 | -4.0 | -4.8 |
| 152.0 | 13.727 | -8.3 | -3.6 | -3.6 | -4.5 |
| 152.2 | 13.743 | -8.8 | -3.5 | -3.5 | -4.3 |
| 152.5 | 13.761 | -8.3 | -3.5 | -3.5 | -4.4 |
| 152.8 | 13.779 | -8.6 | -3.9 | -3.9 | -4.8 |
| 153.1 | 13.796 | -9.2 | -4.2 | -4.2 | -5.0 |
| 153.4 | 13.814 | -8.5 | -3.5 | -3.5 | -4.3 |
| 153.7 | 13.832 | -8.6 | -3.3 | -3.3 | -4.2 |
| 154.0 | 13.850 | -8.9 | -3.9 | -3.9 | -4.8 |
| 154.3 | 13.867 | -8.9 | -3.5 | -3.5 | -4.4 |
| 154.6 | 13.885 | -8.7 | -3.5 | -3.5 | -4.3 |
| 154.9 | 13.903 | -8.5 | -3.0 | -3.0 | -3.9 |
| 155.2 | 13.920 | -8.4 | -3.0 | -3.0 | -3.9 |
| 155.5 | 13.938 | -8.4 | -3.0 | -3.0 | -3.8 |
| 155.8 | 13.956 | -8.6 | -3.1 | -3.1 | -3.9 |
| 156.1 | 13.974 | -8.6 | -3.1 | -3.1 | -4.0 |
| 156.4 | 13.991 | -8.6 | -3.0 | -3.0 | -3.9 |
| 156.7 | 14.009 | -8.6 | -3.1 | -3.1 | -4.0 |
| 156.8 | 14.014 | -8.6 | -2.8 | -2.8 | -3.7 |
| 156.9 | 14.019 | -8.4 | -3.2 | -3.2 | -4.1 |
| 157.0 | 14.025 | -8.3 | -3.0 | -3.0 | -3.9 |
| 157.1 | 14.031 | -8.8 | -3.7 | -3.7 | -4.5 |
| 157.2 | 14.037 | -8.9 | -3.7 | -3.7 | -4.6 |
| 157.3 | 14.042 | -8.7 | -3.5 | -3.5 | -4.4 |
| 157.4 | 14.048 | -8.7 | -3.6 | -3.6 | -4.4 |
| 157.5 | 14.054 | -8.5 | -3.2 | -3.2 | -4.1 |
| 157.6 | 14.060 | -8.4 | -3.3 | -3.3 | -4.2 |
| 157.7 | 14.066 | -8.8 | -3.4 | -3.4 | -4.3 |
| 157.8 | 14.071 | -8.5 | -3.2 | -3.2 | -4.1 |
| 157.9 | 14.077 | -8.7 | -3.5 | -3.5 | -4.4 |
| 158.0 | 14.083 | -8.6 | -3.6 | -3.6 | -4.5 |

| Depth (mm) | Age (ka BP) | $\delta^{13}C$ (‰ VPDB) | $\delta^{18}O$ (‰ VPDB) | $\delta^{18}O$ (‰ VPDB) Calcite Corr. | $\delta^{18}O$ (‰ VPDB) Sea Level Corr. |
|---|---|---|---|---|---|
| 158.1 | 14.089 | -8.6 | -3.4 | -3.4 | -4.2 |
| 158.2 | 14.095 | -8.9 | -3.6 | -3.6 | -4.5 |
| 158.3 | 14.100 | -9.0 | -3.6 | -3.6 | -4.5 |
| 158.4 | 14.106 | -8.9 | -3.7 | -3.7 | -4.7 |
| 158.5 | 14.112 | -8.7 | -3.4 | -3.4 | -4.3 |
| 158.6 | 14.118 | -8.7 | -3.5 | -3.5 | -4.4 |
| 158.7 | 14.124 | -8.4 | -3.2 | -3.2 | -4.2 |
| 158.8 | 14.129 | -8.6 | -3.7 | -3.7 | -4.6 |
| 158.9 | 14.135 | -8.3 | -3.0 | -3.0 | -3.9 |
| 159.0 | 14.141 | -8.4 | -3.2 | -3.2 | -4.1 |
| 159.1 | 14.147 | -8.6 | -3.5 | -3.5 | -4.4 |
| 159.2 | 14.153 | -8.4 | -3.3 | -3.3 | -4.2 |
| 159.3 | 14.158 | -8.7 | -3.7 | -3.7 | -4.6 |
| 159.4 | 14.164 | -8.3 | -3.2 | -3.2 | -4.2 |
| 159.5 | 14.170 | -8.4 | -3.5 | -3.5 | -4.4 |
| 159.6 | 14.176 | -8.0 | -2.8 | -2.8 | -3.7 |
| 159.7 | 14.181 | -8.4 | -3.3 | -3.3 | -4.2 |
| 159.8 | 14.187 | -8.4 | -3.1 | -3.1 | -4.0 |
| 159.9 | 14.193 | -8.5 | -3.2 | -3.2 | -4.1 |
| 160.0 | 14.199 | -8.7 | -3.5 | -3.5 | -4.5 |
| 160.1 | 14.205 | -9.4 | -4.0 | -4.0 | -4.9 |
| 160.2 | 14.210 | -8.3 | -3.5 | -3.5 | -4.5 |
| 160.2 | 14.216 | -8.5 | -3.3 | -3.3 | -4.3 |
| 160.3 | 14.222 | -8.3 | -3.3 | -3.3 | -4.3 |
| 160.4 | 14.228 | -8.4 | -3.8 | -3.8 | -4.8 |
| 160.5 | 14.234 | -7.9 | -2.9 | -2.9 | -3.8 |
| 160.6 | 14.239 | -8.0 | -2.9 | -2.9 | -3.8 |
| 160.7 | 14.245 | -8.1 | -3.2 | -3.2 | -4.2 |
| 160.8 | 14.251 | -8.0 | -3.0 | -3.0 | -3.9 |
| 160.9 | 14.257 | -8.4 | -3.0 | -3.0 | -4.0 |
| 161.0 | 14.263 | -8.5 | -3.2 | -3.2 | -4.1 |
| 161.1 | 14.268 | -8.3 | -2.9 | -2.9 | -3.8 |
| 161.2 | 14.274 | -8.2 | -3.2 | -3.2 | -4.1 |
| 161.3 | 14.280 | -8.2 | -3.0 | -3.0 | -4.0 |
| 161.4 | 14.286 | -8.4 | -3.1 | -3.1 | -4.1 |
| 161.5 | 14.292 | -8.2 | -2.8 | -2.8 | -3.7 |
| 161.6 | 14.297 | -8.1 | -2.8 | -2.8 | -3.8 |
| 161.7 | 14.303 | -7.9 | -3.0 | -3.0 | -4.0 |
| 161.8 | 14.309 | -7.9 | -2.9 | -2.9 | -3.9 |
| 161.9 | 14.315 | -7.8 | -2.8 | -2.8 | -3.8 |
| 162.0 | 14.320 | -7.5 | -2.6 | -2.6 | -3.6 |
| 162.1 | 14.326 | -7.4 | -2.4 | -2.4 | -3.3 |
| 162.2 | 14.332 | -7.6 | -2.7 | -2.7 | -3.7 |

| Depth (mm) | Age (ka BP) | $\delta^{13}C$ (‰ VPDB) | $\delta^{18}O$ (‰ VPDB) | $\delta^{18}O$ (‰ VPDB) Calcite Corr. | $\delta^{18}O$ (‰ VPDB) Sea Level Corr. |
|---|---|---|---|---|---|
| 162.3 | 14.338 | -7.7 | -2.8 | -2.8 | -3.8 |
| 162.4 | 14.344 | -7.7 | -2.7 | -2.7 | -3.7 |
| 162.5 | 14.349 | -7.5 | -2.5 | -2.5 | -3.5 |
| 162.6 | 14.355 | -7.6 | -2.7 | -2.7 | -3.7 |
| 162.7 | 14.361 | -7.7 | -3.0 | -3.0 | -4.0 |
| 162.8 | 14.367 | -7.7 | -2.7 | -2.7 | -3.7 |
| 162.9 | 14.373 | -7.8 | -2.9 | -2.9 | -3.9 |
| 163.0 | 14.378 | -7.8 | -2.9 | -2.9 | -3.9 |
| 163.1 | 14.384 | -7.9 | -2.9 | -2.9 | -3.9 |
| 163.2 | 14.390 | -8.1 | -3.1 | -3.1 | -4.1 |
| 163.3 | 14.396 | -8.0 | -3.0 | -3.0 | -4.0 |
| 163.4 | 14.402 | -7.9 | -2.8 | -2.8 | -3.8 |
| 163.5 | 14.407 | -7.9 | -2.7 | -2.7 | -3.7 |
| 163.6 | 14.413 | -7.9 | -2.9 | -2.9 | -3.9 |
| 163.7 | 14.419 | -7.7 | -2.8 | -2.8 | -3.8 |
| 163.8 | 14.425 | -7.7 | -3.0 | -3.0 | -4.1 |
| 163.9 | 14.431 | -7.4 | -2.8 | -2.8 | -3.8 |
| 164.0 | 14.436 | -7.4 | -2.7 | -2.7 | -3.7 |
| 164.1 | 14.442 | -7.2 | -2.7 | -2.7 | -3.7 |
| 164.2 | 14.448 | -7.1 | -2.6 | -2.6 | -3.7 |
| 164.3 | 14.454 | -7.2 | -2.3 | -2.3 | -3.3 |
| 164.4 | 14.459 | -7.1 | -2.4 | -2.4 | -3.4 |
| 164.5 | 14.465 | -7.1 | -2.3 | -2.3 | -3.4 |
| 164.6 | 14.471 | -7.1 | -2.5 | -2.5 | -3.5 |
| 164.7 | 14.477 | -7.0 | -2.3 | -2.3 | -3.4 |
| 164.8 | 14.483 | -7.0 | -2.3 | -2.3 | -3.3 |
| 164.9 | 14.488 | -7.0 | -2.4 | -2.4 | -3.5 |
| 165.0 | 14.494 | -7.1 | -2.6 | -2.6 | -3.6 |
| 165.1 | 14.500 | -7.0 | -2.4 | -2.4 | -3.5 |
| 165.1 | 14.506 | -7.2 | -2.7 | -2.7 | -3.7 |
| 165.2 | 14.512 | -7.3 | -2.9 | -2.9 | -3.9 |
| 165.4 | 14.523 | -7.3 | -2.6 | -2.6 | -3.6 |
| 165.5 | 14.529 | -7.3 | -2.7 | -2.7 | -3.7 |
| 165.6 | 14.535 | -7.3 | -2.5 | -2.5 | -3.6 |
| 165.7 | 14.541 | -7.5 | -2.8 | -2.8 | -3.8 |
| 165.8 | 14.546 | -7.6 | -2.8 | -2.8 | -3.8 |
| 165.9 | 14.552 | -7.8 | -2.9 | -2.9 | -4.0 |
| 166.0 | 14.558 | -7.7 | -2.9 | -2.9 | -3.9 |
| 166.1 | 14.564 | -7.6 | -2.8 | -2.8 | -3.8 |
| 166.2 | 14.570 | -7.6 | -2.8 | -2.8 | -3.8 |
| 166.3 | 14.575 | -7.6 | -2.7 | -2.7 | -3.7 |
| 166.5 | 14.587 | -7.9 | -2.6 | -2.6 | -3.7 |
| 166.6 | 14.593 | -7.9 | -2.6 | -2.6 | -3.7 |

| Depth (mm) | Age (ka BP) | $\delta^{13}C$ (‰ VPDB) | $\delta^{18}O$ (‰ VPDB) | $\delta^{18}O$ (‰ VPDB) Calcite Corr. | $\delta^{18}O$ (‰ VPDB) Sea Level Corr. |
|---|---|---|---|---|---|
| 166.7 | 14.599 | -8.0 | -2.9 | -2.9 | -3.9 |
| 166.8 | 14.604 | -8.0 | -3.1 | -3.1 | -4.1 |
| 166.9 | 14.610 | -8.0 | -3.2 | -3.2 | -4.2 |
| 167.0 | 14.616 | -8.1 | -3.0 | -3.0 | -4.0 |
| 167.1 | 14.622 | -8.3 | -3.0 | -3.0 | -4.1 |
| 167.2 | 14.627 | -8.3 | -3.1 | -3.1 | -4.1 |
| 167.3 | 14.633 | -8.3 | -3.0 | -3.0 | -4.0 |
| 167.4 | 14.639 | -8.3 | -3.2 | -3.2 | -4.2 |
| 167.5 | 14.645 | -8.2 | -3.1 | -3.1 | -4.2 |
| 167.6 | 14.651 | -8.1 | -2.9 | -2.9 | -3.9 |
| 167.7 | 14.656 | -8.1 | -2.8 | -2.8 | -3.8 |
| 167.8 | 14.662 | -8.2 | -2.8 | -2.8 | -3.8 |
| 167.9 | 14.668 | -8.4 | -2.8 | -2.8 | -3.9 |
| 168.0 | 14.674 | -8.5 | -3.1 | -3.1 | -4.2 |
| 168.1 | 14.680 | -8.3 | -2.8 | -2.8 | -3.9 |
| 168.2 | 14.685 | -8.3 | -2.7 | -2.7 | -3.7 |
| 168.3 | 14.691 | -8.2 | -3.1 | -3.1 | -4.1 |
| 168.4 | 14.697 | -7.8 | -2.6 | -2.6 | -3.7 |
| 168.5 | 14.703 | -7.6 | -2.4 | -2.4 | -3.4 |
| 168.6 | 14.709 | -8.0 | -2.7 | -2.7 | -3.8 |
| 168.7 | 14.714 | -8.0 | -2.8 | -2.8 | -3.9 |
| 168.8 | 14.720 | -7.7 | -2.9 | -2.9 | -4.0 |
| 168.9 | 14.726 | -8.1 | -3.1 | -3.1 | -4.2 |
| 169.0 | 14.732 | -8.0 | -2.8 | -2.8 | -3.9 |
| 169.1 | 14.738 | -8.0 | -2.7 | -2.7 | -3.7 |
| 169.2 | 14.743 | -8.4 | -3.0 | -3.0 | -4.1 |
| 169.3 | 14.749 | -8.2 | -2.9 | -2.9 | -4.0 |
| 169.4 | 14.755 | -8.1 | -2.8 | -2.8 | -3.9 |
| 169.5 | 14.761 | -7.9 | -2.8 | -2.8 | -3.8 |
| 169.6 | 14.766 | -7.8 | -2.9 | -2.9 | -3.9 |
| 169.7 | 14.772 | -7.8 | -2.7 | -2.7 | -3.7 |
| 169.8 | 14.778 | -7.9 | -2.9 | -2.9 | -3.9 |
| 169.9 | 14.784 | -8.2 | -3.0 | -3.0 | -4.0 |
| 170.0 | 14.790 | -8.1 | -2.6 | -2.6 | -3.7 |
| 170.0 | 14.795 | -8.2 | -3.0 | -3.0 | -4.1 |
| 170.1 | 14.801 | -8.3 | -3.3 | -3.3 | -4.3 |
| 170.2 | 14.807 | -8.4 | -3.2 | -3.2 | -4.2 |
| 170.3 | 14.813 | -7.9 | -2.5 | -2.5 | -3.6 |
| 170.5 | 14.824 | -9.0 | -3.3 | -3.3 | -4.4 |
| 170.6 | 14.830 | -8.2 | -2.9 | -2.9 | -4.0 |
| 170.7 | 14.836 | -8.1 | -2.7 | -2.7 | -3.8 |
| 170.8 | 14.842 | -8.0 | -2.4 | -2.4 | -3.4 |
| 170.9 | 14.848 | -8.2 | -2.8 | -2.8 | -3.8 |

| Depth (mm) | Age (ka BP) | $\delta^{13}C$ (‰ VPDB) | $\delta^{18}O$ (‰ VPDB) | $\delta^{18}O$ (‰ VPDB) Calcite Corr. | $\delta^{18}O$ (‰ VPDB) Sea Level Corr. |
|---|---|---|---|---|---|
| 171.0 | 14.853 | -8.2 | -3.0 | -3.0 | -4.0 |
| 171.1 | 14.859 | -8.5 | -3.1 | -3.1 | -4.2 |
| 171.2 | 14.865 | -8.6 | -2.9 | -2.9 | -3.9 |
| 171.3 | 14.871 | -8.5 | -2.7 | -2.7 | -3.8 |
| 171.4 | 14.877 | -8.2 | -2.6 | -2.6 | -3.6 |
| 171.5 | 14.882 | -8.3 | -2.8 | -2.8 | -3.9 |
| 171.6 | 14.888 | -7.7 | -2.8 | -2.8 | -3.9 |
| 171.7 | 14.894 | -8.3 | -2.4 | -2.4 | -3.5 |
| 171.8 | 14.900 | -8.4 | -2.7 | -2.7 | -3.7 |
| 171.9 | 14.905 | -8.2 | -2.8 | -2.8 | -3.9 |
| 172.0 | 14.911 | -8.3 | -2.7 | -2.7 | -3.7 |
| 172.1 | 14.917 | -8.2 | -2.6 | -2.6 | -3.6 |
| 172.2 | 14.923 | -8.8 | -3.0 | -3.0 | -4.1 |
| 172.3 | 14.929 | -8.9 | -2.4 | -2.4 | -3.5 |
| 172.4 | 14.934 | -8.5 | -2.8 | -2.8 | -3.9 |
| 172.5 | 14.940 | -8.4 | -3.1 | -3.1 | -4.1 |
| 172.6 | 14.946 | -8.3 | -2.6 | -2.6 | -3.7 |
| 172.7 | 14.952 | -8.4 | -2.9 | -2.9 | -3.9 |
| 172.8 | 14.958 | -8.1 | -2.6 | -2.6 | -3.7 |
| 172.9 | 14.963 | -7.8 | -2.3 | -2.3 | -3.4 |
| 173.0 | 14.969 | -8.2 | -2.8 | -2.8 | -3.8 |
| 173.1 | 14.975 | -8.0 | -2.4 | -2.4 | -3.5 |
| 173.2 | 14.981 | -8.2 | -3.1 | -3.1 | -4.2 |
| 173.3 | 14.987 | -8.3 | -3.0 | -3.0 | -4.0 |
| 173.4 | 14.992 | -7.9 | -2.3 | -2.3 | -3.4 |
| 173.5 | 14.998 | -7.8 | -2.4 | -2.4 | -3.5 |
| 173.6 | 15.004 | -7.8 | -2.3 | -2.3 | -3.3 |
| 173.7 | 15.010 | -7.8 | -2.4 | -2.4 | -3.5 |
| 173.8 | 15.016 | -8.1 | -2.9 | -2.9 | -4.0 |
| 173.9 | 15.021 | -7.8 | -2.4 | -2.4 | -3.5 |
| 174.0 | 15.027 | -8.2 | -2.6 | -2.6 | -3.7 |
| 174.1 | 15.033 | -8.1 | -2.8 | -2.8 | -3.9 |
| 174.2 | 15.039 | -8.0 | -2.3 | -2.3 | -3.4 |
| 174.3 | 15.044 | -8.3 | -2.8 | -2.8 | -3.9 |
| 174.4 | 15.050 | -8.3 | -2.8 | -2.8 | -3.9 |
| 174.5 | 15.056 | -7.9 | -2.6 | -2.6 | -3.7 |
| 174.6 | 15.062 | -7.6 | -2.6 | -2.6 | -3.7 |
| 174.7 | 15.068 | -7.1 | -2.2 | -2.2 | -3.2 |
| 174.8 | 15.073 | -6.8 | -2.3 | -2.3 | -3.4 |
| 174.9 | 15.079 | -7.1 | -2.6 | -2.6 | -3.6 |
| 174.9 | 15.089 | -7.5 | -2.6 | -2.6 | -3.7 |
| 175.0 | 15.095 | -8.0 | -2.7 | -2.7 | -3.8 |
| 175.1 | 15.109 | -8.2 | -2.9 | -2.9 | -4.0 |

| Depth (mm) | Age (ka BP) | $\delta^{13}C$ (‰ VPDB) | $\delta^{18}O$ (‰ VPDB) | $\delta^{18}O$ (‰ VPDB) Calcite Corr. | $\delta^{18}O$ (‰ VPDB) Sea Level Corr. |
|---|---|---|---|---|---|
| 175.2 | 15.123 | -7.9 | -2.6 | -2.6 | -3.7 |
| 175.3 | 15.137 | -8.2 | -2.9 | -2.9 | -4.0 |
| 175.4 | 15.150 | -8.2 | -2.8 | -2.8 | -3.9 |
| 175.5 | 15.164 | -8.2 | -2.9 | -2.9 | -4.0 |
| 175.6 | 15.178 | -8.2 | -2.7 | -2.7 | -3.8 |
| 175.7 | 15.191 | -7.9 | -2.5 | -2.5 | -3.6 |
| 175.8 | 15.205 | -8.1 | -2.4 | -2.4 | -3.5 |
| 175.9 | 15.219 | -8.7 | -3.3 | -3.3 | -4.4 |
| 176.0 | 15.233 | -8.4 | -2.7 | -2.7 | -3.8 |
| 176.1 | 15.246 | -8.6 | -2.7 | -2.7 | -3.8 |
| 176.2 | 15.260 | -8.1 | -2.4 | -2.4 | -3.5 |
| 176.3 | 15.274 | -8.1 | -2.5 | -2.5 | -3.6 |
| 176.4 | 15.287 | -7.8 | -2.9 | -2.9 | -4.0 |
| 176.5 | 15.301 | -7.2 | -2.8 | -2.8 | -3.9 |
| 176.6 | 15.315 | -7.4 | -3.2 | -3.2 | -4.3 |
| 176.8 | 15.342 | -7.6 | -3.1 | -3.1 | -4.2 |
| 176.9 | 15.356 | -7.4 | -2.7 | -2.7 | -3.8 |
| 177.0 | 15.370 | -7.6 | -2.9 | -2.9 | -4.0 |
| 177.1 | 15.383 | -7.5 | -2.9 | -2.9 | -4.0 |
| 177.2 | 15.397 | -7.8 | -3.2 | -3.2 | -4.3 |
| 177.3 | 15.411 | -7.5 | -3.4 | -3.4 | -4.5 |
| 177.4 | 15.424 | -7.9 | -3.4 | -3.4 | -4.5 |
| 177.5 | 15.438 | -8.8 | -3.7 | -3.7 | -4.9 |
| 177.6 | 15.452 | -8.6 | -3.5 | -3.5 | -4.6 |
| 177.7 | 15.466 | -8.7 | -3.7 | -3.7 | -4.9 |
| 177.8 | 15.479 | -7.7 | -3.1 | -3.1 | -4.2 |
| 177.9 | 15.493 | -7.4 | -2.8 | -2.8 | -4.0 |
| 178.0 | 15.507 | -7.3 | -2.8 | -2.8 | -4.0 |
| 178.1 | 15.520 | -7.6 | -3.0 | -3.0 | -4.1 |
| 178.2 | 15.534 | -7.4 | -2.6 | -2.6 | -3.7 |
| 178.3 | 15.548 | -8.0 | -3.0 | -3.0 | -4.1 |
| 178.4 | 15.569 | -7.5 | -2.3 | -2.3 | -3.5 |
| 178.5 | 15.571 | -7.1 | -2.5 | -2.5 | -3.6 |
| 178.6 | 15.577 | -7.1 | -2.4 | -2.4 | -3.5 |
| 178.7 | 15.583 | -7.2 | -2.3 | -2.3 | -3.4 |
| 178.8 | 15.588 | -6.7 | -2.0 | -2.0 | -3.1 |
| 178.9 | 15.594 | -7.4 | -2.5 | -2.5 | -3.7 |
| 179.0 | 15.600 | -8.0 | -2.3 | -2.3 | -3.5 |
| 179.1 | 15.605 | -7.7 | -2.4 | -2.4 | -3.5 |
| 179.2 | 15.611 | -6.9 | -2.1 | -2.1 | -3.3 |
| 179.3 | 15.617 | -6.2 | -1.9 | -1.9 | -3.1 |
| 179.4 | 15.622 | -6.1 | -2.5 | -2.5 | -3.7 |
| 179.5 | 15.628 | -5.7 | -2.2 | -2.2 | -3.3 |

| Depth (mm) | Age (ka BP) | $\delta^{13}C$ (‰ VPDB) | $\delta^{18}O$ (‰ VPDB) | $\delta^{18}O$ (‰ VPDB) Calcite Corr. | $\delta^{18}O$ (‰ VPDB) Sea Level Corr. |
|---|---|---|---|---|---|
| 179.6 | 15.634 | -5.7 | -2.1 | -2.1 | -3.2 |
| 179.7 | 15.639 | -6.0 | -2.2 | -2.2 | -3.3 |
| 179.8 | 15.645 | -6.2 | -2.1 | -2.1 | -3.2 |
| 179.8 | 15.651 | -6.5 | -2.2 | -2.2 | -3.4 |
| 179.9 | 15.656 | -6.4 | -2.3 | -2.3 | -3.4 |
| 180.0 | 15.662 | -6.7 | -2.7 | -2.7 | -3.8 |
| 180.1 | 15.668 | -6.6 | -2.5 | -2.5 | -3.7 |
| 180.2 | 15.673 | -6.4 | -2.1 | -2.1 | -3.3 |
| 180.3 | 15.679 | -6.3 | -2.2 | -2.2 | -3.4 |
| 180.4 | 15.685 | -6.4 | -2.3 | -2.3 | -3.4 |
| 180.5 | 15.690 | -6.4 | -2.7 | -2.7 | -3.8 |
| 180.6 | 15.696 | -6.6 | -2.5 | -2.5 | -3.7 |
| 180.7 | 15.702 | -6.7 | -2.9 | -2.9 | -4.0 |
| 180.8 | 15.707 | -6.3 | -3.1 | -3.1 | -4.2 |
| 180.9 | 15.713 | -6.5 | -3.5 | -3.5 | -4.6 |
| 181.0 | 15.719 | -6.7 | -3.7 | -3.7 | -4.9 |
| 181.1 | 15.724 | -7.1 | -3.4 | -3.4 | -4.6 |
| 181.2 | 15.730 | -8.3 | -3.4 | -3.1 | -4.2 |
| 181.5 | 15.746 | -7.0 | -3.9 | -3.6 | -4.8 |
| 181.8 | 15.761 | -7.0 | -3.5 | -3.2 | -4.3 |
| 182.0 | 15.777 | -6.9 | -3.3 | -3.0 | -4.2 |
| 182.3 | 15.792 | -7.1 | -3.6 | -3.3 | -4.4 |
| 182.6 | 15.808 | -7.3 | -3.7 | -3.4 | -4.5 |
| 182.8 | 15.823 | -7.3 | -3.7 | -3.4 | -4.6 |
| 183.1 | 15.839 | -7.3 | -3.7 | -3.4 | -4.5 |
| 183.4 | 15.854 | -7.1 | -3.5 | -3.2 | -4.3 |
| 183.6 | 15.870 | -7.2 | -3.6 | -3.3 | -4.5 |
| 183.9 | 15.885 | -7.3 | -3.6 | -3.3 | -4.5 |
| 184.2 | 15.901 | -7.2 | -3.6 | -3.3 | -4.5 |
| 184.4 | 15.916 | -7.0 | -3.4 | -3.1 | -4.3 |
| 184.7 | 15.932 | -7.4 | -3.6 | -3.3 | -4.5 |
| 185.0 | 15.947 | -7.6 | -3.9 | -3.6 | -4.8 |
| 185.2 | 15.963 | -7.1 | -3.6 | -3.3 | -4.5 |
| 185.5 | 15.978 | -7.3 | -4.0 | -3.7 | -4.9 |
| 185.8 | 15.994 | -7.1 | -4.0 | -3.7 | -4.8 |
| 186.0 | 16.009 | -6.8 | -3.8 | -3.5 | -4.6 |
| 186.3 | 16.025 | -7.0 | -4.1 | -3.8 | -5.0 |
| 186.6 | 16.040 | -7.3 | -4.1 | -3.8 | -5.0 |
| 186.8 | 16.056 | -7.3 | -3.9 | -3.6 | -4.8 |
| 187.1 | 16.071 | -7.3 | -3.9 | -3.6 | -4.8 |
| 187.4 | 16.087 | -7.4 | -4.1 | -3.8 | -5.0 |
| 187.7 | 16.104 | -7.5 | -4.1 | -3.8 | -4.9 |
| 188.0 | 16.121 | -7.1 | -3.6 | -3.3 | -4.5 |

| Depth (mm) | Age (ka BP) | $\delta^{13}C$ (‰ VPDB) | $\delta^{18}O$ (‰ VPDB) | $\delta^{18}O$ (‰ VPDB) Calcite Corr. | $\delta^{18}O$ (‰ VPDB) Sea Level Corr. |
|---|---|---|---|---|---|
| 188.3 | 16.138 | -7.2 | -4.0 | -3.7 | -4.9 |
| 188.6 | 16.156 | -7.2 | -4.1 | -3.8 | -5.0 |
| 188.9 | 16.173 | -6.9 | -3.8 | -3.5 | -4.7 |
| 189.2 | 16.190 | -6.6 | -3.0 | -2.7 | -3.9 |
| 189.5 | 16.207 | -7.3 | -4.1 | -3.8 | -5.0 |
| 189.8 | 16.225 | -7.2 | -3.9 | -3.6 | -4.8 |
| 190.1 | 16.242 | -7.3 | -4.0 | -3.7 | -4.9 |
| 190.4 | 16.259 | -7.2 | -4.1 | -3.8 | -5.0 |
| 190.7 | 16.276 | -7.1 | -4.0 | -3.7 | -4.9 |
| 191.0 | 16.294 | -7.1 | -4.0 | -3.7 | -4.9 |
| 191.3 | 16.311 | -7.1 | -4.1 | -3.8 | -5.0 |
| 191.6 | 16.328 | -7.1 | -4.1 | -3.8 | -5.0 |
| 191.8 | 16.345 | -7.1 | -4.1 | -3.8 | -5.0 |
| 192.1 | 16.363 | -7.3 | -4.3 | -4.0 | -5.2 |
| 192.4 | 16.380 | -7.0 | -3.9 | -3.6 | -4.8 |
| 192.7 | 16.397 | -7.1 | -4.1 | -3.8 | -5.0 |
| 193.0 | 16.414 | -7.1 | -3.9 | -3.6 | -4.8 |
| 193.3 | 16.432 | -7.3 | -4.1 | -3.8 | -5.0 |
| 193.6 | 16.449 | -7.2 | -3.8 | -3.5 | -4.7 |
| 193.9 | 16.466 | -7.3 | -3.8 | -3.5 | -4.7 |
| 194.2 | 16.484 | -7.5 | -4.2 | -3.9 | -5.1 |
| 194.5 | 16.501 | -7.5 | -4.1 | -3.8 | -5.0 |
| 194.8 | 16.518 | -7.6 | -4.4 | -4.1 | -5.3 |
| 195.1 | 16.535 | -7.5 | -4.5 | -4.2 | -5.4 |
| 195.4 | 16.553 | -7.5 | -4.3 | -4.0 | -5.2 |
| 195.7 | 16.570 | -7.4 | -4.1 | -3.8 | -5.0 |
| 196.0 | 16.587 | -6.9 | -3.8 | -3.5 | -4.7 |
| 196.3 | 16.604 | -7.4 | -4.1 | -3.8 | -5.0 |
| 196.6 | 16.622 | -7.0 | -3.3 | -3.0 | -4.2 |
| 196.9 | 16.639 | -7.5 | -4.2 | -3.9 | -5.1 |
| 197.2 | 16.656 | -7.1 | -3.4 | -3.1 | -4.3 |
| 197.5 | 16.673 | -7.2 | -4.0 | -3.7 | -4.9 |
| 197.8 | 16.691 | -7.2 | -4.1 | -3.8 | -5.0 |
| 198.1 | 16.708 | -7.0 | -3.8 | -3.5 | -4.7 |
| 198.7 | 16.742 | -6.7 | -3.1 | -2.8 | -4.0 |
| 199.0 | 16.760 | -7.4 | -4.0 | -3.7 | -4.9 |
| 199.3 | 16.777 | -7.7 | -4.1 | -3.8 | -5.0 |
| 199.6 | 16.795 | -7.3 | -3.8 | -3.5 | -4.8 |
| 199.9 | 16.812 | -6.7 | -3.2 | -2.9 | -4.1 |
| 200.2 | 16.830 | -7.0 | -3.4 | -3.1 | -4.4 |
| 200.5 | 16.847 | -7.7 | -4.3 | -4.0 | -5.2 |
| 200.8 | 16.865 | -7.3 | -3.7 | -3.4 | -4.7 |
| 201.1 | 16.882 | -7.4 | -3.7 | -3.4 | -4.6 |

| Depth (mm) | Age (ka BP) | $\delta^{13}C$ (‰ VPDB) | $\delta^{18}O$ (‰ VPDB) | $\delta^{18}O$ (‰ VPDB) Calcite Corr. | $\delta^{18}O$ (‰ VPDB) Sea Level Corr. |
|---|---|---|---|---|---|
| 201.4 | 16.900 | -7.3 | -3.7 | -3.4 | -4.7 |
| 201.7 | 16.917 | -7.6 | -4.0 | -3.7 | -4.9 |
| 202.0 | 16.935 | -7.2 | -3.5 | -3.2 | -4.4 |
| 202.3 | 16.953 | -7.4 | -3.8 | -3.5 | -4.7 |
| 202.6 | 16.970 | -7.5 | -4.0 | -3.7 | -4.9 |
| 202.9 | 16.988 | -7.6 | -3.9 | -3.6 | -4.8 |
| 203.2 | 17.005 | -7.4 | -3.8 | -3.5 | -4.7 |
| 203.5 | 17.023 | -7.2 | -3.7 | -3.4 | -4.7 |
| 203.8 | 17.040 | -7.2 | -3.7 | -3.4 | -4.6 |
| 204.1 | 17.058 | -7.0 | -3.4 | -3.1 | -4.3 |
| 204.4 | 17.075 | -7.4 | -3.9 | -3.6 | -4.8 |
| 204.8 | 17.093 | -7.4 | -3.8 | -3.5 | -4.8 |
| 205.1 | 17.110 | -7.4 | -3.8 | -3.5 | -4.7 |
| 205.4 | 17.128 | -7.4 | -3.9 | -3.6 | -4.8 |
| 205.7 | 17.145 | -7.3 | -3.9 | -3.6 | -4.8 |
| 206.0 | 17.163 | -7.4 | -4.0 | -3.7 | -5.0 |
| 206.3 | 17.180 | -6.8 | -3.3 | -3.0 | -4.3 |
| 206.6 | 17.198 | -6.9 | -3.6 | -3.3 | -4.5 |
| 206.9 | 17.215 | -6.8 | -3.6 | -3.3 | -4.6 |
| 207.2 | 17.233 | -7.1 | -3.9 | -3.6 | -4.9 |
| 207.5 | 17.250 | -7.1 | -3.8 | -3.5 | -4.8 |
| 207.8 | 17.268 | -7.0 | -3.7 | -3.4 | -4.7 |
| 208.1 | 17.285 | -7.0 | -3.9 | -3.6 | -4.8 |
| 208.4 | 17.303 | -7.1 | -3.8 | -3.5 | -4.7 |
| 208.7 | 17.320 | -7.1 | -3.9 | -3.6 | -4.8 |
| 209.0 | 17.338 | -7.2 | -3.9 | -3.6 | -4.9 |
| 209.3 | 17.355 | -7.3 | -3.8 | -3.5 | -4.8 |
| 209.6 | 17.373 | -7.5 | -4.0 | -3.7 | -4.9 |
| 209.9 | 17.390 | -7.3 | -3.6 | -3.3 | -4.5 |
| 210.2 | 17.408 | -7.6 | -4.1 | -3.8 | -5.1 |
| 210.5 | 17.426 | -7.6 | -4.1 | -3.8 | -5.1 |
| 210.8 | 17.444 | -7.4 | -3.9 | -3.6 | -4.8 |
| 211.1 | 17.461 | -7.2 | -3.4 | -3.1 | -4.3 |
| 211.4 | 17.479 | -7.4 | -3.6 | -3.3 | -4.5 |
| 211.7 | 17.497 | -7.9 | -4.0 | -3.7 | -4.9 |
| 212.0 | 17.515 | -7.2 | -3.6 | -3.3 | -4.6 |
| 212.3 | 17.532 | -7.5 | -4.0 | -3.7 | -4.9 |
| 212.7 | 17.550 | -7.7 | -4.3 | -4.0 | -5.3 |
| 213.0 | 17.568 | -7.7 | -4.3 | -4.0 | -5.2 |
| 213.3 | 17.585 | -7.3 | -3.9 | -3.6 | -4.9 |
| 213.6 | 17.603 | -7.3 | -3.9 | -3.6 | -4.9 |
| 213.9 | 17.621 | -6.9 | -3.6 | -3.3 | -4.6 |
| 214.2 | 17.639 | -7.1 | -3.9 | -3.6 | -4.8 |

| Depth (mm) | Age (ka BP) | $\delta^{13}C$ (‰ VPDB) | $\delta^{18}O$ (‰ VPDB) | $\delta^{18}O$ (‰ VPDB) Calcite Corr. | $\delta^{18}O$ (‰ VPDB) Sea Level Corr. |
|---|---|---|---|---|---|
| 214.5 | 17.656 | -7.3 | -4.2 | -3.9 | -5.1 |
| 214.8 | 17.674 | -7.2 | -3.9 | -3.6 | -4.9 |
| 215.1 | 17.692 | -7.1 | -4.0 | -3.7 | -4.9 |
| 215.4 | 17.710 | -7.1 | -3.9 | -3.6 | -4.8 |
| 215.7 | 17.727 | -7.3 | -4.0 | -3.7 | -4.9 |
| 216.0 | 17.745 | -7.1 | -3.6 | -3.3 | -4.6 |
| 216.3 | 17.763 | -6.9 | -3.5 | -3.2 | -4.5 |
| 216.6 | 17.781 | -6.9 | -3.7 | -3.4 | -4.6 |
| 216.9 | 17.798 | -7.2 | -4.0 | -3.7 | -4.9 |
| 217.2 | 17.816 | -7.2 | -4.0 | -3.7 | -5.0 |
| 217.6 | 17.834 | -7.1 | -3.7 | -3.4 | -4.7 |
| 217.9 | 17.851 | -7.1 | -3.7 | -3.4 | -4.7 |
| 218.2 | 17.869 | -6.9 | -4.1 | -3.8 | -5.0 |
| 218.5 | 17.887 | -7.0 | -3.8 | -3.5 | -4.7 |
| 218.8 | 17.905 | -6.9 | -3.9 | -3.6 | -4.8 |
| 219.1 | 17.922 | -7.0 | -3.9 | -3.6 | -4.9 |
| 219.4 | 17.940 | -6.9 | -3.8 | -3.5 | -4.7 |
| 219.7 | 17.958 | -6.9 | -3.8 | -3.5 | -4.8 |
| 220.0 | 17.976 | -7.0 | -3.9 | -3.6 | -4.9 |
| 220.3 | 17.993 | -7.0 | -3.8 | -3.5 | -4.8 |
| 220.6 | 18.011 | -7.0 | -3.7 | -3.4 | -4.7 |
| 220.9 | 18.029 | -7.1 | -3.7 | -3.4 | -4.7 |
| 221.2 | 18.047 | -7.2 | -4.0 | -3.7 | -4.9 |
| 221.5 | 18.064 | -7.2 | -4.0 | -3.7 | -4.9 |
| 221.8 | 18.082 | -7.2 | -4.0 | -3.7 | -5.0 |
| 222.1 | 18.100 | -7.1 | -3.7 | -3.4 | -4.6 |
| 222.5 | 18.117 | -7.1 | -4.1 | -3.8 | -5.1 |
| 222.8 | 18.135 | -7.2 | -3.9 | -3.6 | -4.9 |
| 223.1 | 18.153 | -7.1 | -3.8 | -3.5 | -4.8 |
| 223.4 | 18.171 | -6.9 | -3.9 | -3.6 | -4.8 |
| 223.7 | 18.188 | -6.8 | -3.7 | -3.4 | -4.7 |
| 224.0 | 18.206 | -6.7 | -3.7 | -3.4 | -4.6 |
| 224.3 | 18.224 | -6.8 | -3.7 | -3.4 | -4.7 |
| 224.6 | 18.242 | -7.0 | -3.8 | -3.5 | -4.8 |
| 224.9 | 18.258 | -6.9 | -3.7 | -3.4 | -4.6 |
| 225.2 | 18.275 | -6.9 | -3.8 | -3.5 | -4.8 |
| 225.5 | 18.292 | -6.8 | -3.8 | -3.5 | -4.7 |
| 225.8 | 18.309 | -6.8 | -3.7 | -3.4 | -4.6 |
| 226.0 | 18.326 | -6.8 | -3.8 | -3.5 | -4.7 |
| 226.3 | 18.342 | -6.8 | -3.5 | -3.2 | -4.5 |
| 226.6 | 18.359 | -7.1 | -3.7 | -3.4 | -4.7 |
| 226.9 | 18.376 | -7.0 | -3.8 | -3.5 | -4.8 |
| 227.2 | 18.393 | -7.0 | -3.7 | -3.4 | -4.7 |

| Depth (mm) | Age (ka BP) | $\delta^{13}C$ (‰ VPDB) | $\delta^{18}O$ (‰ VPDB) | $\delta^{18}O$ (‰ VPDB) Calcite Corr. | $\delta^{18}O$ (‰ VPDB) Sea Level Corr. |
|---|---|---|---|---|---|
| 227.5 | 18.410 | -6.8 | -3.8 | -3.5 | -4.7 |
| 227.8 | 18.427 | -6.9 | -3.9 | -3.6 | -4.8 |
| 228.1 | 18.443 | -6.9 | -3.8 | -3.5 | -4.8 |
| 228.4 | 18.460 | -6.8 | -3.9 | -3.6 | -4.8 |
| 228.7 | 18.477 | -6.9 | -3.9 | -3.6 | -4.9 |
| 229.0 | 18.494 | -6.8 | -3.9 | -3.6 | -4.8 |
| 229.2 | 18.511 | -6.8 | -3.6 | -3.3 | -4.6 |
| 229.5 | 18.527 | -6.9 | -3.8 | -3.5 | -4.7 |
| 229.8 | 18.544 | -6.8 | -3.8 | -3.5 | -4.8 |
| 230.1 | 18.561 | -6.8 | -3.8 | -3.5 | -4.7 |
| 230.4 | 18.578 | -6.8 | -3.9 | -3.6 | -4.9 |
| 230.7 | 18.595 | -6.8 | -3.9 | -3.6 | -4.8 |
| 231.0 | 18.612 | -6.8 | -3.8 | -3.5 | -4.8 |
| 231.3 | 18.628 | -6.8 | -3.9 | -3.6 | -4.9 |
| 231.6 | 18.645 | -6.9 | -3.8 | -3.5 | -4.8 |
| 231.9 | 18.662 | -6.7 | -3.8 | -3.5 | -4.7 |
| 232.1 | 18.679 | -6.8 | -3.8 | -3.5 | -4.8 |
| 232.4 | 18.696 | -6.9 | -3.8 | -3.5 | -4.8 |
| 232.7 | 18.712 | -6.8 | -3.9 | -3.6 | -4.9 |
| 233.0 | 18.729 | -7.0 | -3.7 | -3.4 | -4.7 |
| 233.3 | 18.746 | -7.0 | -4.0 | -3.7 | -5.0 |
| 233.6 | 18.763 | -6.9 | -3.8 | -3.5 | -4.8 |
| 233.9 | 18.780 | -6.9 | -3.9 | -3.6 | -4.8 |
| 234.2 | 18.797 | -7.0 | -3.8 | -3.5 | -4.8 |
| 234.5 | 18.813 | -6.9 | -4.0 | -3.7 | -5.0 |
| 234.8 | 18.830 | -7.1 | -4.1 | -3.8 | -5.0 |
| 235.1 | 18.847 | -7.1 | -4.2 | -3.9 | -5.1 |
| 235.3 | 18.864 | -6.9 | -4.0 | -3.7 | -4.9 |
| 235.6 | 18.881 | -6.6 | -3.8 | -3.5 | -4.8 |
| 235.9 | 18.897 | -6.8 | -3.6 | -3.3 | -4.6 |
| 236.2 | 18.914 | -6.9 | -4.0 | -3.7 | -4.9 |
| 236.5 | 18.931 | -6.8 | -3.7 | -3.4 | -4.6 |
| 236.8 | 18.948 | -7.0 | -3.9 | -3.6 | -4.9 |
| 237.1 | 18.965 | -7.0 | -3.8 | -3.5 | -4.8 |
| 237.4 | 18.982 | -7.5 | -3.9 | -3.6 | -4.9 |
| 237.7 | 18.998 | -7.0 | -3.8 | -3.5 | -4.7 |
| 238.0 | 19.015 | -7.2 | -3.7 | -3.4 | -4.7 |
| 238.2 | 19.032 | -7.1 | -3.7 | -3.4 | -4.6 |
| 238.5 | 19.049 | -7.0 | -3.9 | -3.6 | -4.8 |
| 238.8 | 19.066 | -7.0 | -3.9 | -3.6 | -4.9 |
| 239.1 | 19.082 | -7.0 | -3.9 | -3.6 | -4.9 |
| 239.4 | 19.099 | -7.1 | -4.2 | -3.9 | -5.2 |
| 239.7 | 19.116 | -7.4 | -4.2 | -3.9 | -5.2 |

| Depth (mm) | Age (ka BP) | $\delta^{13}C$ (‰ VPDB) | $\delta^{18}O$ (‰ VPDB) | $\delta^{18}O$ (‰ VPDB) Calcite Corr. | $\delta^{18}O$ (‰ VPDB) Sea Level Corr. |
|---|---|---|---|---|---|
| 240.0 | 19.133 | -7.2 | -3.8 | -3.5 | -4.8 |
| 240.3 | 19.150 | -7.0 | -4.0 | -3.7 | -4.9 |
| 240.6 | 19.167 | -6.7 | -3.7 | -3.4 | -4.6 |
| 240.9 | 19.183 | -6.7 | -3.7 | -3.4 | -4.7 |
| 241.2 | 19.200 | -7.1 | -4.2 | -3.9 | -5.2 |
| 241.4 | 19.217 | -7.1 | -4.1 | -3.8 | -5.1 |
| 241.7 | 19.234 | -7.1 | -4.0 | -3.7 | -4.9 |
| 242.0 | 19.251 | -6.9 | -3.8 | -3.5 | -4.8 |
| 242.3 | 19.267 | -6.8 | -4.0 | -3.7 | -4.9 |
| 242.6 | 19.284 | -6.7 | -3.6 | -3.3 | -4.5 |
| 242.9 | 19.301 | -6.8 | -3.9 | -3.6 | -4.9 |
| 243.2 | 19.318 | -7.0 | -4.0 | -3.7 | -5.0 |
| 243.5 | 19.335 | -7.0 | -4.0 | -3.7 | -5.0 |
| 243.8 | 19.351 | -7.0 | -3.9 | -3.6 | -4.9 |
| 244.1 | 19.368 | -7.1 | -3.9 | -3.6 | -4.9 |
| 244.3 | 19.385 | -7.1 | -4.0 | -3.7 | -5.0 |
| 244.6 | 19.402 | -7.1 | -4.0 | -3.7 | -5.0 |
| 244.9 | 19.419 | -7.2 | -3.8 | -3.5 | -4.8 |
| 245.2 | 19.436 | -7.0 | -3.7 | -3.4 | -4.7 |
| 245.5 | 19.452 | -7.0 | -3.9 | -3.6 | -4.9 |
| 245.8 | 19.474 | -6.9 | -3.7 | -3.4 | -4.7 |
| 246.1 | 19.499 | -7.1 | -4.0 | -3.7 | -5.0 |
| 246.4 | 19.518 | -6.9 | -3.8 | -3.5 | -4.7 |
| 246.7 | 19.538 | -7.1 | -4.0 | -3.7 | -5.0 |
| 247.0 | 19.557 | -7.1 | -3.8 | -3.5 | -4.8 |
| 247.3 | 19.577 | -7.2 | -3.7 | -3.4 | -4.7 |
| 247.6 | 19.596 | -7.0 | -3.7 | -3.4 | -4.6 |
| 247.9 | 19.616 | -7.2 | -4.0 | -3.7 | -4.9 |
| 248.2 | 19.635 | -6.7 | -3.4 | -3.1 | -4.4 |
| 248.5 | 19.655 | -6.9 | -3.7 | -3.4 | -4.6 |
| 248.7 | 19.674 | -6.8 | -3.6 | -3.3 | -4.6 |
| 249.0 | 19.694 | -6.7 | -3.3 | -3.0 | -4.3 |
| 249.3 | 19.713 | -6.8 | -3.5 | -3.2 | -4.5 |
| 249.6 | 19.733 | -6.9 | -3.6 | -3.3 | -4.6 |
| 249.9 | 19.752 | -6.9 | -3.8 | -3.5 | -4.8 |
| 250.2 | 19.772 | -6.7 | -3.4 | -3.1 | -4.4 |
| 250.5 | 19.791 | -6.9 | -3.7 | -3.4 | -4.7 |
| 250.8 | 19.811 | -6.9 | -3.8 | -3.5 | -4.8 |
| 251.1 | 19.830 | -6.9 | -3.9 | -3.6 | -4.8 |
| 251.4 | 19.850 | -6.7 | -3.8 | -3.5 | -4.8 |
| 251.7 | 19.869 | -6.8 | -3.7 | -3.4 | -4.7 |
| 252.0 | 19.889 | -6.8 | -3.5 | -3.2 | -4.5 |
| 252.3 | 19.908 | -6.8 | -3.6 | -3.3 | -4.5 |

| Depth (mm) | Age (ka BP) | $\delta^{13}C$ (‰ VPDB) | $\delta^{18}O$ (‰ VPDB) | $\delta^{18}O$ (‰ VPDB) Calcite Corr. | $\delta^{18}O$ (‰ VPDB) Sea Level Corr. |
|---|---|---|---|---|---|
| 252.6 | 19.928 | -6.8 | -3.3 | -3.0 | -4.3 |
| 252.9 | 19.947 | -6.9 | -3.8 | -3.5 | -4.8 |
| 253.2 | 19.967 | -6.8 | -3.6 | -3.3 | -4.6 |
| 253.5 | 19.986 | -6.9 | -3.4 | -3.1 | -4.4 |
| 253.8 | 20.006 | -6.9 | -3.9 | -3.6 | -4.9 |
| 254.1 | 20.025 | -6.8 | -3.8 | -3.5 | -4.8 |
| 254.3 | 20.045 | -6.8 | -3.8 | -3.5 | -4.7 |
| 254.6 | 20.064 | -6.8 | -3.5 | -3.2 | -4.5 |
| 254.9 | 20.084 | -7.0 | -3.7 | -3.4 | -4.7 |
| 255.2 | 20.103 | -6.8 | -3.3 | -3.0 | -4.3 |
| 255.5 | 20.123 | -6.7 | -3.3 | -3.0 | -4.3 |
| 255.8 | 20.142 | -6.8 | -3.4 | -3.1 | -4.4 |
| 256.1 | 20.162 | -6.8 | -3.6 | -3.3 | -4.6 |
| 256.4 | 20.181 | -6.8 | -3.6 | -3.3 | -4.6 |
| 256.7 | 20.201 | -6.8 | -3.3 | -3.0 | -4.3 |
| 257.0 | 20.221 | -7.1 | -3.4 | -3.1 | -4.4 |
| 257.3 | 20.240 | -6.8 | -3.5 | -3.2 | -4.5 |
| 257.6 | 20.260 | -6.9 | -3.6 | -3.3 | -4.5 |
| 257.9 | 20.279 | -6.9 | -3.8 | -3.5 | -4.8 |
| 258.2 | 20.299 | -6.6 | -3.5 | -3.2 | -4.5 |
| 258.5 | 20.318 | -6.7 | -3.8 | -3.5 | -4.8 |
| 258.8 | 20.338 | -6.8 | -3.9 | -3.6 | -4.9 |
| 259.1 | 20.358 | -6.9 | -3.7 | -3.4 | -4.7 |
| 259.4 | 20.377 | -6.8 | -3.7 | -3.4 | -4.7 |
| 259.7 | 20.397 | -6.7 | -3.6 | -3.3 | -4.6 |
| 260.0 | 20.417 | -6.9 | -4.0 | -3.7 | -5.0 |
| 260.3 | 20.437 | -6.8 | -4.0 | -3.7 | -5.0 |
| 260.6 | 20.456 | -9.6 | -3.6 | -3.3 | -4.6 |
| 260.9 | 20.476 | -6.8 | -3.5 | -3.2 | -4.5 |
| 261.2 | 20.496 | -6.9 | -3.7 | -3.4 | -4.7 |
| 261.5 | 20.515 | -6.7 | -3.7 | -3.4 | -4.7 |
| 261.8 | 20.535 | -7.0 | -3.6 | -3.3 | -4.6 |
| 262.1 | 20.555 | -7.9 | -2.9 | -2.6 | -3.9 |
| 262.3 | 20.575 | -9.0 | -3.1 | -2.8 | -4.1 |
| 262.6 | 20.594 | -9.4 | -3.5 | -3.2 | -4.5 |
| 262.9 | 20.614 | -8.7 | -3.6 | -3.3 | -4.6 |
| 263.2 | 20.634 | -8.2 | -3.4 | -3.1 | -4.4 |
| 263.5 | 20.654 | -7.7 | -3.8 | -3.5 | -4.8 |
| 263.8 | 20.673 | -7.4 | -3.6 | -3.3 | -4.6 |
| 264.1 | 20.693 | -7.5 | -3.9 | -3.6 | -4.9 |
| 264.4 | 20.713 | -7.3 | -3.8 | -3.5 | -4.8 |
| 264.7 | 20.733 | -7.4 | -3.9 | -3.6 | -4.9 |
| 265.0 | 20.752 | -7.7 | -3.8 | -3.5 | -4.8 |

| Depth (mm) | Age (ka BP) | $\delta^{13}C$ (‰ VPDB) | $\delta^{18}O$ (‰ VPDB) | $\delta^{18}O$ (‰ VPDB) Calcite Corr. | $\delta^{18}O$ (‰ VPDB) Sea Level Corr. |
|---|---|---|---|---|---|
| 265.3 | 20.772 | -7.5 | -3.6 | -3.3 | -4.6 |
| 265.6 | 20.792 | -7.5 | -3.7 | -3.4 | -4.7 |
| 265.9 | 20.812 | -7.5 | -3.7 | -3.4 | -4.7 |
| 266.2 | 20.831 | -7.2 | -3.7 | -3.4 | -4.7 |
| 266.5 | 20.851 | -7.4 | -4.0 | -3.7 | -5.0 |
| 266.8 | 20.871 | -7.4 | -4.0 | -3.7 | -5.0 |
| 267.1 | 20.891 | -7.4 | -4.1 | -3.8 | -5.1 |
| 267.4 | 20.910 | -7.5 | -3.9 | -3.6 | -4.9 |
| 267.7 | 20.930 | -7.3 | -3.8 | -3.5 | -4.8 |
| 268.0 | 20.950 | -7.4 | -4.1 | -3.8 | -5.1 |
| 268.3 | 20.970 | -7.1 | -3.6 | -3.3 | -4.6 |
| 268.6 | 20.989 | -7.2 | -3.8 | -3.5 | -4.8 |
| 268.9 | 21.009 | -7.1 | -3.8 | -3.5 | -4.8 |
| 269.2 | 21.029 | -7.1 | -3.8 | -3.5 | -4.8 |
| 269.5 | 21.049 | -7.1 | -3.8 | -3.5 | -4.8 |
| 269.8 | 21.068 | -7.1 | -3.6 | -3.3 | -4.6 |
| 270.1 | 21.088 | -7.1 | -3.6 | -3.3 | -4.6 |
| 270.4 | 21.108 | -7.3 | -3.9 | -3.6 | -4.9 |
| 270.7 | 21.128 | -7.3 | -3.8 | -3.5 | -4.8 |
| 271.0 | 21.147 | -7.6 | -3.9 | -3.6 | -4.9 |
| 271.3 | 21.167 | -7.7 | -3.6 | -3.3 | -4.7 |
| 271.6 | 21.187 | -7.7 | -3.6 | -3.3 | -4.6 |
| 271.9 | 21.207 | -7.5 | -3.7 | -3.4 | -4.7 |
| 272.2 | 21.226 | -7.4 | -3.6 | -3.3 | -4.6 |
| 272.5 | 21.246 | -7.3 | -3.7 | -3.4 | -4.7 |
| 272.8 | 21.266 | -7.4 | -3.7 | -3.4 | -4.7 |
| 273.1 | 21.285 | -7.3 | -3.7 | -3.4 | -4.7 |
| 273.4 | 21.305 | -7.3 | -3.8 | -3.5 | -4.8 |
| 273.7 | 21.325 | -7.2 | -3.6 | -3.3 | -4.6 |
| 274.0 | 21.345 | -7.2 | -3.9 | -3.6 | -4.9 |
| 274.3 | 21.364 | -6.9 | -3.7 | -3.4 | -4.7 |
| 274.6 | 21.384 | -7.1 | -3.7 | -3.4 | -4.7 |
| 274.9 | 21.404 | -7.3 | -3.6 | -3.3 | -4.6 |
| 275.2 | 21.424 | -6.8 | -3.5 | -3.2 | -4.6 |
| 275.5 | 21.443 | -6.7 | -3.5 | -3.2 | -4.5 |
| 275.8 | 21.463 | -6.4 | -3.4 | -3.1 | -4.4 |
| 276.1 | 21.483 | -6.6 | -3.4 | -3.1 | -4.4 |
| 276.4 | 21.503 | -6.6 | -3.9 | -3.6 | -4.9 |
| 276.7 | 21.522 | -6.2 | -3.4 | -3.1 | -4.4 |
| 277.0 | 21.542 | -6.6 | -3.5 | -3.2 | -4.5 |
| 277.3 | 21.562 | -6.1 | -3.3 | -3.0 | -4.3 |
| 277.6 | 21.582 | -6.3 | -3.5 | -3.2 | -4.5 |
| 277.9 | 21.601 | -6.3 | -3.6 | -3.3 | -4.6 |

| Depth (mm) | Age (ka BP) | $\delta^{13}C$ (‰ VPDB) | $\delta^{18}O$ (‰ VPDB) | $\delta^{18}O$ (‰ VPDB) Calcite Corr. | $\delta^{18}O$ (‰ VPDB) Sea Level Corr. |
|---|---|---|---|---|---|
| 278.2 | 21.621 | -6.6 | -3.7 | -3.4 | -4.7 |
| 278.5 | 21.641 | -6.9 | -3.6 | -3.3 | -4.6 |
| 278.8 | 21.661 | -6.9 | -3.7 | -3.4 | -4.7 |
| 279.1 | 21.680 | -6.9 | -3.8 | -3.5 | -4.8 |
| 279.3 | 21.700 | -6.8 | -3.6 | -3.3 | -4.6 |
| 279.6 | 21.720 | -6.6 | -3.3 | -3.0 | -4.3 |
| 279.9 | 21.740 | -6.8 | -3.7 | -3.4 | -4.7 |
| 280.2 | 21.759 | -6.8 | -3.7 | -3.4 | -4.7 |
| 280.5 | 21.779 | -6.8 | -3.7 | -3.4 | -4.7 |
| 280.8 | 21.799 | -6.5 | -3.5 | -3.2 | -4.5 |
| 281.1 | 21.819 | -6.5 | -3.4 | -3.1 | -4.4 |
| 281.4 | 21.838 | -6.6 | -3.4 | -3.1 | -4.4 |
| 281.7 | 21.858 | -6.8 | -3.5 | -3.2 | -4.5 |
| 282.0 | 21.878 | -7.1 | -3.1 | -2.8 | -4.1 |
| 282.3 | 21.898 | -7.2 | -2.8 | -2.5 | -3.8 |
| 282.6 | 21.917 | -7.0 | -2.8 | -2.5 | -3.8 |
| 282.9 | 21.937 | -7.0 | -2.6 | -2.3 | -3.6 |
| 283.2 | 21.957 | -7.2 | -3.0 | -2.7 | -4.0 |
| 283.5 | 21.977 | -7.2 | -2.7 | -2.4 | -3.7 |
| 283.8 | 21.996 | -6.9 | -3.1 | -2.8 | -4.1 |
| 284.1 | 22.016 | -7.0 | -3.5 | -3.2 | -4.5 |
| 284.4 | 22.036 | -7.1 | -3.7 | -3.4 | -4.7 |
| 284.7 | 22.055 | -7.2 | -3.6 | -3.3 | -4.7 |
| 285.0 | 22.075 | -7.2 | -3.3 | -3.0 | -4.3 |
| 285.3 | 22.089 | -7.4 | -3.5 | -3.2 | -4.5 |
| 285.6 | 22.097 | -7.6 | -3.6 | -3.3 | -4.6 |
| 285.9 | 22.105 | -7.4 | -3.6 | -3.3 | -4.6 |
| 286.2 | 22.112 | -7.4 | -3.5 | -3.2 | -4.5 |
| 286.5 | 22.120 | -7.5 | -3.5 | -3.2 | -4.5 |
| 286.8 | 22.128 | -7.5 | -3.4 | -3.1 | -4.5 |
| 287.1 | 22.136 | -7.4 | -3.1 | -2.8 | -4.1 |
| 287.4 | 22.143 | -7.3 | -2.8 | -2.5 | -3.9 |
| 287.7 | 22.151 | -7.2 | -3.0 | -2.7 | -4.0 |
| 288.0 | 22.159 | -7.1 | -2.8 | -2.5 | -3.8 |
| 288.3 | 22.167 | -6.8 | -2.8 | -2.5 | -3.8 |
| 288.6 | 22.174 | -6.7 | -2.6 | -2.3 | -3.6 |
| 288.9 | 22.182 | -6.6 | -2.5 | -2.2 | -3.5 |
| 289.2 | 22.190 | -6.5 | -2.4 | -2.1 | -3.4 |
| 289.5 | 22.198 | -6.6 | -2.5 | -2.2 | -3.5 |
| 289.8 | 22.206 | -6.7 | -3.4 | -3.1 | -4.4 |
| 290.1 | 22.213 | -6.8 | -3.5 | -3.2 | -4.6 |
| 290.4 | 22.221 | -6.8 | -3.7 | -3.4 | -4.7 |
| 290.7 | 22.229 | -6.8 | -3.6 | -3.3 | -4.6 |

| Depth (mm) | Age (ka BP) | $\delta^{13}C$ (‰ VPDB) | $\delta^{18}O$ (‰ VPDB) | $\delta^{18}O$ (‰ VPDB) Calcite Corr. | $\delta^{18}O$ (‰ VPDB) Sea Level Corr. |
|---|---|---|---|---|---|
| 291.0 | 22.237 | -6.7 | -3.7 | -3.4 | -4.7 |
| 291.3 | 22.244 | -6.8 | -3.6 | -3.3 | -4.6 |
| 291.6 | 22.252 | -6.8 | -4.0 | -3.7 | -5.0 |
| 291.9 | 22.260 | -6.8 | -3.9 | -3.6 | -4.9 |
| 292.2 | 22.268 | -6.8 | -3.6 | -3.3 | -4.6 |
| 292.5 | 22.276 | -6.9 | -3.6 | -3.3 | -4.6 |
| 292.8 | 22.283 | -7.0 | -3.8 | -3.5 | -4.8 |
| 293.1 | 22.291 | -7.1 | -3.8 | -3.5 | -4.8 |
| 293.4 | 22.299 | -7.2 | -4.1 | -3.8 | -5.1 |
| 293.7 | 22.307 | -7.1 | -3.8 | -3.5 | -4.8 |
| 294.0 | 22.314 | -7.3 | -3.8 | -3.5 | -4.8 |
| 294.3 | 22.322 | -7.2 | -3.6 | -3.3 | -4.6 |
| 294.6 | 22.330 | -7.2 | -3.6 | -3.3 | -4.6 |
| 294.9 | 22.338 | -7.3 | -3.8 | -3.5 | -4.8 |
| 295.2 | 22.345 | -7.2 | -3.6 | -3.3 | -4.6 |
| 295.5 | 22.353 | -7.4 | -3.6 | -3.3 | -4.6 |
| 295.8 | 22.361 | -7.5 | -3.9 | -3.6 | -4.9 |
| 296.1 | 22.369 | -7.4 | -3.6 | -3.3 | -4.6 |
| 296.4 | 22.377 | -7.4 | -3.7 | -3.4 | -4.7 |
| 296.7 | 22.384 | -7.4 | -3.7 | -3.4 | -4.7 |
| 297.0 | 22.392 | -7.4 | -3.4 | -3.1 | -4.4 |
| 297.3 | 22.400 | -7.2 | -3.7 | -3.4 | -4.7 |
| 297.6 | 22.408 | -7.4 | -3.7 | -3.4 | -4.7 |
| 297.9 | 22.415 | -7.5 | -3.8 | -3.5 | -4.8 |
| 298.2 | 22.423 | -7.3 | -3.5 | -3.2 | -4.5 |
| 298.5 | 22.431 | -7.4 | -3.4 | -3.1 | -4.4 |
| 298.8 | 22.439 | -7.5 | -3.7 | -3.4 | -4.7 |
| 299.0 | 22.446 | -7.4 | -3.4 | -3.1 | -4.4 |
| 299.3 | 22.454 | -7.4 | -3.6 | -3.3 | -4.6 |
| 299.6 | 22.462 | -7.3 | -3.6 | -3.3 | -4.6 |
| 299.9 | 22.470 | -7.2 | -3.7 | -3.4 | -4.7 |
| 300.2 | 22.478 | -7.3 | -3.4 | -3.1 | -4.4 |
| 300.5 | 22.485 | -7.3 | -3.6 | -3.3 | -4.6 |
| 300.8 | 22.493 | -7.4 | -3.6 | -3.3 | -4.6 |
| 301.1 | 22.501 | -7.4 | -3.6 | -3.3 | -4.6 |
| 301.4 | 22.509 | -7.8 | -3.7 | -3.4 | -4.7 |
| 301.7 | 22.516 | -7.5 | -3.6 | -3.3 | -4.6 |
| 302.0 | 22.524 | -7.8 | -3.7 | -3.4 | -4.7 |
| 302.3 | 22.532 | -7.3 | -3.3 | -3.0 | -4.3 |
| 302.6 | 22.540 | -7.2 | -3.6 | -3.3 | -4.7 |
| 302.9 | 22.548 | -7.2 | -3.5 | -3.2 | -4.5 |
| 303.2 | 22.555 | -7.1 | -3.4 | -3.1 | -4.4 |
| 303.5 | 22.563 | -7.3 | -3.6 | -3.3 | -4.6 |

| Depth (mm) | Age (ka BP) | $\delta^{13}C$ (‰ VPDB) | $\delta^{18}O$ (‰ VPDB) | $\delta^{18}O$ (‰ VPDB) Calcite Corr. | $\delta^{18}O$ (‰ VPDB) Sea Level Corr. |
|---|---|---|---|---|---|
| 303.8 | 22.571 | -7.3 | -3.8 | -3.5 | -4.8 |
| 304.1 | 22.579 | -7.2 | -3.8 | -3.5 | -4.8 |
| 304.4 | 22.586 | -7.1 | -3.5 | -3.2 | -4.6 |
| 304.7 | 22.594 | -7.2 | -3.6 | -3.3 | -4.6 |
| 305.0 | 22.602 | -7.2 | -3.8 | -3.5 | -4.8 |
| 305.3 | 22.610 | -7.3 | -3.9 | -3.6 | -4.9 |
| 305.6 | 22.617 | -7.3 | -3.9 | -3.6 | -4.9 |
| 305.9 | 22.625 | -7.4 | -3.9 | -3.6 | -4.9 |
| 306.2 | 22.633 | -7.3 | -3.8 | -3.5 | -4.8 |
| 306.5 | 22.641 | -7.3 | -3.8 | -3.5 | -4.8 |
| 306.8 | 22.649 | -7.5 | -3.7 | -3.4 | -4.7 |
| 307.1 | 22.656 | -7.4 | -3.7 | -3.4 | -4.7 |
| 307.4 | 22.664 | -7.4 | -3.6 | -3.3 | -4.6 |
| 307.7 | 22.672 | -7.5 | -3.5 | -3.2 | -4.5 |
| 308.0 | 22.680 | -7.8 | -3.7 | -3.4 | -4.7 |
| 308.3 | 22.687 | -8.3 | -3.3 | -3.0 | -4.3 |
| 308.6 | 22.695 | -8.9 | -3.5 | -3.2 | -4.5 |
| 308.9 | 22.703 | -8.6 | -3.1 | -2.8 | -4.1 |
| 309.2 | 22.711 | -8.7 | -3.1 | -2.8 | -4.1 |
| 309.5 | 22.718 | -8.6 | -3.5 | -3.2 | -4.5 |
| 309.8 | 22.726 | -8.5 | -3.4 | -3.1 | -4.4 |
| 310.1 | 22.734 | -7.7 | -3.5 | -3.2 | -4.5 |
| 310.4 | 22.742 | -7.3 | -3.4 | -3.1 | -4.4 |
| 310.7 | 22.750 | -7.9 | -3.5 | -3.2 | -4.5 |
| 311.0 | 22.757 | -7.9 | -3.5 | -3.2 | -4.5 |
| 311.3 | 22.765 | -7.7 | -3.6 | -3.3 | -4.6 |
| 311.6 | 22.773 | -7.7 | -3.5 | -3.2 | -4.5 |
| 311.9 | 22.781 | -7.3 | -4.1 | -3.8 | -5.1 |
| 312.2 | 22.788 | -7.1 | -4.0 | -3.7 | -5.0 |
| 312.5 | 22.796 | -7.1 | -3.8 | -3.5 | -4.8 |
| 312.8 | 22.804 | -7.3 | -3.6 | -3.3 | -4.6 |
| 313.1 | 22.812 | -7.3 | -3.7 | -3.4 | -4.7 |
| 313.4 | 22.820 | -7.2 | -3.7 | -3.4 | -4.7 |
| 313.7 | 22.827 | -7.2 | -3.6 | -3.3 | -4.6 |
| 314.0 | 22.835 | -7.2 | -3.7 | -3.4 | -4.7 |
| 314.3 | 22.843 | -7.2 | -3.7 | -3.4 | -4.7 |
| 314.6 | 22.851 | -7.1 | -3.8 | -3.5 | -4.8 |
| 314.9 | 22.859 | -7.1 | -3.8 | -3.5 | -4.8 |
| 315.2 | 22.867 | -7.1 | -3.8 | -3.5 | -4.8 |
| 315.5 | 22.874 | -7.0 | -3.8 | -3.5 | -4.8 |
| 315.8 | 22.882 | -7.1 | -3.7 | -3.4 | -4.7 |
| 316.1 | 22.890 | -7.0 | -3.8 | -3.5 | -4.8 |
| 316.4 | 22.898 | -7.1 | -3.8 | -3.5 | -4.8 |

| Depth (mm) | Age (ka BP) | $\delta^{13}C$ (‰ VPDB) | $\delta^{18}O$ (‰ VPDB) | $\delta^{18}O$ (‰ VPDB) Calcite Corr. | $\delta^{18}O$ (‰ VPDB) Sea Level Corr. |
|---|---|---|---|---|---|
| 316.7 | 22.906 | -7.0 | -3.8 | -3.5 | -4.8 |
| 317.0 | 22.914 | -6.9 | -3.9 | -3.6 | -4.9 |
| 317.3 | 22.922 | -6.9 | -4.1 | -3.8 | -5.1 |
| 317.6 | 22.930 | -6.9 | -4.0 | -3.7 | -5.1 |
| 317.9 | 22.939 | -6.7 | -4.1 | -3.8 | -5.1 |
| 318.2 | 22.947 | -6.6 | -3.8 | -3.5 | -4.8 |
| 318.5 | 22.955 | -6.7 | -3.9 | -3.6 | -4.9 |
| 318.7 | 22.963 | -6.9 | -3.9 | -3.6 | -4.9 |
| 319.0 | 22.972 | -7.1 | -3.8 | -3.5 | -4.8 |
| 319.3 | 22.980 | -7.1 | -4.0 | -3.7 | -5.0 |
| 319.6 | 22.988 | -7.0 | -4.0 | -3.7 | -5.0 |
| 319.9 | 22.996 | -7.0 | -4.1 | -3.8 | -5.1 |
| 320.2 | 23.005 | -7.0 | -4.0 | -3.7 | -5.0 |
| 320.5 | 23.013 | -7.0 | -4.0 | -3.7 | -5.0 |
| 320.7 | 23.021 | -6.9 | -4.0 | -3.7 | -5.0 |
| 321.0 | 23.030 | -6.8 | -4.0 | -3.7 | -5.0 |
| 321.3 | 23.038 | -7.0 | -4.1 | -3.8 | -5.1 |
| 321.6 | 23.046 | -7.1 | -4.0 | -3.7 | -5.0 |
| 321.9 | 23.054 | -7.0 | -4.3 | -4.0 | -5.3 |
| 322.2 | 23.063 | -7.1 | -4.1 | -3.8 | -5.1 |
| 322.5 | 23.071 | -7.1 | -4.0 | -3.7 | -5.0 |
| 322.7 | 23.079 | -7.1 | -3.8 | -3.5 | -4.8 |
| 323.0 | 23.087 | -6.9 | -3.7 | -3.4 | -4.7 |
| 323.3 | 23.096 | -6.8 | -3.6 | -3.3 | -4.6 |
| 323.6 | 23.104 | -6.7 | -3.6 | -3.3 | -4.6 |
| 323.9 | 23.112 | -6.9 | -3.9 | -3.6 | -4.9 |
| 324.2 | 23.121 | -6.8 | -3.9 | -3.6 | -4.9 |
| 324.5 | 23.129 | -6.9 | -3.9 | -3.6 | -4.9 |
| 324.8 | 23.137 | -7.4 | -3.9 | -3.6 | -5.0 |
| 325.1 | 23.146 | -7.2 | -4.1 | -3.8 | -5.1 |
| 325.4 | 23.155 | -7.0 | -3.9 | -3.6 | -4.9 |
| 325.6 | 23.163 | -7.2 | -3.8 | -3.5 | -4.8 |
| 325.9 | 23.172 | -7.1 | -3.7 | -3.4 | -4.7 |
| 326.2 | 23.181 | -7.4 | -4.1 | -3.8 | -5.1 |
| 326.5 | 23.189 | -6.9 | -3.9 | -3.6 | -4.9 |
| 326.8 | 23.198 | -6.8 | -4.0 | -3.7 | -5.0 |
| 327.1 | 23.207 | -7.0 | -4.2 | -3.9 | -5.2 |
| 327.4 | 23.216 | -7.0 | -4.5 | -4.2 | -5.6 |
| 327.7 | 23.224 | -7.0 | -4.0 | -3.7 | -5.0 |
| 328.0 | 23.233 | -7.0 | -4.1 | -3.8 | -5.1 |
| 328.3 | 23.242 | -6.8 | -3.8 | -3.5 | -4.9 |
| 328.6 | 23.250 | -6.8 | -3.8 | -3.5 | -4.8 |
| 328.9 | 23.259 | -7.0 | -3.7 | -3.4 | -4.7 |

| Depth (mm) | Age (ka BP) | $\delta^{13}C$ (‰ VPDB) | $\delta^{18}O$ (‰ VPDB) | $\delta^{18}O$ (‰ VPDB) Calcite Corr. | $\delta^{18}O$ (‰ VPDB) Sea Level Corr. |
|---|---|---|---|---|---|
| 329.2 | 23.268 | -7.0 | -3.9 | -3.6 | -4.9 |
| 329.5 | 23.276 | -7.3 | -3.6 | -3.3 | -4.7 |
| 329.8 | 23.285 | -7.1 | -3.8 | -3.5 | -4.8 |
| 330.1 | 23.294 | -7.2 | -3.7 | -3.4 | -4.7 |
| 330.4 | 23.302 | -7.1 | -3.7 | -3.4 | -4.7 |
| 330.7 | 23.311 | -7.1 | -3.7 | -3.4 | -4.7 |
| 331.0 | 23.320 | -7.1 | -3.7 | -3.4 | -4.7 |
| 331.3 | 23.328 | -7.0 | -3.8 | -3.5 | -4.8 |
| 331.6 | 23.337 | -7.1 | -3.7 | -3.4 | -4.8 |
| 331.9 | 23.346 | -7.0 | -3.8 | -3.5 | -4.8 |
| 332.2 | 23.355 | -7.2 | -3.6 | -3.3 | -4.7 |
| 332.5 | 23.363 | -7.1 | -3.8 | -3.5 | -4.8 |
| 332.8 | 23.372 | -7.2 | -3.9 | -3.6 | -4.9 |
| 333.1 | 23.381 | -7.1 | -3.9 | -3.6 | -4.9 |
| 333.4 | 23.389 | -7.1 | -4.0 | -3.7 | -5.0 |
| 333.7 | 23.398 | -7.0 | -3.9 | -3.6 | -4.9 |
| 334.0 | 23.407 | -7.0 | -3.6 | -3.3 | -4.6 |
| 334.3 | 23.415 | -7.0 | -3.7 | -3.4 | -4.7 |
| 334.6 | 23.424 | -7.0 | -3.9 | -3.6 | -4.9 |
| 334.9 | 23.433 | -7.3 | -3.9 | -3.6 | -4.9 |
| 335.2 | 23.441 | -7.1 | -3.9 | -3.6 | -4.9 |
| 335.5 | 23.450 | -7.3 | -3.9 | -3.6 | -4.9 |
| 335.8 | 23.459 | -7.3 | -3.9 | -3.6 | -4.9 |
| 336.1 | 23.467 | -7.0 | -3.7 | -3.4 | -4.7 |
| 336.4 | 23.476 | -7.4 | -3.4 | -3.1 | -4.4 |
| 336.7 | 23.485 | -7.3 | -3.4 | -3.1 | -4.5 |
| 337.0 | 23.493 | -6.4 | -3.3 | -3.0 | -4.4 |
| 337.3 | 23.502 | -6.4 | -3.7 | -3.4 | -4.7 |
| 337.6 | 23.511 | -6.3 | -3.5 | -3.2 | -4.5 |
| 337.9 | 23.519 | -6.3 | -3.6 | -3.3 | -4.6 |
| 338.2 | 23.528 | -6.2 | -3.4 | -3.1 | -4.5 |
| 338.5 | 23.536 | -6.4 | -3.5 | -3.2 | -4.5 |
| 338.8 | 23.545 | -7.0 | -3.4 | -3.1 | -4.4 |
| 339.1 | 23.554 | -8.0 | -3.0 | -2.7 | -4.0 |
| 339.4 | 23.562 | -8.4 | -3.2 | -2.9 | -4.2 |
| 339.7 | 23.571 | -7.6 | -3.3 | -3.0 | -4.3 |
| 340.0 | 23.579 | -7.8 | -3.4 | -3.1 | -4.4 |
| 340.3 | 23.588 | -7.5 | -3.3 | -3.0 | -4.3 |
| 340.6 | 23.597 | -7.1 | -3.3 | -3.0 | -4.3 |
| 340.9 | 23.605 | -7.5 | -3.1 | -2.8 | -4.1 |
| 341.2 | 23.614 | -8.0 | -2.9 | -2.6 | -3.9 |
| 341.5 | 23.622 | -8.4 | -2.8 | -2.5 | -3.9 |
| 341.8 | 23.631 | -8.5 | -2.9 | -2.6 | -3.9 |

| Depth (mm) | Age (ka BP) | $\delta^{13}C$ (‰ VPDB) | $\delta^{18}O$ (‰ VPDB) | $\delta^{18}O$ (‰ VPDB) Calcite Corr. | $\delta^{18}O$ (‰ VPDB) Sea Level Corr. |
|---|---|---|---|---|---|
| 342.1 | 23.639 | -9.0 | -3.1 | -2.8 | -4.1 |
| 342.4 | 23.648 | -9.2 | -3.0 | -2.7 | -4.0 |
| 342.7 | 23.657 | -9.0 | -3.2 | -2.9 | -4.2 |
| 343.0 | 23.665 | -9.7 | -3.2 | -2.9 | -4.2 |
| 343.3 | 23.674 | -9.3 | -3.4 | -3.1 | -4.4 |
| 343.6 | 23.682 | -8.4 | -3.5 | -3.2 | -4.5 |
| 343.8 | 23.691 | -7.9 | -3.6 | -3.3 | -4.6 |
| 344.1 | 23.700 | -8.4 | -3.5 | -3.2 | -4.5 |
| 344.4 | 23.708 | -8.5 | -3.5 | -3.2 | -4.5 |
| 344.7 | 23.717 | -8.0 | -3.7 | -3.4 | -4.7 |
| 345.0 | 23.725 | -7.9 | -3.7 | -3.4 | -4.8 |
| 345.3 | 23.734 | -7.5 | -3.5 | -3.2 | -4.6 |
| 345.6 | 23.743 | -7.7 | -3.6 | -3.3 | -4.6 |
| 345.9 | 23.751 | -7.9 | -3.5 | -3.2 | -4.5 |
| 346.2 | 23.760 | -8.3 | -3.4 | -3.1 | -4.4 |
| 346.5 | 23.768 | -9.7 | -3.4 | -3.1 | -4.4 |
| 346.8 | 23.777 | -9.9 | -3.2 | -2.9 | -4.2 |
| 347.1 | 23.786 | -9.9 | -3.2 | -2.9 | -4.2 |
| 347.4 | 23.794 | -10.0 | -3.3 | -3.0 | -4.3 |
| 347.7 | 23.803 | -9.7 | -3.3 | -3.0 | -4.3 |
| 348.0 | 23.811 | -8.2 | -3.4 | -3.1 | -4.4 |
| 348.3 | 23.820 | -7.9 | -3.3 | -3.0 | -4.3 |
| 348.6 | 23.829 | -7.8 | -3.4 | -3.1 | -4.4 |
| 348.9 | 23.837 | -7.0 | -3.4 | -3.1 | -4.4 |
| 349.2 | 23.846 | -7.0 | -3.3 | -3.0 | -4.3 |
| 349.5 | 23.854 | -7.3 | -3.5 | -3.2 | -4.5 |
| 349.8 | 23.863 | -7.9 | -3.3 | -3.0 | -4.3 |
| 350.1 | 23.871 | -7.5 | -3.6 | -3.3 | -4.6 |
| 350.4 | 23.880 | -7.2 | -3.5 | -3.2 | -4.5 |
| 350.7 | 23.889 | -7.3 | -3.4 | -3.1 | -4.4 |
| 351.0 | 23.897 | -7.1 | -3.5 | -3.2 | -4.5 |
| 351.3 | 23.906 | -7.6 | -3.5 | -3.2 | -4.6 |
| 351.6 | 23.914 | -7.6 | -3.4 | -3.1 | -4.4 |
| 351.9 | 23.923 | -7.5 | -3.4 | -3.1 | -4.4 |
| 352.1 | 23.932 | -8.0 | -3.4 | -3.1 | -4.4 |
| 352.4 | 23.940 | -8.2 | -3.3 | -3.0 | -4.3 |
| 352.7 | 23.949 | -8.3 | -3.3 | -3.0 | -4.3 |
| 353.0 | 23.957 | -8.2 | -3.3 | -3.0 | -4.3 |
| 353.3 | 23.966 | -8.7 | -3.5 | -3.2 | -4.5 |
| 353.6 | 23.975 | -8.5 | -3.2 | -2.9 | -4.3 |
| 353.9 | 23.983 | -8.5 | -3.3 | -3.0 | -4.3 |
| 354.2 | 23.992 | -8.4 | -3.2 | -2.9 | -4.3 |
| 354.5 | 24.000 | -8.5 | -3.4 | -3.1 | -4.5 |

| Depth (mm) | Age (ka BP) | $\delta^{13}C$ (‰ VPDB) | $\delta^{18}O$ (‰ VPDB) | $\delta^{18}O$ (‰ VPDB) Calcite Corr. | $\delta^{18}O$ (‰ VPDB) Sea Level Corr. |
|---|---|---|---|---|---|
| 354.8 | 24.009 | -8.3 | -3.4 | -3.1 | -4.4 |
| 355.1 | 24.018 | -8.1 | -3.4 | -3.1 | -4.4 |
| 355.4 | 24.026 | -8.1 | -3.4 | -3.1 | -4.4 |
| 355.7 | 24.035 | -7.9 | -3.3 | -3.0 | -4.3 |
| 356.0 | 24.043 | -8.1 | -3.6 | -3.3 | -4.6 |
| 356.3 | 24.052 | -8.0 | -3.5 | -3.2 | -4.5 |
| 356.6 | 24.061 | -7.9 | -3.6 | -3.3 | -4.6 |
| 356.9 | 24.069 | -8.4 | -3.7 | -3.4 | -4.7 |
| 357.2 | 24.078 | -7.9 | -3.6 | -3.3 | -4.6 |
| 357.5 | 24.086 | -7.1 | -3.3 | -3.0 | -4.3 |
| 357.8 | 24.095 | -6.9 | -3.2 | -2.9 | -4.3 |
| 358.1 | 24.104 | -7.0 | -3.2 | -2.9 | -4.2 |
| 358.4 | 24.112 | -6.9 | -3.4 | -3.1 | -4.5 |
| 358.7 | 24.121 | -6.8 | -3.4 | -3.1 | -4.4 |
| 359.0 | 24.129 | -6.9 | -3.4 | -3.1 | -4.4 |
| 359.3 | 24.138 | -6.9 | -3.6 | -3.3 | -4.6 |
| 359.6 | 24.146 | -7.1 | -3.7 | -3.4 | -4.7 |
| 359.9 | 24.155 | -6.9 | -3.6 | -3.3 | -4.6 |
| 360.2 | 24.164 | -6.9 | -3.8 | -3.5 | -4.8 |
| 360.4 | 24.172 | -6.8 | -3.7 | -3.4 | -4.7 |
| 360.7 | 24.181 | -6.7 | -3.6 | -3.3 | -4.7 |
| 361.0 | 24.189 | -6.8 | -3.9 | -3.6 | -4.9 |
| 361.3 | 24.198 | -6.8 | -3.6 | -3.3 | -4.6 |
| 361.6 | 24.207 | -6.8 | -3.7 | -3.4 | -4.7 |
| 361.9 | 24.215 | -6.6 | -3.8 | -3.5 | -4.8 |
| 362.2 | 24.224 | -6.7 | -3.7 | -3.4 | -4.8 |
| 362.5 | 24.232 | -6.5 | -3.7 | -3.4 | -4.7 |
| 362.8 | 24.241 | -6.6 | -3.7 | -3.4 | -4.7 |
| 363.1 | 24.249 | -6.6 | -3.8 | -3.5 | -4.8 |
| 363.4 | 24.256 | -6.6 | -3.8 | -3.5 | -4.9 |
| 363.7 | 24.264 | -6.7 | -3.7 | -3.4 | -4.7 |
| 364.0 | 24.272 | -6.5 | -3.9 | -3.6 | -5.0 |
| 364.3 | 24.279 | -6.7 | -3.8 | -3.5 | -4.8 |
| 364.6 | 24.287 | -6.6 | -3.9 | -3.6 | -4.9 |
| 364.9 | 24.295 | -6.7 | -3.8 | -3.5 | -4.8 |
| 365.2 | 24.303 | -6.7 | -3.6 | -3.3 | -4.6 |
| 365.5 | 24.310 | -6.6 | -3.6 | -3.3 | -4.6 |
| 365.8 | 24.318 | -6.4 | -3.6 | -3.3 | -4.6 |
| 366.1 | 24.326 | -6.5 | -3.5 | -3.2 | -4.5 |
| 366.4 | 24.333 | -6.4 | -3.5 | -3.2 | -4.5 |
| 366.7 | 24.341 | -6.3 | -3.6 | -3.3 | -4.7 |
| 367.0 | 24.349 | -6.4 | -3.5 | -3.2 | -4.5 |
| 367.3 | 24.357 | -6.2 | -3.7 | -3.4 | -4.7 |

| Depth (mm) | Age (ka BP) | $\delta^{13}C$ (‰ VPDB) | $\delta^{18}O$ (‰ VPDB) | $\delta^{18}O$ (‰ VPDB) Calcite Corr. | $\delta^{18}O$ (‰ VPDB) Sea Level Corr. |
|---|---|---|---|---|---|
| 367.6 | 24.364 | -6.3 | -3.7 | -3.4 | -4.7 |
| 367.9 | 24.372 | -6.5 | -3.7 | -3.4 | -4.7 |
| 368.1 | 24.380 | -6.5 | -3.7 | -3.4 | -4.8 |
| 368.4 | 24.387 | -6.5 | -3.7 | -3.4 | -4.7 |
| 368.7 | 24.395 | -6.4 | -3.8 | -3.5 | -4.8 |
| 369.0 | 24.403 | -6.5 | -3.6 | -3.3 | -4.7 |
| 369.3 | 24.410 | -6.5 | -4.0 | -3.7 | -5.0 |
| 369.6 | 24.418 | -6.5 | -4.0 | -3.7 | -5.0 |
| 369.9 | 24.426 | -6.6 | -4.0 | -3.7 | -5.0 |
| 370.2 | 24.434 | -6.7 | -3.8 | -3.5 | -4.9 |
| 370.5 | 24.441 | -6.6 | -3.8 | -3.5 | -4.8 |
| 370.8 | 24.449 | -6.5 | -3.9 | -3.6 | -4.9 |
| 371.1 | 24.457 | -6.6 | -3.7 | -3.4 | -4.7 |
| 371.4 | 24.464 | -6.4 | -3.9 | -3.6 | -4.9 |
| 371.7 | 24.472 | -6.4 | -3.8 | -3.5 | -4.8 |
| 372.0 | 24.480 | -6.4 | -3.8 | -3.5 | -4.8 |
| 372.3 | 24.487 | -6.4 | -3.8 | -3.5 | -4.8 |
| 372.6 | 24.495 | -6.6 | -3.9 | -3.6 | -4.9 |
| 372.9 | 24.503 | -6.6 | -3.8 | -3.5 | -4.8 |
| 373.2 | 24.511 | -6.4 | -3.7 | -3.4 | -4.7 |
| 373.5 | 24.518 | -6.6 | -3.7 | -3.4 | -4.7 |
| 373.8 | 24.526 | -6.7 | -3.6 | -3.3 | -4.6 |
| 374.1 | 24.534 | -6.6 | -3.5 | -3.2 | -4.5 |
| 374.4 | 24.541 | -6.6 | -3.4 | -3.1 | -4.4 |
| 374.7 | 24.549 | -6.8 | -3.3 | -3.0 | -4.3 |
| 375.0 | 24.557 | -6.5 | -3.5 | -3.2 | -4.5 |
| 375.3 | 24.564 | -6.4 | -3.3 | -3.0 | -4.3 |
| 375.6 | 24.572 | -6.3 | -3.3 | -3.0 | -4.3 |
| 375.8 | 24.580 | -6.5 | -3.3 | -3.0 | -4.3 |
| 376.1 | 24.588 | -6.5 | -3.2 | -2.9 | -4.2 |
| 376.4 | 24.595 | -6.4 | -3.4 | -3.1 | -4.4 |
| 376.7 | 24.603 | -6.5 | -3.5 | -3.2 | -4.5 |
| 377.0 | 24.611 | -6.3 | -3.5 | -3.2 | -4.5 |
| 377.3 | 24.618 | -6.2 | -3.5 | -3.2 | -4.5 |
| 377.6 | 24.626 | -6.0 | -3.3 | -3.0 | -4.3 |
| 377.9 | 24.634 | -6.4 | -3.2 | -2.9 | -4.2 |
| 378.2 | 24.641 | -6.6 | -3.6 | -3.3 | -4.6 |
| 378.5 | 24.649 | -6.8 | -3.6 | -3.3 | -4.6 |
| 378.8 | 24.657 | -6.8 | -3.8 | -3.5 | -4.8 |
| 379.1 | 24.665 | -6.5 | -3.5 | -3.2 | -4.6 |
| 379.4 | 24.672 | -6.5 | -3.3 | -3.0 | -4.4 |
| 379.7 | 24.680 | -6.3 | -3.2 | -2.9 | -4.2 |
| 380.0 | 24.688 | -6.1 | -3.2 | -2.9 | -4.3 |

| Depth (mm) | Age (ka BP) | $\delta^{13}C$ (‰ VPDB) | $\delta^{18}O$ (‰ VPDB) | $\delta^{18}O$ (‰ VPDB) Calcite Corr. | $\delta^{18}O$ (‰ VPDB) Sea Level Corr. |
|---|---|---|---|---|---|
| 380.3 | 24.695 | -6.4 | -3.4 | -3.1 | -4.4 |
| 380.6 | 24.703 | -6.8 | -3.6 | -3.3 | -4.6 |
| 380.9 | 24.711 | -6.9 | -3.5 | -3.2 | -4.5 |
| 381.2 | 24.718 | -6.8 | -3.3 | -3.0 | -4.3 |
| 381.5 | 24.726 | -6.7 | -3.2 | -2.9 | -4.2 |
| 381.8 | 24.734 | -6.6 | -3.2 | -2.9 | -4.2 |
| 382.1 | 24.742 | -6.6 | -3.2 | -2.9 | -4.2 |
| 382.4 | 24.749 | -6.8 | -3.3 | -3.0 | -4.3 |
| 382.7 | 24.757 | -6.8 | -3.6 | -3.3 | -4.6 |
| 383.0 | 24.765 | -6.7 | -3.3 | -3.0 | -4.3 |
| 383.2 | 24.772 | -6.9 | -3.3 | -3.0 | -4.3 |
| 383.5 | 24.780 | -6.7 | -3.5 | -3.2 | -4.5 |
| 383.8 | 24.788 | -6.6 | -3.7 | -3.4 | -4.7 |
| 384.1 | 24.796 | -6.6 | -3.6 | -3.3 | -4.7 |
| 384.4 | 24.803 | -6.7 | -3.7 | -3.4 | -4.7 |
| 384.7 | 24.811 | -6.5 | -3.8 | -3.5 | -4.8 |
| 385.0 | 24.819 | -6.4 | -3.6 | -3.3 | -4.6 |
| 385.3 | 24.826 | -6.4 | -3.7 | -3.4 | -4.8 |
| 385.6 | 24.834 | -6.5 | -3.6 | -3.3 | -4.7 |
| 385.9 | 24.841 | -6.5 | -3.6 | -3.3 | -4.6 |
| 386.2 | 24.849 | -6.4 | -3.6 | -3.3 | -4.7 |
| 386.5 | 24.856 | -6.4 | -3.6 | -3.3 | -4.6 |
| 386.8 | 24.864 | -6.5 | -3.4 | -3.1 | -4.4 |
| 387.0 | 24.871 | -6.6 | -3.3 | -3.0 | -4.3 |
| 387.3 | 24.879 | -6.6 | -3.3 | -3.0 | -4.3 |
| 387.6 | 24.886 | -6.6 | -3.3 | -3.0 | -4.3 |
| 387.9 | 24.893 | -6.5 | -3.3 | -3.0 | -4.3 |
| 388.2 | 24.901 | -6.6 | -3.5 | -3.2 | -4.5 |
| 388.5 | 24.908 | -6.5 | -3.7 | -3.4 | -4.7 |
| 388.8 | 24.916 | -6.5 | -3.5 | -3.2 | -4.5 |
| 389.1 | 24.923 | -6.6 | -3.5 | -3.2 | -4.5 |
| 389.3 | 24.931 | -6.4 | -3.2 | -2.9 | -4.2 |
| 389.6 | 24.938 | -6.4 | -3.3 | -3.0 | -4.3 |
| 389.9 | 24.946 | -6.5 | -3.2 | -2.9 | -4.2 |
| 390.2 | 24.953 | -6.5 | -3.2 | -2.9 | -4.3 |
| 390.5 | 24.961 | -6.5 | -3.1 | -2.8 | -4.1 |
| 390.8 | 24.968 | -6.4 | -3.0 | -2.7 | -4.1 |
| 391.1 | 24.976 | -6.5 | -3.4 | -3.1 | -4.4 |
| 391.3 | 24.983 | -7.0 | -3.4 | -3.1 | -4.4 |
| 391.6 | 24.991 | -6.7 | -3.3 | -3.0 | -4.3 |
| 391.9 | 24.998 | -6.5 | -3.3 | -3.0 | -4.4 |
| 392.2 | 25.005 | -6.5 | -3.3 | -3.0 | -4.3 |
| 392.5 | 25.013 | -6.5 | -3.3 | -3.0 | -4.3 |

| Depth (mm) | Age (ka BP) | $\delta^{13}C$ (‰ VPDB) | $\delta^{18}O$ (‰ VPDB) | $\delta^{18}O$ (‰ VPDB) Calcite Corr. | $\delta^{18}O$ (‰ VPDB) Sea Level Corr. |
|---|---|---|---|---|---|
| 392.8 | 25.020 | -6.4 | -3.4 | -3.1 | -4.4 |
| 393.1 | 25.028 | -6.3 | -3.3 | -3.0 | -4.3 |
| 393.4 | 25.035 | -6.4 | -3.4 | -3.1 | -4.5 |
| 393.6 | 25.043 | -6.2 | -3.3 | -3.0 | -4.3 |
| 393.9 | 25.050 | -6.3 | -3.1 | -2.8 | -4.1 |
| 394.2 | 25.058 | -6.4 | -3.3 | -3.0 | -4.4 |
| 394.5 | 25.065 | -6.4 | -3.6 | -3.3 | -4.6 |
| 394.8 | 25.073 | -6.4 | -3.4 | -3.1 | -4.4 |
| 395.1 | 25.080 | -6.4 | -3.4 | -3.1 | -4.4 |
| 395.4 | 25.088 | -6.5 | -3.1 | -2.8 | -4.1 |
| 395.7 | 25.095 | -6.4 | -3.1 | -2.8 | -4.1 |
| 395.9 | 25.102 | -6.5 | -3.1 | -2.8 | -4.1 |
| 396.2 | 25.110 | -6.6 | -3.0 | -2.7 | -4.0 |
| 396.5 | 25.117 | -6.7 | -3.1 | -2.8 | -4.1 |
| 396.8 | 25.125 | -6.7 | -3.0 | -2.7 | -4.0 |
| 397.1 | 25.132 | -6.8 | -3.2 | -2.9 | -4.2 |
| 397.4 | 25.140 | -6.7 | -3.0 | -2.7 | -4.0 |
| 397.7 | 25.147 | -6.9 | -3.2 | -2.9 | -4.2 |
| 397.9 | 25.155 | -7.6 | -3.2 | -2.9 | -4.2 |
| 398.2 | 25.162 | -7.1 | -3.1 | -2.8 | -4.1 |
| 398.5 | 25.170 | -7.0 | -3.1 | -2.8 | -4.1 |
| 398.8 | 25.177 | -6.7 | -2.8 | -2.5 | -3.8 |
| 399.1 | 25.185 | -6.4 | -3.3 | -3.0 | -4.3 |
| 399.4 | 25.192 | -6.2 | -3.5 | -3.2 | -4.5 |
| 399.7 | 25.200 | -6.3 | -3.5 | -3.2 | -4.5 |
| 400.0 | 25.207 | -6.5 | -3.3 | -3.0 | -4.3 |
| 400.3 | 25.215 | -6.9 | -3.3 | -3.0 | -4.3 |
| 400.6 | 25.224 | -6.9 | -3.2 | -2.9 | -4.2 |
| 400.9 | 25.232 | -7.0 | -3.1 | -2.8 | -4.1 |
| 401.3 | 25.241 | -7.1 | -3.1 | -2.8 | -4.1 |
| 401.6 | 25.249 | -7.0 | -3.1 | -2.8 | -4.1 |
| 401.9 | 25.258 | -7.0 | -3.1 | -2.8 | -4.1 |
| 402.2 | 25.266 | -7.0 | -3.0 | -2.7 | -4.0 |
| 402.6 | 25.275 | -7.1 | -3.1 | -2.8 | -4.1 |
| 402.9 | 25.283 | -7.0 | -3.3 | -3.0 | -4.3 |
| 403.2 | 25.292 | -7.0 | -3.0 | -2.7 | -4.0 |
| 403.5 | 25.300 | -7.2 | -3.1 | -2.8 | -4.1 |
| 403.9 | 25.309 | -7.1 | -3.3 | -3.0 | -4.3 |
| 404.2 | 25.317 | -7.0 | -3.2 | -2.9 | -4.2 |
| 404.5 | 25.325 | -6.8 | -3.2 | -2.9 | -4.2 |
| 404.8 | 25.334 | -6.6 | -3.3 | -3.0 | -4.3 |
| 405.2 | 25.342 | -6.5 | -3.5 | -3.2 | -4.5 |
| 405.5 | 25.351 | -6.6 | -3.4 | -3.1 | -4.5 |

| Depth (mm) | Age (ka BP) | $\delta^{13}C$ (‰ VPDB) | $\delta^{18}O$ (‰ VPDB) | $\delta^{18}O$ (‰ VPDB) Calcite Corr. | $\delta^{18}O$ (‰ VPDB) Sea Level Corr. |
|---|---|---|---|---|---|
| 405.8 | 25.359 | -6.8 | -3.3 | -3.0 | -4.3 |
| 406.1 | 25.368 | -6.8 | -3.4 | -3.1 | -4.4 |
| 406.5 | 25.376 | -7.1 | -3.0 | -2.7 | -4.0 |
| 406.8 | 25.385 | -7.3 | -3.3 | -3.0 | -4.3 |
| 407.1 | 25.393 | -7.4 | -3.4 | -3.1 | -4.4 |
| 407.4 | 25.402 | -7.4 | -3.2 | -2.9 | -4.2 |
| 407.8 | 25.410 | -7.2 | -3.0 | -2.7 | -4.0 |
| 408.1 | 25.419 | -7.2 | -3.3 | -3.0 | -4.3 |
| 408.4 | 25.427 | -7.1 | -3.2 | -2.9 | -4.2 |
| 408.7 | 25.435 | -7.1 | -3.0 | -2.7 | -4.0 |
| 409.1 | 25.444 | -7.0 | -3.1 | -2.8 | -4.1 |
| 409.4 | 25.452 | -6.9 | -3.0 | -2.7 | -4.0 |
| 409.7 | 25.461 | -7.1 | -3.1 | -2.8 | -4.1 |
| 410.0 | 25.469 | -6.9 | -3.0 | -2.7 | -4.0 |
| 410.4 | 25.478 | -7.3 | -3.1 | -2.8 | -4.1 |
| 410.7 | 25.486 | -7.5 | -3.1 | -2.8 | -4.1 |
| 411.0 | 25.495 | -7.4 | -3.1 | -2.8 | -4.1 |
| 411.3 | 25.503 | -7.3 | -3.2 | -2.9 | -4.2 |
| 411.7 | 25.512 | -7.3 | -3.0 | -2.7 | -4.0 |
| 412.0 | 25.520 | -7.5 | -3.1 | -2.8 | -4.1 |
| 412.3 | 25.528 | -7.4 | -3.1 | -2.8 | -4.1 |
| 412.6 | 25.537 | -7.4 | -3.0 | -2.7 | -4.0 |
| 413.0 | 25.545 | -7.3 | -3.1 | -2.8 | -4.1 |
| 413.3 | 25.554 | -7.3 | -2.8 | -2.5 | -3.8 |
| 413.6 | 25.562 | -7.3 | -3.1 | -2.8 | -4.1 |
| 413.9 | 25.571 | -7.3 | -3.3 | -3.0 | -4.3 |
| 414.3 | 25.579 | -7.3 | -3.2 | -2.9 | -4.2 |
| 414.6 | 25.588 | -7.3 | -3.1 | -2.8 | -4.1 |
| 414.9 | 25.596 | -7.3 | -3.3 | -3.0 | -4.3 |
| 415.2 | 25.605 | -7.4 | -3.2 | -2.9 | -4.2 |
| 415.6 | 25.613 | -7.2 | -3.1 | -2.8 | -4.1 |
| 415.9 | 25.622 | -7.4 | -3.1 | -2.8 | -4.1 |
| 416.2 | 25.630 | -7.4 | -2.8 | -2.5 | -3.8 |
| 416.5 | 25.638 | -7.3 | -3.1 | -2.8 | -4.1 |
| 416.9 | 25.647 | -7.2 | -3.1 | -2.8 | -4.1 |
| 417.2 | 25.655 | -7.4 | -3.2 | -2.9 | -4.2 |
| 417.5 | 25.664 | -7.3 | -3.1 | -2.8 | -4.1 |
| 417.8 | 25.672 | -7.3 | -3.1 | -2.8 | -4.1 |
| 418.2 | 25.681 | -7.4 | -3.2 | -2.9 | -4.2 |
| 418.5 | 25.689 | -7.2 | -3.0 | -2.7 | -4.0 |
| 418.8 | 25.698 | -7.1 | -3.1 | -2.8 | -4.1 |
| 419.1 | 25.706 | -7.0 | -3.2 | -2.9 | -4.2 |
| 419.5 | 25.715 | -7.2 | -3.6 | -3.3 | -4.6 |

| Depth (mm) | Age (ka BP) | $\delta^{13}C$ (‰ VPDB) | $\delta^{18}O$ (‰ VPDB) | $\delta^{18}O$ (‰ VPDB) Calcite Corr. | $\delta^{18}O$ (‰ VPDB) Sea Level Corr. |
|---|---|---|---|---|---|
| 419.8 | 25.723 | -7.0 | -3.2 | -2.9 | -4.2 |
| 420.1 | 25.732 | -6.8 | -3.2 | -2.9 | -4.2 |
| 420.4 | 25.740 | -6.8 | -3.2 | -2.9 | -4.2 |
| 420.8 | 25.748 | -6.5 | -3.5 | -3.2 | -4.5 |
| 421.1 | 25.757 | -6.5 | -3.4 | -3.1 | -4.4 |
| 421.4 | 25.765 | -7.0 | -3.3 | -3.0 | -4.3 |
| 421.7 | 25.774 | -6.5 | -3.7 | -3.4 | -4.7 |
| 422.1 | 25.782 | -6.6 | -3.6 | -3.3 | -4.6 |
| 422.3 | 25.789 | -6.9 | -3.7 | -3.4 | -4.7 |
| 422.6 | 25.795 | -6.7 | -3.2 | -2.9 | -4.2 |
| 422.8 | 25.801 | -6.5 | -3.3 | -3.0 | -4.3 |
| 423.0 | 25.807 | -6.6 | -3.4 | -3.1 | -4.4 |
| 423.3 | 25.813 | -6.6 | -3.4 | -3.1 | -4.5 |
| 423.5 | 25.820 | -6.9 | -3.4 | -3.1 | -4.4 |
| 423.7 | 25.826 | -7.2 | -3.3 | -3.0 | -4.3 |
| 424.0 | 25.832 | -7.3 | -3.2 | -2.9 | -4.2 |
| 424.2 | 25.838 | -7.1 | -3.2 | -2.9 | -4.2 |
| 424.5 | 25.845 | -7.2 | -3.0 | -2.7 | -4.0 |
| 424.7 | 25.851 | -7.0 | -3.0 | -2.7 | -4.0 |
| 424.9 | 25.857 | -7.1 | -3.1 | -2.8 | -4.1 |
| 425.2 | 25.863 | -7.4 | -3.4 | -3.1 | -4.4 |
| 425.4 | 25.870 | -7.2 | -3.1 | -2.8 | -4.1 |
| 425.7 | 25.876 | -7.0 | -3.1 | -2.8 | -4.1 |
| 425.9 | 25.882 | -7.0 | -3.2 | -2.9 | -4.2 |
| 426.1 | 25.888 | -7.0 | -3.0 | -2.7 | -4.0 |
| 426.4 | 25.895 | -7.0 | -3.1 | -2.8 | -4.1 |
| 426.6 | 25.901 | -7.0 | -2.8 | -2.5 | -3.8 |
| 426.9 | 25.907 | -7.0 | -3.3 | -3.0 | -4.3 |
| 427.1 | 25.913 | -7.0 | -3.4 | -3.1 | -4.4 |
| 427.3 | 25.919 | -7.1 | -3.3 | -3.0 | -4.3 |
| 427.6 | 25.926 | -7.9 | -3.4 | -3.1 | -4.4 |
| 427.8 | 25.932 | -8.3 | -3.3 | -3.0 | -4.3 |
| 428.1 | 25.938 | -8.3 | -3.3 | -3.0 | -4.4 |
| 428.3 | 25.944 | -7.8 | -3.2 | -2.9 | -4.2 |
| 428.5 | 25.951 | -7.7 | -3.2 | -2.9 | -4.2 |
| 428.8 | 25.957 | -7.4 | -2.9 | -2.6 | -3.9 |
| 429.0 | 25.963 | -7.3 | -2.8 | -2.5 | -3.8 |
| 429.3 | 25.969 | -7.3 | -2.9 | -2.6 | -3.9 |
| 429.5 | 25.976 | -7.5 | -3.2 | -2.9 | -4.2 |
| 429.7 | 25.982 | -7.1 | -2.9 | -2.6 | -3.9 |
| 430.0 | 25.988 | -7.1 | -2.7 | -2.4 | -3.7 |
| 430.2 | 25.994 | -7.3 | -2.9 | -2.6 | -3.9 |
| 430.5 | 26.000 | -7.4 | -3.1 | -2.8 | -4.1 |

| Depth (mm) | Age (ka BP) | $\delta^{13}C$ (‰ VPDB) | $\delta^{18}O$ (‰ VPDB) | $\delta^{18}O$ (‰ VPDB) Calcite Corr. | $\delta^{18}O$ (‰ VPDB) Sea Level Corr. |
|---|---|---|---|---|---|
| 430.7 | 26.007 | -7.3 | -3.0 | -2.7 | -4.0 |
| 430.9 | 26.013 | -7.4 | -3.4 | -3.1 | -4.4 |
| 431.2 | 26.019 | -7.4 | -3.2 | -2.9 | -4.2 |
| 431.4 | 26.025 | -7.3 | -3.1 | -2.8 | -4.1 |
| 431.7 | 26.032 | -7.3 | -2.9 | -2.6 | -3.9 |
| 431.9 | 26.038 | -7.1 | -3.0 | -2.7 | -4.0 |
| 432.1 | 26.044 | -7.2 | -2.9 | -2.6 | -3.9 |
| 432.4 | 26.050 | -7.3 | -3.1 | -2.8 | -4.1 |
| 432.6 | 26.057 | -7.2 | -3.0 | -2.7 | -4.0 |
| 432.9 | 26.063 | -7.4 | -3.1 | -2.8 | -4.1 |
| 433.1 | 26.069 | -7.3 | -3.2 | -2.9 | -4.2 |
| 433.3 | 26.075 | -7.4 | -3.4 | -3.1 | -4.4 |
| 433.6 | 26.082 | -7.4 | -3.3 | -3.0 | -4.3 |
| 433.8 | 26.088 | -7.6 | -3.3 | -3.0 | -4.3 |
| 434.1 | 26.094 | -8.0 | -3.5 | -3.2 | -4.5 |
| 434.3 | 26.106 | -7.7 | -3.2 | -2.9 | -4.2 |
| 434.6 | 26.118 | -7.5 | -3.2 | -2.9 | -4.1 |
| 434.9 | 26.130 | -7.6 | -3.2 | -2.9 | -4.2 |
| 435.2 | 26.141 | -7.8 | -2.9 | -2.6 | -3.9 |
| 435.5 | 26.153 | -7.8 | -3.1 | -2.8 | -4.0 |
| 435.8 | 26.165 | -8.4 | -3.4 | -3.1 | -4.4 |
| 436.1 | 26.177 | -8.8 | -3.2 | -2.9 | -4.2 |
| 436.4 | 26.189 | -9.9 | -3.5 | -3.2 | -4.5 |
| 436.7 | 26.201 | -10.4 | -3.5 | -3.2 | -4.5 |
| 437.0 | 26.212 | -10.2 | -3.4 | -3.1 | -4.4 |
| 437.3 | 26.224 | -9.4 | -3.3 | -3.0 | -4.3 |
| 437.6 | 26.236 | -9.1 | -3.3 | -3.0 | -4.3 |
| 437.9 | 26.248 | -8.7 | -3.2 | -2.9 | -4.2 |
| 438.2 | 26.260 | -7.8 | - | - | - |
| 438.5 | 26.272 | -8.1 | -3.2 | -2.9 | -4.2 |
| 438.8 | 26.283 | -8.3 | -3.2 | -2.9 | -4.2 |
| 439.1 | 26.295 | -7.8 | -3.1 | -2.8 | -4.0 |
| 439.4 | 26.307 | -7.7 | -2.9 | -2.6 | -3.9 |
| 439.7 | 26.319 | -7.6 | -3.2 | -2.9 | -4.1 |
| 440.0 | 26.331 | -7.7 | -3.0 | -2.7 | -4.0 |
| 440.2 | 26.343 | -8.1 | -3.1 | -2.8 | -4.0 |
| 440.5 | 26.354 | -8.7 | -3.4 | -3.1 | -4.4 |
| 440.8 | 26.366 | -8.6 | -3.1 | -2.8 | -4.1 |
| 441.1 | 26.378 | -8.0 | -3.1 | -2.8 | -4.1 |
| 441.4 | 26.390 | -7.8 | -3.0 | -2.7 | -4.0 |
| 441.7 | 26.402 | -7.7 | -3.1 | -2.8 | -4.1 |
| 442.0 | 26.414 | -7.8 | -3.2 | -2.9 | -4.2 |
| 442.3 | 26.425 | -8.8 | -3.7 | -3.4 | -4.7 |

| Depth (mm) | Age (ka BP) | $\delta^{13}C$ (‰ VPDB) | $\delta^{18}O$ (‰ VPDB) | $\delta^{18}O$ (‰ VPDB) Calcite Corr. | $\delta^{18}O$ (‰ VPDB) Sea Level Corr. |
|---|---|---|---|---|---|
| 442.6 | 26.437 | -9.4 | -3.5 | -3.2 | -4.5 |
| 442.9 | 26.449 | -9.5 | -3.6 | -3.3 | -4.6 |
| 443.2 | 26.461 | -8.4 | -3.4 | -3.1 | -4.4 |
| 443.5 | 26.473 | -8.1 | -3.5 | -3.2 | -4.5 |
| 443.8 | 26.485 | -8.0 | -3.5 | -3.2 | -4.4 |
| 444.1 | 26.496 | -7.9 | -3.2 | -2.9 | -4.1 |
| 444.4 | 26.508 | -7.9 | -3.3 | -3.0 | -4.2 |
| 444.7 | 26.520 | -7.9 | -3.3 | -3.0 | -4.3 |
| 445.0 | 26.532 | -7.8 | -3.4 | -3.1 | -4.3 |
| 445.3 | 26.544 | -8.0 | -3.1 | -2.8 | -4.0 |
| 445.6 | 26.556 | -8.0 | -3.4 | -3.1 | -4.4 |
| 445.9 | 26.567 | -8.0 | -3.2 | -2.9 | -4.2 |
| 446.1 | 26.579 | -7.9 | -2.8 | -2.5 | -3.8 |
| 446.4 | 26.591 | -7.7 | -2.9 | -2.6 | -3.9 |
| 446.7 | 26.603 | -7.8 | -3.0 | -2.7 | -3.9 |
| 447.0 | 26.615 | -7.8 | -3.0 | -2.7 | -3.9 |
| 447.3 | 26.627 | -7.7 | -3.2 | -2.9 | -4.2 |
| 447.6 | 26.638 | -7.8 | -3.1 | -2.8 | -4.0 |
| 447.9 | 26.650 | -7.9 | -3.2 | -2.9 | -4.1 |
| 448.2 | 26.662 | -7.9 | -3.2 | -2.9 | -4.2 |
| 448.5 | 26.674 | -7.9 | -3.2 | -2.9 | -4.1 |
| 448.8 | 26.686 | -7.9 | -3.2 | -2.9 | -4.2 |
| 449.1 | 26.698 | -8.0 | -3.6 | -3.3 | -4.5 |
| 449.4 | 26.709 | -7.9 | -3.6 | -3.3 | -4.5 |
| 449.7 | 26.721 | -7.7 | -3.5 | -3.2 | -4.4 |
| 450.0 | 26.733 | -8.0 | -3.6 | -3.3 | -4.6 |
| 450.3 | 26.745 | -8.0 | -3.5 | -3.2 | -4.5 |
| 450.6 | 26.757 | -8.0 | -3.4 | -3.1 | -4.3 |
| 450.9 | 26.769 | -8.0 | -3.8 | -3.5 | -4.7 |
| 451.2 | 26.780 | -8.1 | -3.9 | -3.6 | -4.8 |
| 451.5 | 26.792 | -7.9 | -3.8 | -3.5 | -4.7 |
| 451.8 | 26.804 | -7.6 | -3.4 | -3.1 | -4.4 |
| 452.0 | 26.816 | -7.8 | -3.2 | -2.9 | -4.2 |
| 452.3 | 26.828 | -7.6 | -3.5 | -3.2 | -4.5 |
| 452.6 | 26.839 | -7.7 | -3.3 | -3.0 | -4.2 |
| 452.9 | 26.851 | -7.6 | -3.7 | -3.4 | -4.6 |
| 453.2 | 26.863 | -7.6 | -3.7 | -3.4 | -4.6 |
| 453.5 | 26.875 | -7.6 | -3.3 | -3.0 | -4.3 |
| 453.8 | 26.886 | -7.7 | -3.3 | -3.0 | -4.3 |
| 454.1 | 26.898 | -7.8 | -3.5 | -3.2 | -4.5 |
| 454.4 | 26.910 | -7.7 | -3.3 | -3.0 | -4.3 |
| 454.7 | 26.922 | -7.7 | -3.6 | -3.3 | -4.5 |
| 455.0 | 26.933 | -7.9 | -3.5 | -3.2 | -4.4 |

| Depth (mm) | Age (ka BP) | $\delta^{13}C$ (‰ VPDB) | $\delta^{18}O$ (‰ VPDB) | $\delta^{18}O$ (‰ VPDB) Calcite Corr. | $\delta^{18}O$ (‰ VPDB) Sea Level Corr. |
|---|---|---|---|---|---|
| 455.3 | 26.945 | -7.9 | -3.1 | -2.8 | -4.0 |
| 455.6 | 26.957 | -7.8 | -3.2 | -2.9 | -4.1 |
| 455.9 | 26.969 | -8.0 | -3.1 | -2.8 | -4.0 |
| 456.2 | 26.981 | -7.9 | -3.0 | -2.7 | -3.9 |
| 456.4 | 26.992 | -8.0 | -3.1 | -2.8 | -4.0 |
| 456.7 | 27.004 | -8.0 | -3.1 | -2.8 | -4.1 |
| 457.0 | 27.016 | -7.9 | -3.2 | -2.9 | -4.1 |
| 457.3 | 27.028 | -8.2 | -3.1 | -2.8 | -4.0 |
| 457.6 | 27.039 | -8.0 | -3.1 | -2.8 | -4.0 |
| 457.9 | 27.051 | -8.1 | -3.0 | -2.7 | -3.9 |
| 458.2 | 27.063 | -8.1 | -2.9 | -2.6 | -3.9 |
| 458.5 | 27.074 | -8.1 | -3.1 | -2.8 | -4.0 |
| 458.8 | 27.086 | -7.0 | -2.9 | -2.6 | -3.8 |
| 459.1 | 27.098 | -8.0 | -2.9 | -2.6 | -3.8 |
| 459.4 | 27.109 | -7.9 | -2.9 | -2.6 | -3.9 |
| 459.6 | 27.121 | -8.0 | -3.1 | -2.8 | -4.0 |
| 459.9 | 27.132 | -8.3 | -3.2 | -2.9 | -4.2 |
| 460.2 | 27.144 | -8.4 | -3.2 | -2.9 | -4.2 |
| 460.5 | 27.156 | -8.3 | -3.2 | -2.9 | -4.1 |
| 460.8 | 27.167 | -8.2 | -3.2 | -2.9 | -4.1 |
| 461.1 | 27.179 | -8.7 | -3.3 | -3.0 | -4.2 |
| 461.4 | 27.190 | -8.2 | -3.3 | -3.0 | -4.2 |
| 461.7 | 27.202 | -8.0 | -3.3 | -3.0 | -4.2 |
| 462.0 | 27.214 | -8.1 | -3.3 | -3.0 | -4.2 |
| 462.3 | 27.225 | -8.2 | -3.4 | -3.1 | -4.3 |
| 462.5 | 27.237 | -7.9 | -3.1 | -2.8 | -4.0 |
| 462.8 | 27.248 | -8.5 | -3.3 | -3.0 | -4.2 |
| 463.1 | 27.260 | -8.2 | -3.3 | -3.0 | -4.2 |
| 463.4 | 27.272 | -8.1 | -2.9 | -2.6 | -3.8 |
| 463.7 | 27.283 | -8.0 | -3.3 | -3.0 | -4.2 |
| 464.0 | 27.295 | -8.1 | -3.2 | -2.9 | -4.1 |
| 464.3 | 27.306 | -8.1 | -3.0 | -2.7 | -3.8 |
| 464.6 | 27.318 | -8.1 | -3.2 | -2.9 | -4.1 |
| 464.9 | 27.330 | -8.4 | -3.3 | -3.0 | -4.2 |
| 465.1 | 27.341 | -8.5 | -3.3 | -3.0 | -4.2 |
| 465.4 | 27.353 | -8.3 | -3.2 | -2.9 | -4.0 |
| 465.7 | 27.364 | -8.6 | -3.5 | -3.2 | -4.4 |
| 466.0 | 27.376 | -8.4 | -3.4 | -3.1 | -4.3 |
| 466.3 | 27.388 | -8.4 | -3.4 | -3.1 | -4.3 |
| 466.6 | 27.399 | -8.4 | -3.4 | -3.1 | -4.2 |
| 466.9 | 27.411 | -8.4 | -3.5 | -3.2 | -4.3 |
| 467.2 | 27.422 | -8.3 | -3.1 | -2.8 | -4.0 |
| 467.5 | 27.434 | -8.1 | -3.2 | -2.9 | -4.1 |

| Depth (mm) | Age (ka BP) | $\delta^{13}C$ (‰ VPDB) | $\delta^{18}O$ (‰ VPDB) | $\delta^{18}O$ (‰ VPDB) Calcite Corr. | $\delta^{18}O$ (‰ VPDB) Sea Level Corr. |
|---|---|---|---|---|---|
| 467.7 | 27.446 | -8.3 | -3.3 | -3.0 | -4.1 |
| 468.0 | 27.457 | -8.1 | -3.5 | -3.2 | -4.4 |
| 468.3 | 27.469 | -8.3 | -3.2 | -2.9 | -4.1 |
| 468.6 | 27.481 | -8.2 | -3.2 | -2.9 | -4.0 |
| 468.9 | 27.492 | -8.2 | -3.1 | -2.8 | -4.0 |
| 469.2 | 27.504 | -8.0 | -3.3 | -3.0 | -4.2 |
| 469.5 | 27.515 | -8.3 | -3.4 | -3.1 | -4.3 |
| 469.8 | 27.527 | -7.8 | -3.4 | -3.1 | -4.2 |
| 470.1 | 27.539 | -7.8 | -3.4 | -3.1 | -4.3 |
| 470.4 | 27.550 | -7.8 | -3.5 | -3.2 | -4.3 |
| 470.6 | 27.562 | -8.0 | -3.2 | -2.9 | -4.1 |
| 470.9 | 27.573 | -7.8 | -3.3 | -3.0 | -4.1 |
| 471.2 | 27.585 | -7.8 | -3.1 | -2.8 | -4.0 |
| 471.5 | 27.597 | -7.8 | -3.2 | -2.9 | -4.0 |
| 471.8 | 27.608 | -8.0 | -3.0 | -2.7 | -3.9 |
| 472.1 | 27.620 | -7.8 | -3.2 | -2.9 | -4.1 |
| 472.4 | 27.631 | -7.9 | -3.1 | -2.8 | -3.9 |
| 472.7 | 27.643 | -7.9 | -3.1 | -2.8 | -4.0 |
| 473.0 | 27.655 | -8.0 | -3.4 | -3.1 | -4.3 |
| 473.2 | 27.666 | -8.1 | -3.3 | -3.0 | -4.1 |
| 473.5 | 27.678 | -8.2 | -3.4 | -3.1 | -4.2 |
| 473.8 | 27.689 | -7.8 | -3.3 | -3.0 | -4.2 |
| 474.1 | 27.701 | -7.8 | -3.1 | -2.8 | -3.9 |
| 474.4 | 27.713 | -7.7 | -3.3 | -3.0 | -4.1 |
| 474.7 | 27.724 | -7.9 | -3.3 | -3.0 | -4.1 |
| 475.0 | 27.736 | -7.8 | -3.1 | -2.8 | -3.9 |
| 475.3 | 27.748 | -8.0 | -3.2 | -2.9 | -4.0 |
| 475.6 | 27.759 | -8.1 | -3.3 | -3.0 | -4.1 |
| 475.9 | 27.771 | -8.0 | -3.2 | -2.9 | -4.1 |
| 476.1 | 27.783 | -7.8 | -3.2 | -2.9 | -4.0 |
| 476.4 | 27.794 | -7.8 | -3.2 | -2.9 | -4.1 |
| 476.7 | 27.806 | -7.7 | -3.3 | -3.0 | -4.1 |
| 477.0 | 27.818 | -7.8 | -3.3 | -3.0 | -4.2 |
| 477.3 | 27.829 | -8.9 | -3.3 | -3.0 | -4.2 |
| 477.6 | 27.841 | -7.8 | -3.2 | -2.9 | -4.1 |
| 477.9 | 27.853 | -8.0 | -3.2 | -2.9 | -4.1 |
| 478.2 | 27.864 | -8.0 | -3.2 | -2.9 | -4.0 |
| 478.5 | 27.876 | -7.8 | -3.0 | -2.7 | -3.8 |
| 478.8 | 27.887 | -7.7 | -3.2 | -2.9 | -4.0 |
| 479.1 | 27.899 | -8.1 | -3.2 | -2.9 | -4.0 |
| 479.3 | 27.911 | -7.6 | -3.1 | -2.8 | -3.9 |
| 479.6 | 27.922 | -7.7 | -3.0 | -2.7 | -3.8 |
| 479.9 | 27.934 | -8.3 | -3.1 | -2.8 | -3.9 |

| Depth (mm) | Age (ka BP) | $\delta^{13}C$ (‰ VPDB) | $\delta^{18}O$ (‰ VPDB) | $\delta^{18}O$ (‰ VPDB) Calcite Corr. | $\delta^{18}O$ (‰ VPDB) Sea Level Corr. |
|---|---|---|---|---|---|
| 480.2 | 27.946 | -8.1 | -3.1 | -2.8 | -3.9 |
| 480.5 | 27.957 | -8.0 | -3.1 | -2.8 | -3.9 |
| 480.8 | 27.969 | -7.9 | -3.1 | -2.8 | -3.9 |
| 481.1 | 27.981 | -7.8 | -2.9 | -2.6 | -3.7 |
| 481.4 | 27.992 | -7.8 | -3.2 | -2.9 | -4.0 |
| 481.7 | 28.004 | -7.9 | -3.3 | -3.0 | -4.1 |
| 482.0 | 28.016 | -8.0 | -3.5 | -3.2 | -4.3 |
| 482.3 | 28.027 | -7.6 | -3.0 | -2.7 | -3.8 |
| 482.5 | 28.039 | -7.6 | -3.2 | -2.9 | -4.0 |
| 482.8 | 28.051 | -7.6 | -3.2 | -2.9 | -4.0 |
| 483.1 | 28.062 | -7.9 | -3.3 | -3.0 | -4.1 |
| 483.4 | 28.074 | -7.8 | -3.4 | -3.1 | -4.2 |
| 483.7 | 28.086 | -7.5 | -3.4 | -3.1 | -4.2 |
| 484.0 | 28.097 | -7.7 | -3.4 | -3.1 | -4.2 |
| 484.3 | 28.109 | -7.5 | -3.5 | -3.2 | -4.3 |
| 484.6 | 28.121 | -7.4 | -3.5 | -3.2 | -4.3 |
| 484.9 | 28.132 | -7.4 | -3.5 | -3.2 | -4.3 |
| 485.2 | 28.144 | -7.5 | -3.4 | -3.1 | -4.2 |
| 485.5 | 28.156 | -7.5 | -3.5 | -3.2 | -4.3 |
| 485.7 | 28.167 | -7.6 | -3.5 | -3.2 | -4.3 |
| 486.0 | 28.179 | -7.5 | -3.7 | -3.4 | -4.5 |
| 486.3 | 28.191 | -7.9 | -3.6 | -3.3 | -4.4 |
| 486.6 | 28.202 | -7.7 | -3.4 | -3.1 | -4.2 |
| 486.9 | 28.214 | -7.4 | -3.7 | -3.4 | -4.5 |
| 487.2 | 28.226 | -7.5 | -3.7 | -3.4 | -4.5 |
| 487.5 | 28.237 | -8.1 | -3.5 | -3.2 | -4.2 |
| 487.8 | 28.249 | -7.5 | -3.6 | -3.3 | -4.4 |
| 488.1 | 28.261 | -7.4 | -3.6 | -3.3 | -4.4 |
| 488.4 | 28.272 | -7.4 | -3.6 | -3.3 | -4.4 |
| 488.6 | 28.284 | -7.5 | -3.5 | -3.2 | -4.2 |
| 488.9 | 28.296 | -7.5 | -3.7 | -3.4 | -4.5 |
| 489.2 | 28.307 | -7.5 | -3.6 | -3.3 | -4.4 |
| 489.5 | 28.319 | -7.6 | -3.6 | -3.3 | -4.3 |
| 489.8 | 28.331 | -7.4 | -3.2 | -2.9 | -4.0 |
| 490.1 | 28.342 | -7.4 | -3.1 | -2.8 | -3.8 |
| 490.4 | 28.354 | -7.6 | -3.1 | -2.8 | -3.9 |
| 490.7 | 28.372 | -7.8 | -3.1 | -2.8 | -3.9 |
| 491.0 | 28.389 | -8.5 | -3.2 | -2.9 | -4.0 |
| 491.2 | 28.407 | -9.0 | -3.2 | -2.9 | -3.9 |
| 491.5 | 28.425 | -9.7 | -3.4 | -3.1 | -4.1 |
| 491.8 | 28.443 | -9.6 | -3.4 | -3.1 | -4.1 |
| 492.1 | 28.460 | -9.6 | -3.3 | -3.0 | -4.1 |
| 492.4 | 28.478 | -8.9 | -3.3 | -3.0 | -4.1 |

| Depth (mm) | Age (ka BP) | $\delta^{13}C$ (‰ VPDB) | $\delta^{18}O$ (‰ VPDB) | $\delta^{18}O$ (‰ VPDB) Calcite Corr. | $\delta^{18}O$ (‰ VPDB) Sea Level Corr. |
|---|---|---|---|---|---|
| 492.7 | 28.496 | -8.8 | -3.3 | -3.0 | -4.0 |
| 493.0 | 28.515 | -9.0 | -3.3 | -3.0 | -4.0 |
| 493.2 | 28.532 | -8.8 | -3.3 | -3.0 | -4.0 |
| 493.5 | 28.549 | -9.2 | -3.3 | -3.0 | -4.0 |
| 493.8 | 28.566 | -9.6 | -3.4 | -3.1 | -4.2 |
| 494.1 | 28.583 | -9.6 | -3.4 | -3.1 | -4.1 |
| 494.3 | 28.600 | -9.8 | -3.5 | -3.2 | -4.2 |
| 494.6 | 28.617 | -9.7 | -3.4 | -3.1 | -4.2 |
| 494.9 | 28.634 | -9.7 | -3.2 | -2.9 | -3.9 |
| 495.2 | 28.651 | -9.5 | -3.0 | -2.7 | -3.8 |
| 495.4 | 28.669 | -9.3 | -3.0 | -2.7 | -3.7 |
| 495.7 | 28.686 | -9.1 | -2.9 | -2.6 | -3.7 |
| 496.0 | 28.703 | -9.0 | -3.1 | -2.8 | -3.9 |
| 496.3 | 28.721 | -8.7 | -2.9 | -2.6 | -3.6 |
| 496.6 | 28.740 | -9.0 | -3.0 | -2.7 | -3.8 |
| 496.9 | 28.758 | -9.5 | -3.0 | -2.7 | -3.7 |
| 497.2 | 28.777 | -9.5 | -3.1 | -2.8 | -3.8 |
| 497.5 | 28.795 | -9.3 | -2.8 | -2.5 | -3.5 |
| 497.8 | 28.814 | -9.4 | -3.0 | -2.7 | -3.7 |
| 498.1 | 28.832 | -9.0 | -4.2 | -3.9 | -4.9 |
| 498.4 | 28.851 | -8.9 | -3.0 | -2.7 | -3.7 |
| 498.7 | 28.869 | -8.7 | -3.0 | -2.7 | -3.7 |
| 499.0 | 28.888 | -8.5 | -3.0 | -2.7 | -3.7 |
| 499.3 | 28.907 | -8.9 | -2.8 | -2.5 | -3.5 |
| 499.6 | 28.925 | -8.2 | -2.8 | -2.5 | -3.5 |
| 499.9 | 28.944 | -8.0 | -3.0 | -2.7 | -3.7 |
| 500.2 | 28.962 | -8.9 | -3.1 | -2.8 | -3.8 |
| 500.5 | 28.981 | -8.8 | -3.1 | -2.8 | -3.8 |
| 500.8 | 29.000 | -8.2 | -3.1 | -2.8 | -3.8 |
| 501.1 | 29.018 | -8.2 | -3.2 | -2.9 | -3.8 |
| 501.4 | 29.037 | -7.9 | -3.4 | -3.1 | -4.1 |
| 501.7 | 29.056 | -8.4 | -3.4 | -3.1 | -4.1 |
| 502.0 | 29.075 | -8.4 | -3.1 | -2.8 | -3.8 |
| 502.3 | 29.093 | -8.5 | -2.9 | -2.6 | -3.6 |
| 502.6 | 29.112 | -8.3 | -3.0 | -2.7 | -3.7 |
| 502.9 | 29.131 | -7.9 | -3.1 | -2.8 | -3.8 |
| 503.2 | 29.150 | -8.4 | -3.0 | -2.7 | -3.7 |
| 503.5 | 29.168 | -8.9 | -2.9 | -2.6 | -3.6 |
| 503.8 | 29.187 | -9.1 | -3.3 | -3.0 | -4.0 |
| 504.1 | 29.206 | -8.9 | -3.2 | -2.9 | -3.8 |
| 504.4 | 29.224 | -8.9 | -3.2 | -2.9 | -3.8 |
| 504.7 | 29.243 | -8.2 | -2.9 | -2.6 | -3.6 |
| 505.0 | 29.262 | -7.7 | -3.1 | -2.8 | -3.8 |

| Depth (mm) | Age (ka BP) | $\delta^{13}C$ (‰ VPDB) | $\delta^{18}O$ (‰ VPDB) | $\delta^{18}O$ (‰ VPDB) Calcite Corr. | $\delta^{18}O$ (‰ VPDB) Sea Level Corr. |
|---|---|---|---|---|---|
| 505.3 | 29.281 | -7.9 | -3.3 | -3.0 | -4.0 |
| 505.6 | 29.299 | -8.1 | -3.4 | -3.1 | -4.1 |
| 505.9 | 29.318 | -8.7 | -3.6 | -3.3 | -4.2 |
| 506.2 | 29.337 | -9.1 | -3.5 | -3.2 | -4.2 |
| 506.5 | 29.355 | -8.8 | -3.4 | -3.1 | -4.1 |
| 506.8 | 29.374 | -9.0 | -3.4 | -3.1 | -4.1 |
| 507.1 | 29.393 | -9.1 | -3.7 | -3.4 | -4.3 |
| 507.4 | 29.412 | -9.0 | -3.3 | -3.0 | -4.0 |
| 507.7 | 29.430 | -8.8 | -3.1 | -2.8 | -3.8 |
| 508.0 | 29.449 | -8.7 | -3.0 | -2.7 | -3.6 |
| 508.3 | 29.468 | -8.7 | -2.9 | -2.6 | -3.6 |
| 508.6 | 29.486 | -8.8 | -3.0 | -2.7 | -3.7 |
| 508.9 | 29.505 | -8.7 | -3.1 | -2.8 | -3.8 |
| 509.2 | 29.524 | -8.4 | -3.5 | -3.2 | -4.2 |
| 509.5 | 29.543 | -8.8 | -3.2 | -2.9 | -3.8 |
| 509.8 | 29.561 | -9.1 | -3.7 | -3.4 | -4.4 |
| 510.1 | 29.580 | -8.8 | -3.4 | -3.1 | -4.1 |
| 510.4 | 29.599 | -9.0 | -3.3 | -3.0 | -3.9 |
| 510.7 | 29.618 | -8.8 | -3.4 | -3.1 | -4.1 |
| 511.0 | 29.636 | -8.7 | -3.4 | -3.1 | -4.0 |
| 511.3 | 29.655 | -8.8 | -3.6 | -3.3 | -4.2 |
| 511.6 | 29.674 | -8.8 | -3.5 | -3.2 | -4.1 |
| 511.9 | 29.692 | -8.7 | -3.5 | -3.2 | -4.2 |
| 512.2 | 29.711 | -8.4 | -3.5 | -3.2 | -4.1 |
| 512.5 | 29.730 | -8.4 | -3.3 | -3.0 | -4.0 |
| 512.8 | 29.749 | -8.1 | -3.4 | -3.1 | -4.1 |
| 513.1 | 29.767 | -8.4 | -3.5 | -3.2 | -4.2 |
| 513.4 | 29.786 | -8.4 | -3.3 | -3.0 | -3.9 |
| 513.7 | 29.805 | -8.5 | -3.3 | -3.0 | -4.0 |
| 514.0 | 29.823 | -8.6 | -3.4 | -3.1 | -4.0 |
| 514.3 | 29.842 | -8.7 | -3.2 | -2.9 | -3.9 |
| 514.6 | 29.861 | -8.7 | -3.3 | -3.0 | -3.9 |
| 514.9 | 29.880 | -8.5 | -3.2 | -2.9 | -3.9 |
| 515.2 | 29.898 | -8.3 | -3.4 | -3.1 | -4.1 |
| 515.5 | 29.917 | -8.1 | -3.4 | -3.1 | -4.1 |
| 515.8 | 29.936 | -8.3 | -3.5 | -3.2 | -4.1 |
| 516.1 | 29.954 | -8.5 | -3.5 | -3.2 | -4.2 |
| 516.4 | 29.973 | -8.5 | -3.4 | -3.1 | -4.0 |
| 516.7 | 29.992 | -8.2 | -3.3 | -3.0 | -4.0 |
| 517.0 | 30.011 | -8.5 | -3.4 | -3.1 | -4.1 |
| 517.3 | 30.029 | -8.4 | -3.2 | -2.9 | -3.9 |
| 517.6 | 30.048 | -8.1 | -3.5 | -3.2 | -4.1 |
| 517.9 | 30.067 | -7.9 | -3.4 | -3.1 | -4.0 |

| Depth (mm) | Age (ka BP) | $\delta^{13}C$ (‰ VPDB) | $\delta^{18}O$ (‰ VPDB) | $\delta^{18}O$ (‰ VPDB) Calcite Corr. | $\delta^{18}O$ (‰ VPDB) Sea Level Corr. |
|---|---|---|---|---|---|
| 518.2 | 30.086 | -8.1 | -3.4 | -3.1 | -4.1 |
| 518.5 | 30.104 | -8.0 | -3.6 | -3.3 | -4.2 |
| 518.8 | 30.123 | -8.0 | -3.6 | -3.3 | -4.2 |
| 519.1 | 30.142 | -8.0 | -3.5 | -3.2 | -4.1 |
| 519.4 | 30.160 | -7.6 | -3.5 | -3.2 | -4.2 |
| 519.7 | 30.179 | -7.6 | -3.3 | -3.0 | -3.9 |
| 520.0 | 30.198 | -8.1 | -3.3 | -3.0 | -4.0 |
| 520.3 | 30.217 | -9.1 | -3.6 | -3.3 | -4.2 |
| 520.6 | 30.235 | -8.8 | -3.4 | -3.1 | -4.0 |
| 520.9 | 30.254 | -8.9 | -3.6 | -3.3 | -4.2 |
| 521.2 | 30.273 | -9.2 | -3.5 | -3.2 | -4.1 |
| 521.5 | 30.291 | -9.1 | -3.4 | -3.1 | -4.0 |
| 521.8 | 30.310 | -8.5 | -3.5 | -3.2 | -4.2 |
| 522.1 | 30.329 | -8.8 | -3.7 | -3.4 | -4.4 |
| 522.4 | 30.347 | -8.7 | -3.8 | -3.5 | -4.4 |
| 522.7 | 30.366 | -9.0 | -3.6 | -3.3 | -4.3 |
| 523.0 | 30.384 | -9.0 | -3.4 | -3.1 | -4.1 |
| 523.2 | 30.402 | -8.8 | -3.7 | -3.4 | -4.3 |
| 523.5 | 30.421 | -8.8 | -3.7 | -3.4 | -4.4 |
| 523.8 | 30.439 | -9.0 | -3.7 | -3.4 | -4.4 |
| 524.1 | 30.458 | -9.1 | -3.6 | -3.3 | -4.3 |
| 524.4 | 30.476 | -9.1 | -3.7 | -3.4 | -4.3 |
| 524.7 | 30.494 | -9.2 | -3.7 | -3.4 | -4.3 |
| 525.0 | 30.513 | -9.3 | -3.8 | -3.5 | -4.4 |
| 525.3 | 30.531 | -9.2 | -3.7 | -3.4 | -4.4 |
| 525.6 | 30.549 | -9.2 | -3.7 | -3.4 | -4.4 |
| 525.9 | 30.568 | -9.1 | -3.9 | -3.6 | -4.5 |
| 526.2 | 30.586 | -9.2 | -3.9 | -3.6 | -4.5 |
| 526.5 | 30.605 | -9.0 | -3.9 | -3.6 | -4.5 |
| 526.8 | 30.623 | -8.4 | -3.7 | -3.4 | -4.3 |
| 527.1 | 30.641 | -8.0 | -3.6 | -3.3 | -4.2 |
| 527.4 | 30.660 | -7.9 | -3.5 | -3.2 | -4.1 |
| 527.7 | 30.678 | -8.3 | -3.8 | -3.5 | -4.4 |
| 528.0 | 30.696 | -8.6 | -3.8 | -3.5 | -4.4 |
| 528.3 | 30.715 | -8.7 | -3.9 | -3.6 | -4.5 |
| 528.6 | 30.733 | -8.8 | -3.9 | -3.6 | -4.5 |
| 528.8 | 30.752 | -8.6 | -3.8 | -3.5 | -4.4 |
| 529.1 | 30.770 | -9.0 | -4.0 | -3.7 | -4.6 |
| 529.4 | 30.788 | -9.1 | -4.1 | -3.8 | -4.7 |
| 529.7 | 30.807 | -8.9 | -3.8 | -3.5 | -4.5 |
| 530.0 | 30.825 | -9.0 | -3.8 | -3.5 | -4.4 |
| 530.3 | 30.843 | -9.1 | -3.9 | -3.6 | -4.6 |
| 530.6 | 30.862 | -9.3 | -4.0 | -3.7 | -4.7 |

| Depth (mm) | Age (ka BP) | $\delta^{13}C$ (‰ VPDB) | $\delta^{18}O$ (‰ VPDB) | $\delta^{18}O$ (‰ VPDB) Calcite Corr. | $\delta^{18}O$ (‰ VPDB) Sea Level Corr. |
|---|---|---|---|---|---|
| 530.9 | 30.880 | -9.3 | -3.9 | -3.6 | -4.6 |
| 531.2 | 30.899 | -8.9 | -3.8 | -3.5 | -4.4 |
| 531.5 | 30.917 | -8.9 | -4.1 | -3.8 | -4.7 |
| 531.8 | 30.935 | -9.0 | -3.8 | -3.5 | -4.5 |
| 532.1 | 30.954 | -8.8 | -3.6 | -3.3 | -4.2 |
| 532.4 | 30.972 | -8.7 | -3.7 | -3.4 | -4.3 |
| 532.7 | 30.990 | -8.7 | -3.5 | -3.2 | -4.2 |
| 533.0 | 31.009 | -8.8 | -3.6 | -3.3 | -4.2 |
| 533.3 | 31.027 | -8.8 | -3.5 | -3.2 | -4.2 |
| 533.6 | 31.046 | -8.3 | -3.3 | -3.0 | -4.0 |
| 533.9 | 31.064 | -8.2 | -3.4 | -3.1 | -4.0 |
| 534.2 | 31.082 | -8.2 | -3.6 | -3.3 | -4.2 |
| 534.5 | 31.101 | -8.3 | -3.4 | -3.1 | -4.0 |
| 534.7 | 31.119 | -7.9 | -3.5 | -3.2 | -4.2 |
| 535.0 | 31.137 | -7.9 | -3.5 | -3.2 | -4.1 |
| 535.3 | 31.156 | -7.9 | -3.4 | -3.1 | -4.0 |
| 535.6 | 31.174 | -8.1 | -3.6 | -3.3 | -4.2 |
| 535.9 | 31.193 | -8.3 | -3.7 | -3.4 | -4.4 |
| 536.2 | 31.211 | -8.5 | -3.7 | -3.4 | -4.4 |
| 536.5 | 31.229 | -8.5 | -3.8 | -3.5 | -4.4 |
| 536.8 | 31.248 | -8.3 | -3.7 | -3.4 | -4.3 |
| 537.1 | 31.266 | -7.9 | -3.6 | -3.3 | -4.3 |
| 537.4 | 31.284 | -7.9 | -3.7 | -3.4 | -4.3 |
| 537.7 | 31.303 | -8.1 | -3.4 | -3.1 | -4.1 |
| 538.0 | 31.321 | -8.3 | -3.5 | -3.2 | -4.2 |
| 538.3 | 31.340 | -8.5 | -3.4 | -3.1 | -4.0 |
| 538.6 | 31.358 | -8.5 | -3.5 | -3.2 | -4.1 |
| 538.9 | 31.376 | -8.6 | -3.5 | -3.2 | -4.1 |
| 539.2 | 31.395 | -8.5 | -3.4 | -3.1 | -4.1 |
| 539.5 | 31.413 | -7.9 | -3.4 | -3.1 | -4.1 |
| 539.8 | 31.432 | -8.1 | -3.7 | -3.4 | -4.3 |
| 540.1 | 31.450 | -8.2 | -3.8 | -3.5 | -4.5 |
| 540.3 | 31.468 | -8.7 | -3.5 | -3.2 | -4.1 |
| 540.6 | 31.487 | -8.5 | -3.6 | -3.3 | -4.2 |
| 540.9 | 31.505 | -8.8 | -3.7 | -3.4 | -4.3 |
| 541.2 | 31.523 | -8.7 | -3.8 | -3.5 | -4.4 |
| 541.5 | 31.542 | -8.9 | -3.8 | -3.5 | -4.4 |
| 541.8 | 31.560 | -9.1 | -4.0 | -3.7 | -4.7 |
| 542.1 | 31.579 | -9.3 | -3.9 | -3.6 | -4.5 |
| 542.4 | 31.597 | -9.1 | -3.7 | -3.4 | -4.4 |
| 542.7 | 31.616 | -8.7 | -3.6 | -3.3 | -4.3 |
| 543.0 | 31.634 | -9.0 | -3.8 | -3.5 | -4.4 |
| 543.3 | 31.652 | -9.5 | -3.6 | -3.3 | -4.3 |

| Depth (mm) | Age (ka BP) | $\delta^{13}C$ (‰ VPDB) | $\delta^{18}O$ (‰ VPDB) | $\delta^{18}O$ (‰ VPDB) Calcite Corr. | $\delta^{18}O$ (‰ VPDB) Sea Level Corr. |
|---|---|---|---|---|---|
| 543.6 | 31.671 | -9.7 | -3.5 | -3.2 | -4.2 |
| 543.9 | 31.689 | -10.9 | -3.8 | -3.5 | -4.4 |
| 544.2 | 31.708 | -10.1 | -3.9 | -3.6 | -4.5 |
| 544.5 | 31.726 | -10.8 | -3.6 | -3.3 | -4.2 |
| 544.8 | 31.745 | -11.5 | -3.6 | -3.3 | -4.2 |
| 545.1 | 31.763 | -11.2 | -3.7 | -3.4 | -4.3 |
| 545.4 | 31.781 | -11.0 | -3.6 | -3.3 | -4.3 |
| 545.7 | 31.800 | -10.5 | -3.6 | -3.3 | -4.2 |
| 546.0 | 31.818 | -10.8 | -3.5 | -3.2 | -4.2 |
| 546.3 | 31.837 | -11.0 | -3.6 | -3.3 | -4.2 |
| 546.6 | 31.855 | -10.9 | -3.4 | -3.1 | -4.1 |
| 546.8 | 31.873 | -10.6 | -3.0 | -2.7 | -3.7 |
| 547.1 | 31.892 | -10.7 | -3.3 | -3.0 | -4.0 |
| 547.4 | 31.910 | -10.9 | -3.3 | -3.0 | -4.0 |

**APPENDIX 4.3.**

(DSSG-3 STABLE ISOTOPE DATA)

| Depth (mm) | $\delta^{13}C$ (‰ VPDB) | $\delta^{18}O$ (‰ VPDB) |
|---|---|---|
| 0.0 | -5.8 | -4.3 |
| 0.3 | -5.0 | -3.8 |
| 0.6 | -4.1 | -4.0 |
| 0.9 | -3.9 | -3.7 |
| 1.2 | -5.1 | -4.0 |
| 1.5 | -5.0 | -3.8 |
| 1.8 | -4.9 | -4.2 |
| 2.1 | -4.6 | -3.7 |
| 2.4 | -4.5 | -3.6 |
| 2.7 | -4.6 | -3.7 |
| 3.0 | -4.9 | -3.5 |
| 3.3 | -4.7 | -3.7 |
| 3.6 | -4.8 | -3.8 |
| 3.9 | -4.9 | -3.9 |
| 4.2 | -5.0 | -3.7 |
| 4.5 | -4.8 | -3.8 |
| 4.8 | -5.2 | -3.7 |
| 5.1 | -5.0 | -3.7 |
| 5.4 | -4.7 | -3.7 |
| 5.7 | -4.5 | -3.8 |
| 6.0 | -4.1 | -3.8 |
| 6.3 | -3.2 | -3.9 |
| 6.6 | -3.7 | -4.0 |
| 6.9 | -3.8 | -3.9 |
| 7.2 | -4.3 | -4.1 |
| 7.5 | -6.6 | -4.8 |
| 7.8 | -6.7 | -4.6 |
| 8.1 | -5.5 | -4.2 |
| 8.4 | -4.2 | -3.9 |
| 8.7 | -3.7 | -3.9 |
| 9.0 | -4.2 | -4.1 |
| 9.3 | -5.8 | -4.2 |
| 9.6 | -6.1 | -4.4 |
| 9.9 | -5.5 | -4.6 |
| 10.2 | -6.8 | -4.4 |
| 10.5 | -6.8 | -4.2 |
| 10.8 | -8.1 | -4.0 |
| 11.1 | -9.0 | -4.1 |
| 11.4 | -9.9 | -4.1 |
| 11.7 | -9.7 | -4.2 |
| 12.0 | -9.4 | -4.1 |
| 12.3 | -9.4 | -3.8 |
| 12.6 | -9.6 | -4.1 |

| Depth (mm) | $\delta^{13}C$ (‰ VPDB) | $\delta^{18}O$ (‰ VPDB) |
|---|---|---|
| 12.9 | -9.9 | -4.2 |
| 13.2 | -9.9 | -4.3 |
| 13.5 | -9.8 | -4.0 |
| 13.8 | -9.9 | -4.1 |
| 14.1 | -10.1 | -4.2 |
| 14.4 | -10.1 | -4.1 |
| 14.7 | -9.9 | -4.2 |
| 15.3 | -9.5 | -3.8 |
| 15.6 | -9.7 | -3.9 |
| 15.9 | -10.0 | -4.1 |
| 16.2 | -9.7 | -3.8 |
| 16.5 | -9.6 | -3.9 |
| 16.8 | -9.7 | -4.0 |
| 17.1 | -9.6 | -3.9 |
| 17.4 | -9.5 | -4.0 |
| 17.7 | -9.6 | -3.8 |
| 18.0 | -9.7 | -4.0 |
| 18.3 | -9.9 | -3.9 |
| 18.6 | -9.8 | -4.0 |
| 18.9 | -9.4 | -3.8 |
| 19.2 | -9.9 | -4.1 |
| 19.5 | -9.9 | -3.9 |
| 19.8 | -9.8 | -3.8 |
| 20.1 | -9.8 | -3.9 |
| 20.4 | -9.8 | -3.8 |
| 20.7 | -9.9 | -3.8 |
| 21.0 | -10.0 | -4.0 |
| 21.6 | -9.5 | -3.8 |
| 21.9 | -9.7 | -3.9 |
| 22.2 | -10.0 | -3.9 |
| 22.5 | -9.7 | -3.8 |
| 22.8 | -9.7 | -3.8 |
| 23.1 | -9.9 | -4.1 |
| 23.4 | -9.8 | -3.8 |
| 23.7 | -9.7 | -4.0 |
| 24.0 | -9.9 | -4.1 |
| 24.3 | -9.7 | -4.0 |
| 24.6 | -9.6 | -3.9 |
| 24.9 | -9.7 | -4.1 |
| 25.2 | -9.7 | -4.1 |
| 25.5 | -9.8 | -3.9 |
| 25.8 | -9.6 | -3.8 |
| 26.1 | -9.5 | -3.8 |
| 26.4 | -9.8 | -3.9 |

| Depth (mm) | $\delta^{13}C$ (‰ VPDB) | $\delta^{18}O$ (‰ VPDB) |
|---|---|---|
| 26.7 | -9.9 | -4.0 |
| 27.0 | -9.8 | -3.7 |
| 27.3 | -10.0 | -3.9 |
| 27.6 | -9.7 | -3.7 |
| 27.9 | -9.7 | -3.8 |
| 28.2 | -9.4 | -3.5 |
| 28.5 | -9.4 | -3.5 |
| 28.8 | -9.3 | -3.5 |
| 29.1 | -9.3 | -3.5 |
| 29.4 | -9.4 | -3.4 |
| 29.7 | -9.5 | -3.6 |
| 30.0 | -9.7 | -3.4 |
| 30.3 | -9.3 | -3.4 |
| 30.6 | -9.5 | -3.3 |
| 30.9 | -9.4 | -3.4 |
| 31.2 | -9.5 | -3.4 |
| 31.5 | -9.5 | -3.4 |
| 31.8 | -9.4 | -3.6 |
| 32.1 | -9.5 | -3.6 |
| 32.4 | -9.6 | -3.7 |
| 32.7 | -9.4 | -3.6 |
| 33.0 | -9.4 | -3.6 |
| 33.3 | -9.6 | -3.9 |
| 33.6 | -9.6 | -3.8 |
| 33.9 | -9.5 | -3.8 |
| 34.2 | -9.5 | -3.8 |
| 34.5 | -9.4 | -4.0 |
| 34.8 | -9.7 | -4.1 |
| 35.1 | -9.8 | -4.2 |
| 35.4 | -9.7 | -4.0 |
| 35.7 | -9.8 | -4.0 |
| 36.0 | -9.8 | -4.2 |
| 36.3 | -9.7 | -4.0 |
| 36.6 | -9.8 | -4.1 |
| 36.9 | -9.8 | -4.0 |
| 37.2 | -9.8 | -4.0 |
| 37.5 | -9.7 | -3.9 |
| 37.8 | -9.6 | -3.9 |
| 38.1 | -9.5 | -3.8 |
| 38.4 | -9.3 | -3.6 |
| 38.7 | -9.6 | -3.8 |
| 39.0 | -9.9 | -3.8 |
| 39.3 | -9.9 | -3.7 |
| 39.6 | -9.9 | -3.7 |

| Depth (mm) | $\delta^{13}C$ (‰ VPDB) | $\delta^{18}O$ (‰ VPDB) |
|---|---|---|
| 39.9 | -9.7 | -3.7 |
| 40.2 | -9.8 | -3.6 |
| 40.5 | -9.7 | -3.7 |
| 40.8 | -9.6 | -3.8 |
| 41.1 | -9.6 | -3.7 |
| 41.4 | -9.5 | -4.0 |
| 41.7 | -9.5 | -4.0 |
| 42.0 | -9.6 | -3.9 |
| 42.3 | -9.8 | -4.0 |
| 42.6 | -9.8 | -3.8 |
| 42.9 | -9.8 | -3.8 |
| 43.2 | -10.0 | -3.9 |
| 43.5 | -9.9 | -4.0 |
| 43.8 | -10.0 | -3.8 |
| 44.1 | -10.0 | -3.5 |
| 44.4 | -10.0 | -3.8 |
| 44.7 | -9.8 | -3.9 |
| 45.0 | -9.7 | -3.8 |
| 45.3 | -9.8 | -3.7 |
| 45.6 | -10.0 | -3.8 |
| 45.9 | -10.3 | -4.0 |
| 46.2 | -10.5 | -4.0 |
| 46.5 | -10.1 | -3.7 |
| 46.8 | -10.3 | -3.7 |
| 47.1 | -10.7 | -4.2 |
| 47.4 | -10.0 | -3.9 |
| 47.7 | -9.9 | -3.5 |
| 48.0 | -9.7 | -3.6 |
| 48.3 | -10.0 | -3.3 |
| 48.6 | -9.8 | -3.6 |
| 48.9 | -9.8 | -3.6 |
| 49.2 | -9.9 | -3.5 |
| 49.5 | -9.7 | -3.3 |
| 49.8 | -9.7 | -3.1 |
| 50.1 | -9.7 | -3.5 |
| 50.4 | -9.7 | -3.6 |
| 50.7 | -9.8 | -3.8 |
| 51.0 | -9.4 | -3.2 |
| 51.3 | -10.4 | -3.7 |
| 51.6 | -10.9 | -4.1 |
| 51.9 | -11.2 | -4.4 |
| 52.2 | -11.5 | -4.5 |
| 52.5 | -11.5 | -4.3 |
| 52.8 | -11.6 | -4.3 |

| Depth (mm) | $\delta^{13}C$ (‰ VPDB) | $\delta^{18}O$ (‰ VPDB) |
|---|---|---|
| 53.1 | -11.7 | -4.7 |
| 53.4 | -11.5 | -4.4 |
| 53.7 | -11.5 | -4.5 |
| 54.0 | -11.6 | -4.2 |
| 54.3 | -11.6 | -4.1 |
| 54.6 | -11.7 | -4.3 |
| 54.9 | -11.7 | -4.6 |
| 55.2 | -11.9 | -4.4 |
| 55.5 | -11.9 | -4.7 |
| 55.8 | -12.0 | -4.5 |
| 56.1 | -11.8 | -4.6 |
| 56.4 | -12.0 | -4.6 |